

# **Conversions of hydrocarbons with hydrogen over Pd model catalysts: A molecular beam and IRAS study**

DISSERTATION

zur Erlangung des akademischen Grades

**doctor rerum naturalium**

(Dr. rer. nat.)

im Fach Chemie

eingereicht an der

Mathematisch-Naturwissenschaftlichen Fakultät I

Humboldt-Universität zu Berlin

von

**M. Sc. Wiebke Ludwig**

08.06.1981, Eutin

Präsident der Humboldt-Universität zu Berlin:

Prof. Dr. Jan-Hendrik Olbertz

Dekan der Mathematisch-Naturwissenschaftlichen Fakultät I:

Prof. Dr. Andreas Herrmann

Gutachter:

1. Prof. Dr. Hans-Joachim Freund

2. Prof. Dr. Klaus Rademann

**eingereicht am:** 18.10.2010

**Tag der mündlichen Prüfung:** 08.12.2010







## Abstract

The conversion of hydrocarbons with hydrogen over well-defined Pd model catalysts has been studied using pulsed molecular beam (MB) techniques and IR spectroscopy with a special focus on the understanding of microscopic factors governing the activity and selectivity in the conversion reactions.

Exemplarily, we studied the conversion of *cis*-2-butene with H<sub>2</sub>(D<sub>2</sub>) toward *cis*-*trans* isomerization and hydrogenation over a supported Pd/Fe<sub>3</sub>O<sub>4</sub>/Pt(111) model catalyst and a Pd(111) single crystal surface by pulsed isothermal molecular beam (MB) experiments.

Analysis of the transient and steady state kinetics showed that the activity and selectivity of the Pd model catalyst depend strongly on its ability to build up and maintain a sufficiently high concentration of different hydrogen species - on and in the Pd particles - under reaction conditions. While isomerization proceeds effectively when merely surface adsorbed H(D) is available, for the hydrogenation pathway a second hydrogen species is required. Using a combination of nuclear reaction analysis (in collaboration with M. Wilde and K. Fukutani) and transient MB experiments, it could be demonstrated that the second hydrogen species is associated with the presence of subsurface adsorbed hydrogen.

Strongly-dehydrogenated carbonaceous deposits located on low-coordinated sites of the Pd particles were found to induce persisting hydrogenation activity over the supported Pd/Fe<sub>3</sub>O<sub>4</sub> model catalyst already at low temperatures (220 – 260 K) which could be attributed to facilitation of H(D) diffusion to subsurface sites under reaction conditions. Theoretical calculations (in collaboration with K. M. Neyman) suggest that C on atomically flexible particle edges reduces the activation barrier for H diffusion to subsurface sites mainly due to C-induced expansions of the Pd lattice.

Co-adsorbed hydrocarbon species, in contrast, were found to inhibit the formation of both surface and subsurface H(D). This effect was more pronounced for the replenishment of subsurface H(D) species.

Pulsed isothermal MB experiments on the H/D exchange over Pd model catalysts to probe the H(D) distribution more directly showed that - next to regular surface H(D) - a second type of hydrogen species is involved in the formation of HD, most likely subsurface hydrogen. In line with theoretical calculations, C deposited on low-coordinated sites was shown to affect the HD formation presumably by facilitating subsurface H diffusion and increasing the concentration of highly reactive subsurface H species. Co-adsorbed hydrocarbons, in contrast, strongly inhibit the H/D exchange presumably due to breaking up ensembles of free adsorption sites.

The first results on the adsorption and reaction of isophorone, a  $\alpha,\beta$ -unsaturated ketone, with hydrogen over a Pd(111) single crystal surface investigated by surface science techniques under well-defined UHV conditions are presented. Changes in the adsorption geometry with increasing coverage and due to co-adsorbed H(D) affecting, in particular, also the C=C and/or the C=O bonds were detected using IRAS. In line with realistic catalytic studies, a strong chemoselectivity toward the hydrogenation of the C=C double bond was found in TPR measurements. These promising results constitute the base for further investigations on the microscopic factors governing the selectivity in the hydrogenation reactions of more complex molecules.



## Zusammenfassung

Die Umsetzung von Kohlenwasserstoffen mit Wasserstoff auf wohldefinierten Pd-Modellkatalysatoren wurde anhand von Molekularstrahlmethoden (MB) und IR-Spektroskopie mit besonderem Schwerpunkt auf dem Verständnis von mikroskopischen Faktoren, die die Aktivität und Selektivität bestimmen, studiert.

Exemplarisch wurden die Reaktionen von *cis*-2-Buten mit  $H_2(D_2)$ , *cis-trans*-Isomerisierung und Hydrierung, über einem geträgerten Pd/Fe<sub>3</sub>O<sub>4</sub>-Modellkatalysator und einem Pd(111)-Einkristall mit Hilfe von gepulsten, isothermen MB-Experimenten erforscht.

Analyse der transienten und stationären Kinetik ergab, dass die Aktivität und Selektivität des Pd-Modellkatalysators stark von dessen Fähigkeit abhängt, ausreichend hohe Konzentrationen von unterschiedlichen Wasserstoffspezies - auf und in den Pd-Partikeln - unter Reaktionsbedingungen aufzubauen und aufrechtzuerhalten. Während Isomerisierung effektiv abläuft, selbst wenn nur oberflächenadsorbierter H(D) verfügbar ist, wird für die Hydrierung eine zweite Art von H(D)-Spezies benötigt. Durch Kombination von Nuclear Reaction Analysis (in Kooperation mit M. Wilde und K. Fukutani) und transienten MB-Experimenten konnten wir zeigen, dass die zweite Art von H-Spezies mit der Anwesenheit von im Pd-Partikelvolumen absorbierten H korreliert ist.

Unsere Untersuchungen demonstrierten, dass stark-dehydrogenierte Kohlenstoffablagerungen auf niedrig-kooordinierten Adsorptionsplätzen der Pd-Partikel anhaltende Hydrierungsaktivität über dem Pd/Fe<sub>3</sub>O<sub>4</sub>-Modellkatalysator schon bei niedrigen Temperaturen (220 – 260 K) ermöglichen. Dies wurde einer Begünstigung der H(D)-Diffusion zu Adsorptionsplätzen im Partikelvolumen unter Reaktionsbedingungen zugeschrieben. Theoretische Rechnungen (in Kooperation mit K. M. Neyman) deuten an, dass C auf atomarflexiblen Partikelkanten die Aktivierungsbarriere für H(D)-Diffusion ins Partikelvolumen hauptsächlich durch C-induzierte Aufweitungen des Pd-Gitters reduziert.

Die experimentellen Ergebnisse zeigten, dass co-adsorbierte Kohlenwasserstoffspezies hingegen die Bildung von sowohl oberflächenadsorbiertem als auch im Partikelvolumen absorbiertem H(D) inhibieren. Dieser Effekt war für die Regeneration von volumen-absorbierten H(D) stärker ausgeprägt.

Gepulste isotherme MB-Experimente zum H/D-Austausch auf Pd-Modellkatalysatoren zur direkteren Untersuchung der H(D)-Verteilung zeigten, dass neben regulärem Oberflächenwasserstoff, eine zweite Art von H-Spezies, vermutlich volumen-absorbierter H(D), in die Bildung von HD involviert ist. In Übereinstimmung mit theoretischen Rechnungen, zeigten die Experimente, dass C auf niedrig-kooordinierten Plätzen die HD-Bildung vermutlich durch eine Erleichterung der H(D)-Diffusion ins Partikelvolumen und durch eine somit höhere Konzentration des hochreaktiven, volumen-absorbierten H(D) beeinflusst. Co-adsorbierte Kohlenwasserstoffspezies hingegen inhibieren den H/D-Austausch stark, vermutlich dadurch, dass sie Ensembles von freien Adsorptionsplätzen aufbrechen.

Die ersten Ergebnisse zur Adsorption und Reaktion von Isophoron, einem  $\alpha, \beta$ -ungesättigtem Keton, mit Wasserstoff auf einer Pd(111)-Einkristalloberfläche, die mit Hilfe von oberflächensensitiven Methoden unter wohldefinierten UHV-Bedingungen untersucht wurden, werden präsentiert. Veränderungen der Adsorptionsgeometrie, die insbesondere auch die C=C- und/oder die C=O-Bindungen betreffen,

wurden mit steigender Bedeckung und in Anwesenheit von co-adsorbierten H(D) anhand von IRAS-Messungen detektiert. In Übereinstimmung mit realistischen Katalysestudien wurde in TPR-Messungen eine deutliche Chemoselektivität in Richtung der Hydrierung der C=C-Doppelbindung festgestellt. Diese vielversprechenden Ergebnisse bilden die Basis für weitere Untersuchungen zu mikroskopischen Faktoren, die die Selektivität in Hydrierungsreaktionen von komplexeren Molekülen bestimmen.



# Contents

<b>1</b>	<b>Introduction</b>	<b>1</b>
<b>2</b>	<b>Theory</b>	<b>7</b>
2.1	Kinetics on surfaces . . . . .	7
2.1.1	Basic processes on surfaces . . . . .	7
2.1.2	Kinetic effects on oxide supported metal particles . . . . .	11
2.2	Adsorption and absorption on Pd . . . . .	13
2.2.1	CO adsorption on Pd . . . . .	14
2.2.2	Hydrogen adsorption and absorption on Pd . . . . .	15
2.2.3	Carbon on Pd . . . . .	17
2.3	Experimental methods . . . . .	18
2.3.1	Molecular beams . . . . .	18
2.3.2	Detection methods . . . . .	22
<b>3</b>	<b>Experimental setup</b>	<b>29</b>
3.1	Preparation chamber and sample holder . . . . .	30
3.1.1	Sample holder . . . . .	30
3.2	Scattering chamber . . . . .	31
3.2.1	Supersonic beam . . . . .	33
3.2.2	Effusive beams . . . . .	34
3.2.3	Stationary mass spectrometer . . . . .	35
3.2.4	FT-IR setup . . . . .	36
3.3	Time control of the pulsed molecular beam experiments . . . . .	36
<b>4</b>	<b>Pd/Fe<sub>3</sub>O<sub>4</sub> model catalyst</b>	<b>37</b>
4.1	Fe <sub>3</sub> O <sub>4</sub> film on Pt(111) . . . . .	38
4.2	Pd-particles supported on Fe <sub>3</sub> O <sub>4</sub> /Pt(111) . . . . .	39
<b>5</b>	<b>2-butene conversion with D<sub>2</sub> over Pd/Fe<sub>3</sub>O<sub>4</sub>/Pt(111): The role of hydrogen</b>	<b>43</b>
5.1	Introduction . . . . .	43
5.2	Reactivity of the Pd/Fe <sub>3</sub> O <sub>4</sub> model catalyst between 190 and 260 K . . . . .	45
5.3	Reactivity of the C-containing Pd/Fe <sub>3</sub> O <sub>4</sub> model catalyst . . . . .	48
5.4	The role of surface and subsurface deuterium . . . . .	52
5.5	Conclusion . . . . .	56
<b>6</b>	<b>2-butene conversion with D<sub>2</sub> over Pd/Fe<sub>3</sub>O<sub>4</sub>/Pt(111): A kinetic study</b>	<b>59</b>
6.1	Introduction . . . . .	59

6.2	Dependence on the D <sub>2</sub> pressure . . . . .	62
6.2.1	Reactivity of the C-covered Pd/Fe <sub>3</sub> O <sub>4</sub> model catalyst . . . . .	63
6.2.2	Reactivity of the C-free Pd/Fe <sub>3</sub> O <sub>4</sub> model catalyst . . . . .	70
6.3	Dependence on the <i>cis</i> -2-butene pressure . . . . .	74
6.3.1	Reactivity of the C-covered Pd/Fe <sub>3</sub> O <sub>4</sub> model catalyst . . . . .	74
6.3.2	Reactivity of the C-free Pd/Fe <sub>3</sub> O <sub>4</sub> model catalyst . . . . .	78
6.4	Temperature dependence . . . . .	80
6.4.1	Reactivity of the C-covered Pd/Fe <sub>3</sub> O <sub>4</sub> model catalyst . . . . .	80
6.4.2	Reactivity of the C-free Pd/Fe <sub>3</sub> O <sub>4</sub> model catalyst . . . . .	83
6.5	Conversion and selectivity . . . . .	85
6.6	Conclusion . . . . .	87
<b>7</b>	<b>2-butene conversion with D<sub>2</sub> over Pd model catalysts: The role of carbon</b>	<b>91</b>
7.1	Introduction . . . . .	91
7.2	Isomerization activity . . . . .	92
7.3	Hydrogenation activity . . . . .	96
7.4	The role of carbon . . . . .	102
7.5	Conclusion . . . . .	107
<b>8</b>	<b>H/D exchange over Pd model catalysts: Probing the hydrogen distribution</b>	<b>109</b>
8.1	Introduction . . . . .	109
8.2	The influence of C-modification of low-coordinated sites . . . . .	112
8.3	The influence of subsurface H . . . . .	116
8.3.1	Temperature dependence . . . . .	116
8.3.2	Pressure dependence . . . . .	122
8.3.3	Transient kinetics . . . . .	128
8.4	Effect of hydrocarbons . . . . .	134
8.5	Conclusion . . . . .	136
<b>9</b>	<b>Isophorone adsorption and reaction with D<sub>2</sub> on Pd(111)</b>	<b>139</b>
9.1	Introduction . . . . .	139
9.2	Adsorption on Pd(111) . . . . .	141
9.2.1	Isophorone on Pd(111) . . . . .	141
9.2.2	3,3,5-trimethyl-cyclohexanone on Pd(111) . . . . .	144
9.3	Reactivity on Pd(111) . . . . .	148
9.4	Conclusion and outlook . . . . .	152
<b>10</b>	<b>Summary</b>	<b>155</b>

# 1 Introduction

Heterogeneous catalysis is used to kinetically control many important processes in the chemical industry, in environmental technology and in energy technology [1–4]. The conversion of hydrocarbons and alkenes, *e.g.* from oil feedstocks or from biomass, is one major application for heterogeneous catalysts. In particular, Pd catalysts are often employed for hydrogenation and isomerization reactions of alkenes.

Catalysts, by definition, alter the kinetics of chemical reactions, control thus reaction rates and thereby influence the selectivity of a reaction as well as the required reaction conditions. To achieve higher yields at milder reaction conditions in combination with a high purity of the products is both economically and environmentally beneficial and therefore one of the main goals in catalysis research. For a rational improvement of catalysts, the reaction mechanisms on the surface as well as the correlation between the electronic and geometric surface structure and the interaction with adsorbed reactants, intermediates and products need to be understood.

Heterogeneous catalysts typically consist of a support, in many cases a metal oxide, on which the active phase, metals or metal oxides, is dispersed in small particles. Next to the oxidation state, also the particle size, particle size distribution and morphology of the catalyst particles were found to influence the catalytic activity [2, 5–8]. Often minority species, like defects, promoters or poisons critically control the reactivity of a catalyst. Also the support can have a significant influence on the reactivity either due to electronic or structural effects on the active particles or due to direct involvement in certain reactions. Under reaction conditions, catalysts often restructure, so that a detailed knowledge of the interaction of adsorbates and the catalyst is required for a microscopic understanding of the processes taking place on the surface [2, 9, 10]. Due to the high complexity of these systems, a detailed enough or even general understanding of surface processes required for the rational design of new catalysts has not yet been achieved and the improvement of catalysts is still mainly accomplished by empirical methods (*catalyst screening*).

There are in principle two different approaches in catalysis research: Either the reactivity of catalysts is studied under conditions as realistic as possible or it is studied on model systems.

In the first approach, the structural parameters of the catalyst, *e.g.* particle size and metal loading, are varied over a wide range and subsequently the influence on the reactivity is determined. Despite the problem that it is often not easy to vary just one

## 1 Introduction

parameter individually, the distinct advantage of this approach is that the obtained results are directly relevant for application. The main disadvantage is that it is usually possible to obtain only *macroscopic* information on the structure of the catalyst, while the *atomic* details are not accessible and thus, also a truly microscopic understanding of the reaction mechanism is not possible.

In the second approach, the structural and chemical complexity of the real catalytic system is reduced by the use of model systems, in the most simple case, a metal single crystal is investigated under ultra-high vacuum (UHV) conditions. On one hand, the reduced structural complexity of the catalyst ensures that atomic details on the surface can be captured by spectroscopic methods. On the other hand, UHV conditions provide a very well-controlled, chemically clean environment and thus, allow for a high control of the molecules adsorbed on the catalytic surface. Even though UHV studies on metal single crystals have contributed significantly to the understanding of catalytic processes [9], the conditions are very different from those of industrially applied processes, both in the pressure range (*pressure gap*) as well as in the complexity and composition of the catalyst (*materials gap*). Therefore, the results of these strongly reduced model systems often cannot reproduce the catalytic processes of realistic systems sufficiently [11, 12].

One promising approach to better mimic the structure of oxide supported metal catalysts as well as the pressure conditions of realistic systems, while still working in a well-defined chemical environment and knowing the structural details at an atomic level, is the combination of molecular beam experiments [2, 12–17] and oxide supported model catalysts [11, 12, 18–22].

Next to a simple Pd(111) single crystal, a model catalyst was used in this work consisting of Pd metal particles deposited on a thin Fe<sub>3</sub>O<sub>4</sub> oxide film that was epitaxially grown onto a Pt(111) metal single crystal substrate. Compared to real catalysts, these well-defined model catalyst exhibit a reduced complexity, but still mimic some important structural characteristics of real supported systems. With respect to real catalysts, the main advantage of supported model catalysts is that due to the good electrical conductance of the underlying metal single crystal substrate a large number of surface science techniques can be used to investigate the structure and morphology at an atomic level [19, 22–25]. By variation of the preparation conditions, it is moreover possible to modify the structure and morphology, *e.g.* particle size and crystallinity, of the model catalyst in a wide range.

In dynamic and kinetic studies, molecular beams are a well-established and very valuable tool [12, 15, 16, 26–29]. By using molecular beams, it is possible to provide a well-defined flux of molecules that can be precisely modulated on short time scales which is a prerequisite to study both the transient and the steady state kinetics of chemical reactions under well-defined conditions. In this work, a molecular beam apparatus was used for kinetic experiments on reactions at surfaces that is equipped with three molecular beams which can be controlled independently from each other. It is possible to

simultaneously cross all three beams on the sample surface so that the sample can be exposed in a well-defined way with up to three different reactants. The reaction can simultaneously be followed by time-resolved infrared-reflection-absorption spectroscopy (IRAS) and quadrupole mass spectrometry (QMS) [30].

In this work, the conversion of olefins with hydrogen over Pd catalysts has been investigated with a special focus on the factors governing the selectivity.

When a simple alkene, in this study *cis*-2-butene, reacts with hydrogen over a Pd catalyst, several reactions may occur: hydrogenation, H/D exchange/*cis-trans* isomerization and decomposition/dehydrogenation. For molecules exhibiting next to a C=C also a C=O double bond, like the  $\alpha,\beta$ -unsaturated ketone isophorone, hydrogenation can occur on either of the two double bonds or on both resulting in the formation of different products. Usually, it is desired that just one and not a mix of products forms. Therefore, it is important to reveal which factors influence the selectivity toward the different competitive reaction pathways.

From catalytic studies conducted under realistic conditions, several macroscopic properties, like reaction orders in the alkene and hydrogen pressure as well as the temperature dependence, of the reaction of alkenes with hydrogen over Pd catalysts are known. Hydrogenation over Pd catalysts for example is favored over isomerization at higher hydrogen and lower alkene partial pressures as well as at higher temperatures [31–38]. Even though these macroscopic trends give indication on how the selectivity can be influenced, a microscopic picture of the processes occurring on the surface is lacking.

While numerous surface science studies were conducted on the reactions of acetylene and ethylene with hydrogen over transition metal surfaces, relatively few were published on longer alkenes. Only few surface science studies on C4 alkene conversion over Pd exist focusing mainly on 1,3-butadiene and 1-butene while 2-butene is often discussed merely as a possible product [39–46]. Surface science studies on the reactions of hydrogen with molecules including both a C=C and a C=O double bond, like  $\alpha,\beta$ -unsaturated aldehydes or ketones, became more numerous only in recent years and focus mainly on acrolein and crotonaldehyde [47–52]; to our best knowledge, no surface science studies on the reactivity in the conversion of isophorone with hydrogen over Pd catalysts exist. The majority of surface science studies is, moreover, conducted on extended metal single crystals despite the fact that small metal particles, as applied in real catalysts, may exhibit a significantly different reactivity in alkene conversions [43, 53]. While previous surface science studies helped to identify, *e.g.* adsorption states and reaction intermediates in alkene conversions with hydrogen, a number of fundamental questions still remain under debate.

On Pd, hydrogen can not only adsorb on the surface, but can also occupy more weakly-binding subsurface sites (see *e.g.* [54, 55]). It has been suggested that the weakly-bound subsurface hydrogen plays a significant role in the hydrogenation of alkenes [43, 53, 56–

## 1 Introduction

59]. Even though recent studies gave first experimental evidence [43, 53, 58], the involvement of different hydrogen species in alkene conversions still remains under discussion.

Under realistic conditions, the catalytic surface is usually covered with a variety of carbonaceous species formed in the decomposition of alkenes. Most surface science studies are however conducted on *clean*, C-free surfaces. Pd exhibits the prominent ability to dissolve relatively large quantities of carbon in the bulk. While amorphous carbonaceous deposits residing on the surface mainly deactivate the catalyst by blocking of active sites, subsurface absorbed carbon has been suggested to influence also the *selectivity* in diene and alkyne conversions with hydrogen [38, 60, 61]. It has been moreover suggested that different carbonaceous deposits may have a distinct influence on the hydrogen distribution which is expected to critically affect the reactivity of the Pd catalyst in reactions involving hydrogen [58, 62–65]. The exact mechanism how different carbonaceous deposits influence the hydrogen distribution and the selectivities in alkene conversions with hydrogen has not yet been unraveled.

### The aim of this work

The aim of this work is to reveal important factors influencing the activity and selectivity of Pd catalysts in hydrocarbon conversions with hydrogen. A special emphasis is put on the role of the hydrogen distribution on the surface and in the subsurface of Pd particles which has been previously suggested to influence the selectivity in olefin reactions with hydrogen [43, 53, 56–59]. Moreover, the effect of strongly-dehydrogenated carbonaceous deposits and co-adsorbed hydrocarbon species on the activity and selectivity in olefin conversions as well as on the hydrogen distribution should be investigated. These species which are usually present on the catalysts under applied reaction conditions were previously suggested to affect not only the activity, but also the selectivity in hydrocarbon conversions with hydrogen [38, 60, 61].

Exemplarily, the conversion of *cis*-2-butene with  $\text{H}_2(\text{D}_2)$  is chosen as a model reaction for alkene conversions with hydrogen. The activity and selectivity toward the two main reaction pathways, *cis-trans* isomerization and hydrogenation, is studied over well-defined Pd model catalysts under chemically-clean UHV conditions using pulsed molecular beam (MB) techniques and IR spectroscopy. The influence on the hydrogen distribution as well as the effect of carbonaceous deposits and co-adsorbed hydrocarbon species is exemplarily investigated for this reaction. Complementing measurements with an independent method are conducted to directly probe the hydrogen distribution on and in the Pd particles under reaction conditions and how it is influenced by carbonaceous deposits and co-adsorbed hydrocarbon species. To advance the understanding of the microscopic factors governing the selectivity in the hydrogenation of more complex molecules, first measurements on the adsorption and reaction of isophorone with hydrogen over a Pd(111) single crystal are performed under well-defined UHV conditions using surface science techniques to build a base for further, detailed investigations.

In the first part of the thesis, the theoretical background of the experiments conducted in this study will be discussed (chapter 2). Subsequently, the experimental MB setup used for the measurements (chapter 3) and the structural properties of the supported Pd/Fe<sub>3</sub>O<sub>4</sub> model catalyst (chapter 4) will be described. In the following chapters (5 to 9), the results obtained in this study are discussed. First, the activity and selectivity of the Pd/Fe<sub>3</sub>O<sub>4</sub> model catalyst in the conversion of *cis*-2-butene with D<sub>2</sub> is investigated for low temperatures (190 – 260 K) by pulsed isothermal MB experiments (chapter 5). It can be demonstrated that the availability of different hydrogen species, surface adsorbed H(D) and subsurface absorbed H(D), critically controls the reactivity toward *cis-trans* isomerization and hydrogenation and that strongly dehydrogenated carbonaceous deposits located on low-coordinated sites of the Pd particles dramatically alter the activity and selectivity of the Pd model catalyst. In chapter 6, kinetic measurements on the influence of the reaction conditions, such as reactant pressures, their relative ratio and the reaction temperature, on the activity and selectivity in *cis*-2-butene conversion are presented. By comparison of the reaction rates on the D-saturated surface and the surface under steady state conditions the effect of co-adsorbed hydrocarbon species on the reactivity of the catalyst and on the hydrogen distribution is further investigated. Moreover, the results obtained for the model system are compared to macroscopic trends reported for realistic systems. Subsequently, the role of low-coordinated sites and their modification by C is studied by comparative measurements over a Pd(111) single crystal and the supported Pd model catalyst (chapter 7). Our experimental results are consistent with the interpretation that C deposited on low-coordinated sites of Pd particles facilitates H(D) diffusion to subsurface sites under reaction conditions. Results on the H/D exchange over Pd model catalysts to study the hydrogen distribution more directly are presented in the following demonstrating that a second hydrogen species, likely subsurface hydrogen, is involved in the formation of HD next to regular surface H(D) (chapter 8). Moreover, the effect of C on the HD formation is investigated. In chapter 9, the first results on the adsorption and reaction with hydrogen of a more complex molecule, the  $\alpha, \beta$ -unsaturated ketone isophorone, over Pd surfaces are presented. It can be demonstrated that changes in the adsorption geometry are detectable and that the selectivity of the model system is in line with reports of applied catalytic systems. The most important results of this work are summarized in chapter 10.





## 2 Theory

In this chapter, the theoretical background for the most important aspects of this work will be discussed. In the first section of this chapter (2.1), some specific aspects of kinetics on surfaces in general as well as kinetic phenomena on oxide supported catalysts will be presented. The adsorption and absorption properties of Pd catalysts is discussed in the second section (2.2). In the third section (2.3), the physical working principle of the most important experimental methods applied in this work will be described.

### 2.1 Kinetics on surfaces

Catalysis is by definition a kinetic phenomenon and is based on the interactions between the gas phase and the surface. Even a very simple catalytic reaction consists of a number of elementary reaction steps. In the first part of this section (2.1.1), basic processes that can occur on a surface will be shortly discussed. When a heterogeneous catalysts consists not only of a single phase, but of metal particles supported on a metal oxide, additional kinetic effects can occur that are not observed on a simple homogeneous metal single crystal surface. The kinetic phenomena that can occur on oxide supported metal particles are discussed in the second part of this section (2.1.2).

#### 2.1.1 Basic processes on surfaces

In this part, elementary processes occurring on surfaces will be presented only briefly. A more detailed discussion can be found in the literature [15–17, 66, 67]. A schematical representation of the different processes is given in fig. 2.1.

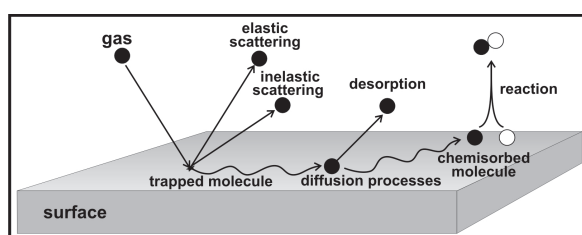


Figure 2.1: Schematical representation of elementary processes on surfaces.

**Scattering:** Molecules or atoms from the gas phase can be elastically or inelastically scattered from the surface. The scattering angle for an elastic scattering process is identical with the angle of incidence. While no energy transfer occurs in an elastic scattering

## 2 Theory

process, in an inelastic scattering event, energy is transferred between the molecule and the surface. Thus, it is possible to heat or cool the surface by inelastic scattering events [15–17].

**Trapping:** When a molecule loses its kinetic energy perpendicular to the surface, *e.g.* by energy transfer to the surface phonons or by excitation of internal vibrations, and becomes thermally equilibrated with the surface, it becomes trapped on the surface. The trapped molecule can either adsorb directly in a more strongly binding state or diffuse over the surface before desorbing or adsorbing in a stronger binding state [15–17].

**Adsorption:** An adsorbed molecule is a molecule that is bound to the surface. If the binding to the surface is due to relatively weak dispersive (*Van-der-Waals*) forces, this type of adsorption is called physisorption. When the binding is due to strong covalent bonds, it is called chemisorption. The strong interactions of chemisorbed molecules with the surface can lead to pronounced distortions of the adsorbed molecule (compared to the gas phase structure) and even to dissociation. Often chemisorption occurs after a molecule has passed a more weakly bound precursor state.

The rate of adsorption of a molecule  $A$  depends on the incoming flux of molecules which can also be expressed as the collision frequency  $Z_A$ , the number of free adsorption sites  $\theta_*$  (with  $\theta_* = 1 - \theta_A - \theta_B - \dots$ ) and the sticking coefficient  $S_A$ :

$$\frac{d\theta_A}{dt} = Z_A \cdot \theta_* \cdot S_A(\theta_A, \theta_B, \dots) \quad (2.1)$$

The collision frequency  $Z_A$  is given by  $Z_A = p_A / \sqrt{2\pi \cdot m_A \cdot k_B \cdot T}$  with  $p_A$  and  $m_A$  denoting the partial pressure and the molecular mass of the adsorbing molecule  $A$ . The sticking coefficient  $S_A$  is defined as the ratio of the sticking molecules relative to the overall number of incoming molecules  $S_A(\theta) = \frac{dN_{ads}}{dN}$ .

The rate of adsorption can strongly depend on the presence of other adsorbates. This effect is mainly due to simple site blocking, but some adsorption processes require also an ensemble of several free neighboring adsorption sites to accommodate the adsorbate on the surface. In this case even a relatively low number of other adsorbates on the surface can strongly decrease the adsorption rate. For other cases, *e.g.* precursor mediated processes, the adsorption rate may also be independent of the surface coverage.

The adsorption of molecules can either be activated or non-activated. The two cases differ in the temperature dependence of the sticking coefficient [67]. Usually physisorption processes are rather non-activated, while chemisorption processes often have a pronounced activation barrier. There are however, also cases of dissociative adsorption that are basically non-activated, such as dissociative adsorption of  $H_2$  on Pd.

**Diffusion:** Diffusion of molecules over surfaces is typically an activated process. The diffusion coefficient  $D$  can be expressed as (see *e.g.* [67]):

$$D = D_0 \exp\left(\frac{-E_{diff}}{RT_s}\right) \quad (2.2)$$

with  $D_0$  and  $E_{diff}$  denoting the pre-exponential factor and the activation energy for diffusion, respectively.  $T_s$  indicates the surface temperature. For strongly-bound species that have to overcome a significant activation barrier between different adsorption sites (where  $RT_s$  is not  $\gg E_{diff}$ ), the diffusion over the surface resembles a hopping motion along the path of minimum activation energy. When  $RT_s \gg E_{diff}$ , the molecules diffuse freely over the surface in a kind of *Brownian* motion (2-dimensional gas).

For temperatures where  $RT_s$  is not  $\gg E_{diff}$ , the diffusion coefficient  $D$  can be interpreted also as [67]:

$$D = \frac{vd^2}{4} \quad (2.3)$$

with  $v$  denoting the hopping frequency and  $d$  the hopping length which is related to the distance between the adsorption sites. The mean distance  $\bar{x}$  traveled of a diffusing molecule is given by  $\bar{x} = \sqrt{4Dt_r}$  with  $t_r$  denoting the average residence time on the surface. For weakly-bound species the residence time is usually short limiting, thus, the mean path  $\bar{x}$ , while for strongly-bound species that exhibit relatively long residence times, the mean path is rather limited by low diffusion coefficients due to relatively large diffusion barriers.

In some cases, adsorbates do not only diffuse over the surface, but can also diffuse into the region beneath the surface and even further into the bulk. On Pd, both H and C can diffuse also to absorption sites within the bulk (see *e.g.* [54, 55, 68, 69]). Diffusion into the subsurface or into the bulk is often an activated process with the size of the activation barrier depending on the surface structure and diffusion site which was suggested to be also the case for *e.g.* H diffusion to subsurface sites [70–75]. For H diffusion into the subsurface region of Pd, the activation energy for diffusion through a (111)-facet is significantly larger than that for a (100)-facet [70]. The atoms or molecules absorbed in the bulk can also diffuse within the bulk. For H in Pd the activation barrier for diffusion with the bulk metal is moderate, so that diffusion within bulk Pd occurs at significant rates already at relatively low temperatures [76, 77].

**Reactions on surfaces:** Reactions on transition metal surfaces can occur either via the so-called Eley-Rideal (ER) mechanism or the Langmuir-Hinshelwood (LH) mechanism [78–80]. Most surface reactions occur via the Langmuir-Hinshelwood mechanism where two surface adsorbed species react with each other, while only very few examples are known following the Eley-Rideal mechanism where an atom or molecule from the gas phase directly reacts with a surface adsorbed species [15, 16, 67]. Also the reactions studied in this work follow a LH mechanism, which will be discussed therefore using a simple example reaction  $A_{gas} + B_{gas} + surface \rightarrow AB$  with the elementary reaction steps:



## 2 Theory

with  $\star$  representing the respective surface sites. Even a seemingly simple catalytic reaction consists of a multitude of elementary reaction steps. If the adsorption of  $A$  and  $B$  (eq. 2.4 and 2.5) and the desorption of  $AB$  (eq. 2.7) are fast and thus the reaction of  $A$  and  $B$  (eq. 2.6) is rate limiting, the reaction rate can be calculated by:

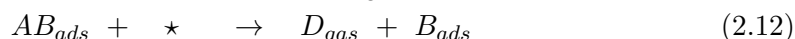
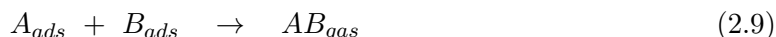
$$\frac{d\theta_{AB}}{dt} = k \cdot \exp\left(-\frac{E_a}{RT_s}\right) \cdot \theta_A \cdot \theta_B \quad (2.8)$$

with  $k$  denoting the pre-exponential factor,  $E_A$  the activation energy,  $\theta_A$  and  $\theta_B$  denoting the surface coverages of molecules  $A$  and  $B$ , respectively. Reactions on surfaces often exhibit strong deviations from the simple Arrhenius type behavior as denoted in eq. 2.8. One reason for this is the temperature dependence of the coverages of the reactants  $A$  and  $B$ . When the temperature is increased, the reaction rates can decrease due to increased desorption and thus, decreased coverages, despite an increase in the reaction rate constant.

The rate equation also becomes significantly more involved, when the two adsorbates  $A$  and  $B$  compete for the same adsorption site or one adsorbate inhibits the adsorption of the other reactant. In this case, the coverage of molecule  $A$  depends on the coverage of molecule  $B$ :  $\theta_A = f(\theta_B)$  and *vice versa*, so that analytical solutions of the rate equations often become impossible. One important aspect of competing or inhibited adsorption is that the reaction rates may not increase linearly with increasing flux or coverage of the reactants. An increase in the flux of the inhibiting molecule can even result in decreasing reaction rates.

It should be noted that also the pre-exponential factor  $k$  and the activation energy  $E_a$  may depend strongly on the coverage of different adsorbates which further complicates the kinetic equations of surface reactions.

Even more complex kinetic systems arise, when several reaction pathways are accessible for the reaction:



For directly competing reaction rates, as in eq. 2.9 and 2.10, the relative reaction rates depend on the ratio of the reaction rate constants. In consecutive reactions, like eq. 2.9, 2.11 and 2.12, the relative reaction rates depend not only on the reaction rate constants, but also on the coverages of molecules  $A$  and  $B$  as well as on the availability of free surface sites  $\star$ . For such complex reaction systems, an analytical solution of the rate equations is often not possible. In this case, numerical solutions can be attempted. Another possibility to test the importance of individual reaction steps is to make simplifications in the reaction mechanism and subsequently test, if the resulting simplified reaction mechanism can describe the observed kinetics.

**Desorption:** An adsorbed molecule can leave the surface again, when the temperature of the surface and thus, the energy transferred to molecule becomes high enough to leave the potential well. The temperature dependence of the desorption can be described with an Arrhenius type equation:

$$\frac{d\theta_A}{dt} = -k_{des} \cdot \exp\left(-\frac{E_{des}}{RT_s}\right) \cdot (\theta_A)^n \quad (2.13)$$

with  $k_{des}$  denoting the pre-exponential factor for desorption,  $E_{des}$  the activation energy for desorption,  $\theta_A$  the coverage of the adsorbed molecule  $A$  and  $n$  denoting the desorption order. The order of desorption is typically 0 for multilayer desorption, 1 for molecular desorption and 2 for associative or recombinative desorption. When the adsorbates have attractive or repulsive interactions, also non-integral numbers can be observed for the desorption orders.

### 2.1.2 Kinetic effects on oxide supported metal particles

When the catalyst is composed not just of a single phase but of metal particles supported on a metal oxide, the kinetic processes become more complex. On one hand, the oxide support can be directly or indirectly involved in the reaction kinetics, on the other hand also on a metal particle - a confined system with a variety of different adsorption sites - special kinetic processes that are not possible on a simple metal single crystal surface can occur.

In the first part, the influence of the *support* on the reaction kinetics will be discussed briefly, while in the second part distinct kinetic effects of metal *particles* in comparison with extended metal single crystals will be presented. In the third part, the importance of the *thermal stability* of metal particles will be addressed briefly.

#### The role of the metal oxide support

The metal oxide is often not just an inactive phase that simply supports the metal particles, but it can actively participate in the reaction. It is possible that a reaction occurs entirely on the oxide support or that the support is just in some reaction steps active, while other reactions steps only proceed effectively on the metal particles.

Next to this direct involvement in the reaction, the oxide support can also be more indirectly involved in the reaction kinetics (see also fig. 2.2). In a supported metal oxide catalyst, the reactants can not only adsorb on the metal particles, but they can also be trapped on the oxide support. When the mean path of the reactants on the oxide support is long enough, these can diffuse to the metal particles. This way the support can capture additional reactants. The zone around the metal particle providing additional reactants for the particle by trapping is called *capture zone*. Intermediates formed by an activated process on the metal particles can also diffuse onto the oxide support (*spillover*) which either acts just as a reservoir or is active for further reactions. The

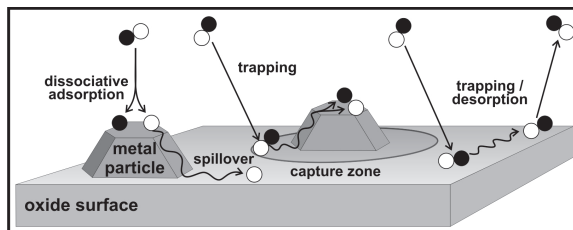


Figure 2.2: Schematical representation of processes on a catalyst consisting of metal particles supported on a metal oxide.

reverse process is called *reverse spillover*.

The interactions between the oxide support and the metal particles can modify the electronic structure and the morphology of the metal particles. Thereby, the oxide support may also significantly alter the adsorption properties and the reactivity of the metal particles.

### Kinetic effects on supported particles

Compared to extended metal single crystal surfaces, metal particles exhibit a variety of different adsorption sites, such as different facets, edges, corners and defects with distinct reactivities. Even though it is possible to mimic these sites to a certain extent by stepped single crystal surfaces, not all effects observed for particles can be reproduced [11, 12].

Modification of the reaction kinetics on small metal particles can arise from the limited size of the particles. Due to electron confinement and lattice distortions, the size of a particle may significantly influence the electronic structure and thus, the reactivity compared to an extended bulk metal. This effect is most significant for very small particles [81–83].

The surface metal atoms in small particles exhibit moreover a high flexibility compared to relatively rigid extended single crystal surfaces. Therefore, adsorbate induced restructuring that can dramatically alter the reaction kinetics is expected to be even more important for small metal particles than for extended metal surfaces.

On small particles, adsorbates or reactive intermediates can diffuse quickly between regions of different reactivity, such as different facets, edges and corners. This coupling can result in distinct reaction kinetics that are not expected from a simple combination of the respective regions.

The kinetics on small particles can further exhibit unique kinetic properties due to confinement of the adsorbates to the metal particle. This effect can lead to *e.g.* coverage

fluctuations or restricted diffusion. The latter is especially important for the case of H bulk diffusion on Pd where H absorbed in the near-surface region is present on small Pd particles while on Pd single crystals H diffuses further into the bulk [53].

### Thermal stability and sintering

Metal particles supported on a metal oxide reduce their surface free energy on one hand by surface reduction and on the other hand by interaction with the underlying support which stabilizes the particles and prevents the formation of one large metal agglomerate. For a given metal loading and a certain metal oxide support, the equilibrium shape of the metal particles is determined by the surface free energy of the metal, the support and the metal-support interface and depends on temperature as well as on the surrounding gas atmosphere.

When a metal is deposited onto a cold oxide surface, the mobility of the metal atoms can be - depending on the activation energy for diffusion - low, so that at low temperature deposited metal particles often exhibit a high island density and a relatively small particle size compared to deposition at higher surface temperatures which was *e.g.* reported for Pd particles deposited on Al<sub>2</sub>O<sub>3</sub> thin films [19]. When heating these particles to higher temperatures usually two processes occur. On one hand the metal atoms rearrange in the particle to a more ordered, crystalline and thermodynamically favorable structure. On the other hand, the smaller particles sinter to bigger particles so that the island density decreases and the average particle size increases leading to a reduction of the surface free energy.

In the investigation of reaction kinetics, to ensure a high reproducibility, it is very important that in a series of experiments, the catalyst structure and thus, the average size and shape of the metal particles is the same at the beginning of each measurement. Moreover, the catalyst should be free from unwanted contaminants to exclude an influence of these species on the studied reaction. When working with hydrocarbons, carbonaceous residue formed in preceding experiment needs to be removed from the catalyst by oxidative treatment. It has been previously shown that the sintering of Pd particles supported on Fe<sub>3</sub>O<sub>4</sub> is enhanced by an atmosphere of oxygen [84, 85]. Therefore, the metal particles in this work were always stabilized before use by repeated oxidation-reduction cycles until an equilibrium shape was attained.

## 2.2 Adsorption and absorption on Pd

In the following section the adsorption behavior of CO, hydrogen and carbon on Pd will be discussed shortly. CO was used as a probe to investigate the distribution of different adsorption sites on the Pd particles. Its adsorption behavior on Pd will be described in the first part of the section (2.2.1). The adsorption and absorption behavior of both hydrogen and carbon is important in the investigation of alkene conversions with hydrogen over Pd model catalysts. Therefore, some prominent aspects will be discussed

## 2 Theory

for hydrogen and carbon in the second (2.2.2) and third part (2.2.3) of this section, respectively.

### 2.2.1 CO adsorption on Pd

In this work, CO was used to probe the structure of the Pd particles by IRAS measurements. Therefore, the adsorption of CO on Pd surfaces with a special emphasis on the frequency shifts in the CO stretching vibration depending on the adsorption site will be discussed in the following.

The interaction of CO with transition metal surfaces is usually described using the model introduced by Blyholder [86]. When CO adsorbs on a transition metal surface, charge can be transferred from the  $5\sigma$ -HOMO (highest occupied molecular orbital) into lower-lying metal states leading to the formation of a  $\sigma$ -donor bond between the C atom and the metal (electron donation). The formally negatively charged surface can transfer charge back into the  $2\pi^*$ -LUMO (lowest unoccupied molecular orbital) orbital resulting in a  $\pi$ -acceptor bond which increases the binding energy of the metal-CO bond, but weakens the C-O bond (back donation). The electron donation and back donation strongly depend on the electron density of the metal surface which varies for different transition metals and also for individual adsorption sites. Therefore, the C-O bond strength and thus, the C-O stretching frequency are a very sensitive probe for the underlying structure. As the CO adsorption on Pd has been studied in much detail, CO can be used to investigate the structure and morphology of supported Pd particles.

#### CO on Pd(111)

For CO adsorption on Pd(111), a variety of ordered adsorption structures depending on the coverage has been found [87]. At low coverage, islands of CO adsorbed in hollow sites with an internal  $(\sqrt{3} \times \sqrt{3}) R30^\circ$  adsorbate structure are observed that grow with increasing coverage until a closed  $(\sqrt{3} \times \sqrt{3}) R30^\circ$  adsorbate structure is formed at a coverage of  $\theta = 0.33$ . The C-O stretching frequency for this coverage is observed at  $1840 \text{ cm}^{-1}$  [88–90]. Upon further increase of the coverage, a  $c(4 \times 2)$ -2CO-structure with a C-O stretching frequency of  $1936 \text{ cm}^{-1}$  is found at  $\theta = 0.5$  which is the saturation coverage at 300 K under UHV conditions [90]. In this adsorption structure at 300 K, CO occupies next to *fcc*- and *hcp*-hollow sites also bridge sites [89, 91–93]. At  $\theta = 0.75$ , the saturation coverage under UHV conditions below 120 K, a  $c(2 \times 2)$ -3CO structure is observed with CO linearly bound to Pd atoms (C-O stretching frequency at  $2110 \text{ cm}^{-1}$ ) and CO adsorbed in *fcc*- and *hcp*-hollow sites (C-O stretching frequency at  $1895 \text{ cm}^{-1}$ ) [89, 93–95].

#### CO on Pd(100)

CO adsorbed on Pd(100) occupies, independent of coverage, bridge sites with the C-O stretching frequency shifting from  $1895 \text{ cm}^{-1}$  at low coverages to  $1997 \text{ cm}^{-1}$  at the maxi-



mum coverage of  $\theta = 0.8$  [90, 96]. Under UHV conditions, an ordered  $c(2\sqrt{2} \times \sqrt{2}) R45^\circ$  adsorbate structure with a saturation coverage of  $\theta = 0.5$  and a C-O stretching frequency of  $1955 \text{ cm}^{-1}$  is observed.

### CO on Pd particles

Supported particles exhibit a variety of different adsorption sites, such as different facets, corners, edges and defects. CO adsorption on supported particles has been investigated in detail before [95, 97–102]. A typical spectrum of CO adsorbed at 300 K on supported Pd particles is shown in fig. 2.3. Based on CO adsorption on Pd single crystal surfaces, the signals in the region  $1960\text{--}1870 \text{ cm}^{-1}$  were assigned to CO occupying mainly hollow sites on regular (111)-facets. The sharp peak at  $1978 \text{ cm}^{-1}$  was attributed to CO adsorbed on bridge sites on both (100)-facets and edges, while the signal at  $2078 \text{ cm}^{-1}$  was assigned to CO bound in on-top sites of the particle edges. It should be mentioned that the signal due to CO adsorbed on the (100)-side facets of the particles is expected to be attenuated due to the metal surface selection rule (MSSR) as these facets are strongly tilted with respect to the surface normal. In contrast, due to dipole coupling effects, known also as *intensity borrowing*, the signal attributed to CO adsorbed in bridge sites on the particle edges ( $1978 \text{ cm}^{-1}$ ) is expected to gain intensity at the expense of signals attributed to CO adsorbed on regular (111)-facets. Due to these effects, the intensity of the adsorption signals does not reflect the population of the different adsorption sites quantitatively (see also 2.3.2 and [103]).

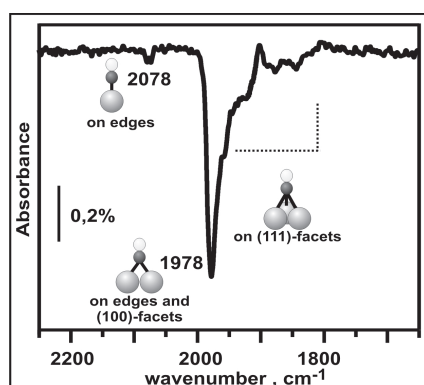


Figure 2.3: IRAS of CO adsorbed at 300 K on supported Pd particles.

### 2.2.2 Hydrogen adsorption and absorption on Pd

Hydrogen can adsorb and absorb on and in Pd in several distinct states. Since it has been suggested in the literature that the different hydrogen species exhibit distinct reactivities in alkene conversions, some important aspects of hydrogen sorption on Pd that has been extensively investigated before, will be briefly discussed [27, 104–108].

## 2 Theory

When hydrogen adsorbs on Pd(111) and Pd(100), it dissociates in a basically non-activated process [27, 104, 105, 109]. It has been found that for dissociation an ensemble of at least three free adjacent adsorption sites is required [104, 110, 111]. This prerequisite becomes important at high coverages or when other adsorbates are present on the Pd surface.

At low coverage, hydrogen atoms adsorb on Pd at strongly-binding, highly coordinating surface sites. On Pd(111), atomic hydrogen occupies *fcc*-threefold-hollow sites with a Pd-H distance of 1.8 Å and a binding energy of 43.5 kJ/mol [55, 71, 112]. On Pd(100), atomic hydrogen is adsorbed in fourfold-hollow sites with a Pd-H distance of 2.0 Å and a slightly higher binding energy of 51.1 kJ/mol [104, 106].

While hydrogen adsorbs at low coverages and/or high temperatures in a non-ordered fashion, ordered adsorbate structures are observed at rather high coverages and low temperatures [27, 104]. For Pd(111),  $(\sqrt{3} \times \sqrt{3})R30^\circ$  structures form at  $\theta = 0.33$  and at  $\theta = 0.66$ , while at  $\theta = 1.0$  a  $(1 \times 1)$  overlayer is observed between 50-250 K, always with H adsorbing in threefold-hollow sites [113–115]. On Pd(100), a  $c(2 \times 2)$  structure is observed at 130 K with a maximum ordering at a coverage of  $\theta = 0.5$  and a  $p(1 \times 1)$  structure at  $\theta = 1.0$  with H adsorbed in fourfold-hollow sites; at higher temperatures, a transition to a disordered phase is found [104, 106].

The desorption of surface adsorbed hydrogen follows a Langmuir-Hinshelwood mechanism exhibiting a second order behavior which indicates that the rate limiting step is the recombination of two hydrogen atoms [27, 104].

For high coverages, when surface sites become saturated, H can also diffuse to more weakly-binding sites beneath the Pd surface in the bulk (heat of dissolution is in the range of 10-20 kJ/mol) [54, 55]. Due to the weaker bonding, subsurface adsorbed hydrogen is suggested to be more reactive in hydrogenation reactions than strongly-bound surface hydrogen [57–59]. The diffusion into the bulk is usually an activated process [70, 76] with the height of the activation barrier depending on the diffusion site. Hydrogen diffusion into the subsurface was found to be significantly slower on (111)-facets than on other, more open Pd surfaces [70–75]. For small Pd particles, it is therefore expected that open sites, like edges and corners, are especially important for H diffusion into the subsurface region. Subsurface adsorbed hydrogen can diffuse further within the Pd bulk with a moderate activation energy of  $E_{diff} = 22.2$  kJ/mol [76, 77].

Unlike surface adsorbed hydrogen, desorption associated with subsurface adsorbed hydrogen was found to exhibit rather a first or zero than second order behavior for the Pd(111), Pd(100) and Pd(110) surfaces and the observed desorption temperatures were lower than those of surface adsorbed hydrogen [70, 71, 104]. This behavior may indicate that for the desorption of subsurface adsorbed hydrogen the rate limiting step is not the recombination of two hydrogen atoms.

At high hydrogen concentrations in the subsurface of Pd, an expansion of the Pd-Pd bond lengths was observed in LEED and XRD measurements with respect to the pristine system. This effect is reported for both bulk Pd crystals and small Pd particles [113, 116–118]. A change in the Pd-Pd distance is expected to influence also the bond strength of the surface adsorbed hydrogen residing in highly-coordinating hollow sites.

When large amounts of H are accommodated in the Pd bulk, a phase transition from dissolved hydrogen ( $\alpha$ - phase stable up to H:Pd  $\geq$  0.1) *via* a mixed  $\alpha, \beta$ -phase to a stable hydride phase at high H:Pd ratios ( $\beta$ -phase stable for H:Pd  $\geq$  0.6) is observed [70, 107]. While the  $\beta$ -phase might be important in alkene conversions under realistic conditions, a stable hydride phase is not formed under the conditions applied in this work. The exposures of H<sub>2</sub>(D<sub>2</sub>) are however large enough for the formation of weakly-bound subsurface absorbed H(D) ( $\alpha$ -phase).

### 2.2.3 Carbon on Pd

In the reaction of alkenes, always a variety of strongly-dehydrogenated carbonaceous deposits are formed on the catalyst which have been suggested to exhibit distinct influences on the activity and selectivity of the catalyst - ranging from harmful to beneficial [60, 119]. Therefore, it is important to differentiate between different C species [65]. On Pd, in principle three different kinds of strongly-dehydrogenated carbonaceous deposits can form: amorphous, graphitic and dissolved carbon that is absorbed in sites below the Pd surface. The formation of the different species depends strongly on the temperature and the amount of carbon present on the surface.

On Pd, amorphous carbon can be formed from the decomposition of C-containing molecules which leads for high C contents to blackening of the catalyst. Amorphous carbon is usually thought to deactivate the catalyst by blocking of active sites [61, 120]. The formation temperature typically depends on the decomposition temperatures of the carbon source, *e.g.* alkenes. At higher temperatures amorphous carbon can either diffuse to subsurface sites in Pd or undergo a transition to graphitic carbon.

Compared to other transition metals like Ni and Fe, Pd is significantly less active in the formation of graphitic carbon [65]. On Pd, graphitic carbon forms only at very high temperatures ( $\geq$  870 K) and at high C concentrations [121–123]. Under the reaction conditions applied in this work, the formation of graphitic carbon can be excluded.

Carbon can also diffuse to sites located below the Pd surface. Theoretical calculations even suggest that C absorbed in subsurface sites is energetically favored over adsorption on surface sites [123–125]. Diffusion to subsurface sites is an activated process that starts to occur at significant rates at temperatures  $\approx$  400 K [68, 69]. In theoretical calculations it was found that the C diffusion into the subsurface of Pd depends strongly on the diffusion site. While diffusion through (111)-facets was found to have an activation barrier

## 2 Theory

of 107 kJ/mol [126], significantly smaller barriers are calculated for C diffusion through more open edge or step sites [124, 127, 128]. For Pd particles, C diffusion into the subsurface is expected to occur thus preferentially on open edge and corner sites. Carbon can also diffuse within the Pd bulk with an overall diffusion barrier of  $E_{diff} = 117$  kJ/mol [68]. In calculations, it is predicted that C diffusion in the subsurface parallel to the surface is energetically favored compared to diffusion further into the bulk [128, 129]. In accordance with these calculations, it has been observed that C initially accumulates in layers parallel to the surface before this front of dissolved C migrates further into the bulk [62].

XRD and STM measurements as well as theoretical calculations indicated that dissolved carbon occupies interstitial sites and is situated in octahedral holes in the Pd lattice [129–132]. At high carbon contents an increase of the Pd lattice by  $\approx 2 - 3\%$  is observed in XRD measurements [60, 130, 131]. A maximum of 15 atom% of carbon can be accommodated in Pd [60, 61, 68, 121, 130, 131]. The  $\beta$ -PdC $_{\geq 0.13}$  phase is only metastable and decomposes at higher temperatures ( $\approx 600$  K) to Pd and carbon [121].

It has been found that formation of the  $\beta$ -phase with PdC $_{\geq 0.13}$  inhibits the formation of the hydride phase of Pd which is expected to have a strong impact on the reactivity of the catalyst in alkene conversions with hydrogen [58, 62–65]. Under the conditions applied in this work, the formation of a fully closed carbide phase can clearly be excluded. However, it is expected that some carbon will be dissolved in the subsurface of Pd particles after heating the alkene covered model catalyst to  $\approx 500$  K.

## 2.3 Experimental methods

In this section, the theoretical working principle together with the technical setup will be presented for the main experimental methods applied in this thesis. In the first part (2.3.1), the working principle of molecular beams, *i.e.* supersonic and effusive beam sources will be discussed. The second part (2.3.2) is concerned with the physical background and the technical setup of the detection methods, infrared-reflection-absorption spectroscopy (IRAS) and quadrupole mass spectrometry (QMS).

### 2.3.1 Molecular beams

A molecular beam (MB) is a directed, spatially well-defined, collision free flux of atoms or molecules that is produced by an expansion from a gas reservoir into a vacuum chamber which is then collimated by apertures to obtain a directed beam (see fig. 2.4). Choppers and shutters can be used to precisely modulate the molecular beam on short time scales.

Molecular beams are especially important for kinetic and dynamic studies due to their unique properties. Due to single collision conditions, it is possible to determine absolute reaction probabilities, *e.g.* measurements of the sticking probability [133, 134]. The

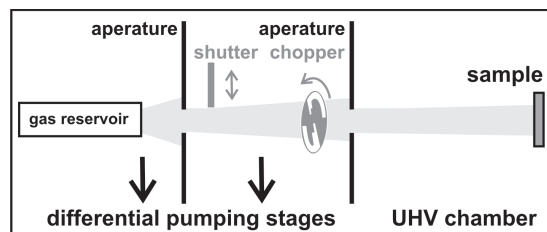


Figure 2.4: Schematical display of a molecular beam.

fast and precise modulation of molecular beams allows to study the transient kinetics of chemical reactions which can give further insights into the microscopic reaction mechanism of a reaction. Reactions with low-reaction probabilities can be quantitatively investigated because molecular beams allow for high local pressures on the sample, while the overall chamber pressure remains low and thus, background reactions are reduced. Moreover, the collision free environment enables the investigation of energy- and angle-resolved scattering and desorption processes from surfaces.

The dynamic properties of the molecules or atoms in the beam depend largely on the expansion conditions, *i.e.* the pressure and temperature in the gas reservoir and in the expansion stage. Basically, two different kinds of molecular beam sources are used which differ fundamentally in the expansion conditions that can be described by the dimensionless *Knudsen number* ( $Kn = \lambda/d$ ; with  $\lambda =$  mean free path of the molecules and  $d =$  diameter of the nozzle). In supersonic beams, a high pressure in the gas reservoir is applied resulting in a low *Knudsen number* ( $Kn \ll 1$ ). Due to the short mean free path of the molecules, collisions in the expansion govern the dynamic properties of the molecules in the molecular beam. In effusive beam sources operated at higher *Knudsen numbers*, a relatively low pressure in the gas reservoir ensures a collision free expansion, so that the dynamic properties of molecules in an effusive beam are mainly determined by the temperature and pressure in the gas reservoir. The working principle and technical setup of supersonic and effusive beam sources will be discussed briefly in the following sections. A more detailed description of molecular beam sources can be found in the literature (see *e.g.* [14]).

### Supersonic beams

A supersonic beam is formed by the expansion of a gas from a reservoir with a high pressure through a small nozzle into a vacuum chamber. The high pressure ( $p > 1$  bar) in the gas reservoir causes a small mean free path of the molecules, so that supersonic beams are operated at low *Knudsen numbers* ( $Kn \ll 1$ ).

The gas in the reservoir,  $M \ll 1$  (*Mach number*  $M = v/c$ , with  $v =$  gas velocity and  $c =$  sonic speed), is accelerated by the pressure drop in the nozzle to sonic speed  $M = 1$  and then further in the vacuum chamber to supersonic speed,  $M \gg 1$ . The different

## 2 Theory

flow zones of the supersonic expansion are schematically depicted in fig. 2.5. A skimmer extracts part of the expansion in the zone of silence. The resulting molecular beam is then further collimated by apertures.

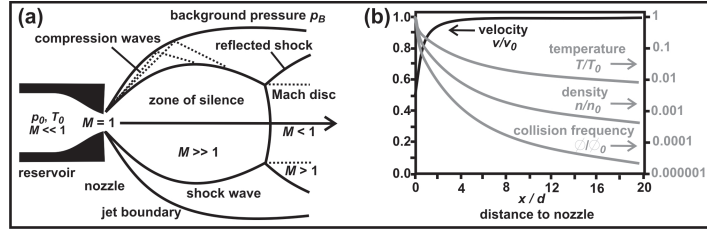


Figure 2.5: (a) Schematic display of the flow zones in a supersonic expansion; (b) profiles of the velocity, temperature, density and collision frequency along the center axis of the expansion.

Due to the small mean free path of the molecules, numerous collisions occur in the nozzle during the expansion. In these collisions, energy is transferred between the molecules resulting in a narrow energy distribution in the direction of the expansion with respect to the Maxwell-Boltzmann distribution expected for the nozzle temperature. This effect is most pronounced for the translational and rotational degrees of freedom. For vibrational modes this effect is smaller due to the larger difference in energy levels. The resulting velocity distribution for the flux  $I_{\parallel}$  can be described by a shifted Boltzmann distribution with  $T_{\parallel}$  characterizing the width of the distribution:

$$I_{\parallel} \propto v^2 \exp\left(-\frac{M(v - v_{\parallel})^2}{2kT_{\parallel}}\right) \quad (2.14)$$

with  $v_{\parallel}$  denoting the parallel flow velocity and  $M$  the molecular mass of the molecules or atoms in the beam.

The maximal parallel velocity of the molecules  $v_{\parallel,\infty}$  in the beam can be estimated assuming an ideal gas using the molecular mass  $M$  and the adiabatic exponent  $\gamma$ :

$$v_{\parallel,\infty} = \sqrt{\frac{2RT_0}{M} \frac{\gamma}{\gamma - 1}} \quad (2.15)$$

In principle, it is thus possible to adjust the velocity of the supersonic beam by heating or cooling the reservoir or experimentally more simple, the nozzle. The net effect is however rather small. For a variation of the velocity over a broad range, in practice supersonic beams are *seeded* with heavier or lighter molecules resulting in lower or higher velocities of the beam gas, respectively (see *e.g.* [14, 67]).

The main advantages of supersonic beams are the narrow energy distribution and the possibility of adjusting the kinetic energy which is of great interest in kinetic and especially dynamic measurements. A drawback of the method is however the relatively high experimental costs and a low control of the beam intensity.

### Effusive beams

In contrast to supersonic beams, effusive beam sources are operated at high Knudsen numbers. A relatively low pressure in the gas reservoir ( $p < 1$  mbar) is applied ensuring due to the low collision frequency that the energy distribution remains basically unchanged in the expansion. Therefore it is possible to describe the properties of effusive beam by the gas kinetic theory, *e.g.* the velocity distribution in an effusive beam is given by the Maxwell-Boltzmann distribution:

$$I \propto v^2 \exp\left(-\frac{Mv^2}{2kT_0}\right) \quad (2.16)$$

The simplest case of an effusive beam source is a simple thin walled orifice through which the gas expands to a vacuum chamber. The resulting intensity distribution is a cosine distribution. Therefore additional apertures are required to form a *directed* beam flux. Due to the low directionality of the expansion, a large part of the molecules do not contribute to the beam causing low intensities and requiring high pumping speeds. Using a tube rather than a 1-dimensional nozzle opening improves the directionality of the beam. The collimation by a tube or a capillary is determined by the length to radius ratio. It is usually described by the dimensionless *peaking factor*  $\kappa$  which is defined as the flux in the expansion direction relative to the flux for a simple cosine distribution at an identical overall flux. For long enough tubes it can be written:

$$\kappa = \frac{\pi}{N_0} I(0) = \frac{3L}{8r} \quad (2.17)$$

With typical length to radius ratios of  $L/r = 40$  enhancements of 15 can be achieved, while a supersonic beam source displays enhancements of less than 2. By minimizing the flux of molecules into unwanted directions, also the requirement on the pumping power in the differential pumping stages are strongly reduced compared to supersonic beams.

However, while a small diameter to length ratio of the tubes enhances the directionality of the beam, it also reduces the maximum flux. In order to achieve a highly directed flux combined with high beam intensities, glass capillary arrays can be used. Here the capillaries ensure on one hand that the beam is directed and on the other hand, a multitude of capillaries allow for a high overall flux. A schematical display of an effusive beam source using a glass capillary array is depicted in fig. 2.6. The flux of effusive beam sources can be varied by several orders of magnitude simply by changing the pressure in the gas reservoir. The maximum flux of effusive beam sources is usually determined by the free mean path of the molecules. When the pressure in the gas reservoir is too high and the mean free path decreases, collisions inside the glass capillaries inhibit a further

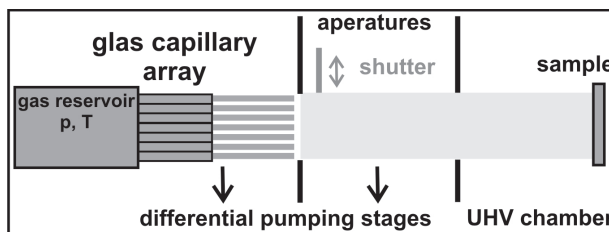


Figure 2.6: Schematical display of an effusive beam source.

increase of the flux.

The main advantages of effusive beam sources are the high maximum flux requiring only moderate pumping speeds, the easily adjustable flux (by several orders of magnitude), and the low backing pressures which allow to use chemicals with low vapor pressures and which also reduce the consumption of gas, in particular important when using expensive reactants like isotopically labeled molecules.

### 2.3.2 Detection methods

In this part, the working principle and the technical setup of the most important detection methods applied in this work, *i.e.* surface sensitive IR spectroscopy and quadrupole mass spectrometry, will be shortly presented. A more detailed introduction can be found in the literature (mass spectrometry: [135–137]; IRAS [138–141]).

#### Mass spectrometry

In this work, quadrupole mass spectrometry has been used for the detection of gas phase products of chemical surface reactions. Quadrupole mass spectrometry is a widely used detection technique in vacuum setups. Gas is ionized, selected according to the mass  $m$  to charge  $z$  ratio ( $m/z$ ) and subsequently quantitatively detected. A quadrupole mass spectrometer (QMS) consists of an ion source, a quadrupole mass filter and a detector, as schematically depicted in fig. 2.7.

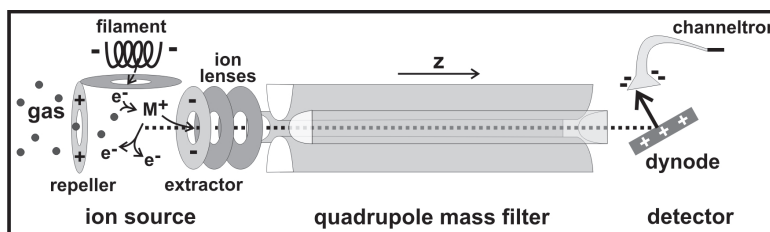


Figure 2.7: Schematical display of a quadrupole mass spectrometer including an electron impact ion source, the quadrupole mass filter and a channeltron detector.



For an effective mass selection process, it is important that the ions pass the mass filter collision free. Therefore, the use of QMS requires low pressures ( $< 10^{-4}$  mbar).

In the following sections, the individual components of the QMS and their working principle will be described in more detail.

### Ion source

Neutral gas phase molecules can be ionized by various means, however, a very common method, also applied in this work, is the ionization by electron impact (EI). For this, electrons  $e^-$  emitted from a cathode are accelerated onto the neutral molecules with energies ranging typically from 10-100 eV. Part of the kinetic energy can be transferred from the electron  $e^-$  to the molecule  $M$  which is thereby ionized:



If the transferred energy is large enough, the molecule can undergo further transformations. Typically an excess energy leads to fragmentation of the molecule:



At the usually applied acceleration voltage of 70 eV, these fragmentation reactions happen frequently and are especially important for larger molecules, *e.g.* 2-butene and isophorone that were used in this work. For these molecules, the highest intensity is observed on fragment peaks which are therefore used to follow the temporal evolution of these molecules to obtain a better signal to noise ratio. For larger, relatively similar molecules that exhibit a number of common fragments, like isophorone and its hydrogenation products, it is essential for an unambiguous assignment of the signal to monitor also the parent ion, *i.e.* the unfragmented ionized molecule.

Especially when working at high pressures, next to fragmentation reactions also recombination reactions can occur and need to be accounted for:



### Quadrupole mass filter

A linear quadrupole mass filter consists of four cylindrical or hyperbolic electrodes which are positioned parallel to each other (see fig. 2.8). Ions generated in the ion source fly parallel to the electrodes through the quadrupole mass filter where they are separated by mass  $m$  to charge  $z$  ( $m/z$ ) ratio. Opposing electrodes are on the same potential, while on neighboring electrodes a potential consisting of a direct voltage  $U$  and a high-frequency alternating component  $V$  of a radio frequency  $\omega$  is applied:

$$U(t) = U + V \cos(\omega t) \quad (2.21)$$

## 2 Theory

The resulting oscillating motion of the ions can be described by differential, so-called *Mathieu* equations (see [135] for details):

$$\frac{d^2x}{dt^2} + \frac{e}{m_i r_0^2} (U + V \cos \omega t) x = 0 \quad ; \quad \frac{d^2y}{dt^2} - \frac{e}{m_i r_0^2} (U + V \cos \omega t) y = 0 \quad (2.22)$$

The ions move in an oscillating motion through the quadrupole mass filter. For a given parameter set  $U$ ,  $V$ ,  $\omega$ , only ions with a fitting  $m/z$  ratio pass the filter on a stable trajectory in the  $z$ -direction parallel to the electrodes. All other ions on unstable trajectories leave the mass filter and are thus, not detected. During this mass selection, the ions are not accelerated or decelerated along the  $z$ -direction.

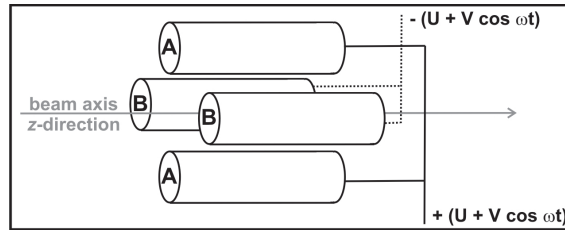


Figure 2.8: Schematical display of a quadrupole mass filter.

### Detector

For the detection of ions different detectors may be used. In our setup, a channeltron electron multiplier (CEM) is applied as detector. CEM detectors are very commonly used today due to their high temporal resolution and high signal to noise ratio. However, CEM detectors require very high vacuum conditions ( $< 10^{-6}$  mbar) because of possible spark overs.

CEM detectors consist of a small tube, typically made out of glass which is coated with a highly resistive material that emits electrons. Along the tube, a potential of  $\approx 1 - 3$  kV is applied. The positively charged cations are accelerated to the negatively charged entrance of the CEM where their impact onto the surface leads to the emission of electrons. These are attracted by the anode on the other side of the CEM. On their way, they create an avalanche of secondary electrons. In this way, amplification factors of up to  $10^8$  can be achieved.

When working at high fluxes, it is important to realize that the detected signal increases with flux only up to a certain threshold. When too many ions simultaneously arrive on the detector, the resulting electron flux will not increase linearly. This can be circumvented by *e.g.* reduction of the acceleration voltage. However, when signals of very high and very low intensities should be quantitatively detected simultaneously, this approach is not advantageous. In this case, one possibility is to follow the high intensity

signal not on the maximum of the mass signal, but rather on a flank.

### Infrared-reflection-absorption spectroscopy

Time resolved infrared-reflection-absorption spectroscopy (TR-IRAS) is a very valuable technique for detection of surface adsorbates [103, 138–144]. Molecular vibrations are excited by the absorption of infrared light. It is not only possible to chemically identify molecules by the absorption frequency but also to gain information on the interaction of the molecules with the surface. The absorption frequencies of some molecules, *e.g.* CO, are very sensitive to the morphology of the surface and the adsorption site. Therefore, CO adsorption can be used to characterize the morphology of the surface (see also 2.2.1). Next to adsorbed molecules, it is also possible to study lattice vibrations, phonons, using IRAS.

A typical IRAS setup is shown in fig. 2.9. IR light is directed by a set of mirrors onto a highly reflecting surface at a grazing incidence where it is partially absorbed and the remainder is reflected onto another mirror which directs the IR light onto the detector. A high reflectivity of the surface is required for a good signal intensity.

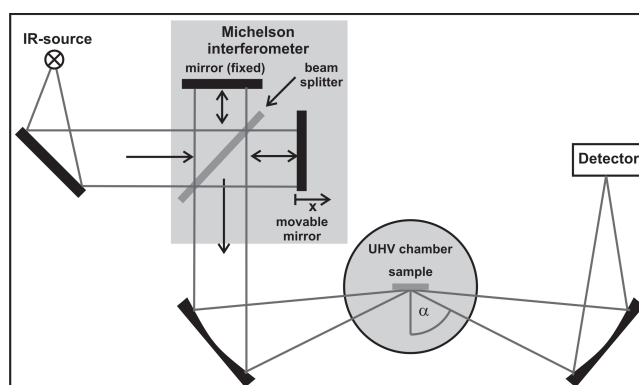


Figure 2.9: Schematical display of the IRAS setup including the Michelson interferometer.

In the beginning of IR spectroscopy, dispersive spectrometers were used to determine the absorption of IR light as a function of the wavelength. In these setups, the sample is exposed to monochromatic light and the absorption is measured for each individual wavelength separately. Instead of dispersive spectrometers, usually Fourier-transform (FT) spectrometers with a Michelson interferometer are used when studying adsorbates on surfaces. Compared to dispersive spectrometers, FT spectrometers exhibit fast acquisition times allowing for a good signal to noise ratio within a reasonable time even for small signals as expected for a small number of molecules adsorbed on a surface. In FT-IR setups, the sample is not exposed to monochromatic, but to light from broad spectral region which allows to significantly reduce the acquisition time. To determine

## 2 Theory

the IR absorption as a function of the wavelength despite the use of polychromatic light, a Michelson interferometer is used. The beam path within the Michelson interferometer is schematically depicted in fig. 2.9. One part of the IR light is directed by a beam splitter onto a stationary mirror, while the second part is reflected off a moving mirror. When the two beams are subsequently overlapped, constructive or destructive interference is observed for different wavelengths as a function of the path difference. The detector collects the overall beam intensity  $I(x)$  as a function of the displacement  $x$  of the movable mirror, the so-called interferogram  $I(x)$  from which the single channel spectrum can be calculated by Fourier transformation. The single channel spectrum is however strongly dominated by the characteristics of the optical setup. To eliminate these contributions, typically the sample spectrum is divided by a reference spectrum, which is obtained in the same setup, but in the absence of the adsorbates.

The excitation of molecular vibrations by electromagnetic radiation can be described by the time-dependent perturbation theory. For wavelengths  $\lambda$  that are much bigger than the dimensions of the excited vibration, which is always true for IR light, the electric field induced by the electromagnetic radiation can be described by the dipole approximation, so that the perturbation operator can be expressed as:

$$H^{(1)} = -\vec{\mu} \cdot \vec{E} \quad (2.23)$$

with  $\vec{\mu}$  the electric dipole moment of the molecule and  $\vec{E}$  the electric field vector of the electromagnetic radiation. Using Fermi's Golden Rule, the transition probability is given by:

$$W \propto \left| \langle \psi_f | \vec{\mu} \cdot \vec{E} | \psi_i \rangle \right| \quad (2.24)$$

with  $\psi_f$  and  $\psi_i$  being the eigenfunctions of the vibration in the excited and in the ground state [145]. Thus, only vibrations where the dynamic dipole moment ( $\partial\vec{\mu}/\partial Q_k$ ) changes along the normal coordinate  $Q_k$  of the vibration get excited (see *e.g.* [145, 146] for further details).

For molecules adsorbed on metal surfaces additional selection rules apply. The interaction with the surface also has to be taken into account. The most important aspect is that on surfaces only vibrational modes can be detected that have a dipole moment with a component perpendicular to the surface. The part of the IR light with a polarization parallel to the surface (*s*-polarisation) is reflected with a phase shift of  $180^\circ$  leading to a vanishing of the electric field parallel to the surface. Moreover, surface adsorbed molecules induce a mirror charge in the metal surface. For dipole moments parallel to the surface the induced mirror charge simply compensates the dipole of the molecule [97, 138]. Thus, only vibrations with a dipole component perpendicular to the surface can be detected (metal surface selection rule, MSSR):

$$\frac{\partial\mu_\perp}{\partial Q_k} \neq 0 \quad (2.25)$$

Taking this additional selection rule into account, IRAS measurements of adsorbates can give valuable information on the adsorption geometry of adsorbates. The absence or reduction in intensity of certain vibrational modes compared to the gas phase spectrum can be an indication that the corresponding bonds are oriented parallel to the surface.

Working with  $p$ -polarized light enhances the surface selectivity, because possible additional gas phase absorptions from the  $s$ -polarized light component are suppressed. The phase shift of the  $p$ -polarized light and thus, the resulting electrical field on the surface as well as the reflectivity are strongly dependent on the incidence angle. It has been demonstrated that a maximal absorption can be achieved with an incidence angle of  $83^\circ$  (see [138] and references therein).

The vibrational frequencies and intensities of adsorbed molecules can be significantly changed from those in the gas phase due to the interactions with the surface. The most important aspects on how adsorption influences the vibrational frequencies and intensities are summarized in the following paragraphs (see [103, 138, 139] for further details).

*Frequency shifts:* The binding of a molecule to a rigid surface causes a shift of the vibrational modes to higher frequencies (blue shift) which can be rationalized based on mechanical considerations with a model of vibrating masses and oscillators. Additionally, the dynamic dipole moment of the adsorbate induces an image charge in the substrate which in turn changes the local electrical field of the adsorbate. This effect leads to a shift to lower frequencies (red shift). The frequency of a vibration is also influenced by the changes in the electronic structure of the adsorbed molecule due to charge transfer with the surface. Depending on the exact nature of the interaction, the frequencies can be shifted to higher or lower wavenumbers. A further reason for frequency shifts are interactions with other adsorbates which become especially important at higher coverages. The molecular vibrations of neighboring dipoles can either interact directly due to the local electric field of the vibrations or through the electrons of the substrate resulting in both cases in a shift to higher frequencies [147, 148]. This effect is known as *dipole coupling effect*. Neighboring adsorbates can also alter the electronic structure of the surface and therefore change the interaction and charge transfer with an adsorbed molecule compared to the adsorbate free surface. The frequency shift depends on the exact nature of the changes.

*Intensity changes:* Due to the metal surface selection rule (MSSR), the adsorption geometry of the adsorbate on a metallic surface is particularly important for the observed intensities. The intensity critically depends on the magnitude of the dipole moment perpendicular to the surface. At higher coverages, also dipole interactions within the adsorbate phase leading to depolarisation can cause a strongly non-linear behavior of the absorption intensities at high coverages. Upon increasing coverage, the intensity either does not increase further or even decreases due to this effect. For adsorbate phases consisting of two species with similar absorption frequencies in spatial proximity, a part of the intensity of the low-frequency absorption can be transferred to the high-frequency

## 2 Theory

species due to dipole coupling [103]. Due to this effect, denoted as *intensity borrowing*, minority species often appear in IRAS with unusually high intensities.

All these effects make the interpretation and especially a quantitative analysis of IRAS measurements more difficult. However, as mentioned before, the absence and presence of certain phenomena provides valuable information on the interaction between the molecules and the surface as well as on the interaction between adsorbed molecules.

### 3 Experimental setup

All experiments described in this thesis were conducted in an ultra-high vacuum (UHV) setup which allows to study the kinetics of chemical reactions on model catalysts under well-defined conditions. A scheme of the apparatus is displayed in fig. 3.1. The setup was built before and has been described in detail previously [30, 149].

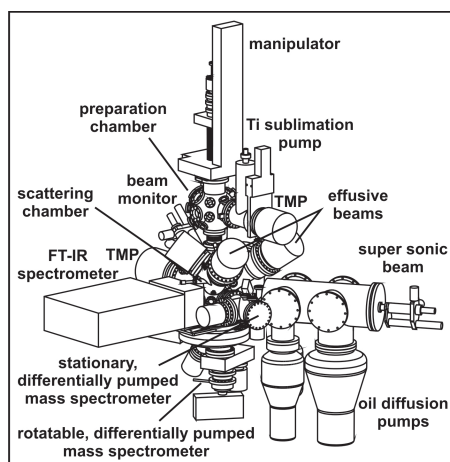


Figure 3.1: Scheme of the molecular beam setup (adapted from [30]).

The experimental setup consists of two chambers, the preparation chamber and the scattering chamber. Both chambers are operated at a base pressure of  $\approx 1 \cdot 10^{-10}$  mbar and are connected by a gate valve. The sample can be transferred on a manipulator from one chamber to the other remaining at all times under *clean* UHV conditions.

In the preparation chamber, the sample can be cleaned by fast ion bombardment (*sputtering*), oxidation and by heating to high temperatures (*annealing*). Subsequently, it can be further prepared by physical vapor deposition and oxidation. Techniques like low-energy electron diffraction (LEED), Auger electron spectroscopy (AES) and temperature programmed desorption/reaction (TPD/TPR) using a quadrupole mass spectrometer (QMS) shielded by a Feulner cup allow for the characterization of the prepared samples.

In the scattering chamber, kinetic measurements of chemical reactions are conducted on the model catalyst as prepared in the preparation chamber. The reactants are dosed onto the catalytic surface using molecular beams providing a well-defined flux which can

### 3 Experimental setup

be precisely modulated to study the transient kinetic behavior of chemical reactions. The kinetics of the reactions can be followed by both time-resolved infrared-reflection-absorption-spectroscopy (TR-IRAS) detecting species adsorbed on the catalytic surface and by time-resolved mass spectrometry (TR-MS) monitoring the evolution of gas phase products.

The chapter is divided into two sections. In the first section (3.1), the preparation chamber together with the sample holder is described and in the second section (3.2), the scattering chamber including the molecular beams, the stationary quadrupole mass spectrometer and the FT-IR setup is presented.

## 3.1 Preparation chamber and sample holder

The preparation chamber is equipped for the preparation of thin metal oxide films and small metal particles by physical vapor deposition and oxidation in oxygen under well-defined ultra-high vacuum conditions. The base pressure of the chamber is maintained at  $\approx 1 \cdot 10^{-10}$  mbar using a turbo-molecular pump (TMP, Pfeiffer, TMU500MC, 500 L/s) and a titanium sublimation pump (Pfeiffer).

For sample cleaning, an ion gun for fast ion bombardment (*sputtering*, Omicron ISE10) is available. Two electron beam evaporators (Omicron Focus EFM3) are available for the deposition of metals, in this study iron (Fe) and palladium (Pd). A quartz microbalance (Caburn MDC, controller: Intellemetrics IL 150) is used to calibrate the metal deposition rate of the electron beam evaporators.

For the characterization of samples, a low-energy electron diffraction (LEED) and Auger electron spectroscopy (AES) combination (Omicron, ErLEED 150) is available. Furthermore, a shielded mass spectrometer (MS, HIDEN Analytical RC PIC) can be used for TPR (temperature programmed reaction) measurements.

### 3.1.1 Sample holder

A picture of the sample holder is shown in fig. 3.2. In this work, a rectangular Pt(111) or Pd(111) single crystal ( $10 \times 11$ mm) were used as samples. The metal single crystal is mounted on a tantalum foil by spot welding. In order to move the sample between and inside the chambers, the tantalum foil is connected by sapphire plates to the metal rod manipulator (Vacuum Generators, Omniax MX800), which can be rotated and translated in three directions.

A reservoir for liquid nitrogen inside the manipulator can be used for cooling of the sample down to 110 K. The connection of the tantalum foil with the manipulator rod by sapphire plates ensures a good thermal conductivity, while the sample remains electrically isolated. Connected to the back of the sample holder, a heating plate (boron



nitride, Advanced Ceramics Corp., Boralectrics HT-01) allows for very stable, precise and spatially homogeneous heating of the sample up to 1300 K. A thermocouple (Ni/CrNi, Type K) spot-welded to the side of the sample is used for accurate measurement of the sample temperature. An electrical connection to the sample holder is made to ground the sample (*e.g.* during LEED and AES measurements) or to apply high voltage (*e.g.* during physical vapor deposition to avoid sputtering damage).

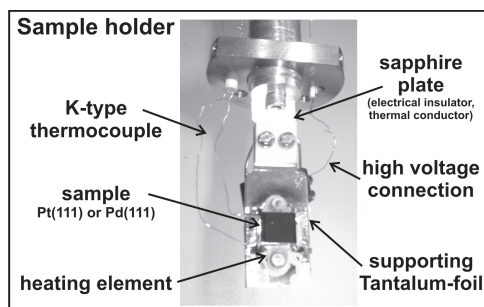


Figure 3.2: Setup of the sample holder.

### 3.2 Scattering chamber

The scattering chamber is equipped for kinetic measurements of chemical reactions on model catalysts under well-defined UHV conditions. The chamber including three molecular beams, two QMS, one stationary and one rotatable, and the IRAS setup, is schematically depicted in fig. 3.3 and fig. 3.4.

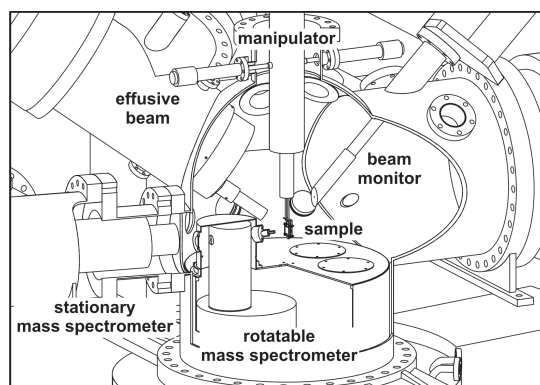


Figure 3.3: Schematic display of the scattering chamber (from [30]).

The base pressure of  $\approx 1 \cdot 10^{-10}$  mbar is maintained by a turbomolecular pump (TMP, Pfeiffer TMU1600MC) providing a high pumping speed (1380 L/s). The high pumping capacity is required during the kinetic measurements where high pressures are applied

### 3 Experimental setup

onto the sample surface. On one hand, fast pumping ensures that the overall chamber pressure remains up to a factor of 100 lower than the local pressure on the sample surface which minimizes background reactions and thus, allows to study also reactions with low reaction probabilities. On the other hand, high pumping speeds are necessary for studying reactions in a time-resolved mode. The temporal resolution depends on the changes of the reactants and products in the gas phase which is strongly limited by the pumping capacity. In this setup, a temporal resolution of  $\approx 50$  ms can be achieved.

For the supply of reactants, three molecular beams, one supersonic beam and two effusive beams, are available which can be simultaneously crossed on the sample surface. By using molecular beams, well-controlled, stable fluxes can be realized that can be precisely modulated. The use of molecular beams further allows for high local pressures on the sample at an overall low chamber pressure. The beam intensities can be measured by a beam monitor consisting of a high-precision ion gauge housed in a movable gold-coated tube with a 1 mm small orifice.

For the *in-situ* detection of species adsorbed on the sample surface, the scattering chamber is equipped with a FT-IR setup working at grazing incidence that allows for time-resolved measurements. Gas phase species can be monitored by two mass spectrometers (MS), one stationary for the integral evolution of products in the chamber and a rotatable MS for angular-resolved measurements detecting just a small angular contribution (acceptance angle  $\approx 7^\circ$ ).

A schematic display of the scattering geometry in the chamber is given in fig. 3.4 and summarized in table 3.1.

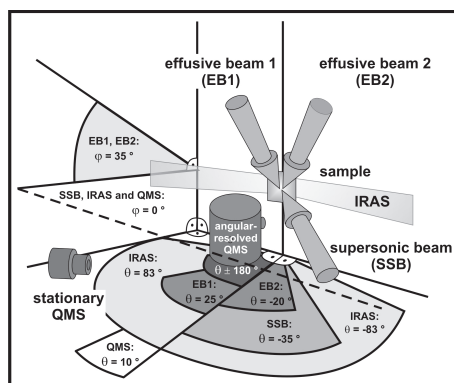


Figure 3.4: Scheme of the scattering geometry in the experimental chamber (adapted from [30] and [150]).

In the following sections, the different parts of the scattering chamber used in this work will be described in more detail, *i.e.* the molecular beams, the FT-IR setup and the stationary mass spectrometer.

Table 3.1: Geometry of molecular beams and detection methods relative to the sample in the scattering chamber.

Component	$\theta$	$\varphi$	resulting incidence angle
effusive beam 1	$25^\circ$	$35^\circ$	$42.1^\circ$
effusive beam 2	$-20^\circ$	$35^\circ$	$39.7^\circ$
supersonic beam	$-35^\circ$	$0^\circ$	$35^\circ$
stationary QMS	$-10^\circ$	$0^\circ$	
rotatable QMS	$\pm 180^\circ$	$0^\circ$	
FT-IR spectrometer	$-83^\circ/83^\circ$	$0^\circ$	

### 3.2.1 Supersonic beam

The supersonic beam consists of an expansion chamber pumped by an oil diffusion pump (Edwards Diffstak, 250/2000, 2000 L/s) and two differential pumping stages evacuated by an oil diffusion (Edwards Diffstak CR 160/700, 700 L/s) and a turbomolecular pump (Pfeiffer, 50 L/s). A scheme of the supersonic beam is displayed in fig. 3.5. From the supersonic expansion through a magnetic nozzle (100  $\mu\text{m}$ ), a small part is extracted by a 0.7 mm skimmer situated between the expansion chamber and the first differential pumping stage. In the differential pumping stages, the molecular beam is further collimated by apertures. Beside the magnetic nozzle in the expansion stage, the flux onto the sample can be controlled on short time scales ( $t < 1$  ms) manually or automatically by a shutter and a chopper, both situated in the first differential pumping stage. The beam size can be regulated by apertures positioned in the first differential pumping stage such that the beam size is either smaller, bigger or the same sizes as the sample (7.6, 11.0 or 14.3 mm).

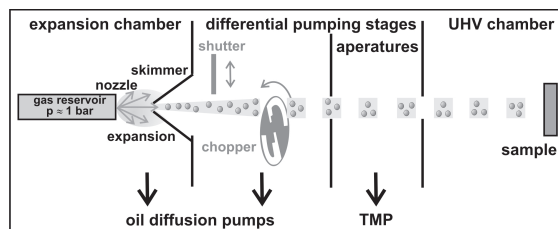


Figure 3.5: Schematic display of the supersonic beam setup.

The flux of the beam depends mainly on the gas and can only be further regulated using the chopper which allows for a reduction of the beam intensity to 50%, 3.3% and 1.6% of the original, unattenuated flux. The flux for 2-butene is typically  $1.7 \cdot 10^{14}$  molecules $\cdot\text{cm}^{-2}\cdot\text{s}^{-1}$  ( $8.2 \cdot 10^{-7}$  mbar) on the sample surface. During all experiments, this flux was reduced using the chopper. Typically the 3.3% setting was applied resulting in a flux of  $5.6 \cdot 10^{12}$  molecules $\cdot\text{cm}^{-2}\cdot\text{s}^{-1}$  ( $2.7 \cdot 10^{-8}$  mbar). In order to avoid possible reactions of 2-butene on the sample holder, the beam diameter was in all

### 3 Experimental setup

experiments chosen to be smaller than the sample using the smallest aperture.

A typical beam profile of the supersonic beam using Argon, a non-sticking gas, and the smallest aperture, as used in the experiments, is shown in fig. 3.6. It can be seen that the beam is smaller than the sample and that the pressure is very evenly distributed over the sample before it sharply decreases toward the beam edges. Under these conditions, the pressure on the sample is at  $\approx 4.5 \cdot 10^{-6}$  mbar, while the background pressure of the scattering chamber only amounts to  $3.0 \cdot 10^{-8}$  mbar.

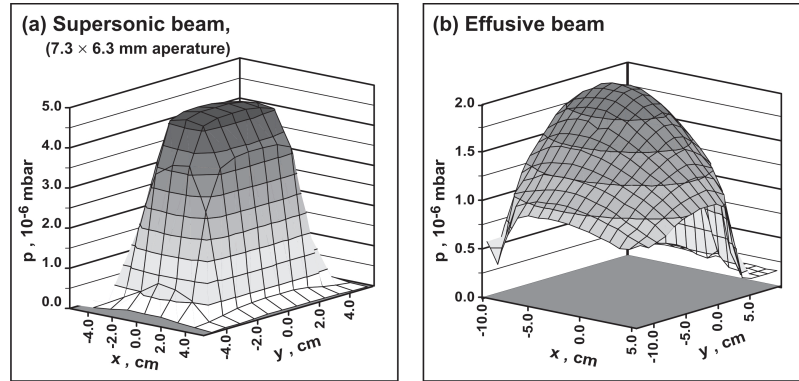


Figure 3.6: The beam profiles of (a) the supersonic beam ( $7.6 \times 6.3$  mm aperture) and (b) the effusive beam (adapted from [84]).

#### 3.2.2 Effusive beams

The experimental setup has two independent effusive beam sources. A scheme of the effusive beams is displayed in fig. 3.7. Both beams are doubly differentially pumped by two turbo molecular pumps (TMU520U, Pfeiffer). The flux of each beam can be regulated with a pneumatic valve and a shutter, manually or automatically controlled, both positioned in the differential pumping stages. The size of the beam diameter can not be changed as for the supersonic beam. It exceeds the size of the sample (see fig. 3.6).

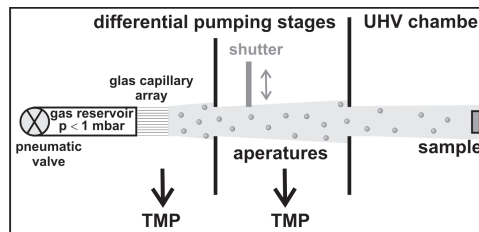


Figure 3.7: Schematic display of the effusive beam setup.

Contrary to the supersonic beam, the beam intensity of the effusive sources can be continuously adjusted by approx. two orders of magnitude. As can be seen in fig. 3.8, the beam flux on the sample increases linearly with increasing backing pressure. Strong deviations from a linear behavior are observed only for backing pressures  $\geq 3 \cdot 10^{-1}$  mbar. The flux onto the sample does not increase further and even decreases for higher backing pressures. The glass capillaries of the multi channel plate (MCP) have a diameter of  $50 \mu\text{m}$  and a length of 1 mm. At high backing pressures, the mean free path of the molecules decreases and collisions inside the capillaries inhibit a further increase of the flux.

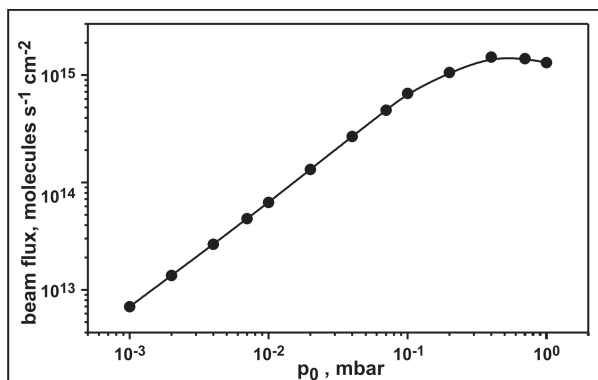


Figure 3.8: Beam intensity (Argon) of the effusive beam as a function of the backing pressure (from [30]).

### 3.2.3 Stationary mass spectrometer

The stationary quadrupole mass spectrometer (ABB Extrel) for the integral detection of gas phase products in kinetic measurements is positioned in plane with the supersonic beam. During the experiments, the rotatable QMS can be positioned between sample and stationary QMS to ensure a correct ratio of reactant to product signals and to avoid artificially high reactant signals due to direct scattering from the sample surface.

In the stationary QMS, molecules are ionized in the ion source by electron impact ionization. These ions are then mass selected in a quadrupole mass filter with a high transmission and subsequently detected by a channeltron detector in single ion counting mode.

The controller of the stationary MS provides several transistor-transistor-logic (TTL) as well as analog ports which are used for the automatic control of the experiments.

### 3 Experimental setup

#### 3.2.4 FT-IR setup

For the IRAS measurements to detect surface adsorbed species, a commercial high-resolution FT-IR spectrometer (Bruker IFS 66 v/s) with slight modifications was used. In this system, the IR source, a hot SiC rod ("Globar"), together with the Michelson interferometer is housed in a separate vacuum system from the at liquid N<sub>2</sub> temperature working MCT-IR-detector (mercury-cadmium-telluride, HgCdTe). The *p*-polarized IR light enters the scattering chamber through a KBr window and is reflected on the sample at grazing incidence (83°) toward the detector, which it enters through a second KBr window on the other side of the chamber. The IR light illuminates a rectangle of 6 × 8 mm on the sample. The resolution of the IR-spectra usually was 2 cm<sup>-1</sup> and for one spectrum 256 interferograms were averaged (160 ms per interferogram). Due to the short accumulation time per interferogram (160 ms), the FT-IR spectrometer can also be used in a time-resolved mode.

### 3.3 Time control of the pulsed molecular beam experiments

For an exact temporal control and a high reproducibility of the kinetic experiments, all relevant parameters of the experiment can be controlled by a computer. In this work most important is the automatic control of the temporal modulation of the molecular beams, but also the flux of the beams, the temperature of the sample as well as the mass spectrometer and the IR-setup can be automatically controlled. Automation of the experiments allows for a fast and exact modulation of the molecular beam flux which is especially important in kinetic experiments, where both the *steady state* and the *transient* behavior of the reaction rates are followed. It ensures a high reproducibility and thus enables signal averaging as well as a direct comparison of different measurements in one series.

The isothermal pulsed experiments consist of a complex pulse sequence with opening times of the beams in the second-range. The signals to control the shutters and valves of the molecular beams are provided by the control unit of the stationary mass spectrometer (ABB Extrel, Merlin QMS Series 5500 controller). Up to 8 TTL in- and 8 TTL out-puts, 6 analog in- (1 × ±1V, 5 × ±10V, 12 bit) and 5 analog out-puts (5 × ±10V, 1 × 0 – 10V, 12 bit) together with up to 6 internal clocks can be used for the automatic control.

The controller of the stationary mass spectrometer can be programmed by macros written in Extrel PAW. This programming language allows to start and stop measurements, control the in- and out-puts as well as internal clocks and to react on input data, *e.g.* the sample temperature. For all isothermal pulsed molecular beam experiments, according macros were written for the pulse sequence and used to control the beam fluxes.

## 4 Pd/Fe<sub>3</sub>O<sub>4</sub> model catalyst

In this chapter, the structure and morphology of the Pd/Fe<sub>3</sub>O<sub>4</sub>/Pt(111) model catalyst are discussed. Model catalysts exhibit compared to real catalysts a well-defined structure and a reduced complexity. The structure and morphology of these model systems can be investigated in detail using surface science techniques. Their use in combination with reactivity studies enables then a better microscopic understanding of the relation between the structure and the reactivity of the catalyst.

For the last decades, metal single crystals with highly polished surfaces have been successfully used as model catalysts [9]. Reactivity studies on metal single crystals can give valuable information on the reactivity of differently oriented surfaces which are often found as large facets on particles. In this work, a Pd(111) single crystal was used to investigate the adsorption properties and the intrinsic reactivity of large (111)-facets.

In real catalysts however, small metal particles reside on a support, often a metal oxide. Metal single crystals as a model system cannot mimic the interaction of the metal particles and the support nor the interaction of different adsorption sites on one particle (see also chapter 2.1). Application of model catalysts based on thin metal oxide films allows to overcome these limitations. In recent years, a variety of methods for the preparation of well-defined model catalyst surfaces have been developed [11, 12, 18–22]. For the preparation of such a model catalyst, a well-defined thin metal oxide film is grown onto a metal single crystal. On the oxide film, metal particles are subsequently deposited as the *active* phase. The preparation of such a model catalyst is schematically displayed in fig. 4.1. The metal single crystal as a substrate ensures a macroscopically planar structure as well as good electrical and thermal conductivity allowing thereby for the use of a variety of surface science techniques.

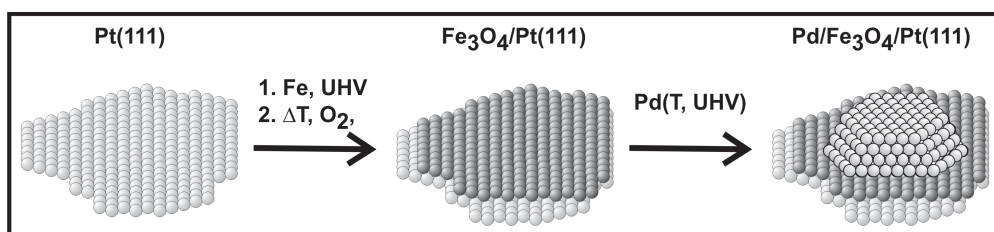


Figure 4.1: Preparation of the Pd/Fe<sub>3</sub>O<sub>4</sub>/Pt(111) model catalyst schematically displayed.

Table 4.1: Cleaning of Pt(111) substrate and preparation of Fe<sub>3</sub>O<sub>4</sub> thin film.

Pt(111) cleaning	repeated cycles of		
sputtering	for 30 min	in Ar ( $p = 1 \cdot 10^{-6}$ mbar)	at $\approx 300$ K
oxidation	for 3 min	in O <sub>2</sub> ( $p = 1 \cdot 10^{-6}$ mbar)	at 1000 K
annealing	for 3 min	in UHV	at 1270 K
Fe <sub>3</sub> O <sub>4</sub> preparation	6 cycles of		
Fe deposition	$\approx 4$ ML	in UHV	at 115 K
oxidation	for 5 min	in O <sub>2</sub> ( $p = 1 \cdot 10^{-6}$ mbar)	at 875 K

In this work, a thin Fe<sub>3</sub>O<sub>4</sub> film ( $\approx 100$  Å thick) grown on a Pt(111) single crystal substrate was used as support. It has been shown that the relatively thick Fe<sub>3</sub>O<sub>4</sub> film exhibits a good thermal and chemical stability [84]. This is a prerequisite to use the same Fe<sub>3</sub>O<sub>4</sub> preparation in several kinetic experiments which is desirable for a better reproducibility and comparability of the experiments. In the first section of this chapter (4.1), the preparation and structure of the Fe<sub>3</sub>O<sub>4</sub> film will be discussed. On the iron oxide film, small Pd particles are subsequently deposited as the active phase of the catalyst. After stabilization involving several oxidation-reduction cycles, the Pd particles supported on Fe<sub>3</sub>O<sub>4</sub>/Pt(111) can be cleaned after an experiment from carbonaceous deposits by oxidative treatment and used for further kinetic experiments. The growth, structure and morphology of the stabilized Pd particles supported on Fe<sub>3</sub>O<sub>4</sub>/Pt(111) are described in the second section (4.2).

## 4.1 Fe<sub>3</sub>O<sub>4</sub> film on Pt(111)

The preparation and growth of iron oxide thin films on a Pt(111) substrate have been described and discussed in detail in the literature [151–163]. Initially, a clean, well-ordered and flat Pt(111) surface is prepared by repeated cycles of Ar sputtering, oxidation and annealing. Iron is deposited in vacuum on the clean Pt(111) surface ( $\approx 4$  monolayers (ML) at 125 K) and subsequently oxidized in O<sub>2</sub> ( $p = 1 \cdot 10^{-6}$  mbar at 875 K). This procedure is repeated six times to obtain a  $\approx 100$  Å thick film (see also table 4.1).

On the Pt(111) substrate initially a thin FeO film grows. When the FeO film reaches a thickness of one monolayer, large flat 3-dimensional islands of Fe<sub>3</sub>O<sub>4</sub> start to grow. With increasing coverage, the Fe<sub>3</sub>O<sub>4</sub> islands increase in size and coalesce to form a closed, flat Fe<sub>3</sub>O<sub>4</sub> surface. The sharpness of the spots in the LEED diffraction pattern shows that the film has a well-ordered long-range structure (see fig. 4.2 (a)). The STM picture in fig. 4.2 (b) displays extended ( $\approx 50$  nm), atomically flat terraces which are separated by steps of 5 Å or a multiple in height.

The Fe<sub>3</sub>O<sub>4</sub> film has been previously characterized in detail using PES (photoelectron spectroscopy) [153, 159, 164], AES (Auger electron spectroscopy) [153], STM (Scanning



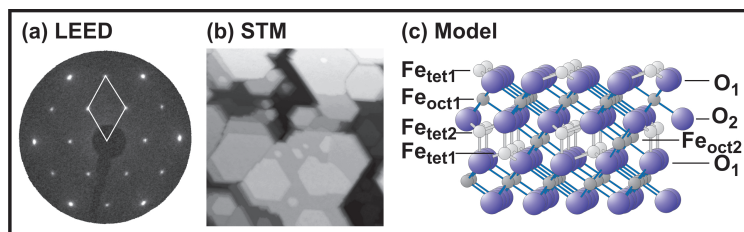


Figure 4.2: (a) LEED diffraction pattern and (b) STM picture of Fe<sub>3</sub>O<sub>4</sub> film; (c) crystal structure of Fe<sub>3</sub>O<sub>4</sub> (from [161]).

tunneling microscopy) [155, 157, 158], XPD (X-ray photoelectron diffraction) [155, 164], LEED [152, 153, 156], TDS (Thermal desorption spectroscopy) [161, 165], IRAS [161] and HREELS (High-resolution electron energy loss spectroscopy) [161]. By PES and XPD [155], it could be demonstrated that the thin Fe<sub>3</sub>O<sub>4</sub> film has the same crystal structure as the bulk phase of Fe<sub>3</sub>O<sub>4</sub>, magnetite. This is an inverse spinel structure where the oxygen ions are ordered in an *fcc*-grid. Fe<sup>3+</sup> ions fill the tetrahedral vacancies and the octahedral sites are occupied by Fe<sup>2+</sup> and Fe<sup>3+</sup> ions (see also fig. 4.2 (c))[166].

The surface termination of the Fe<sub>3</sub>O<sub>4</sub> film is however still a subject of discussion. Based on dynamic LEED and STM studies combined with theoretical calculations, *Weiss et al.* suggested a film termination with tetrahedrally coordinated Fe<sup>3+</sup> ions [156]. In contrast, *Shaikhutdinov et al.* suggested, based on TDS and IRAS CO adsorption measurements combined with an HREELS study and theoretical calculations, a model where octahedrally coordinated Fe<sup>2+</sup> ions terminate the film [161]. Despite the differences in the exact termination of the Fe<sub>3</sub>O<sub>4</sub> film, both models agree that the Fe<sub>3</sub>O<sub>4</sub> film is rather terminated by iron than by oxygen ions.

In our group, it was found that the IR spectrum of adsorbed CO on the iron oxide film strongly depends on the preparation conditions and is not very reproducible, while the corresponding LEED pattern is basically unchanged [84]. The quality of the Fe<sub>3</sub>O<sub>4</sub> films was therefore verified by LEED.

## 4.2 Pd-particles supported on Fe<sub>3</sub>O<sub>4</sub>/Pt(111)

In this section, the preparation, stabilization and cleaning of the Pd particles of the Pd/Fe<sub>3</sub>O<sub>4</sub>/Pt(111) model catalyst will be discussed together with the structure and morphology of the stabilized Pd particles. The preparation, growth, structure and morphology of Pd particles on oxide supports have been investigated in detail before [19, 97, 167].

In this work, Pd (nominal deposition thickness  $\approx 4 \text{ \AA}$ ) was deposited under UHV conditions onto the previously prepared Fe<sub>3</sub>O<sub>4</sub> film by physical vapor deposition (PVD) from an electron beam evaporator. In order to avoid sputtering damage of the oxide film

Table 4.2: Preparation and stabilization of Pd particles on Fe<sub>3</sub>O<sub>4</sub>/Pt(111).

Pd deposition	$\approx 4 \text{ \AA}$	in UHV	at 115 K
heating	for 1 min	in UHV	to 600 K
Stabilization	> 6 cycles of		
oxidation	for 15 min	in O <sub>2</sub> ( $p = 8 \cdot 10^{-7}$ mbar)	at 500 K
reduction	for 45 min	in CO ( $p = 8 \cdot 10^{-7}$ mbar)	at 500 K

by the deposited Pd, the same potential was applied to the sample as to the evaporator (800 V). During Pd deposition, the flux of Pd was  $4.5 \cdot 10^{12}$  atoms $\cdot$ cm<sup>-2</sup> $\cdot$ s<sup>-1</sup> and the surface temperature was kept at 115 K (see also table 4.2). The freshly deposited Pd particles were heated in vacuum to 600 K. Relatively small crystalline Pd particles of 4 nm in size (approx. 700 atoms per particle) with a high island density of  $3.8 \cdot 10^{12}$  cm<sup>-2</sup> are obtained by this preparation procedure.

It has been shown that these small Pd particles are not stable, when they are heated in oxygen ( $p_{\text{O}_2} = 10^{-6}$  mbar) to 500 K [85]. In order to use the same preparation several times, it is necessary to remove carbonaceous residue after an experiment by oxidative treatment. Therefore, the fresh Pd particles were stabilized before use by repeated oxidation (in O<sub>2</sub>,  $p = 8 \cdot 10^{-7}$  mbar) and reduction (in CO,  $p = 8 \cdot 10^{-7}$  mbar) cycles at 500 K to obtain stable Pd particles (see also table 4.2). In fig. 4.3, a STM picture of the stabilized Pd/Fe<sub>3</sub>O<sub>4</sub>/Pt(111) model catalyst is displayed. The stabilized Pd particles are crystalline and have a regular hexagonal shape. The particles exhibit an average diameter of 7 nm, contain approx. 3000 atoms and are thus, significantly larger than the particles before stabilization. The island density after stabilization is reduced to  $8.3 \cdot 10^{11}$  cm<sup>-2</sup> [85]. The changes due to the stabilization procedure can be explained by sintering of the particles which is enhanced by the presence of oxygen. After several oxidation-reduction-cycles, the sintering process becomes very slow, so that no further changes of the particle morphology are observed. A high stability of the Pd particles is important to ensure a direct and quantitative comparison of different kinetic measurements in a series. Therefore, all measurements in this work were conducted on previously stabilized Pd particles.

The structure of the stabilized Pd particles has been further characterized by STM and IRAS [85]. From the STM picture in fig. 4.3, it can be seen that the Pd particles exhibit a hexagonal crystalline shape. The aspect ratio (height to diameter) is  $\approx 1:3.5$ . The STM measurements show that the particles are terminated on top by a (111)-facet and the sides exhibit three (111)- and three (100)-facets. Based on the STM measurements and the geometric form of the Pd particles, it is possible to estimate that about 80% of the surface are terminated by (111)-facets and that  $\approx 20\%$  are terminated by (100)-facets. Further details on the structure and morphology of Pd particles on Fe<sub>3</sub>O<sub>4</sub> can be found in the literature [85, 168].

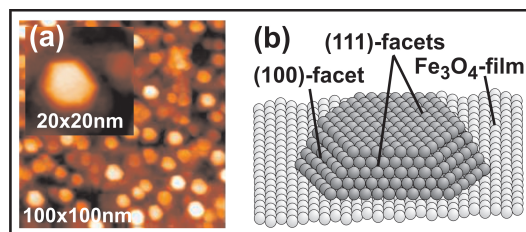


Figure 4.3: (a) STM picture of stabilized Pd particles on Fe<sub>3</sub>O<sub>4</sub>/Pt(111); (b) schematic display of the Pd particles (adapted from [85]).

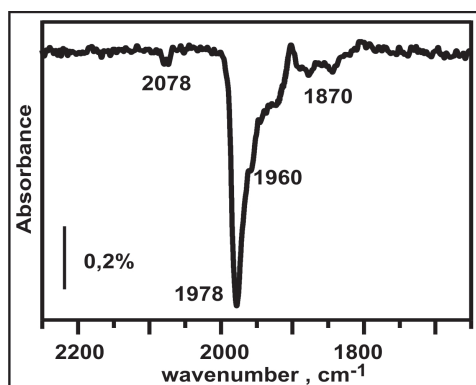


Figure 4.4: IRAS of CO adsorbed at 300 K on stabilized Pd particles on Fe<sub>3</sub>O<sub>4</sub>/Pt(111).

The structure of the Pd particles was also analyzed by IRAS measurements of adsorbed CO molecules [85]. A typical spectrum of CO adsorbed at 300 K (saturation coverage) on the stabilized Pd particles is shown in fig. 4.4. As discussed in more detail in 2.2.1, the signals at 2078 and 1978 cm<sup>-1</sup> are attributed mainly to CO adsorbed on edges occupying on-top and bridge sites respectively, while IR absorption in the region 1960-1870 cm<sup>-1</sup> is assigned to CO occupying mainly hollow sites of regular (111)-facets. Due to the metal surface selection rule (MSSR), signals due to CO adsorbed on strongly inclined (100)-side facets are expected to be strongly attenuated. In contrast, the intensity of signals due CO adsorbed on edge sites is expected to gain intensity at the expense of signals of CO on regular (111)-facets due to dipole coupling effects, also known as *intensity borrowing*. Therefore, it is not possible to derive from IRAS measurements quantitative information on the CO population of different adsorption sites. Based on the STM measurements and previous studies of Pd particles on Al<sub>2</sub>O<sub>3</sub>, it can be however concluded that the particles are well-ordered and exhibit a high crystallinity. The most important structural and morphological parameters of the stabilized Pd particles supported on Fe<sub>3</sub>O<sub>4</sub>/Pt(111) are summarized in table 4.3.

Table 4.3: Structural parameters of the stabilized Pd particles on Fe<sub>3</sub>O<sub>4</sub>/Pt(111).

Parameter		
particle height	$\approx 2$	nm
particle diameter	$\approx 7$	nm
Pd atoms per particle	3000	atoms
Percentage of Pd surface atoms	$\approx 20$	%
Percentage of (111)-facets	$\approx 80$	%
Percentage of (100)-facets	$\approx 20$	%
island density	$8.3 \cdot 10^{11}$	cm <sup>-2</sup>
Percentage of covered support	$\approx 30$	%

# 5 2-butene conversion with D<sub>2</sub> over Pd/Fe<sub>3</sub>O<sub>4</sub>/Pt(111): The role of hydrogen

## 5.1 Introduction

The conversion of olefins with hydrogen, such as *cis-trans* isomerization and hydrogenation, over transition metal catalysts is required for numerous chemical processes, such as fine chemical and pharmaceutical synthesis, petrochemical hydrotreating and food processing, and is thus one of the most important reactions in industrial applications and in catalysis research [31, 37, 169–173]. The chemistry of alkenes has been extensively studied in conventional catalytic studies [31, 169, 170]. More recently, also investigations by modern surface science techniques have been conducted mainly on single crystals [37, 171], but also on supported model catalysts [43, 53]. Surface science studies provided much insight into the mechanistic details, such as key reaction steps. Despite the recent progress, some important issues remain unclear. A complete microscopic picture of the processes controlling the activity and selectivity in alkene conversions is still missing.

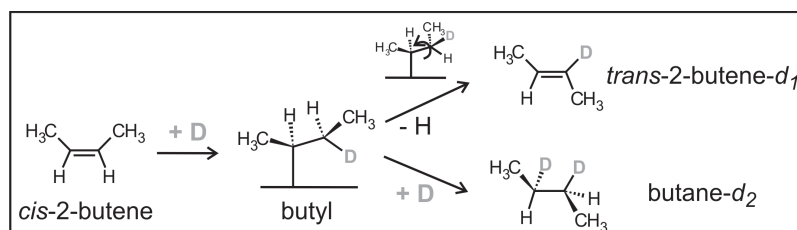


Figure 5.1: *Horiuti-Polanyi* reaction mechanism for *cis*-2-butene conversion with deuterium.

Alkene conversions with hydrogen proceed over transition metal surfaces *via* the generally accepted *Horiuti-Polanyi* mechanism [174] in which the alkene undergoes a series of consecutive hydrogenation and dehydrogenation steps (see also fig. 5.1). In the case of *cis*-2-butene conversion with deuterium, initially a 2-butyl-*d*<sub>1</sub> species is formed in the first half-hydrogenation step, which is the common reaction intermediate for both *cis-trans* isomerization and hydrogenation. The 2-butyl-*d*<sub>1</sub> intermediate can undergo β-hydride elimination resulting in the formation of alkenes, either the original molecule or after a rotation around the C-C axis, the *cis-trans* isomerized molecule. When deuterium is used instead of hydrogen as a reactant, each *cis-trans* isomerization step is accompanied by an H/D exchange [175]. This H/D exchange allows for a distinction between

the reactant *cis*-2-butene- $d_0$  and the product *trans*-2-butene- $d_1$  in the gas phase by mass spectrometry. Alternatively, a second D can be inserted into the carbon metal bond of the 2-butyl- $d_1$  species leading to the formation of the hydrogenation product butane- $d_2$  by reductive elimination. Both the adsorbed 2-butene as well as the 2-butyl intermediate can undergo dehydrogenation resulting in the formation of other carbonaceous species, such as alkylidynes and other partly dehydrogenated species, which remain strongly adsorbed on the surface [176, 177] with their particular stoichiometry depending on the surface temperature.

On Pd, hydrogen cannot only adsorb on strongly-binding *surface* sites, but also occupy more weakly-binding *subsurface* sites [55, 70–76]. There is an ongoing discussion on the involvement of the different hydrogen species in alkene conversion. It has been first suggested by Ceyer *et al.* that *subsurface* adsorbed hydrogen is required for the hydrogenation of olefinic double bonds [56]. Recent studies on supported Pd particles gave first experimental evidence that *subsurface* adsorbed hydrogen plays a crucial role in the hydrogenation of alkenes [43, 53]. Specifically, for small Pd particles a high hydrogenation activity was observed under low pressure conditions, but not for Pd single crystals which was attributed to the unique ability of small Pd particles to store relatively large amounts of hydrogen absorbed beneath the surface. These results demonstrate the need for more realistic model systems, such as supported model catalysts. Despite the recent progress, the involvement of different hydrogen species in the conversion of alkenes remains a controversial issue mainly due to the experimental difficulty of quantitative hydrogen detection under reaction conditions.

Under realistic conditions, catalysts are usually covered with a variety of strongly-dehydrogenated carbonaceous deposits resulting from the decomposition of alkenes. Despite suggestions that different carbonaceous deposits may have a distinct influence on the hydrogen distribution in Pd catalysts as well as on the activity and even the selectivity in alkene conversions [38, 58, 60–65], most surface science studies are conducted on clean, carbon free surfaces. A recent surface science study on the hydrogenation of alkynes demonstrated a strong correlation between the presence of a carbide layer, the formation of subsurface adsorbed hydrogen and the selectivity of the reaction [38, 58]. The underlying microscopic mechanisms of how different carbonaceous species can influence the activity and selectivity in olefin conversions remain however largely unclear.

Pulsed isothermal molecular beam experiments on the conversion of *cis*-2-butene with  $D_2$  over a supported Pd/Fe<sub>3</sub>O<sub>4</sub>/Pt(111) model catalyst under well-defined UHV conditions were conducted to investigate the factors governing the activity and selectivity of this reaction. The reactivity of the C-free Pd/Fe<sub>3</sub>O<sub>4</sub> model catalyst is presented in the first section of this chapter (5.2). To investigate the influence of carbonaceous deposits, the reaction was also studied over a C-covered Pd model catalyst. These results are presented in the second section (5.3). A special emphasis was placed on the role of different hydrogen species in the conversion of *cis*-2-butene which will be discussed in the third section of this chapter (5.4).

## 5.2 Reactivity of the Pd/Fe<sub>3</sub>O<sub>4</sub> model catalyst between 190 and 260 K

First, the activity and selectivity of the Pd/Fe<sub>3</sub>O<sub>4</sub> model catalyst in the conversion of *cis*-2-butene with deuterium was investigated in the temperature range between 190 and 260 K. For this, pulsed molecular beam experiments were conducted under isothermal conditions following the time evolution of the gas phase products by QMS. In these experiments, the sample was continuously exposed to a high flux of D<sub>2</sub> (flux<sub>D<sub>2</sub></sub> = 3.2 · 10<sup>15</sup> molecules · cm<sup>-2</sup> · s<sup>-1</sup>, p<sub>D<sub>2</sub></sub> = 4.0 · 10<sup>-6</sup> mbar) during the entire experiment. After 90 s of D<sub>2</sub> exposure to saturate the Pd model catalyst with deuterium, *cis*-2-butene was pulsed onto the sample at a relatively low flux (flux<sub>*cis*-2-butene</sub> = 5.6 · 10<sup>12</sup> molecules · cm<sup>-2</sup> · s<sup>-1</sup>, p<sub>*cis*-2-butene</sub> = 2.7 · 10<sup>-8</sup> mbar) with a corresponding  $N_{D_2}:N_{cis-2-butene}$  ratio of 570 ( $N_{D_2}$  and  $N_{cis-2-butene}$  denoting the number of D<sub>2</sub> and *cis*-2-butene molecules impinging onto the surface per time unit, respectively). A sequence of 50 short (4 s on, 4 s off) and 30 longer (20 s on, 10 s off) *cis*-2-butene pulses was applied in all experiments discussed in the following. The temporal evolution of the reactant *cis*-2-butene-*d*<sub>0</sub> (C<sub>3</sub>H<sub>5</sub><sup>+</sup>-fragment at 41 amu) is displayed in fig. 5.2 (lower trace, black). The start of the 2-butene exposure corresponds to zero on the time axis. The upper traces (gray) in fig. 5.2 display the evolution of the isomerization product *trans*-2-butene-*d*<sub>1</sub> (C<sub>3</sub>H<sub>4</sub>D<sup>+</sup>-fragment at 42 amu) in the temperature range between 190 and 260 K. It should be noted that no gas-phase reaction products were detected in identical isothermal molecular beam experiments on the bare Fe<sub>3</sub>O<sub>4</sub> support indicating that the Fe<sub>3</sub>O<sub>4</sub>-film by itself is not active neither toward *cis-trans*-isomerization nor hydrogenation of 2-butene. This is in good agreement with previous studies reporting a lack of C-H bond activation in alkenes on Fe<sub>3</sub>O<sub>4</sub> [178–180].

The formation of the products, both *trans*-2-butene-*d*<sub>1</sub> and butane-*d*<sub>2</sub>, only starts after an induction period, indicated in fig. 5.2 by the dotted line. The origin of the induction period has been investigated both on the Fe<sub>3</sub>O<sub>4</sub> support and on the Pd/Fe<sub>3</sub>O<sub>4</sub> model catalyst [150, 181]. In fig. 5.3 (a), it can be seen that the temporal evolution of the reactant trace displays two distinct adsorption modes. During the first pulses, *cis*-2-butene sticks effectively on the surface leaving only a small fraction of the initial flux in the gas phase. After this period of high sticking (sticking probability  $S \approx 0.65$ ), the gas phase signal of *cis*-2-butene significantly increases indicating a considerably decreased sticking. While a square pulse shape indicating irreversible 2-butene adsorption is observed in the initial period of high sticking probability, a significantly different pulse shape is detected in the subsequent period of lower sticking (see fig. 5.3 (b) and (c)). The signal increase is initially very fast after switching the butene beam on, but is followed by a slower growth indicating reversible 2-butene adsorption on the Pd/Fe<sub>3</sub>O<sub>4</sub> model catalyst already covered with strongly-bound adsorbate species. During the period of strong *cis*-2-butene adsorption, no product formation in the gas phase is found (see fig. 5.2). When the sticking probability decreases and adsorption becomes reversible, an onset of product formation is observed. Thus, during the induction period strongly-bound hydrocarbon

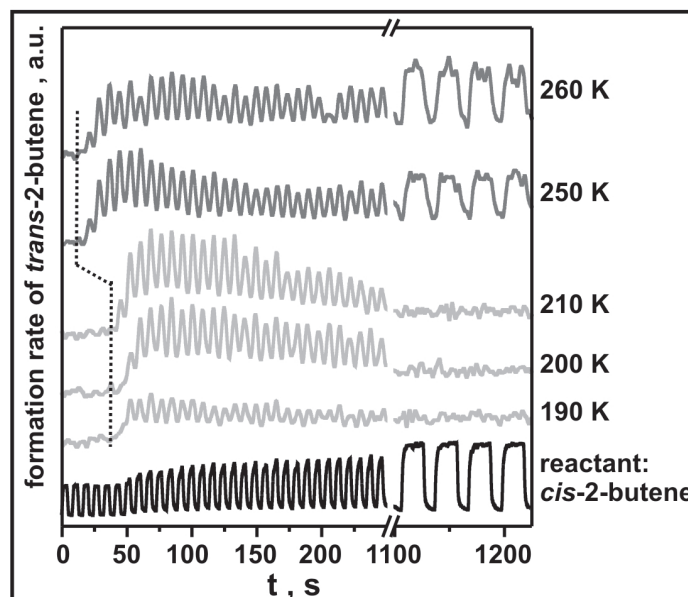


Figure 5.2: Results of pulsed isothermal MB experiments over the Pd/Fe<sub>3</sub>O<sub>4</sub> model catalyst in the temperature range between 190 and 260 K using the pulse sequence described in the text. Displayed is the *cis*-2-butene reactant trace (black) and the time evolution of the *cis-trans* isomerization product *trans*-2-butene-*d*<sub>1</sub> (gray). The dotted line indicates the end of the induction period. While the reaction rates return to zero after prolonged 2-butene exposure at temperatures below 210 K, at higher temperatures, a shorter induction period and sustained *cis-trans* isomerization activity is observed.

species accumulate on the surface that do not lead to the formation of gas phase products. Only when the surface is covered with a relatively high threshold concentration of these strongly-bound hydrocarbon species (for temperatures  $\leq 210\text{K}$ , about  $1 \cdot 10^{14}$  butene molecules per  $6 \cdot 10^{14}$  Pd surface atoms adsorb in the induction period), conversion of *cis*-2-butene is observed. In fig. 5.2, it can be seen that the length of initial induction period decreases at higher temperatures indicating that the formation of the strongly-bound hydrocarbon species involves an activated process such as partial dehydrogenation that occurs faster at higher temperatures. This activation barrier indicates that not only molecularly adsorbed 2-butene is accumulated on the surface, but that also other probably more dehydrogenated species, like butylidyne, are formed. The relative fractions of molecularly adsorbed 2-butene and other partially dehydrogenated species formed in the initial uptake are determined by the ratio of the reaction rate constants for molecular desorption compared to dehydrogenation. Therefore, it is expected that the length of the induction period and also the composition of the adsorbate phase depend in a complex way on the temperature.



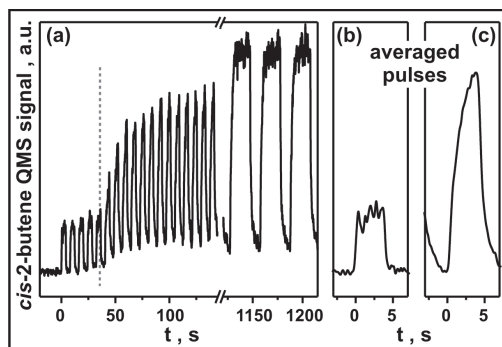


Figure 5.3: (a) Time evolution of the reactant *cis*-2-butene as followed by QMS during a typical isothermal pulsed MB experiment over the Pd/Fe<sub>3</sub>O<sub>4</sub> model catalyst for the conversion of *cis*-2-butene with D<sub>2</sub> at 220 K using the pulse sequence described in the text; (b) average of the first 5 short pulses indicating strong, irreversible sticking; (c) average of the following 45 short pulses displaying weaker reversible adsorption.

In summary, during the induction period, initial irreversible adsorption of the reactant on the Pd/Fe<sub>3</sub>O<sub>4</sub> model catalyst occurs. Only after the surface is saturated with a hydrocarbon species, the production of gas phase products begins. Thus, isomerization and hydrogenation always occur on surfaces covered with hydrocarbon species.

For the *cis-trans* isomerization in the temperature range between 190 and 260 K, two different temperature-dependent regimes can be identified (see fig. 5.2). Between 190 and 210 K, after the induction period, an initially high activity is observed that is followed by a decrease in reaction rate to zero after a few hundred seconds. At higher temperatures (see traces for 250 and 260 K), the reactivity changes significantly. After the induction period, sustained catalytic activity is found for *cis-trans* isomerization even after prolonged 2-butene exposure. The reactivity actually persists over much longer time periods (several hours) than displayed in fig. 5.2 without a significant reduction of the isomerization rate.

The lack of sustained alkene conversion over transition metal under vacuum conditions is usually ascribed to inhibited dissociative adsorption of hydrogen by strongly adsorbed hydrocarbon species [37, 182]. This hypothesis that alkene conversion is limited by the availability of hydrogen due to inhibition of dissociative adsorption by co-adsorbed hydrocarbons is also reflected in the pressure dependence of isomerization and hydrogenation on Pt(111) for which a basically first order dependence on the D<sub>2</sub> pressure is reported, while the dependence on the 2-butene pressure was found to be close to zero order [183]. Based on these results, an interpretation of the reactivity in the temperature range between 190 and 210 K is possible. At the beginning of the MB experiment, before exposure to 2-butene, dissociative D<sub>2</sub> adsorption proceeds effectively forming atomic D on the surface. When the sample is exposed to 2-butene, initially strongly-bound hydro-

carbon species form without the consumption of atomic D. After a threshold coverage of these species is reached, 2-butene isomerization begins initially at high rates consuming the previously adsorbed atomic D. Further dissociative adsorption of D seems to be inhibited however by strongly-bound hydrocarbon species and/or by molecularly adsorbed butene species. When the initially adsorbed D is depleted, the isomerization rate decreases to zero.

In line with this reasoning, it can be concluded that sustained isomerization reactivity at higher temperatures attests to the ability of the Pd model catalyst to dissociatively adsorb  $D_2$  at these temperatures even on the hydrocarbon covered surface and despite of the competition with 2-butene adsorption. There are two possible reasons for this phenomenon. At higher temperatures, molecular 2-butene desorption becomes faster resulting in a lower steady-state coverage, so that more open sites are available for dissociative  $D_2$  adsorption, and thus, decreasing the potential poisoning effect of molecularly adsorbed 2-butene. Another possible reason is that hydrocarbon species are more dehydrogenated at higher temperatures resulting in a smaller footprint of these species on the surface and thus, leaving more metal sites open. Both effects lead to a reduced poisoning of the surface by hydrocarbons allowing for dissociative  $D_2$  adsorption under reaction conditions and thereby for a persisting isomerization activity.

At low temperatures (between 190 and 210 K), the hydrogenation product butane- $d_2$  (followed on the  $C_3H_5D_2^+$  fragment at 45 amu) displays a qualitatively very similar behavior as the isomerization product *trans*-2-butene- $d_1$  (data not shown). After an induction period, initially high hydrogenation rates are observed that decay for longer olefin exposures to zero. At higher temperatures, however a very different reactivity is observed for the hydrogenation pathway compared to the isomerization reaction (see fig. 5.5 (a), left panel). For the hydrogenation, no persisting activity is found at these temperatures contrary to the isomerization reaction. Similarly to the reactivity at low temperatures, the hydrogenation rates also decrease to zero at higher temperatures (250 and 260 K) after initially high activity. The underlying microscopic origins of this effect will be discussed in detail in the following sections.

### 5.3 Reactivity of the C-containing Pd/Fe<sub>3</sub>O<sub>4</sub> model catalyst

Carbonaceous deposits formed by decomposition of hydrocarbons have been suggested to critically affect the activity and selectivity of transition metal catalysts in alkene conversions [31, 37, 38, 60, 61, 119, 171]. The exact microscopic processes resulting in reactivity changes due to carbonaceous deposits remain, however, unclear. In order to investigate the role of carbonaceous deposits in alkene conversions, isothermal pulsed MB reactivity measurements were conducted on a C-precovered Pd/Fe<sub>3</sub>O<sub>4</sub>/Pt(111) model catalyst. For the formation of carbonaceous deposits, the Pd/Fe<sub>3</sub>O<sub>4</sub> model catalyst was exposed at low temperature ( $\approx 115$  K) to 280 L  $D_2$  and 0.8 L *cis*-2-butene and subsequently heated in vacuum to 500 K.

The decomposition of *cis*-2-butene on the D-covered Pd/Fe<sub>3</sub>O<sub>4</sub> model catalyst has been studied in detail before (see [150, 181] for further details), so that here only some important aspect will be briefly discussed. On Pd particles, *cis*-2-butene decomposes step-wise starting already at low temperatures ( $T \leq 200$  K). Based on low-temperature IRAS measurements and similarities of TPR measurements on decomposition over Pt and Pd single crystal surfaces, it was speculated that *cis*-2-butene adsorbs at low temperatures ( $\approx 100$  K) and submonolayer coverages on the Pd model catalyst *via* the formation of a di- $\sigma$ -bound species that dehydrogenates to a di- $\sigma$ -bound 2-butyne species at room temperature and to strongly-dehydrogenated carbonaceous deposits above 400 K (see [181] and references therein). It should be noted that carbon dissolution into the subsurface of Pd was found to occur at temperatures above 400 K [68, 69], so that it is expected that some carbon occupies subsurface sites of the Pd particles after heating of the 2-butene covered model catalyst to  $\approx 500$  K.

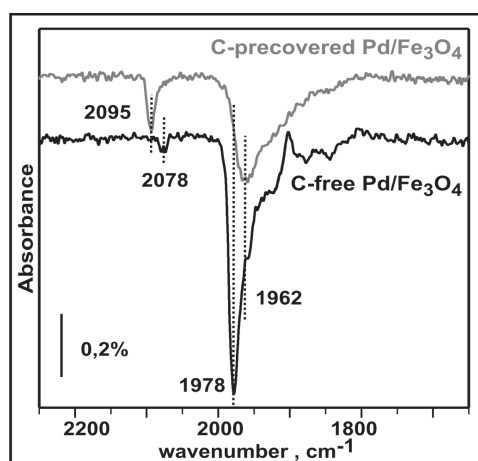


Figure 5.4: CO IRAS spectra for Pd/Fe<sub>3</sub>O<sub>4</sub>/Pt(111) surfaces: C-free (bottom, black) and after C-precovering (top, gray). The surface was saturated with CO at 300 K and subsequently cooled down to a 100 K. The spectra indicate that carbon mainly covers low-coordinates sites like edges and corners and bridge sites on (100)-facets, while the majority of the surface sites on (111)-facets remain C-free.

It has been recognized before that carbonaceous deposits are not uniformly distributed over the surface of the Pd particles [184, 185]. While large (111)-facets remain basically carbon-free, low-coordinated sites, like edges and corners as well as to some extent (100)-facets, are preferentially occupied by carbonaceous deposits. The spatial distribution of carbonaceous deposits formed in the decomposition of 2-butene was studied by IRAS measurements using CO as a probe for different adsorption sites. The spectra obtained for the C-free and the C-covered Pd/Fe<sub>3</sub>O<sub>4</sub> model catalyst are displayed in fig. 5.4.

For the C-free Pd catalyst (black trace), the spectrum of adsorbed CO is dominated by a sharp peak of high intensity around 1978 cm<sup>-1</sup> which can be attributed to CO adsorbed on step and edge sites as well as on (100)-facets (see 2.2.1 and [100, 186] for details). Even though the intensity in IRAS does not scale linearly with the number of adsorption sites and the peak at 1978 cm<sup>-1</sup> appears too large due to intensity transfer (see 2.2.1 and 2.3.2 for further details), significant changes are observed upon carbon deposition. In the CO adsorption spectrum obtained from the C-containing Pd model catalyst (gray trace in fig. 5.4), the peak at 1978 cm<sup>-1</sup> is practically absent, while the signals at lower frequencies attributed to CO adsorbed on (111)-facets remain basically unchanged. Upon C-covering, an additional feature at 2095 cm<sup>-1</sup> appears that can be assigned to CO adsorption on *on-top* sites. These differences suggest that carbonaceous deposits preferentially adsorb and/or form at low-coordinated edge and step sites as well as to a lesser extent also on (100)-facets, while the (111)-facets constituting about 80 % of the particle surface (see 4.2) remain C-free.

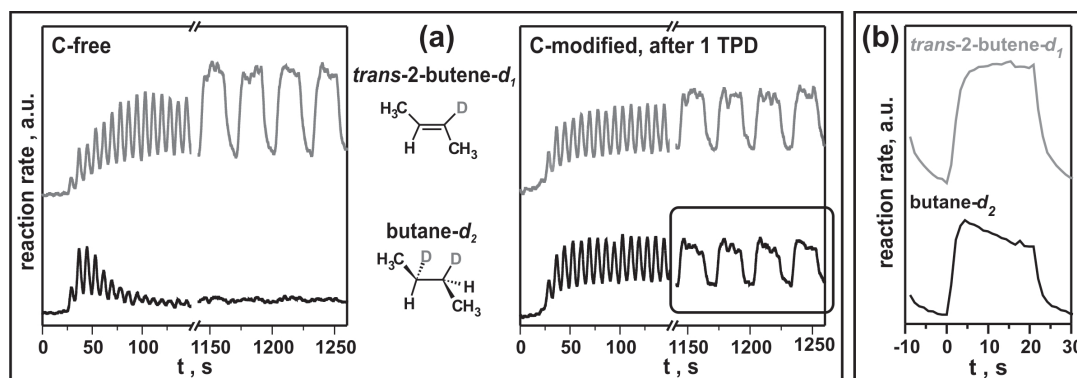


Figure 5.5: (a) Results of pulsed isothermal MB experiments on the conversion of *cis*-2-butene with  $D_2$  at 260 K over the initially C-free (left panel) and the C-precovered (right panel) Pd/Fe<sub>3</sub>O<sub>4</sub>/Pt(111) model catalyst. Displayed is the temporal evolution of the formation rates of the isomerization product *trans*-2-butene- $d_1$  (upper traces, gray) and the hydrogenation product butane- $d_2$  (lower traces, black). While on the initially C-free Pd particles only the *cis-trans* isomerization displays sustained activity, both isomerization and hydrogenation activity persist on the C-precovered model catalyst. (b) Averaged reaction rates obtained for the *cis-trans* isomerization product *trans*-2-butene- $d_1$  (upper row, gray) and the hydrogenation product butane- $d_2$  (lower row, black) at 260 K on the C-precovered Pd/Fe<sub>3</sub>O<sub>4</sub>/Pt(111) model catalyst. The averages were obtained from the last 30 long pulses of the isothermal pulsed MB experiment.

The reactivity of the C-containing Pd/Fe<sub>3</sub>O<sub>4</sub> model catalyst was also investigated by isothermal pulsed MB experiments using the same pulse sequence as described in the previous section (5.2). In fig. 5.5(a), the reaction rates for the isomerization product

### 5.3 Reactivity of the C-containing Pd/Fe<sub>3</sub>O<sub>4</sub> model catalyst

*trans*-2-butene-*d*<sub>1</sub> and the hydrogenation product butane-*d*<sub>2</sub> are displayed for the conversion of *cis*-2-butene over the C-free (left panel) and the C-containing (right panel) Pd particles at 260 K. On the C-free Pd particles the two reaction pathways, *cis-trans* isomerization and hydrogenation exhibit at 260 K a significantly different reactivity behavior. While for isomerization, a persisting high reactivity is observed after an initial induction period, hydrogenation reactivity displays only a transient high reactivity after the induction period which ceases after longer 2-butene exposure. On the C-covered Pd model catalyst (fig. 5.5(a), right panel), the reactivity changes dramatically. Not only isomerization can be sustained over longer time periods, but also a persisting hydrogenation activity is observed. These pronounced differences in the reactivity of the C-free and the C-covered Pd model catalyst clearly demonstrate the promoting role of carbonaceous deposits in sustained alkene hydrogenation at relatively low temperatures.

It should be emphasized that the length of the induction period is basically identical for the C-free and the C-containing Pd particles. Moreover, the initial reaction rates for both isomerization and hydrogenation over the C-free and the C-precovered Pd model catalysts are very similar and also the steady state isomerization rates are of comparable size for the C-free and the C-covered Pd particles. These observations suggest that the carbonaceous deposits on the Pd model catalyst do not significantly alter the total surface area available for 2-butene adsorption as previously indicated by the CO-IRAS measurements. Thus, the (111)-facets constituting the majority of the surface of the Pd particles remain largely unchanged by C deposition.

From the dramatic differences in the hydrogenation reactivity of the C-free and the C-covered Pd model catalyst, two closely related questions arise: Why is the hydrogenation pathway selectively suppressed under steady state conditions on the initially C-free Pd particles, and what is the role of carbon in the induction of the sustained hydrogenation activity?

The persisting isomerization activity on the initially clean Pd particles indicates that both the 2-butyl intermediate and surface adsorbed D are available under steady state conditions on the surface. The selective suppression of the hydrogenation pathway on the initially C-free Pd particles indicates that this reaction pathway does not only require the obviously present surface D species. While the first half-hydrogenation step to the 2-butyl intermediate proceeds effectively as indicated by the persisting isomerization activity, the second half-hydrogenation step from 2-butyl to butane is inhibited under these conditions. The second half-hydrogenation seems to require not only surface D which is abundant on the surface under these conditions, but a different kind of D species present at the beginning of the experiment, but which cannot be replenished under steady state conditions on the C-free Pd particles.

For conversion over the C-covered Pd particles, the transient behavior upon modulation of the 2-butene beam differs significantly for the two reaction pathways giving additional evidence for the involvement of a second kind of D species in the second half-

hydrogenation step. In fig. 5.5(b), the temporal evolution of the reaction rates during the 30 long pulses in *cis*-2-butene conversion with  $D_2$  over the C-precovered Pd/Fe<sub>3</sub>O<sub>4</sub> model catalyst at 260 K is displayed (averaged over the last 30 pulses). The sample is continuously exposed to a large flux of  $D_2$ , so that the sample can be re-saturated with D between the *cis*-2-butene pulses. The reaction rate at the beginning of the pulse corresponds thus, to the rate over a D-saturated catalyst under reaction conditions. For the isomerization product *trans*-2-butene- $d_1$  (black trace), a roughly rectangular pulse profile is observed. Thus, the time-evolution of the reaction rates simply follows the concentration of the reactant *cis*-2-butene. The  $\beta$ -hydride elimination is generally believed to be fast compared to the first half-hydrogenation step [173]. Therefore the isomerization rate is expected to be determined by the formation of the 2-butyl- $d_1$  species which depends on the adsorption rate of *cis*-2-butene and the availability of dissociated D. The constant *cis-trans* isomerization rate observed over the pulse length indicates that the surface concentration of both the 2-butyl- $d_1$  species and surface adsorbed atomic D remain basically constant during the 2-butene pulse.

For the hydrogenation product butane- $d_2$ , in contrast, the initially high reaction rate decreases significantly over the 2-butene pulse duration. This evolution is expected for a situation where the concentration of one reactant is high in the beginning of the pulse, but decreases over the pulse duration leading thereby to a reduction of the reaction rates. As indicated by the isomerization rates, the concentrations of 2-butyl- $d_1$  and surface adsorbed atomic D remain constant. Therefore, a reduction of the hydrogenation rates can only be explained if the second half-hydrogenation step requires a different type of D which is present at high concentrations at the beginning of the 2-butene pulse, but that is depleted over the pulse length.

In summary, both the selective suppression of the hydrogenation pathway on the initially C-free Pd particles as well as the differences in the transient kinetic behavior observed for the isomerization and hydrogenation in the steady state regime on the C-covered Pd particles give strong evidence for the involvement of a second hydrogen species in the second half-hydrogenation step leading to the formation of the hydrogenation product butane- $d_2$ . In the following section, the microscopic nature of this hydrogen species and the role of carbonaceous deposits in enabling persisting hydrogenation activity will be discussed.

## 5.4 The role of surface and subsurface deuterium

As discussed in the previous section, sustained isomerization activity on the C-free catalyst and the transient kinetic behavior in the steady state regime (on both the C-covered and the initially C-free catalysts) imply that both the 2-butyl intermediate and surface adsorbed atomic hydrogen are available on the surface under reaction conditions at 260 K. The selective suppression of the hydrogenation pathway on the C-free Pd particles as well as the differences in the transient kinetic behavior of the hydrogenation rates

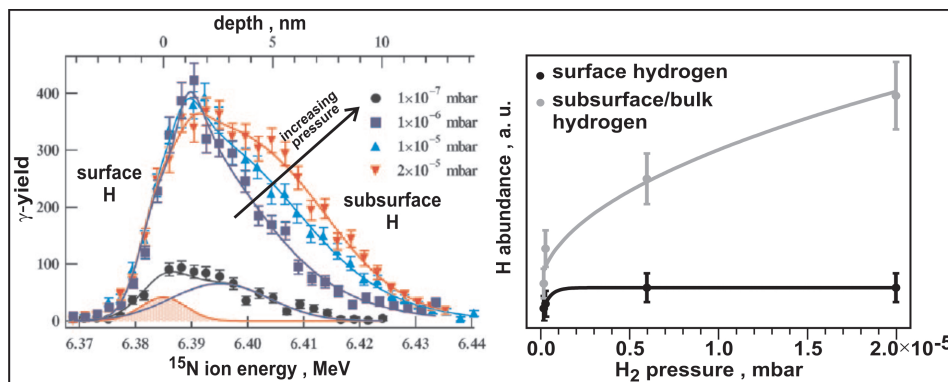


Figure 5.6: Left panel: Grazing incidence NRA yield curves of H on and in Pd particles supported on  $\text{Al}_2\text{O}_3$  at different  $\text{H}_2$  pressures at 94 K. Right panel:  $\text{H}_2$  pressure dependence of the surface adsorbed (black) and volume absorbed (gray) H (data adapted from M. Wilde and K. Fukutani [187]).

in the steady state regime on the C-covered Pd particles, strongly suggest the involvement of a different kind of D species in the second half hydrogenation step.

There are two different types of hydrogen species known for hydrogen sorption on Pd (see *e.g.* [54, 55, 188] and 2.2.2 for further details). Hydrogen dissociatively adsorbs on Pd in a basically non-activated process leading to the formation of surface adsorbed atomic hydrogen. At high coverages, diffusion to absorption sites below the Pd surface begins to proceed at significant rates leading to the formation of subsurface absorbed H(D). Diffusion to subsurface sites is an activated process and the resulting subsurface species are more weakly-bound than surface adsorbed atomic hydrogen (see also 2.2.2 for further details). Recently, the spatial distribution of hydrogen species on and in Pd particles has been investigated as a function of the hydrogen pressure by hydrogen depth profiling using  $^1\text{H}(^{15}\text{N}, \alpha, \beta)^{12}\text{C}$  nuclear reaction analysis (NRA) (see fig. 5.6) [187]. NRA measurements allow to quantitatively detect surface adsorbed and subsurface/volume absorbed (in the following denoted surface and subsurface for simplicity) H species on and in Pd particles. As can be seen in fig. 5.6, the component of the NRA signal attributed to surface hydrogen saturates with increasing  $\text{H}_2$  pressure quickly at pressures  $\leq 1 \cdot 10^{-6}$  mbar. The signal attributed to subsurface hydrogen in contrast increases significantly with increasing  $\text{H}_2$  pressure, at least up to  $2 \cdot 10^{-5}$  mbar. Even at these relatively low pressures, the absolute amount of subsurface hydrogen compared to the saturation coverage of surface adsorbed hydrogen is substantial and even small changes in the  $\text{H}_2$  pressure lead to significant changes in the abundance of subsurface hydrogen. This subsurface absorbed hydrogen has been suggested before to play an important role in olefin hydrogenation [43, 53, 56–59]. Direct experimental proof for this hypothesis has been however lacking.

To test the possible involvement of subsurface hydrogen in the hydrogenation of 2-

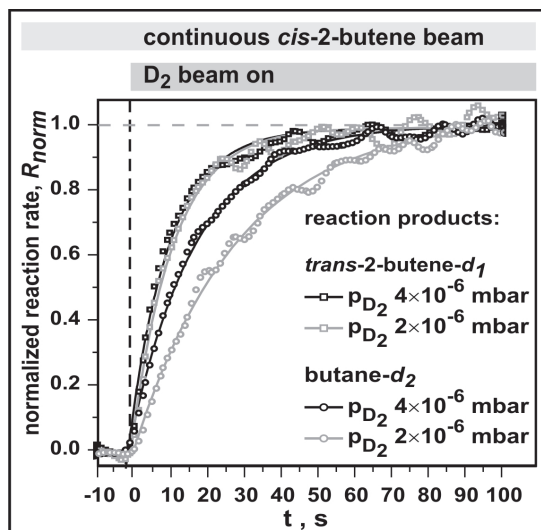


Figure 5.7: Temporal evolution of the normalized reaction rates of *trans*-2-butene- $d_1$  (open squares) and butane- $d_2$  (open circles) in the conversion of *cis*-2-butene with  $D_2$  at 260 K over the C-precovered Pd/Fe<sub>3</sub>O<sub>4</sub>/Pt(111) model catalyst after temporary intermission of the  $D_2$  beam. The experiment was conducted at two different  $D_2$  pressures ( $2 \cdot 10^{-6}$  mbar and  $4 \cdot 10^{-6}$  mbar) at a constant  $N_{D_2}:N_{cis-2-butene}$  ratio of 570.

butene over the Pd/Fe<sub>3</sub>O<sub>4</sub> model catalyst, a series of transient pulsed MB experiments over the C-covered Pd model catalyst was conducted. In these experiments, the surface was pre-exposed to  $D_2$  and *cis*-2-butene at 260 K until a steady state reactivity was reached. Subsequently, the  $D_2$  beam was switched off for 100 s until the surface was depleted from D as indicated by reaction rates decreasing to zero (see fig. 5.7). Then the  $D_2$  beam is switched on again and the temporal evolution of the reaction rate increase is followed by QMS. In this situation, both reaction rates are limited by the formation of D species. The experiment was conducted at two different overall pressures keeping the  $N_{D_2}:N_{cis-2-butene}$  ratio constant at 570 (with  $N_{D_2}$  and  $N_{cis-2-butene}$  denoting the numbers of  $D_2$  and *cis*-2-butene molecules impinging on the surface per unit time, respectively). After re-opening of the  $D_2$  beam, all reaction rates returned to the same steady state level as before. The two reaction pathways exhibit however significant differences in the transient kinetic behavior for the two applied pressures. It can be seen in fig. 5.7 that the isomerization rate returns quickly to the steady state level with almost identical and thus, basically pressure independent time constants of  $\tau_{char} = (11.0 \pm 0.3)$  s and  $\tau_{char} = (11.4 \pm 0.3)$  s at  $D_2$  pressures of  $4 \cdot 10^{-6}$  mbar and  $2 \cdot 10^{-6}$  mbar, respectively. For the hydrogenation pathway, a significantly slower rate increase is observed with the characteristic time constants strongly depending on the overall pressure. At the higher  $D_2$  pressure of  $4 \cdot 10^{-6}$  mbar, the characteristic time constant is with  $\tau_{char} = (18.3 \pm 0.3)$  s clearly smaller than at the lower  $D_2$  pressure of  $2 \cdot 10^{-6}$  mbar with  $\tau_{char} = (28.3 \pm 0.5)$  s.



Upon re-opening of the D<sub>2</sub> beam, the reaction rates are limited by the formation of D species on and in the Pd particles. The pressure independent temporal response of the isomerization rate indicates that this pathway is connected to the coverage of *surface* adsorbed atomic D which is expected to replenish first and reach quickly saturation upon D<sub>2</sub> exposure due to the higher heat of adsorption compared to the subsurface species. The pressure dependence of the hydrogenation rates attests to the involvement of a D species that depends strongly on the D<sub>2</sub> pressure in the second half-hydrogenation step. In combination with the NRA measurements, this strongly suggests that the presence of *subsurface* adsorbed hydrogen is required for the hydrogenation to proceed effectively. It should be emphasized that surface hydrogen cannot be the D species required for the second half-hydrogenation step because in this case, a pressure independent behavior as observed for the isomerization pathway must be detected. Due to the activation barrier for diffusion into the subsurface of Pd, a significantly slower replenishment of the subsurface D species compared to the surface D species which are formed in a basically non-activated process is expected (see [70–76, 105] and 2.2.2 for further details). It should be noted that this model does not imply that subsurface hydrogen is directly involved in the second half-hydrogenation step. Instead, it can merely modify the adsorption properties of the surface such that surface adsorbed hydrogen is more prone to attack the Pd-butyl bond leading to the formation of butane.

Having revealed the nature of the hydrogen species involved in the second half-hydrogenation step, it is possible to understand the observed results for the C-free and the C-covered Pd model catalyst at 260 K (see fig. 5.5). At the beginning of the experiment, before the start of the *cis*-2-butene exposure, both *surface* and *subsurface* D states are populated on the hydrocarbon free surfaces, so that both hydrogenation and isomerization proceed efficiently. On the C-free surface, subsurface adsorbed D cannot be replenished under steady state conditions, when the surface is covered with hydrocarbons. Thus, after the initially adsorbed D is depleted the hydrogenation rates return to zero. The inability to replenish subsurface hydrogen may have several origins: Activated D diffusion into the subsurface competes with effective conversion in the isomerization pathway and with desorption; moreover, hydrocarbons adsorbed under steady state conditions on the surface may block diffusion sites and thereby inhibit diffusion into the Pd bulk. All three effects lead to a reduction of the diffusion into the subsurface of Pd.

On the C-free Pd particles, D diffusion into the Pd volume becomes apparently negligible in the presence of co-adsorbed hydrocarbons resulting in vanishing hydrogenation rates for prolonged olefin exposure. The sustained hydrogenation activity on the C-precovered Pd particles implies in return that replenishment of subsurface D is feasible under steady state conditions. Thus, strongly-dehydrogenated carbonaceous deposits (carbon) likely facilitate hydrogen diffusion into the Pd bulk also in the presence of co-adsorbed hydrocarbons.

This finding seems to be in strong disagreement with recent observations that car-

bonaceous deposits inhibit full hydrogenation of acetylene to ethane and moreover, that carbonaceous deposits inhibit the formation of the bulk dissolved H ( $\beta$ -phase) [58]. However, in these studies the amount of C was substantially higher than in our investigation - the formation of a fully closed PdC phase was observed under the conditions applied in their study, while under the conditions applied in this study, only a submonolayer amount of C is deposited on the Pd particles located mainly at low-coordinated sites of the particles. Recent NRA measurements (at 94 K) show that the saturation coverage of surface and volume absorbed hydrogen is basically identical for C-free and with submonolayer amounts of C covered Pd particles demonstrating that small amounts of carbonaceous deposits do not inhibit the formation subsurface hydrogen [187]. The hydrogen concentration on the C-precovered Pd particles is only slightly reduced closely below the surface indicating that C might partially be dissolved below the surface of the Pd particles which is in good agreement with recent theoretical calculations predicting that C preferentially occupies highly-coordinating subsurface sites [124]. The fact that carbonaceous deposits do not increase the amount of bulk absorbed D supports the hypothesis that the persisting hydrogenation activity on C-covered Pd particles is due to increased D diffusion into the bulk under reaction conditions rather than due to an overall larger capacity of the C-covered Pd particles for storing D in the bulk. Carbonaceous deposits may enhance the rate of D diffusion into the bulk by either destabilizing strongly-bound surface D leading thereby to a reduction of the effective activation barrier for diffusion or C may lower the diffusion barrier by distortions of the Pd lattice making the surface more permeable for hydrogen [189].

## 5.5 Conclusion

In summary, the conversion of *cis*-2-butene with D<sub>2</sub> over a Pd/Fe<sub>3</sub>O<sub>4</sub>/Pt(111) model catalyst was studied by isothermal pulsed molecular beam experiments. A special emphasis was put on the role of different hydrogen species in the activity and selectivity toward *cis-trans* isomerization and hydrogenation. Moreover, the influence of carbonaceous deposits typically present under catalytic reaction conditions on the reactivity of the catalyst was investigated.

The conversion of *cis*-2-butene toward isomerization and hydrogenation products only begins, once the surface is covered with strongly-adsorbed 2-butene or other partially dehydrogenated hydrocarbon species. At low temperatures, these co-adsorbed hydrocarbon species inhibit the dissociative H<sub>2</sub>(D<sub>2</sub>) adsorption leading to vanishing reaction rates when the preadsorbed H(D) is depleted. At higher temperatures, increased 2-butene desorption and/or a smaller footprint of the hydrocarbon species leads to a reduction of the poisoning effect allowing for effective dissociative D<sub>2</sub> adsorption and thus, for sustained isomerization rates.

While isomerization requires the presence of just surface hydrogen, the presence of a second hydrogen species is required for the formation of hydrogenation products. This

hydrogen species could be identified as weakly-bound subsurface absorbed H(D) by a combination of NRA and transient molecular beam experiments.

While persisting isomerization activity is observed at 260 K over the initially clean Pd model catalyst, the hydrogenation rates vanish after a short period of high activity. The deposition of carbon dramatically alters the activity and selectivity of the surface. Over the C-precovered Pd particles, both reaction pathways exhibit activity that can be sustained over long time periods. The selective suppression of the hydrogenation over the C-free catalyst was attributed to the inability of the initially clean Pd catalyst to replenish subsurface absorbed H(D) under reaction conditions, so that the hydrogenation activity ceases once the initially absorbed subsurface hydrogen is depleted. Carbonaceous deposits situated mainly on low-coordinated sites like edges and steps seem to facilitate an effective replenishment of the subsurface hydrogen species under steady state reaction conditions which allows for persisting hydrogenation activity over the C-precovered Pd/Fe<sub>3</sub>O<sub>4</sub>/Pt(111) model catalyst.



# 6 2-butene conversion with D<sub>2</sub> over Pd/Fe<sub>3</sub>O<sub>4</sub>/Pt(111): A kinetic study

## 6.1 Introduction

Studying reactions under clean UHV conditions over well-defined supported model catalysts that reproduce important features of applied catalysts can provide a more detailed insight in the microscopic processes on the surface that govern the activity and selectivity of catalytic reactions. The conversion of *cis*-2-butene with D<sub>2</sub> over a Pd/Fe<sub>3</sub>O<sub>4</sub>/Pt(111) model catalyst has been investigated by isothermal pulsed MB experiments. It was found that the activity and selectivity of the Pd particles in the *cis-trans* isomerization and hydrogenation strongly depend on the availability of *surface* adsorbed and *subsurface* adsorbed H(D) (see chapter 5). While isomerization occurs at significant rates when just *surface* adsorbed D is available, the hydrogenation pathway can only proceed effectively in the presence of *subsurface* hydrogen which either is directly inserted into the molecule or simply modifies the adsorption properties of the surface such that surface adsorbed D is more prone to attack the butyl intermediate. Taking these results into account, an extended reaction mechanism, as depicted in fig. 6.1, for the conversion of *cis*-2-butene with D<sub>2</sub> over Pd toward *cis-trans* isomerization and hydrogenation can be developed. Next to the sequential hydrogenation and dehydrogenation steps of the generally accepted Horiuti-Polanyi mechanism [174], the involvement of different D species in these steps is indicated according to the results presented in chapter 5. D\* denotes a second D species different from regular surface adsorbed D that is involved in the second half-hydrogenation step. It can either be *subsurface* adsorbed hydrogen or by the presence of subsurface D modified *surface* adsorbed D.

From catalytic studies conducted under applied ambient pressure conditions, several macroscopic properties of alkene conversions with hydrogen over Pd catalysts are known including reaction orders with respect to the hydrogen and alkene pressure as well as the temperature dependence. With respect to the hydrogen pressure, formal reaction orders around unity are reported [31, 32, 34–38, 190], while the reaction order in olefin pressure is typically around zero [31, 33, 35–38, 183, 190]. For increasing reaction temperatures, initially the conversion rates increase, however, for even higher temperatures, decreasing conversion rates and thus, negative Arrhenius coefficients are reported which have been attributed to fast desorption of the olefins [37, 191, 192]. The selectivity shifts toward hydrogenation for increasing hydrogen pressures and increasing reaction temperatures, while a selectivity shift toward isomerization is reported for increasing alkene pressures [31–38]. Even though it can be derived from these macroscopic trends how the activity

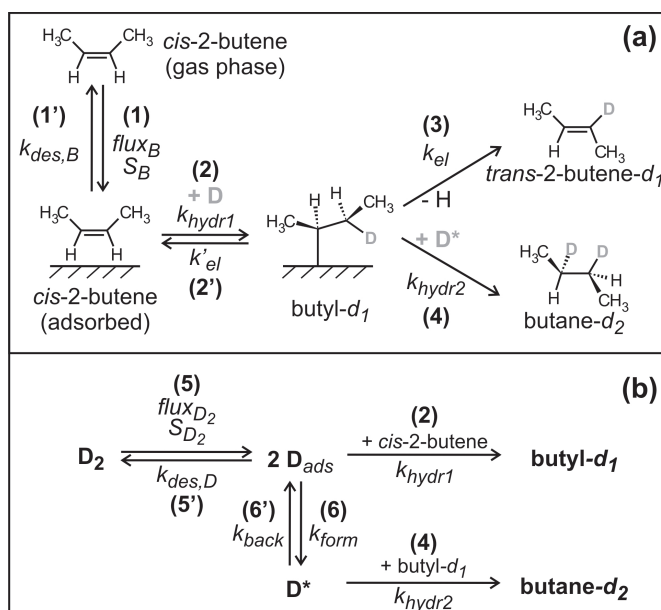


Figure 6.1: Reaction scheme: (a) schematic representation of *cis*-2-butene conversion with  $D_2$  on Pd: (1) molecular adsorption of 2-butene, (2) first half-hydrogenation step of *cis*-2-butene to butyl-*d*<sub>1</sub>, (3) *cis*-*trans* isomerization *via* rotation around the C-C bond followed by  $\beta$ -hydride elimination to *trans*-2-butene-*d*<sub>1</sub>, (4) hydrogenation to butane-*d*<sub>2</sub> by a second half-hydrogenation of butyl-*d*<sub>1</sub>; (b) schematic representation of processes involving deuterium: (5) dissociative  $D_2$  adsorption leading to the formation of surface adsorbed D involved in the formation of the 2-butyl-*d*<sub>1</sub> intermediate, (6) formation of  $D^*$  species involved in the second half-hydrogenation step and connected to the presence of subsurface absorbed D.

and selectivity in alkene conversions over Pd catalysts can be influenced, a microscopic understanding of the occurring processes is lacking.

There are only few surface science studies investigating the conversion of C4 alkenes with hydrogen over Pd catalysts which focus mainly on 1,3-butadiene and 1-butene, while 2-butene is typically only considered as a possible product [39–46]. The kinetics of the 2-butene reactions with hydrogen have been investigated in more detail by Somorjai *et al.* for a Pt(111) single crystal surface. These authors reported reaction orders of unity with respect to the hydrogen pressure for both isomerization and hydrogenation [183]. To the best of our knowledge, no surface science studies have been previously conducted investigating in particular the kinetics of 2-butene conversion with hydrogen over Pd model catalysts.

Isothermal pulsed MB experiments offer the unique possibility to study not only the

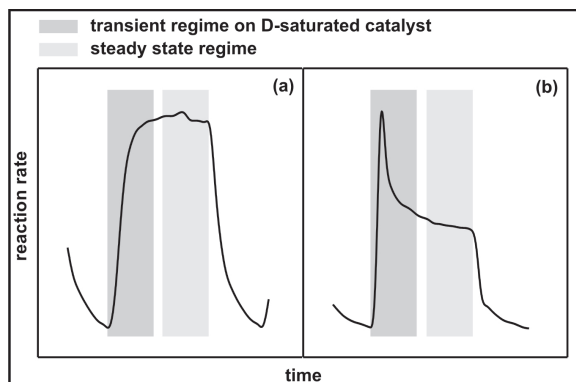


Figure 6.2: Typical product response curves obtained for MB experiments with continuous  $D_2$  exposure and a pulsed 2-butene beam for (a) D-rich and (b) D-deficient steady state conditions. In the transient regime, the surface is saturated with D. The reaction rates remain the same in the steady state, when the D concentration is basically unchanged during the olefin exposure (a) or drop to a lower level, when the D concentration decreases in the presence of additional hydrocarbons (b).

changes of the *steady state* reactivity with varying reaction conditions, but also provide information on the *transient* kinetic behavior and how it is influenced by different reaction conditions. In the isothermal pulsed MB experiments, the catalyst was continuously exposed to a high flux of  $D_2$  and a comparably small flux of *cis*-2-butene was pulsed onto the surface. In the following, the time period between the beginning of the olefin pulse and the establishing of the steady state conditions will be denoted as transient regime. Before the beginning of the 2-butene pulse, the sample is exposed only to  $D_2$  so that the surface can be re-saturated with D between the olefin pulses. In the transient regime, at the beginning of the 2-butene pulse, the reaction proceeds thus, on a D saturated surface. When the reaction continues and steady state conditions are established, basically two responses of the system are possible: Either the D concentration remains basically unchanged upon 2-butene exposure, so that the reaction rates in the steady state are the same as in the transient regime. For such a situation, a roughly rectangular pulse profile is observed following the evolution of the reactant *cis*-2-butene (see fig. 6.2 (a)). Or the D concentration drops significantly due to adsorption of alkenes resulting in decreasing reaction rates as depicted in fig. 6.2 (b). In this case, the reaction takes place under D-deficient conditions in the steady state regime and is limited by the formation of surface or subsurface D. Thus, the form of the product response upon modulation of the 2-butene beam can provide unique information on the involvement of hydrogen related processes in rate limiting steps.

By isothermal pulsed MB experiments, it is thus, possible to investigate the influence of different reaction parameters, like reactant pressures, their relative ratio or the reaction temperature, on the role of *hydrogen* related processes in *cis*-2-butene conversion

over C-free and C-covered Pd/Fe<sub>3</sub>O<sub>4</sub>/Pt(111) model catalysts which may have a crucial influence on the activity and selectivity of the reaction as indicated by the results presented in the preceding chapter 5.

Moreover, such an approach allows to verify that the model system reproduces the macroscopic kinetic trends reported for applied catalytic processes - which differ from our model system significantly both in the pressure regime and the complexity of the catalyst - to ensure thereby the transferability of the obtained results in this surface science study to more realistic conditions.

Based on these two major motivations, pulsed isothermal MB beam experiments on the conversion of *cis*-2-butene with D<sub>2</sub> over the C-free and C-covered Pd/Fe<sub>3</sub>O<sub>4</sub>/Pt(111) model catalyst were conducted as a function of the *cis*-2-butene and D<sub>2</sub> pressure as well as of the reaction temperature. The dependence on the D<sub>2</sub> pressure together with a kinetic model is presented in the first section of this chapter (6.2). In the second section (6.3), the results for different *cis*-2-butene pressures and their implications for the processes on the surface are discussed, while the temperature dependence of the 2-butene conversion is subject of the third section (6.4). At the end of the chapter (6.5), the influence of different reaction conditions on the conversion and selectivity is discussed.

## 6.2 Dependence on the D<sub>2</sub> pressure

First, the influence of the D<sub>2</sub> pressure on the conversion of *cis*-2-butene is investigated both over the C-free and C-precovered Pd/Fe<sub>3</sub>O<sub>4</sub> model catalyst. The isothermal pulsed MB experiments are conducted following the pulse sequence introduced in 5.2. Thus, the sample is initially exposed to 280 L of D<sub>2</sub>, then *cis*-2-butene (50 short pulses (4 s on, 4 s off); 30 long pulses (20 s on, 10 s off)) is pulsed onto the surface, while D<sub>2</sub> is continuously supplied during the entire experiment. The *cis*-2-butene pressure was kept constant ( $2.7 \cdot 10^{-8}$  mbar,  $\text{flux}_{\text{cis-2-butene}} = 5.6 \cdot 10^{12}$  molecules  $\cdot$  cm<sup>-2</sup>  $\cdot$  s<sup>-1</sup>), while the D<sub>2</sub> pressure was varied by a factor of  $\approx 13$  in the range of 0.4 to  $5.3 \cdot 10^{-6}$  mbar. The corresponding  $N_{D_2}:N_{\text{cis-2-butene}}$  ratios lie in the range of 60 to 750, with  $N_{D_2}$  and  $N_{\text{cis-2-butene}}$  denoting the number of D<sub>2</sub> and *cis*-2-butene molecules impinging onto the surface per time unit, respectively. Thus, in all experiments the reaction was conducted in a large excess of D<sub>2</sub>. It is also important to emphasize once more that the surface is exposed to just D<sub>2</sub> between the butene pulses allowing for re-saturation of the Pd particles with D before the next butene pulse so that the reaction in transient regime takes place on a surface with high D concentrations.

In the following part, first the results obtained for *cis*-2-butene conversion with D<sub>2</sub> over the C-precovered Pd model catalyst will be discussed and subsequently compared to results obtained for reaction over the C-free Pd model catalyst.



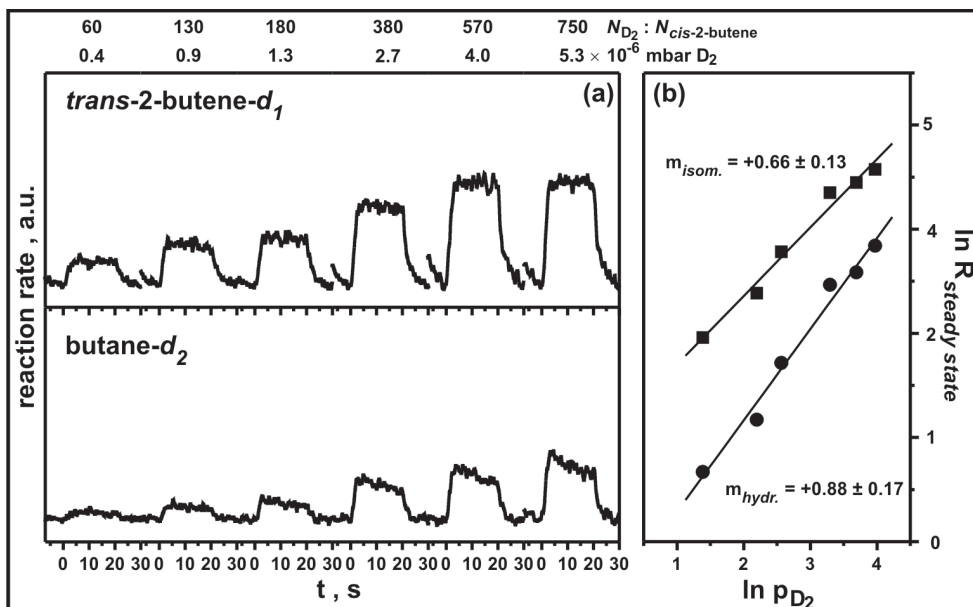


Figure 6.3: (a) Averaged reaction rates of the *cis-trans* isomerization (upper traces, *trans*-2-butene- $d_1$ ) and hydrogenation (lower traces, butane- $d_2$ ) pathways as a function of time obtained from a series of pulsed MB experiments over the C-precovered Pd/Fe<sub>3</sub>O<sub>4</sub> model catalyst at 260 K with a continuous  $D_2$  and a modulated *cis*-2-butene beam. While the *cis*-2-butene pressure was kept constant ( $2.7 \cdot 10^{-8}$  mbar), the  $D_2$  pressure was varied ( $0.4 - 5.3 \cdot 10^{-6}$  mbar). (b) Steady state reaction rates for isomerization (squares) and hydrogenation (circles) as a function of the  $D_2$  pressure plotted in a double logarithmic form together with linear fits.

### 6.2.1 Reactivity of the C-covered Pd/Fe<sub>3</sub>O<sub>4</sub> model catalyst

In fig. 6.3, the results of pulsed MB experiments at 260 K over the C-covered Pd/Fe<sub>3</sub>O<sub>4</sub> model catalyst at a constant *cis*-2-butene pressure are displayed for different  $D_2$  pressures. Fig. 6.3 (a) shows the averaged reaction rates obtained from the 30 last long pulses for different  $D_2$  pressures. For all experiments, the last 30 pulses of the individual experiment exhibited an identical pulse shape indicating that in all cases a quasi steady state reactivity was reached. The upper panel of fig. 6.3 (a) displays the averaged pulse profiles for the *cis-trans* isomerization product *trans*-2-butene- $d_1$ , while the results for the hydrogenation product butane- $d_2$  are shown in the lower panel.

In the applied  $D_2$  pressure range from  $0.4$  to  $5.3 \cdot 10^{-6}$  mbar, the steady state reaction rates for both isomerization and hydrogenation increase with increasing  $D_2$  pressure. In fig. 6.3 (b), the steady state reaction rates as a function of the  $D_2$  pressure are displayed in a double logarithmic form,  $\ln R$  vs.  $\ln p_{D_2}$ . For the hydrogenation pathway, the reaction rate does not always reach a constant value toward the end of the 2-butene pulse.

In this case, the rate value at the end of the 2-butene exposure was taken as a quasi steady state reaction rate. According to a general power law, the reaction rate  $R$  can be expressed as  $R = k \cdot p_{butene}^n \cdot p_{D_2}^m$  with  $k$  denoting the reaction rate constant,  $p_{butene}$  and  $p_{D_2}$  the partial pressures of *cis*-2-butene and D<sub>2</sub> and  $n$ ,  $m$  the formal reaction orders in *cis*-2-butene and D<sub>2</sub> pressure, respectively. In a plot of  $\ln R$  vs.  $\ln p_{D_2}$ , at a constant *cis*-2-butene pressure, the slope of the curve gives the formal reaction order in D<sub>2</sub> pressure  $m$ . As displayed in fig. 6.3 (b), the isomerization and hydrogenation pathway exhibit reaction orders of  $m_{isom.} = +0.66 \pm 0.13$  and  $m_{hydr.} = +0.88 \pm 0.17$ . These values are in good agreement with results by Somorjai *et al.* [183] who reported reaction orders close to unity for both isomerization and hydrogenation of *cis*-2-butene over Pt(111). Also under ambient pressure conditions, typically a formal reaction order around unity is found for olefin hydrogenation over Pd catalysts [31, 32, 34–38, 190] indicating that our model system reproduces the macroscopic trend observed for realistic conditions.

It can be attempted to rationalize the obtained formal reaction orders based on a kinetic model assuming a Langmuir-Hinshelwood mechanism for a low surface coverage and non-competitive adsorption for 2-butene and D<sub>2</sub>. It should be noted that the kinetic model is based on a mean field approximation which implies that the reactive species are homogeneously distributed and that all adsorption sites exhibit an identical reactivity. For the Pd particles exhibiting a variety of adsorption sites, these assumptions are likely not completely fulfilled. Rather than obtaining a complete agreement of the model and the experimental results, comparison of the experimental data with this mean field kinetic model allows to identify reaction steps which can be correctly described by a mean field approximation and those steps that deviate from the predictions. Based on this analysis, information on the structure sensitivity of these reaction steps can be obtained.

Under steady state conditions, the surface concentrations of the main reaction intermediates on the surface, *cis*-2-butene- $d_0$  (for simplicity denoted *butene*- $d_0$  in the kinetic equations) and 2-butyl- $d_1$ , are constant and can be expressed as:

$$\begin{aligned} \frac{d[butene-d_0]}{dt} &= flux_B \cdot S_B - k_{des,B} \cdot [butene-d_0] - k_{hydr1} \cdot [butene-d_0][D] + k'_{el} \cdot [butyl-d_1] \\ &= 0 \end{aligned} \quad (6.1)$$

$$\begin{aligned} \frac{d[butyl-d_1]}{dt} &= k_{hydr1} \cdot [butene-d_0][D] - k'_{el} \cdot [butyl-d_1] - k_{el} \cdot [butyl-d_1] - k_{hydr2} \cdot [butyl-d_1][D^*] \\ &= 0 \end{aligned} \quad (6.2)$$

with  $[butene-d_0]$  signifying the *cis*-2-butene coverage,  $[butyl-d_1]$  the coverage of the 2-butyl- $d_1$  intermediate and  $[D]$  the coverage surface adsorbed D;  $flux_B$  and  $S_B$  denote the flux and sticking coefficient of *cis*-2-butene, respectively;  $k_{des,B}$  is the rate constant for *cis*-2-butene desorption (step 1' in fig. 6.1);  $k_{hydr1}$  and  $k_{hydr2}$  denote the rate constants of the first and second half-hydrogenation step (step 2 and 4 in fig. 6.1), correspondingly; and  $k'_{el}$  and  $k_{el}$  are the rate constants for the  $\beta$ -hydride elimination to *cis*-butene- $d_0$  and

*trans*-2-butene- $d_1$  (step 2' and 3 in fig. 6.1), respectively.

$[D^*]_{st.st.}$  signifies the steady state concentration of a second type of deuterium species that participates in the second half-hydrogenation step, from butyl- $d_1$  to butane- $d_2$ . The  $D^*$  species is associated with subsurface absorbed D. It is however important to emphasize that no assumptions on the exact physical nature of this D species are made in this model. As mentioned before, the  $D^*$  species involved in the second half-hydrogenation step can be either directly subsurface absorbed D or surface adsorbed D which is modified in its adsorption and/or electronic properties by the presence of subsurface D. For simplification, it can be assumed that  $[D^*]$  is under steady state conditions directly proportional to the concentration of surface adsorbed D with the proportionality factor  $\alpha$ :

$$[D^*]_{st.st.} = \alpha \cdot [D]_{st.st.} \quad (6.3)$$

If it is additionally assumed that only a negligible amount of butene- $d_0$  is formed from the decomposition of 2-butyl- $d_1$  compared to butene- $d_0$  formed by *cis*-2-butene adsorption from the gas phase, the following expressions are obtained for the steady state concentrations of the butene- $d_0$  and butyl- $d_1$  intermediates:

$$[butene-d_0]_{st.st.} = \frac{flux_B \cdot S_B}{k_{hydr1} \cdot [D] + k_{des,B}} \quad (6.4)$$

$$[butyl-d_1]_{st.st.} = \frac{flux_B \cdot S_B \cdot k_{hydr2} \cdot [D]}{(k_{hydr1} \cdot [D] + k_{des,B}) \cdot (k_{hydr2} \cdot [D^*] + k'_{el} + k_{el})} \quad (6.5)$$

and the reaction rates for *cis-trans* isomerization ( $R_{isom}$ ) and hydrogenation ( $R_{hydr}$ ) can be expressed as:

$$R_{isom} = k_{el} \cdot [butyl-d_1] \approx \frac{flux_B \cdot S_B \cdot k_{hydr1} \cdot k_{el} \cdot [D]}{(k_{hydr1} \cdot [D] + k_{des,B}) \cdot (k_{hydr2} \cdot [D^*] + k'_{el} + k_{el})} \quad (6.6)$$

$$R_{hydr} = k_{hydr2} \cdot [D^*] \cdot [butyl-d_1] \approx \frac{flux_B \cdot S_B \cdot k_{hydr1} \cdot k_{hydr2} \cdot [D^*] \cdot [D]}{(k_{hydr1} \cdot [D] + k_{des,B}) \cdot (k_{hydr2} \cdot [D^*] + k'_{el} + k_{el})} \quad (6.7)$$

For surface adsorbed deuterium  $[D]$ , the concentration under steady state conditions can be expressed as:

$$\begin{aligned} \frac{d[D]}{dt} &= 2 \cdot flux_{D_2} \cdot S_{D_2} - k_{des,D} \cdot [D]^2 - k_{hydr1} \cdot [butene-d_0][D] - k_{hydr2} \cdot [butyl-d_1][D^*] \\ &= 0 \end{aligned} \quad (6.8)$$

with  $flux_{D_2}$  denoting the  $D_2$  flux,  $S_{D_2}$  the  $D_2$  sticking coefficient and  $k_{des,D}$  the rate constant for associative  $D_2$  desorption (step 5').

A correct analytical solution for this system of kinetic equations that are all depending on each other is not trivial and beyond the scope of this work. In order to circumvent this

problem, two limiting cases can be considered. In the first case, it can be assumed that only a negligible fraction of surface D is consumed by the reactions with hydrocarbons, so that the surface concentration of  $[D]_{st.st.}$  is mainly controlled by the adsorption and desorption of D<sub>2</sub>. This assumption is well justified for the applied conditions considering that all the experiments are carried out under a large excess of D<sub>2</sub> in the gas phase compared to the *cis*-2-butene flux. For this first case, the steady state D coverage can be expressed as:

$$[D]_{st.st.} = \left( \frac{2 \cdot flux_{D_2} \cdot S_{D_2}}{k_{des,D}} \right)^{\frac{1}{2}} \quad (6.9)$$

For a second limiting case, it is possible to assume that D is mainly consumed in reactions with 2-butene and that D desorption is negligible. Admittedly, this assumption seems due to the large excess of D<sub>2</sub> in the gas phase not applicable for the experimental conditions used in this study. However, inhibited D<sub>2</sub> adsorption by co-adsorbed hydrocarbons could possibly result in relatively low D surface concentrations which can potentially lead to a relative increase of D consumption in conversion reactions with 2-butene. Also, associative desorption of D may be slow under the applied reaction conditions either due to relatively low temperatures and/or due to co-adsorbed hydrocarbons breaking up ensembles of free adsorption sites which are necessary for associative D<sub>2</sub> adsorption [104, 110, 111]. For this second case, assuming that D depletion is governed by consumption in conversion reaction with 2-butene and 2-butyl and that D desorption can be neglected, the steady state D coverage can be expressed as:

$$[D]_{st.st.} = \frac{2 \cdot flux_{D_2} \cdot S_{D_2}}{k_{hydr1} \cdot [butene-d_0] + k_{hydr2} \cdot [butyl-d_1]} \quad (6.10)$$

If the following conditions are fulfilled

$$k_{des,B} \gg k_{hydr1} \cdot [D] \quad (6.11)$$

and

$$k'_{el} + k_{el} \gg k_{hydr2} \cdot \alpha [D] \quad (6.12)$$

the reaction rates for both isomerization and hydrogenation are expected to depend positively on the D<sub>2</sub> pressure. Conditions 6.11 and 6.12 imply that the rate of 2-butene desorption is significantly faster than the rate of 2-butene conversion in the first half-hydrogenation step to 2-butyl and that the rate of  $\beta$ -hydride elimination of 2-butyl is faster than the rate of the second half-hydrogenation from 2-butyl to butane.

For the first limiting case, when D depletion is governed by associative D<sub>2</sub> desorption, an upper limit of 0.5 is predicted for the formal isomerization reaction order with respect to the D<sub>2</sub> pressure. For the hydrogenation product, an upper limit of unity is expected for this case. In contrast, when consumption of D in conversion reactions with the hydrocarbons prevails, for the isomerization an upper limit of 1 and for hydrogenation an upper limit of 2 is expected for the formal reaction orders with respect to the

$D_2$  pressure. Deviations from these limiting values are expected either when both D desorption and D consumption in reactions with butene significantly contribute to D depletion or when conditions 6.11 and/or 6.12 are not strictly fulfilled. Moreover, the model is based on a low surface coverage and non-competitive adsorption of *cis*-2-butene and  $D_2$  adsorption as well as on the assumption that  $[D^*]$  is directly proportional to  $[D]$  which may be overly simplified.

The experimentally observed value for the reaction order of the isomerization pathway is +0.7 and lies thus, between the two values predicted by the two limiting cases. An experimental value higher than +0.5, expected as upper limit for a situation where D depletion is governed by desorption, indicates that D consumption in conversion reactions may contribute significantly to D depletion despite the large excess of  $D_2$  in the gas phase. In turn, an experimental value lower than unity which is expected for a situation where D is only consumed in conversion reactions with 2-butene may be caused by several effects. Either  $D_2$  desorption contributes to the depletion of surface D and/or *e.g.* condition 6.12, implying that butyl undergoes mainly  $\beta$ -hydride elimination and not a second half-hydrogenation step, is not strictly fulfilled. From the experimental conditions, it is expected that  $D_2$  desorption contributes significantly to the D depletion as a large excess of  $D_2$  in the gas phase is applied. But it also appears plausible that a significant amount of butyl undergoes a second half-hydrogenation step as indicated by the relatively high hydrogenation rates.

For the hydrogenation pathway a formal reaction order with respect to the  $D_2$  pressure of +0.9 is observed. This value is very close to the upper limit of unity expected for a situation where D depletion is governed by  $D_2$  desorption. The value of 2 expected for a situation where D consumption in conversion reactions with 2-butene prevails is clearly not in agreement with the experimentally observed reaction order of +0.9. Thus, the reaction order obtained for the hydrogenation pathway suggests that D depletion by desorption prevails, while the reaction order for *cis-trans* isomerization indicated that D consumption in conversion reactions with 2-butene is not negligible. The kinetic model is based on a number of simplifications, like a low surface coverage and non-competitive adsorption for *cis*-2-butene and  $D_2$ , while the conditions in the experiments are expected to be significantly more complex. Apart from the simplifications concerning both isomerization and hydrogenation similarly, the assumption that the  $D^*$  concentration is directly proportional to the concentration of surface D (eq. 6.3) affects mostly the hydrogenation pathway. A more precise, however still strongly simplified rate equation for the  $[D^*]$  species under steady state conditions is:

$$\frac{d[D^*]}{dt} = k_{form} \cdot [D] - k_{back} \cdot [D^*] - k_{hydr2} \cdot [butyl-d_1] \cdot [D^*] = 0 \quad (6.13)$$

If, thus, just  $[D^*]$  consumption in the second half-hydrogenation step is additionally

taken into account,  $[D^*]_{st.st.}$  is given by:

$$[D^*]_{st.st.} = \frac{k_{form} \cdot [D]}{k_{back} + k_{hydr2} \cdot [butyl-d_1]} \quad (6.14)$$

Following equation 6.2, the 2-butyl concentration depends positively on the  $[D]$  concentration which results for  $[D^*]$  and consequently also for the hydrogenation in a *reduced* reaction order with respect to the D<sub>2</sub> pressure. In contrast, the isomerization rate, which does not directly depend on the D\* concentration, is expected to be influenced only to a much smaller extend by this over-simplification.

In summary, the model obviously does not have enough detail to predict the experimentally observed reaction orders precisely. The overall agreement of the experimental and the predicted reaction orders is however quite good indicating that the assumed mechanism is in general reasonable.

A qualitative analysis of the temporal evolution of the reaction rates can help to better understand the microscopic processes taking place on the surface. In fig. 6.4, pulse profiles of the isomerization (upper traces, *trans*-2-butene-*d*<sub>1</sub>) and the hydrogenation (lower traces, butane-*d*<sub>2</sub>) products are depicted for five D<sub>2</sub> pressures in the pressure range from 0.9 to  $5.3 \cdot 10^{-6}$  mbar. For a more convenient examination of the changes in the pulse shapes, the pulse heights are normalized. At the two highest applied D<sub>2</sub> pressures, the pulse profiles of the isomerization product *trans*-2-butene-*d*<sub>1</sub> display a roughly rectangular shape following the temporal evolution of the reactant *cis*-2-butene attesting to equal reaction rates in the steady state regime as on the D-saturated surface. This indicates that the rates are not limited by a reduced availability of D due to co-adsorbed 2-butene. Consequently, each of the steps (1), (2) or (3) can potentially be rate limiting (see fig. 6.1). It is generally agreed that  $\beta$ -hydride elimination from butyl is fast compared to the formation of butyl species [193, 194], so that this step is not expected to be rate limiting. Consequently, the isomerization is either limited by the rate of *cis*-2-butene adsorption (step 1 in fig. 6.1) or by formation of the butyl intermediate (step 2 in fig. 6.1). Analysis of the kinetic model implied that *cis*-2-butene desorption is presumably faster than the first half-hydrogenation step to 2-butyl (see condition 6.11,  $k_{des,B} \gg k_{hydr1} \cdot [D]$ ), so that formation of the 2-butyl species is most likely the rate limiting step in the *cis-trans* isomerization pathway.

The hydrogenation product butane-*d*<sub>2</sub> shows, in contrast, at these D<sub>2</sub> pressures initially high reaction rates that decrease over the length of the *cis*-2-butene pulse indicating a significant reduction of the D concentration in the presence of co-adsorbed 2-butene. It should be emphasized here again that under all applied conditions the reaction is carried out in a large excess of D<sub>2</sub> in the gas phase so that the concentration of D on the surface cannot simply be limited by an insufficient supply of D<sub>2</sub> from the gas phase. As indicated by the rectangular pulse profiles of the isomerization product, the concentrations of 2-butyl and surface adsorbed D remain basically constant under these

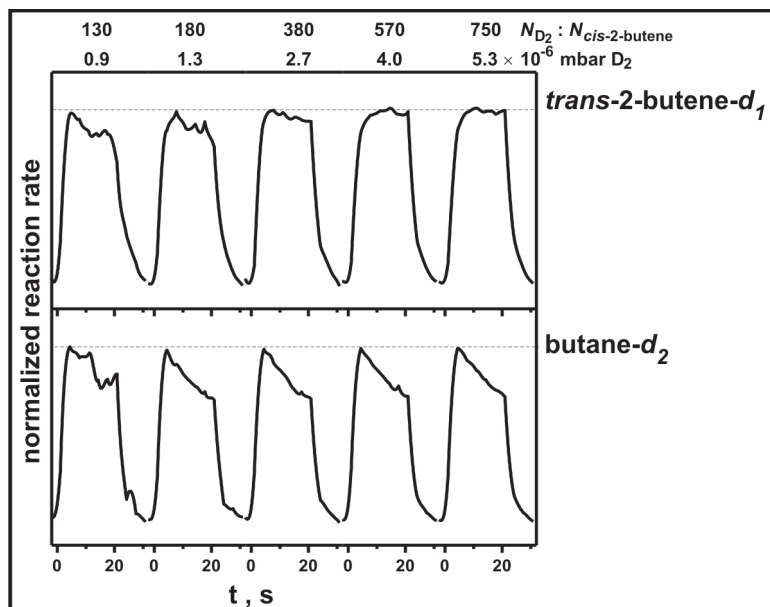


Figure 6.4: Normalized averaged reaction rates obtained for isomerization (upper traces) and hydrogenation (lower traces) in the experiments shown in fig. 6.3 for selected  $D_2$  pressures. At low  $D_2$  pressures the decreasing pulse shape indicates D-deficient steady state conditions for both reaction pathways. At higher  $D_2$  pressures, the rectangular pulse shape indicates for isomerization D-rich steady state conditions, while hydrogenation retains a decaying pulse form indicative of D-deficient steady state conditions.

conditions, so that the decreasing hydrogenation rate can be most likely explained by a decrease of the second D species,  $D^*$ , participating in the second half-hydrogenation step from 2-butyl to butane. At the beginning of the butene pulse, the  $D^*$  species are present in relatively high quantities, but become depleted during the butene pulse resulting in decreasing hydrogenation rates. The depletion of the  $D^*$  species, which are associated with subsurface adsorbed D (see chapter 5 for details), is probably caused by inhibition of D diffusion into the subsurface due to co-adsorbed hydrocarbons. It should be noted once more that a decrease of the hydrogenation rates cannot be due to a decrease of surface adsorbed, regular D as in this case a similar decrease for the isomerization product would be expected (see also 5).

At low  $D_2$  pressures, a different isomerization pulse shape is observed compared to higher  $D_2$  pressures. For low  $D_2$  pressures ( $N_{D_2} : N_{cis-2-butene} \leq 380$ ), the isomerization rate drops from an initially high value over the length of the *cis*-2-butene pulse to a lower steady state value implying that under these conditions also the concentration of regular surface adsorbed D decreases in the presence of co-adsorbed hydrocarbons most likely due to inhibited dissociative  $D_2$  adsorption. With increasing  $N_{D_2} : N_{cis-2-butene}$  ratios

( $\geq 570$ ), a smooth transition from a decreasing pulse shape at low ratios to a rectangular form at high  $D_2$  pressures is observed for the isomerization pathway. This implies that at low  $D_2$  pressures the replenishment of surface adsorbed D is insufficient to retain the initially high rates, while at higher  $N_{D_2}:N_{cis-2-butene}$  ratios the D replenishment is apparently fast under steady state conditions allowing to sustain the initially high rates. The onset of inhibited dissociative  $D_2$  adsorption can be estimated to begin at reactant ratios  $\leq 380$ .

Opposite to this, the hydrogenation product retains a decreasing pulse shape over the entire investigated  $D_2$  pressure range. The reaction rate at the end of the *cis*-2-butene pulse is in all cases diminished by  $\approx 30\%$  from the initial value. Whereas a smooth transition from D-deficient to D-rich steady state conditions is observed with increasing  $N_{D_2}:N_{cis-2-butene}$  ratios for the *cis-trans* isomerization, the hydrogenation profile indicates D-deficient steady state conditions over the entire  $D_2$  pressure range. Thus, there is clearly no correlation of the pulse profiles between the two reaction pathways. In line with the results presented in the previous chapter (5), this indicates that the hydrogenation pathway is governed by the temporal evolution of the concentration of a second D species,  $D^*$ , which is different from the regular, surface adsorbed D involved in the *cis-trans* isomerization. Obviously, the replenishment of the  $D^*$  species associated with subsurface adsorbed D, is under all applied conditions slowed down by co-adsorbed hydrocarbons, even when there are no limitations in the availability of surface adsorbed D. This indicates that co-adsorbed hydrocarbons negatively affect D diffusion into the subsurface. The extent of this inhibition is obviously larger than the inhibition of dissociative  $D_2$  adsorption as there is no transition to D-rich conditions observed for the hydrogenation in the investigated  $D_2$  pressure range. The stronger inhibition of D diffusion into the subsurface compared to the dissociative adsorption most likely originates from different microscopic mechanisms of these processes.

## 6.2.2 Reactivity of the C-free Pd/Fe<sub>3</sub>O<sub>4</sub> model catalyst

In fig. 6.5 (a), the averaged pulse profiles for the *cis-trans* isomerization and hydrogenation products obtained for different  $D_2$  pressures over the initially C-free Pd/Fe<sub>3</sub>O<sub>4</sub> model catalyst are displayed. For a more convenient comparison, next to the results obtained from the C-free Pd particles (black), also the averaged pulse profiles measured for the C-precovered catalyst are displayed (gray). The steady state *cis-trans* isomerization rates (upper trace, *trans*-2-butene- $d_1$ ) over the C-free Pd particles increase linearly with increasing  $D_2$  pressure. In contrast to the C-precovered Pd model catalyst, no significant hydrogenation rates are observed for the C-free surface after prolonged olefin exposure even at the highest applied  $D_2$  pressure (lower trace, butane- $d_2$ ). It is important to note, that for all applied reaction conditions, initially high hydrogenation rates are observed also over the C-free Pd catalyst at the beginning of the experiment. These rates vanish, however, for longer olefin exposures presumably due to inhibited D diffusion into the subsurface (see chapter 5 for details).



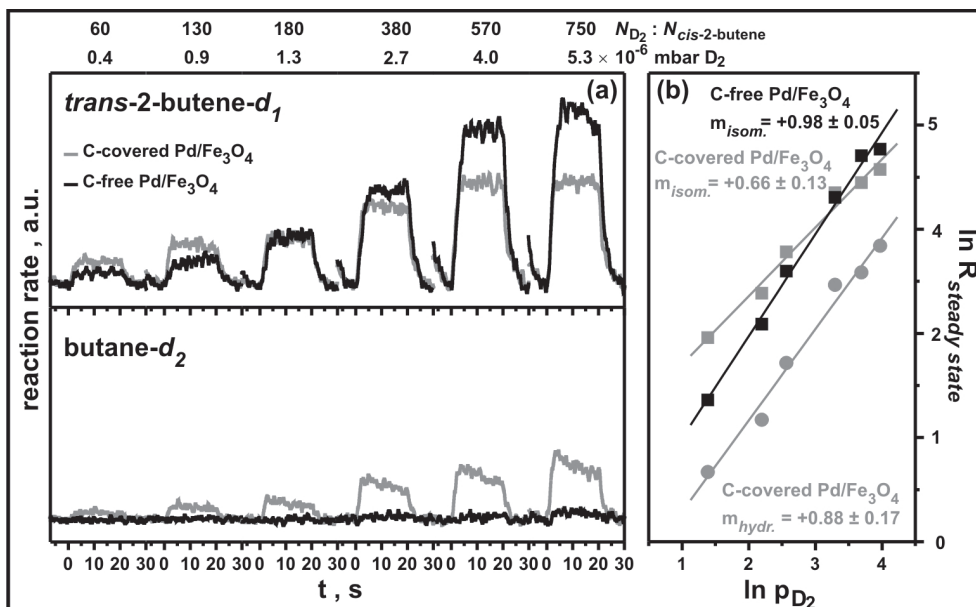


Figure 6.5: (a) Averaged reaction rates of the *cis-trans* isomerization (upper traces, *trans*-2-butene- $d_1$ ) and hydrogenation (lower traces, butane- $d_2$ ) pathways as a function of time obtained from a series of pulsed MB experiments over the C-free (black) Pd/Fe<sub>3</sub>O<sub>4</sub> model catalyst at 260 K with a continuous  $D_2$  exposure and a modulated *cis*-2-butene beam. While the *cis*-2-butene pressure was kept constant ( $2.7 \cdot 10^{-8}$  mbar), the  $D_2$  pressure was varied ( $0.4 - 5.3 \cdot 10^{-6}$  mbar). (b) Steady state reaction rates for isomerization (squares) and hydrogenation (circles) as a function of the  $D_2$  pressure plotted in a double logarithmic form together with linear fits. For comparison, the data obtained over the C-covered model catalyst is also displayed (gray).

Fig. 6.5 (b) displays the plot of the steady state isomerization rates as a function of the  $D_2$  pressure in a double logarithmic form,  $\ln R$  vs.  $\ln p_{D_2}$ , with the slope of the plot giving the formal reaction order with respect to the  $D_2$  pressure (see 6.2.1). Next to the data for the C-free catalyst (black), also the steady state isomerization and hydrogenation rates, obtained from C-precovered catalyst (gray), are shown for comparison. For the *cis-trans* isomerization over the C-free catalyst, a formal reaction order of  $+0.98 \pm 0.05$  is obtained which agrees well with the reaction order of close to unity reported by Somorjai *et al.* [183] for isomerization of *cis*-2-butene over Pt(111).

For the kinetic model introduced in the previous section (6.2.1), two limiting cases were considered. In the first case, depletion of surface adsorbed D was assumed to be governed by  $D_2$  desorption resulting for *cis-trans* isomerization in an upper limit of +0.5 for the formal reaction order in  $D_2$  pressure. In the second case, D consumption in conversion reactions with butene was assumed to prevail giving upper limit of unity for the

reaction order in  $D_2$  pressure. The latter value clearly coincides with the experimentally observed  $+0.98 \pm 0.05$  implying that D depletion is strongly governed by D consumption in reactions with 2-butene. In contrast, the formal reaction orders obtained for isomerization and hydrogenation over the C-covered Pd particles rather suggested a strong contribution of  $D_2$  desorption in the depletion of  $[D]$ .

As previously discussed, due to the large excess of  $D_2$  in the gas phase, the D concentration on the surface is expected to be significantly higher than the 2-butene coverage. Therefore, it seems unlikely that a large part of the D coverage is consumed in reactions with a relatively small number of olefins on the surface. A situation where D depletion is governed by D consumption in conversion reactions can, however, also arise when the  $D_2$  desorption rate under reaction conditions is slow, *e.g.* due to a relatively high activation energy for associative  $D_2$  desorption and/or due to co-adsorbed hydrocarbons breaking up ensembles of free adsorption sites which are required for the recombination of  $D_2$ . A possible explanation for a higher contribution of  $D_2$  desorption in D depletion over the C-covered Pd particles is that deposition of C leads to an overall weaker binding of hydrogen on the Pd particles as indicated by TPD measurements [195]. Microscopically, this effect may be caused by destabilization of surface D in the vicinity of C [125, 128, 196] and/or due to a more effective replenishment of weakly-bound subsurface D under reaction conditions which may lead itself to an additional destabilization of the surface adsorbed D [113, 116, 117, 188]. A reduced binding of hydrogen in the presence of C is expected to result in a relative increase of the  $D_2$  desorption compared to C-free Pd model catalyst as suggested from the analysis of the reaction orders based on the kinetic model. In any case, it should be kept in mind that the kinetic model is based on a number of simplifying assumptions that do not exhibit enough detail to describe the complex experimental conditions accurately.

A qualitative analysis of the temporal evolution of the isomerization rates over the C-free Pd/Fe<sub>3</sub>O<sub>4</sub> model catalyst may aid in the understanding of the processes occurring on the catalyst. The averaged pulse profiles are displayed in fig. 6.6 with the pulse heights normalized for a more convenient examination. It can be seen that the isomerization over the C-free Pd model catalysts exhibits a rectangular pulse shape basically over the entire  $D_2$  pressure range indicating that the steady state reaction rates are *not* reduced compared to the rates at the beginning of the olefin pulse. In other words, the D concentration is *not* significantly reduced by reactions with 2-butene. These results support the assumption that the D concentration on the surface is high and thus, not significantly reduced by reactions with a relatively small number of olefins as implied by the large excess of  $D_2$  in the gas phase.

At the highest applied  $D_2$  pressure (see fig. 6.6), a different pulse shape is observed for *cis-trans* isomerization over the C-free catalysts than at lower  $N_{D_2}:N_{cis-2-butene}$  ratios. For this  $D_2$  pressure, the steady state reaction rates are lower than the isomerization rates observed at the beginning of the 2-butene pulse indicating that the D concentration under steady state conditions is decreased compared to the beginning of the olefin pulse.

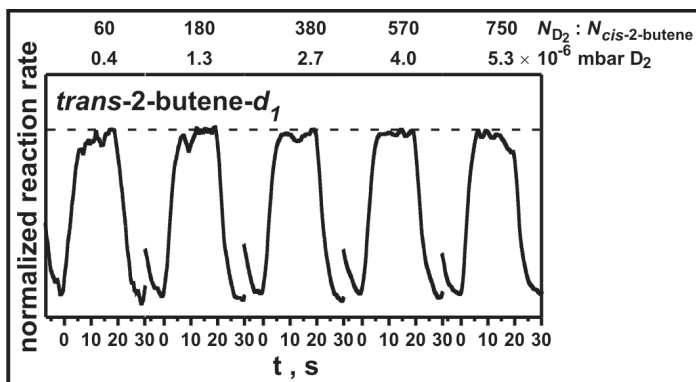


Figure 6.6: Normalized averaged reaction rates obtained for isomerization in the experiments over the C-free Pd/Fe<sub>3</sub>O<sub>4</sub> model catalyst shown in fig. 6.5 for selected  $D_2$  pressures. A rectangular pulse shape is observed for all  $D_2$  pressures except for the highest applied indicating that the D abundance is not significantly changed during the olefin exposure. For the highest applied  $D_2$  pressure, a decreasing pulse form is found indicating that the D concentration in the steady state is lowered.

This pulse shape is very unexpected and stands in strong contrast to the evolution of the pulse shape observed for the C-covered Pd catalyst where a transition from decreasing pulse shapes at low  $N_{D_2} : N_{cis-2-butene}$  ratios to a rectangular pulse shape at higher  $D_2$  pressures was observed. For a higher  $D_2$  pressure, while keeping the *cis*-2-butene flux constant, it is neither expected that the D consumption in conversion with 2-butene is increased compared to lower  $N_{D_2} : N_{cis-2-butene}$  ratios nor that the dissociative  $D_2$  adsorption is more likely inhibited by co-adsorbed hydrocarbons. Thus, the underlying microscopic processes are not obvious.

It can be speculated that for this high  $D_2$  pressure, the surface concentration of D becomes sufficiently high to significantly lower the adsorption strength and thereby, the surface concentration of strongly bound butene/hydrocarbons to allow in turn for a more effective replenishment of D when no butene is supplied from the gas phase. From TPD measurements, it is known that co-adsorbed H(D) considerably lowers the adsorption strength of alkenes [43, 53, 150] resulting in a decrease of the temperature of maximum desorption (140 K for *cis*-2-butene adsorbed on D-saturated Pd particles) with respect to the H(D)-free surface (250 K for *cis*-2-butene adsorbed on H(D)-free Pd particles) [150].

In summary, the isothermal pulsed MB measurements on the *cis*-2-butene conversion with  $D_2$  over C-free and C-covered Pd particles at 260 K as a function of the  $D_2$  pressure showed that the reaction can be roughly described by a kinetic model based on a Langmuir-Hinshelwood mechanism assuming a low surface coverage. This relatively simple model displayed however not enough detail to reproduce all observed effects. Analysis

of the evolution of the pulse profiles showed that processes involving D strongly effect the reactivity of the catalyst. Evidence was found that co-adsorbed hydrocarbons may inhibit both the dissociative adsorption of  $D_2$  as well as D diffusion to subsurface sites in the Pd particles. The results obtained for the C-precovered model catalyst indicate that the inhibiting effect of co-adsorbed hydrocarbons is more pronounced for the D diffusion into the subsurface compared to the dissociative adsorption of  $D_2$ . The pulse profiles observed for isomerization over the C-free catalyst suggested that only a small part of the surface adsorbed D is consumed in reactions with the olefins as expected from the large excess of  $D_2$  in the gas phase applied in all experiments.

### 6.3 Dependence on the *cis*-2-butene pressure

Similarly, the influence of the *cis*-2-butene pressure on the *cis*-2-butene conversion with  $D_2$  over the C-free and the C-covered Pd/Fe<sub>3</sub>O<sub>4</sub> model catalyst at 260 K was investigated by isothermal pulsed MB experiments. While the  $D_2$  pressure was kept constant at  $4.0 \cdot 10^{-6}$  mbar ( $\text{flux}_{D_2} = 3.2 \cdot 10^{15}$  molecules $\cdot\text{cm}^{-2}\cdot\text{s}^{-1}$ ), the *cis*-2-butene pressure was varied in three coarse steps to 1.2, 2.7 and  $40.9 \cdot 10^{-8}$  mbar corresponding to  $N_{D_2}:N_{\text{cis-2-butene}}$  ratios ranging from 1280 to 40. The pulsed MB experiment were conducted at 260 K using the same pulse sequence as described previously (6.2 and 5).

#### 6.3.1 Reactivity of the C-covered Pd/Fe<sub>3</sub>O<sub>4</sub> model catalyst

In fig. 6.7 (a), the averaged pulse profiles for the isomerization (upper trace) and hydrogenation (lower trace) pathway obtained from measurements over the C-precovered Pd model catalyst are displayed. At the lowest applied *cis*-2-butene pressure, both the isomerization and hydrogenation products display a roughly rectangular pulse profile following the temporal evolution of the reactant *cis*-2-butene. At the highest applied olefin pressure, both reaction pathways exhibit high reaction rates at the beginning of the 2-butene pulse that abruptly decrease within a few seconds to a significantly lower steady state value. The pulse profiles observed at the intermediate *cis*-2-butene pressure differ for isomerization and hydrogenation. While the isomerization product *trans*-2-butene-*d*<sub>1</sub> exhibits a roughly rectangular pulse profile, the hydrogenation rates decrease to a lower steady state level.

A qualitative analysis of the pulse shape suggests an interpretation for the microscopic processes taking place on the surface. At the lowest butene pressure ( $1.2 \cdot 10^{-8}$  mbar), the pulse form shows that both *cis-trans* isomerization and hydrogenation simply follow the temporal evolution of the reactant *cis*-2-butene indicating that the D concentration is not significantly reduced under steady state conditions for either reaction pathway. Both reactions are obviously limited under these conditions either by *cis*-2-butene adsorption (step 1) or by the formation of the 2-butyl intermediate (step 2). As mentioned earlier,  $\beta$ -hydride elimination from the butyl intermediate is generally believed to be fast, so that it cannot be the rate limiting step [193, 194]. According to the analysis of the kinetic model, the rate determining step in the *cis-trans* isomerization is likely the

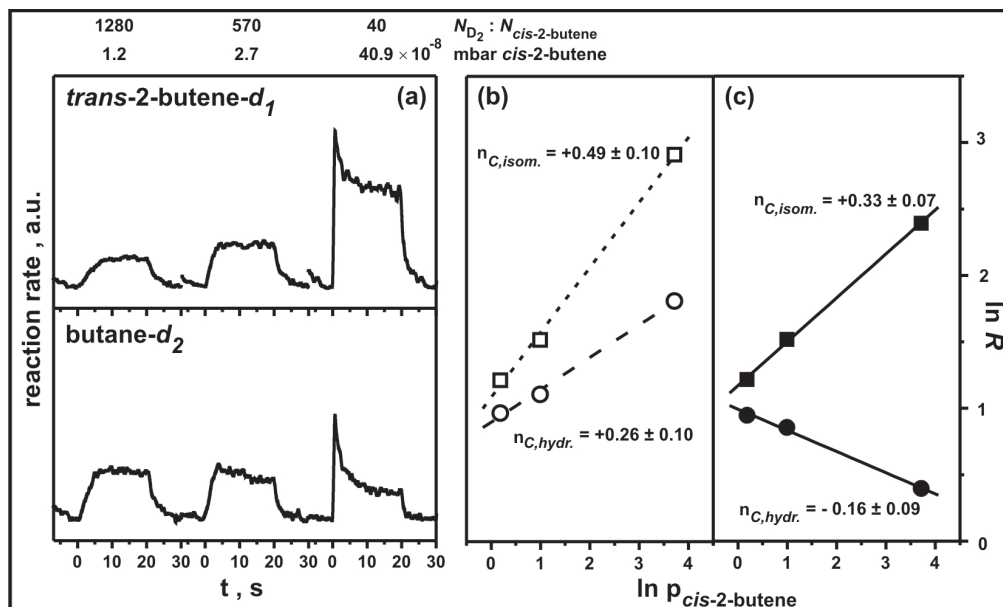


Figure 6.7: (a) Averaged reaction rates of the *cis*-*trans* isomerization (upper traces, *trans*-2-butene-*d*<sub>1</sub>) and hydrogenation (lower traces, butane-*d*<sub>2</sub>) pathways as a function of time obtained from a series of pulsed MB experiments over the C-precovered Pd/Fe<sub>3</sub>O<sub>4</sub> model catalyst at 260 K with a continuous D<sub>2</sub> exposure and a modulated *cis*-2-butene beam. While the D<sub>2</sub> pressure was kept constant ( $4.0 \cdot 10^{-6}$  mbar), the *cis*-2-butene pressure was varied in three steps (1.2, 2.7 and  $40.9 \cdot 10^{-8}$  mbar). Initial (b) (open symbols) and steady state (c) (full symbols) reaction rates for isomerization (squares) and hydrogenation (circles) as a function of the D<sub>2</sub> pressure plotted in a double logarithmic form together with linear fits.

first half-hydrogenation step leading to the formation of the 2-butyl species.

For the intermediate *cis*-2-butene pressure ( $2.7 \cdot 10^{-8}$  mbar), a rectangular pulse shape is observed for the isomerization pathway implying that the concentration of surface adsorbed D is not significantly reduced under steady state conditions, while a decreasing pulse profile for the hydrogenation pathway indicates D-deficient conditions in the steady state. As discussed previously (see 5 and 6.2), this behavior attests to the more pronounced inhibition by co-adsorbed hydrocarbons of D diffusion into the subsurface which is required for the hydrogenation to proceed effectively. In contrast, dissociative D<sub>2</sub> adsorption required for effective isomerization activity is feasible under these conditions.

At the highest *cis*-2-butene pressure ( $40.9 \cdot 10^{-8}$  mbar), both isomerization and hydrogenation show initially high reaction rates that significantly decrease over the length of the butene pulse. This is most easily explained by a strong reduction of the D availability

under steady state conditions affecting both reaction pathways, *i.e.* the concentrations of both surface and subsurface D are considerably decreased by co-adsorbed hydrocarbons. The high *cis*-2-butene pressure leads seemingly to a relatively high surface concentration of hydrocarbon species poisoning the surface for D sorption by *e.g.* inhibition of the dissociative D<sub>2</sub> adsorption and/or D diffusion into the subsurface. It should be emphasized again that even under these conditions, the reaction is conducted in a large excess of D<sub>2</sub> in the gas phase ( $N_{D_2}:N_{cis-2-butene} = 40$ ) so that the decrease in D availability under steady state conditions cannot be simply due to an insufficient supply of D<sub>2</sub> from the gas phase. Thus, dissociative D<sub>2</sub> adsorption required both for the formation of 2-butyl and [*D*\*] species can be identified as a slow, rate determining process under these conditions.

In agreement with the interpretation of the results in the previous section (6.2), the analysis of the pulse profiles as a function of the *cis*-2-butene pressure indicates that the hydrogenation pathway is negatively affected already at lower *cis*-2-butene pressures or corresponding higher  $N_{D_2}:N_{cis-2-butene}$  ratios than the *cis-trans* isomerization. Thus, relatively high concentrations of co-adsorbed hydrocarbons can be adsorbed without affecting the concentration of surface adsorbed D significantly ( $N_{D_2}:N_{cis-2-butene} > 380$ ), while a clear inhibition of the D diffusion into the subsurface by co-adsorbed hydrocarbons is observed already at much higher  $N_{D_2}:N_{cis-2-butene}$  ratios ( $< 1280$ ).

Next a quantitative analysis of the initial rates in the transient regime and the steady state rates at the end of the olefin pulse was performed. In fig. 6.7, the initial (fig. 6.7 (b)) and steady state (fig. 6.7 (c)) rates are displayed as a function of the *cis*-2-butene pressure in a double logarithmic form. For a constant D<sub>2</sub> pressure, the slope of this plot gives the formal reaction order with respect to the *cis*-2-butene pressure (see also 6.2). The initial rates were calculated by determining the reaction rates after a *cis*-2-butene exposure of 0.33 L (the time when this exposure was reached depends on the 2-butene flux). If the reaction rates did not reach a constant value at the end of the olefin exposure, the reaction rate at the end of the pulse was taken as a quasi steady state value.

For the transient regime, the initial rates increase for both *cis-trans* isomerization and hydrogenation with increasing *cis*-2-butene pressure. The formal reaction order for the initial rates are  $n_{isom} = +0.49 \pm 0.10$  for the isomerization and  $n_{hydr} = +0.26 \pm 0.10$  for the hydrogenation pathway (see fig. 6.7 (b)). The steady state reaction rates of the *cis-trans* isomerization also increase with increasing *cis*-2-butene pressure. Under steady state conditions, the increase is however smaller compared to the transient regime resulting in a lower, but positive formal reaction order of  $n_{isom} = +0.33 \pm 0.07$  (see fig. 6.7 (c)). The hydrogenation rates under steady state conditions, contrary to the transient regime, decrease with increasing olefin pressure resulting in a formal reaction order of  $n_{hydr} = -0.16 \pm 0.09$ . The steady state reaction orders are in good agreement with values close to zero obtained from realistic catalytic studies [31, 33, 35–38, 183, 190] indicating that also the dependence on the olefin pressure is well reproduced by our model system.

Based on the Langmuir-Hinshelwood kinetic model introduced in section 6.2, it can

### 6.3 Dependence on the *cis*-2-butene pressure

be attempted to rationalize the observed reaction orders. For both isomerization and hydrogenation, the kinetic model predicts an upper limit of unity for the formal reaction order in *cis*-2-butene pressure. The experimentally observed values are in all cases clearly below this predicted upper limit. Information on the underlying microscopic processes can be obtained however from a comparison of the reaction orders in the transient regime with those obtained for steady state conditions. The reaction orders for both reaction pathways are clearly higher in the *transient* regime where the surface is saturated with D than in the steady state regime. Thus, when D is available in high concentrations, the reaction rate increases clearly with increasing 2-butene flux indicating that the surface concentration of 2-butene increases and that adsorbed D does not inhibit *cis*-2-butene adsorption, a condition implied by the kinetic model.

Under steady state conditions, the reaction orders are significantly lowered implying a strong deviation from the assumption of a low surface coverage and non-competitive butene and D<sub>2</sub> adsorption as assumed in the kinetic model. This drop in the reaction orders indicates that the replenishment of D is reduced under steady state conditions resulting in a weaker dependence of the reaction rates on the *cis*-2-butene pressure.

For the isomerization requiring the presence of surface D, the most likely reason for this reduction is poisoning of the surface for dissociative D<sub>2</sub> adsorption due to co-adsorbed hydrocarbon species. This conclusion is in agreement with the previously discussed analysis of the pulse profiles where a clearly non-rectangular pulse profile at the highest applied 2-butene pressure indicated a strongly reduced availability of surface D under steady state conditions.

For the hydrogenation, the reaction orders with respect to the olefin pressure are both in the transient and in the steady state regime clearly lower than the reaction orders obtained for the isomerization pathway. Under steady state conditions, even a slightly negative dependence is observed implying that the higher hydrocarbon concentration under steady state conditions has a negative effect on the abundance of D species required for hydrogenation. The change from a positive to a negative formal reaction order with respect to the *cis*-2-butene pressure may reflect a change in the rate limiting step with the replenishment of D species becoming rate-limiting. As indicated by our previous results (see chapter 5), the presence of subsurface hydrogen is required for the hydrogenation to proceed effectively. Based on this, it appears reasonable to assume that co-adsorbed hydrocarbons have a more *negative* effect on the abundance of subsurface adsorbed D in comparison to surface adsorbed D resulting in lower and even negative reaction orders in the olefin pressure for the hydrogenation pathway compared to *cis-trans* isomerization. This hypothesis is in line with the qualitative analysis of the pulse profiles where a decreasing pulse profile indicative for D-deficient conditions in the steady state was observed for the hydrogenation product already at the intermediate butene pressure, while the isomerization product displayed at this pressure a rectangular pulse shape implying that the surface D availability is not significantly reduced under steady state conditions. The microscopic reason for this effect is most likely strongly inhibited D

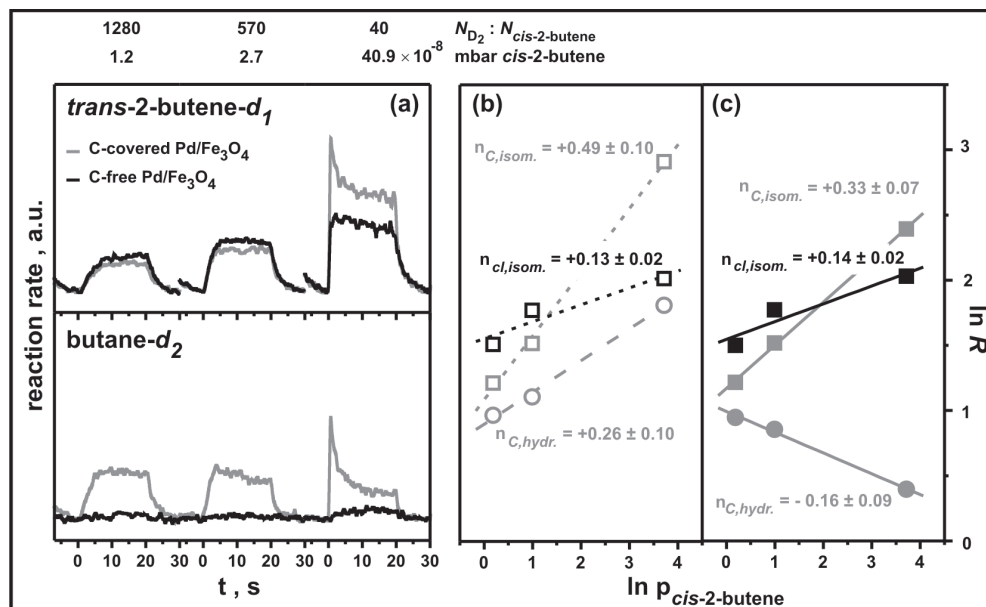


Figure 6.8: (a) Averaged reaction rates of the *cis-trans* isomerization (upper traces, *trans*-2-butene- $d_1$ ) and hydrogenation (lower traces, butane- $d_2$ ) pathways as a function of time obtained from a series of pulsed MB experiments over the C-free (black) Pd/Fe<sub>3</sub>O<sub>4</sub> model catalyst at 260 K with a continuous  $D_2$  exposure and a modulated *cis*-2-butene beam. While the  $D_2$  pressure was kept constant ( $4.0 \cdot 10^{-6}$  mbar), the *cis*-2-butene pressure was varied in three steps (1.2, 2.7 and  $40.9 \cdot 10^{-8}$  mbar). Initial (b) (open symbols) and steady state (c) (full symbols) reaction rates for isomerization (squares) and hydrogenation (circles) as a function of the  $D_2$  pressure plotted in a double logarithmic form together with linear fits. The data obtained for the C-covered Pd model catalyst is displayed for comparison (gray).

diffusion into the subsurface of Pd in the presence of co-adsorbed hydrocarbon species.

### 6.3.2 Reactivity of the C-free Pd/Fe<sub>3</sub>O<sub>4</sub> model catalyst

The dependence on the *cis*-2-butene pressure was also investigated for the C-free Pd model catalyst. The averaged pulses obtained from the isothermal pulsed MB experiments at 260 K at a constant  $D_2$  pressure ( $p_{D_2} = 4.0 \cdot 10^{-6}$  mbar) and three different 2-butene pressures are displayed in fig. 6.8 (a). Next to the results for the C-free Pd particles (black traces), also the pulses obtained from the C-precovered Pd particles (gray traces) are given for comparison.

From fig. 6.8, it can be seen that the isomerization rates over the C-free model catalyst increase with increasing *cis*-2-butene pressure. Over the C-free Pd model catalyst, no persisting hydrogenation activity is observed for the investigated reaction conditions.



### 6.3 Dependence on the *cis*-2-butene pressure

After initially high rates, the hydrogenation ceases due to inhibited D diffusion into the subsurface under reaction conditions.

For the two lower butene pressures ( $N_{D_2}:N_{cis-2-butene} \leq 570$ ), the isomerization product exhibits a rectangular pulse shape following the temporal evolution of the reactant *cis*-2-butene indicating that there is no significant reduction in the D abundance under steady state conditions. This behavior was also observed for the isomerization over a C-precovered surface. At the highest applied 2-butene pressure, a slightly decreasing pulse shape of the isomerization product indicates that the D concentration becomes reduced in the steady state. In comparison with isomerization over the C-covered particles, the drop in the reaction rate is however significantly smaller implying that the steady state D coverage on the C-free catalyst is less affected by the olefin supply from the gas phase. As previously discussed, the reduction of the D abundance is most likely due to inhibited dissociative  $D_2$  adsorption by co-adsorbed hydrocarbon species. A relatively lower inhibition of the dissociative  $D_2$  adsorption during the olefin exposure can either indicate that the D replenishment during the olefin exposure is more effective or that the D replenishment *before* the olefin exposure is *less* effective. The overall lower isomerization rate over the C-free catalyst at the highest 2-butene pressure suggests that the inhibition of the dissociative  $D_2$  adsorption is overall higher compared to the C-covered surface. In line with this, also the high initial rates over the C-covered Pd particles further indicate that the D replenishment before the olefin exposure is more effective in the presence of carbonaceous deposits.

Next a quantitative comparison of the formal reaction orders was performed. The initial and steady state isomerization rates are plotted in a double logarithmic form as a function of the *cis*-2-butene pressure in fig. 6.8 (b) and (c), respectively. For comparison, the data obtained for the C-precovered Pd/Fe<sub>3</sub>O<sub>4</sub> model catalyst is also shown (gray). The reaction rates for *cis-trans* isomerization over the C-free surface increases with increasing butene pressure both in the transient and in the steady state regime resulting in positive formal reaction orders. The formal reaction orders in the transient and in the steady state regime are with  $n_{isom,transient} = +0.13 \pm 0.02$  and  $n_{isom,st.st.} = +0.14 \pm 0.02$  basically identical. In contrast, a strong reduction of the formal steady state reaction order was observed for the C-covered Pd model catalyst which was attributed to a stronger inhibition of  $D_2$  sorption during the olefin exposure. This effect is clearly not observed for the C-free model catalyst. The formal reaction order for isomerization over the C-free surface is with  $+0.14 \pm 0.02$  in absolute numbers clearly smaller than the reaction orders over the C-covered surface, both in the initial and steady state regime ( $n_{isom} = +0.49 \pm 0.10$  and  $n_{isom} = +0.33 \pm 0.07$ , respectively). Following the same reasoning as before, that the reduction of the reaction order from the predicted value of unity can be attributed to inhibited  $D_2$  sorption by co-adsorbed hydrocarbon species, these results show that the  $D_2$  sorption is more strongly poisoned on the C-free than on the C-covered catalyst, especially in the transient, but also in the steady state regime. In line with the analysis of the pulse profiles, these results indicate that the D replenishment especially between the olefin pulses is more effective in the

presence of C.

There are two possible explanations for this C-induced effect: First, the binding strength of hydrocarbons can be reduced in the proximity of C [181, 195] which is expected to result in a lower hydrocarbon coverage compared to the C-free surface and thus, a decreased poisoning of the  $D_2$  sorption. Secondly, co-adsorbed D also can weaken the olefin adsorption strength [43, 53, 181, 197]. Especially, subsurface D - present on the C-covered, but not on the C-free surface under reaction conditions - is expected to lower the olefin binding strength resulting in turn, in an even more decreased poisoning of the surface for  $D_2$  sorption.

In summary, the isothermal pulsed MB experiment at 260 K at a constant  $D_2$  pressure and three different *cis*-2-butene pressures over the C-covered and the C-free Pd/Fe<sub>3</sub>O<sub>4</sub> model catalyst showed that co-adsorbed hydrocarbon species inhibit the  $D_2$  sorption. This inhibition is effective for subsurface adsorbed D already at lower butene pressures ( $N_{D_2}:N_{cis-2-butene} < 1280$ ) than for dissociative  $D_2$  adsorption ( $N_{D_2}:N_{cis-2-butene} < 570$ ). Compared to the C-covered Pd particles, the inhibition of  $D_2$  sorption by co-adsorbed hydrocarbons is more pronounced for the C-free surface, even for the formation of surface adsorbed D.

## 6.4 Temperature dependence

The activity and selectivity in the conversion of *cis*-2-butene with  $D_2$  over the C-covered and the C-free Pd/Fe<sub>3</sub>O<sub>4</sub> model catalyst as a function of temperature was investigated by isothermal pulsed MB beam experiments employing the same pulse sequence as in the preceding sections (6.2 and 6.3). The *cis*-2-butene and the  $D_2$  pressure were kept constant at  $2.7 \cdot 10^{-8}$  mbar and  $4.0 \cdot 10^{-6}$  mbar, respectively, corresponding to a  $N_{D_2}:N_{cis-2-butene}$  ratio of 570, while the temperature was varied in the range between 220 and 400 K for the C-covered Pd particles and between 220 and 340 K for the C-free Pd catalyst. In the first part of this section (6.4.1), the effect of the temperature on the 2-butene conversion over the C-covered model catalyst will be presented, while the second part (6.4.2) is dedicated to the activity and selectivity of the C-free Pd particles as a function of the temperature .

### 6.4.1 Reactivity of the C-covered Pd/Fe<sub>3</sub>O<sub>4</sub> model catalyst

Fig. 6.9 displays the averaged reaction rates of the last 30 long 2-butene pulses for *cis-trans* isomerization (upper trace, *trans*-2-butene-*d*<sub>1</sub>) and hydrogenation (lower trace, butane-*d*<sub>2</sub>) over the C-covered Pd/Fe<sub>3</sub>O<sub>4</sub> model catalyst obtained from a series of isothermal pulsed MB experiments at different temperatures between 220 and 400 K.

Both reaction pathways display a non-monotonic dependence on the reaction temperature reaching a maximum steady state reaction rate around  $T_{max,isom} = 240$  K for the *cis-trans* isomerization and around  $T_{max,hydr} = 300$  K for the hydrogenation pathway.

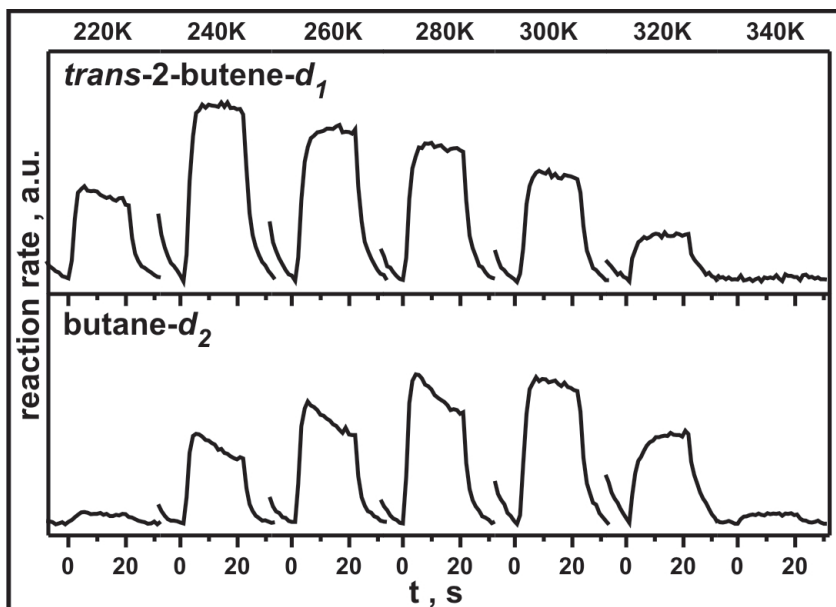


Figure 6.9: Averaged reaction rates as a function of time obtained for the *cis-trans* isomerization (upper traces, *trans*-2-butene-*d*<sub>1</sub>) and hydrogenation (lower traces, butane-*d*<sub>2</sub>) from a series of isothermal pulsed molecular beam experiments over the C-covered Pd/Fe<sub>3</sub>O<sub>4</sub> model catalyst. While the *cis*-2-butene and D<sub>2</sub> pressures were kept constant with a corresponding  $N_{D_2}:N_{cis-2-butene}$  ratio of 570, the reaction temperature was varied in the range between 220 and 400 K.

A maximum in the reaction rates with increasing temperature is also observed for olefin hydrogenation under ambient conditions [37, 191, 192] indicating that the model system reproduces this trend correctly. The *cis-trans* isomerization product *trans*-2-butene-*d*<sub>1</sub> exhibits almost for all studied temperatures a basically rectangular response curve. Only at 220 K, a slightly decreasing pulse shape is found. For the hydrogenation pathway, in contrast, nearly in the entire temperature regime a decaying pulse shape is observed and only above 300 K, rectangular pulse profiles are measured.

The appearance of a maximum with increasing temperature is due to two counteracting processes: On one hand, increasing temperatures lead to a rise of the elementary reaction rate constants, most importantly  $k_{hydr1}$  and  $k_{hydr2}$ , leading to higher reaction rates. On the other hand, also the rate constants for desorption increase, in particular  $k_{des,B}$  and  $k_{des,D}$ , leading to lower coverages of the reactants *cis*-2-butene and D<sub>2</sub> and thus, eventually to decreasing reaction rates. The initial growth of the reaction rates with increasing temperature, for isomerization between 220 – 240 K and for hydrogenation between 220 – 300 K, can be ascribed to an increase of the reaction rate constants  $k_{hydr1}$  and  $k_{hydr2}$  governing the activity in this temperature range. The decrease of the reaction

rates at higher temperatures, despite of the further increase of  $k_{hydr1}$  and  $k_{hydr2}$ , attests to predominant desorption of the reactants causing almost a vanishing of the reaction rates at 400 K. TPD experiments conducted on identical Pd particles support the hypothesis of fast *cis*-2-butene and D<sub>2</sub> desorption in this temperature range [43, 181, 197]. Since pre-adsorbed D weakens the adsorption strength of butene [43, 53, 181, 197] and thus, increasing D desorption is expected to lead to an augmented activation barrier for 2-butene desorption, the *cis*-2-butene coverage might depend in a very complex non-monotonic way on the temperature.

The observation of different positions of the rate maxima for *cis-trans* isomerization and hydrogenation clearly attests to different rate limiting steps for the two reaction pathways. As previously discussed in section 6.2, the isomerization rate reflects the formation rate of the 2-butyl-*d*<sub>1</sub> intermediate which is depending on the temperature either limited by *cis*-2-butene adsorption or the first half-hydrogenation step (step 1 and 2 in fig. 6.1, respectively). The temperature dependence of the isomerization pathway indicates thus, that the concentration of the butyl intermediate increases up to 240 K and decreases at higher temperatures. Despite the decreasing butyl concentration above 240 K, increasing hydrogenation rates are observed up to 300 K indicating that the rate constant of a different rate limiting step which must be the second half-hydrogenation (step 4) is even more strongly growing. From this, it can be derived that the activation barrier of the second half-hydrogenation of the butyl intermediate is higher than the activation barrier of the first half-hydrogenation. With this, direct experimental evidence is provided that the second half-hydrogenation step is rate limiting in olefin hydrogenation up to at least 300 K even in a large excess of D<sub>2</sub> which has been still under debate in the literature [198, 199].

Microscopically, there are two effects which may lead to a higher effective activation barrier of the second half-hydrogenation step compared to the first half-hydrogenation: a high barrier of the elementary reaction step of H(D) insertion into the carbon-metal bond of the butyl intermediate and/or activated D diffusion into the subsurface of the Pd particles. Based on the experimental results, a distinction between these two possibilities is difficult so that theoretical calculation are required to elucidate this question.

The *cis-trans* isomerization exhibits a rectangular pulse shape in almost the entire temperature regime indicating D-rich steady state conditions (see fig. 6.9). Only at the lowest temperature (220 K) a decreasing pulse form attesting to D-deficient steady state conditions is observed. In contrast, the hydrogenation pulse profiles display a decaying form up to 300 K implying thus, that the concentration of D\* (associated with subsurface absorbed D) is decreased during the olefin exposure up to 300 K. Above 300 K, the negative effect of hydrocarbons on the D\* concentration vanishes as indicated by rectangular pulse profiles at higher temperatures. This effect can be either due to increased *cis*-2-butene desorption and/or due to a more effective replenishment of D\* under steady state conditions. A more effective replenishment of D\* may either be caused by a growing rate constant for D diffusion into the subsurface region and/or by

a reduced inhibition of the D diffusion due to a decreased concentration of co-adsorbed hydrocarbons during the olefin pulse.

#### 6.4.2 Reactivity of the C-free Pd/Fe<sub>3</sub>O<sub>4</sub> model catalyst

Fig. 6.10 displays the averaged reaction rates of a series pulsed isothermal MB experiments on the conversion of *cis*-2-butene with D<sub>2</sub> over the C-free Pd/Fe<sub>3</sub>O<sub>4</sub> model catalyst at a constant *cis*-2-butene and D<sub>2</sub> pressure varying the reaction temperature between 220 and 340 K. The response curves of the *cis-trans* isomerization product *trans*-2-butene-*d*<sub>1</sub> (upper traces) display a maximum in the steady state rates around 260 – 280 K, which is slightly higher than on the C-covered Pd model catalyst. The appearance of a rate maximum can be explained by increasing reaction rate constants resulting in growing reaction rates on one hand and increasing desorption of the reactants leading to a reduction of the reaction rates on the other hand (see 6.4.1). A shift of the maximum to higher temperatures with respect to the C-covered Pd particles (maximum ≈ 240 K) indicates that desorption of reactants becomes only at higher temperatures predominant. Thus, the shift in maximum most likely indicates a slightly stronger binding of hydrocarbons on the C-free compared to the C-covered Pd particles [181, 195].

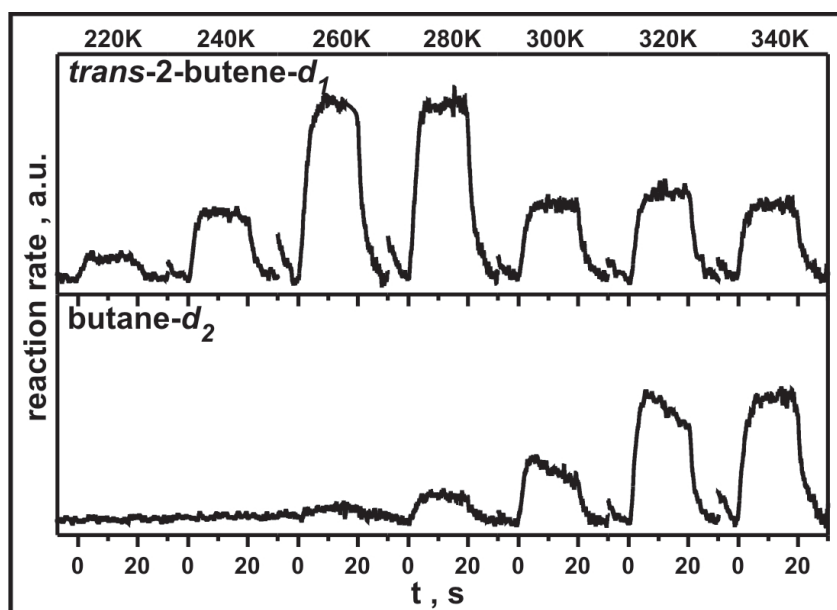


Figure 6.10: Averaged reaction rates as a function of time obtained for the *cis-trans* isomerization (upper traces, *trans*-2-butene-*d*<sub>1</sub>) and hydrogenation (lower traces, butane-*d*<sub>2</sub>) from a series of isothermal pulsed molecular beam experiments over the C-free Pd/Fe<sub>3</sub>O<sub>4</sub> model catalyst. While the *cis*-2-butene and D<sub>2</sub> pressures were kept constant, the reaction temperature was varied in the range between 220 and 340 K.

While no significant steady state hydrogenation activity is observed over the C-free model catalyst up to 260 K, persisting hydrogenation rates are found for higher temperatures ( $\geq 280$  K). With increasing temperature the hydrogenation rates increase. In contrast to the isomerization pathway, no clear maximum is observed in the investigated temperature range. It is important to emphasize once more, that on the C-free model catalyst even at low temperatures a high hydrogenation activity at the beginning of the experiment is observed that ceases however at low temperatures after prolonged olefin exposure. We attributed this effect to inhibited D diffusion into the subsurface under reaction conditions. Persisting hydrogenation attests thus, to the ability of the catalyst to replenish the  $D^*$  species under reaction conditions - at higher temperatures also feasible on the C-free model catalyst. The growing steady state rates with increasing temperature are either caused by an increase of the reaction rate constant of the elementary reaction step where H(D) is inserted into the Pd-butyl bond or by increasing replenishment of the  $D^*$  species (associated with subsurface absorbed D) due to a reduced poisoning of the surface by fast olefin desorption and/or due to higher D diffusion constants.

The pulse shape of the isomerization product exhibits at high temperatures (as of 260 K) a rectangular form, while at low temperatures a slightly decaying pulse profile is observed (see fig. 6.10). This behavior is similar to that observed for the C-covered model catalyst. At high temperatures, the D surface concentration is not significantly affected during the olefin exposure, while at lower temperatures, the steady state concentration of surface D is lowered by co-adsorbed hydrocarbons. With increasing temperature, the olefin desorption becomes faster leading to a reduced poisoning of the surface for dissociative  $D_2$  adsorption. Thus, at low temperatures where olefin desorption is slow the steady state reactivity of the catalyst is strongly governed by the replenishment of D inhibited by high coverages of co-adsorbed hydrocarbons.

For the hydrogenation pathway, a roughly rectangular pulse shape is observed at 280 K, changing to a decaying pulse profile between 300 and 320 K, while at 340 K again a rectangular pulse shape is found. At high temperatures, in line with the reasoning applied in the previous section (6.4.1), the rectangular product response attests to D-rich steady state conditions also with respect to subsurface absorbed D. This can be caused by two effects: a reduced poisoning of D diffusion due to lower hydrocarbon coverages at high temperatures and/or by an increased rate constant for D diffusion into the subsurface.

The decreasing pulse shape at temperatures between 300 and 320 K indicates D-deficient steady state conditions for the hydrogenation pathway. For the isomerization, D-rich steady state conditions are observed in this temperature range showing that D diffusion into the subsurface is more negatively affected by co-adsorbed hydrocarbons than the dissociative  $D_2$  adsorption. This result is in line with measurements over the C-covered catalyst.

In summary, the isothermal pulsed MB experiments on the conversion of *cis*-2-butene with D<sub>2</sub> over the C-covered and C-free Pd/Fe<sub>3</sub>O<sub>4</sub> model catalyst showed a maximum in the steady state reaction rates resulting from two counteracting trends: increasing reaction rate constants leading to growing steady state rates and faster desorption of the reactants causing lower steady state coverages of these and thus, a lowering of the reaction rates. The product response curves indicated that replenishment of D strongly controls the reactivity of the catalyst at low temperatures, while at higher temperatures the replenishment becomes more effective. This observation was attributed to faster olefin desorption at high temperatures resulting in a decreased poisoning of the surface for D<sub>2</sub> sorption. In line with previous results, D diffusion was found to be more sensitive to the inhibiting effect of co-adsorbed hydrocarbons compared to dissociative D<sub>2</sub> adsorption. For higher temperatures, sustained hydrogenation activity was also observed over the C-free Pd model catalyst attesting to an effective replenishment of subsurface D under reaction conditions. This effect can be rationalized by either an increasing rate constant for D diffusion into the subsurface and/or by a reduced poisoning of the surface due to faster olefin desorption.

## 6.5 Conversion and selectivity

In fig. 6.11, the overall conversion and selectivity toward the competing hydrogenation and *cis-trans* isomerization pathways in the steady state is displayed for different reaction conditions. The conversion is calculated as  $\frac{R_{isom}+R_{hydr}}{flux_B}$ . The selectivity is determined by the ratio of the formation rate of the hydrogenation product butane-*d*<sub>2</sub> to the isomerization product *trans*-2-butene-*d*<sub>1</sub>:  $\frac{R_{hydr}}{R_{isom}}$  (in the following denoted simply as butane-*d*<sub>2</sub>:*trans*-2-butene-*d*<sub>1</sub> ratio). Using such values, the overall activity and selectivity of the model system can be directly compared to results obtained under ambient conditions for realistic systems allowing to verify the transferability of the results obtained in this study to processes taking place under more realistic catalytic conditions.

The dependence on the D<sub>2</sub> pressure is displayed in fig. 6.11 (a). Increasing D<sub>2</sub> pressures result in higher overall conversions both for the C-covered and the C-free Pd/Fe<sub>3</sub>O<sub>4</sub> model catalyst. As there is no sustained hydrogenation activity on the C-free Pd particles, the overall conversion is slightly lower than for the C-covered catalyst. The selectivity over the C-covered surface shifts with increasing D<sub>2</sub> pressure toward the hydrogenation pathway attesting to a stronger dependence of this pathway on the D<sub>2</sub> pressure which is in line with the kinetic model introduced in section 6.2. A similar conversion increase and selectivity shift was reported for olefin conversion under ambient conditions [36, 38, 200].

In fig. 6.11 (b), the dependence on the *cis*-2-butene pressure is displayed. An increase of the olefin pressure leads to strongly decreasing conversions on the C-free and the C-covered Pd model catalyst. For the C-covered Pd particles that exhibit persisting isomerization and hydrogenation activity, a strong shift toward the isomerization pathway is

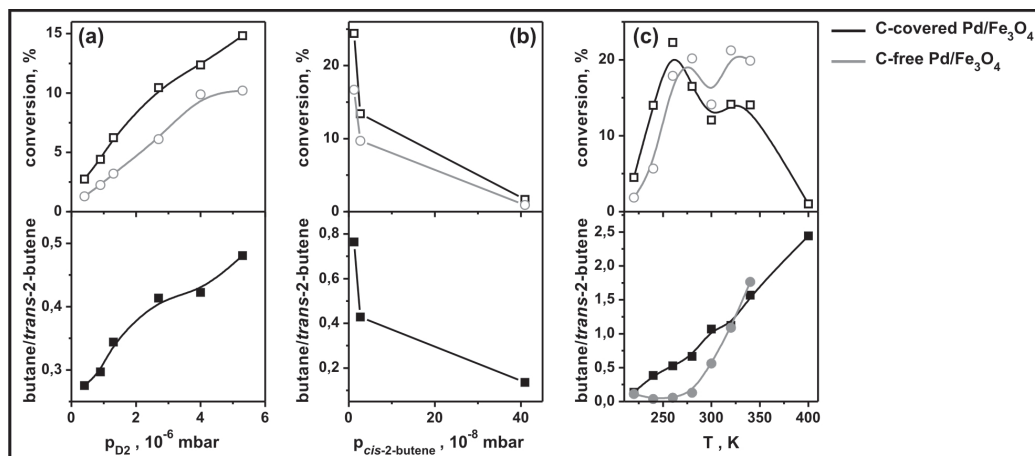


Figure 6.11: Displayed is the overall conversion (upper panels) and the ratio of butane- $d_2$ : $trans$ -2-butene- $d_1$  production (lower panels) as a function of (a) the  $D_2$  pressure (at 260 K with a  $cis$ -2-butene pressure of  $2.7 \cdot 10^{-8}$  mbar), (b) the  $cis$ -2-butene pressure (at 260 K with a  $D_2$  pressure of  $4.0 \cdot 10^{-6}$  mbar) and (c) the reaction temperature (at a  $cis$ -2-butene pressure of  $2.7 \cdot 10^{-8}$  mbar and a  $D_2$  pressure of  $4.0 \cdot 10^{-6}$  mbar) for both the C-covered (black) and the C-free (gray)  $Pd/Fe_3O_4$  model catalyst. Since there is no steady state hydrogenation activity on the C-free  $Pd$  particles at 260 K and thus only isomerization activity, no ratio of butane- $d_2$ : $trans$ -2-butene- $d_1$  production is given for dependence on the  $D_2$  and on the butene pressure (both measured at 260 K) for the C-free catalyst.

found for higher 2-butene pressures indicated by a strongly decreasing butane- $d_2$ : $trans$ -2-butene- $d_1$  ratio. As discussed in section 6.3, the decreasing steady state reactivity can be attributed to a limited availability of D which is probably caused by poisoning of the surface for hydrogen sorption due to co-adsorbed hydrocarbon species. The pronounced drop of the butane- $d_2$ : $trans$ -2-butene- $d_1$  ratio between the two lowest  $cis$ -2-butene pressures indicates, in line with previous results, that subsurface D required for hydrogenation is more negatively affected by co-adsorbed hydrocarbons than surface D required for  $cis$ - $trans$  isomerization.

The temperature dependence of the overall conversion and the selectivity is displayed in fig. 6.11 (c). For the C-covered  $Pd/Fe_3O_4$  catalyst, maximum is observed around 260 K found which results from two opposing trends: on one hand, increasing rate constants for the conversion reactions leading to *increasing* rates and faster desorption of the reactants resulting in *decreased* conversions. The decrease in reaction rates at higher temperatures is in good agreement with negative Arrhenius coefficients reported for alkene conversions under ambient-pressure conditions which were attributed to alkene desorption [37, 191, 192]. For the C-free catalyst in the investigated range, just a broad



maximum in conversion between 280 - 340 K is observed, but no clear decrease in conversion at higher temperatures. This is due to strongly increasing hydrogenation activity at higher temperatures as well as probably due to a slightly higher binding of the olefin on the C-free Pd particles as suggested in 6.3. As indicated by the maximum in isomerization rate, the appearance of a maximum in overall conversion is expected also for the C-free Pd particles for higher temperatures ( $> 340$  K).

Increasing temperatures strongly favor the formation of the hydrogenation product as attested by the strongly increasing butane- $d_2$ :*trans*-2-butene- $d_1$  ratio. As discussed in section 6.4, two effects can account for this selectivity shift: a high activation energy of the second half-hydrogenation step from butyl to butane and/or a more effective replenishment of subsurface D either due to an increased diffusion rate and/or due to reduced poisoning of the surface caused by faster olefin desorption. In line with these results, a similar selectivity shift toward hydrogenation with increasing temperatures was reported for hydrogenation and isomerization of 1-butene under more realistic conditions over Pd catalysts [32, 37].

Despite the overall low reactant pressures, the overall conversion values obtained in this study are with 10-20% surprisingly high. Under realistic conditions, the reaction probabilities are with  $10^{-5}$  to  $10^{-10}$  reported for olefin conversion with hydrogen at ambient pressures much lower [31, 37]. One possible explanation is that large amounts of carbonaceous deposits build up under ambient conditions resulting in a decrease of the active surface area and thus, lower reaction probabilities. The combination of high conversions together with a similar pressure and temperature dependence for the activity and selectivity justifies however the study of the supported model catalysts under well-defined UHV conditions as a suitable proxy for realistic catalytic systems.

## 6.6 Conclusion

The kinetics of the *cis*-2-butene conversion with  $D_2$  over a well-defined Pd/Fe $_3$ O $_4$  model catalyst were investigated under UHV conditions by isothermal pulsed MB experiments with a special emphasis on the understanding of the microscopic factors governing the activity and selectivity of the system. In particular, the role of hydrogen-related processes, such as dissociative  $D_2$  adsorption and D diffusion into the subsurface, in the *cis-trans* isomerization and hydrogenation pathway was investigated by comparison of the transient and the steady state reaction rates obtained in the pulsed MB experiments. The influence of the particular reaction conditions, such as the reactant pressures, the  $N_{D_2}:N_{cis-2-butene}$  ratio and the temperature on the initial and steady state reactivity was investigated over a broad parameter range over both the C-free and the C-precovered Pd particles. C-precovering was found to dramatically affect the activity and selectivity of the Pd particles at 260 K. At 260 K, C-deposition induces sustained hydrogenation activity presumably by facilitating H(D) diffusion to subsurface sites under reaction conditions. It should be however noted that only a relatively small amount of C is deposited

onto the Pd particles which is mainly located on low-coordinated edge sites of the Pd particles, while the majority of the regular (111)-facets remains C-free (see 5.3 for details).

First, the influence of the  $D_2$  pressure was investigated. The steady state isomerization and hydrogenation rates over the C-covered Pd model catalyst at 260 K increase with increasing  $D_2$  pressure exhibiting formal reaction orders of  $m_{isom} = +0.66 \pm 0.13$  and  $m_{hydr} = +0.88 \pm 0.17$ , respectively. These values are in fair agreement with a simple kinetic model based on a Langmuir-Hinshelwood mechanism assuming low coverage conditions. The clearly positive reaction orders imply that the following conditions are basically fulfilled: the rate of 2-butene desorption (step 1') is faster than the first half-hydrogenation step to butyl (step 2) and the rate of  $\beta$ -hydride elimination of the 2-butyl- $d_1$  species (step 2' and 3) is fast compared to the second half-hydrogenation to butane (step 4).

Over the C-free catalyst, the steady state isomerization rates increase with increasing  $D_2$  pressure exhibiting a formal reaction order of  $m_{isom} = +0.98 \pm 0.05$  at 260 K which is also in agreement with the kinetic model. Comparison of the reaction orders obtained for the C-free and the C-covered catalyst shows however that the model does not exhibit enough detail to reproduce all observed effects. At 260 K, no sustained hydrogenation activity is observed over the C-free catalyst - even at the highest applied  $D_2$  pressures - indicating that D diffusion into the subsurface is strongly inhibited on this surface.

On the C-covered Pd particles, a smooth transition from D-deficient to D-rich steady state conditions with increasing  $D_2$  pressures is observed at 260 K for the *isomerization* pathway requiring just the presence of *surface* adsorbed H(D). The analysis of the pulse profiles indicates that this transition to D-rich steady state conditions occurs for reactant ratios of  $N_{D_2}:N_{cis-2-butene}$  larger than 380. Probably, co-adsorbed hydrocarbon species inhibit the dissociative  $D_2$  adsorption leading thereby to reduced steady state concentrations of *surface* adsorbed D at low  $D_2$  pressures. For the *hydrogenation* reaction requiring also the presence of *subsurface* adsorbed D, in contrast, no transition from D-deficient to D-rich steady state conditions is observed at 260 K in the entire investigated  $D_2$  pressure range, even when isomerization requiring just surface D proceeds under D-rich steady state conditions. This observation indicates that co-adsorbed hydrocarbon species affect the concentration of *subsurface* adsorbed D required for hydrogenation more negatively than the concentration of *surface* adsorbed D required for isomerization.

The pulse shape for isomerization over the C-free Pd particles implies D-rich conditions almost in the entire  $D_2$  pressure range indicating that the concentration of surface D is *not* significantly reduced by conversion with butene which is also expected from the large excess of  $D_2$  applied in all experiments. Only at the highest applied  $D_2$  pressure, D-deficient steady state conditions were observed. The microscopic origins of this effect are not clear, although, it can be speculated that high concentrations of co-adsorbed D weaken the adsorption strength of the olefins sufficiently to reduce the hydrocarbon

coverage between the pulses allowing thus for a more effective D replenishment compared to the steady state.

The experimentally obtained formal reaction orders with respect to the *cis*-2-butene pressure were all smaller than the reaction order of unity predicted by the kinetic model. For conversion over the C-covered Pd model catalyst, the reaction orders in the transient regime were with  $n_{isom} = +0.49 \pm 0.10$  for *cis-trans* isomerization and  $n_{hydr} = +0.26 \pm 0.10$  for hydrogenation clearly higher than the formal reaction orders for the steady state regime,  $n_{isom} = +0.33 \pm 0.07$  and  $n_{hydr} = -0.16 \pm 0.09$ , respectively. The difference can be ascribed to a strongly negative effect of adsorbed olefin species on D sorption. Analysis of the pulse profiles as well as a negative steady state reaction order in hydrogenation indicated that the concentration of subsurface D is more negatively affected by co-adsorbed hydrocarbons than the surface D concentration.

For the C-free Pd/Fe<sub>3</sub>O<sub>4</sub> model catalyst, basically identical reaction orders in 2-butene pressure were found for the transient and the steady state isomerization activity. The obtained value of  $n_{isom} = +0.14 \pm 0.02$  is clearly below the value predicted by the kinetic model and also below the steady state reaction order obtained for isomerization over the C-covered Pd surface. This implies that dissociative D<sub>2</sub> adsorption is even more negatively affected by co-adsorbed hydrocarbons on the C-free catalyst. This effect can probably be attributed to a stronger olefin binding and thus a higher coverage of hydrocarbon species on the C-free compared to the C-covered surface.

Both isomerization and hydrogenation over the C-covered Pd model catalyst display a non-monotonous behavior with increasing temperature exhibiting maxima of the reaction rates around  $T_{max} = 240$  K for isomerization and  $T_{max} = 300$  K for hydrogenation. From the different positions of the maxima, it can be concluded that different elementary reaction steps determine the activity for *cis-trans* isomerization and hydrogenation. Up to 300 K, the second half-hydrogenation step limits the hydrogenation rates. The isomerization rates can be either governed by the adsorption of 2-butene or by the first half-hydrogenation step. The activation energy for the second half-hydrogenation step was concluded to be higher than the first half-hydrogenation step presumably due to an intrinsically higher activation barrier for H(D) insertion into the Pd-butyl bond.

The temperature dependence of the *isomerization* over the C-free model catalyst is similar to that observed on the C-covered surface. The maximum in isomerization rate is shifted for the C-free Pd particles to slightly higher temperatures ( $T_{max} = 260 - 280$  K) probably due to a slightly stronger adsorption of olefins on the C-free Pd particles. For the *hydrogenation* pathway, in contrast, a significantly different reactivity is observed for the C-free and the C-precovered Pd particles. In contrast to the C-covered Pd particles, no sustained hydrogenation activity is found on the C-free Pd particles at low temperatures up to 260 K which was attributed to inhibited H(D) diffusion to subsurface sites under reaction conditions. It should be noted again that only a small amount of C is deposited onto the Pd particles which is located mainly on low-coordinated edge sites,

while the majority of the regular (111)-facets remains C-free. For higher temperatures ( $\geq 280$  K), persisting hydrogenation at significant rates is observed also on the C-free Pd particles. This may indicate that subsurface absorbed D can be effectively replenished also on the C-free Pd particles under reaction conditions at these temperatures either due to a reduced poisoning of the surface caused by faster olefin desorption or due to an increased D diffusion rate into the subsurface.

With increasing  $D_2$  pressures an increasing overall conversion is observed for a reaction temperature of 260 K. For the C-covered Pd model catalyst exhibiting at 260 K both sustained isomerization and hydrogenation activity, a selectivity shift toward hydrogenation is observed with increasing  $D_2$  pressures. This effect can probably be attributed to the more pronounced dependence of the hydrogenation on the availability of D species. Increasing 2-butene pressures result in strongly decreased overall conversions and for the C-covered surface a selectivity shift to isomerization products is found. Both effects can be attributed to the inhibition of D sorption by co-adsorbed hydrocarbons poisoning the surface. An increase of the reaction temperature leads to a shift toward hydrogenation which is connected to the overall higher activation barrier for hydrogenation compared to *cis-trans* isomerization.

High overall conversion values combined with similar pressure and temperature dependencies as reported for catalytic studies under ambient pressure conditions justify the study of this reaction over well-defined model catalysts under UHV conditions as a proxy for realistic catalytic systems to gain fundamental insights in the microscopic processes governing the reactivity.

# 7 2-butene conversion with D<sub>2</sub> over Pd model catalysts: The role of carbon

## 7.1 Introduction

The activity and selectivity of Pd catalysts in the conversion of olefins with hydrogen was recognized to depend sensitively on the availability of hydrogen adsorbed on the *surface* and absorbed in the *subsurface* of Pd particles [43, 58]. Using a combination of pulsed isothermal MB experiments and NRA measurements (see chapter 5), experimental evidence was provided demonstrating that the presence of subsurface absorbed hydrogen is required for the hydrogenation of *cis*-2-butene. Under a broad range of reaction conditions, the diffusion of D to subsurface sites was recognized to be a slow and thus, rate determining process (see chapter 6). Therefore, the permeability of the surface for hydrogen diffusion under reaction conditions is expected to be crucial for the hydrogenation activity of Pd catalysts. As hydrogen diffusion into the subsurface is a structure-sensitive process [105], it is expected that the degree of coordination of the Pd atoms is important in the formation rate of subsurface hydrogen species and thus, for the hydrogenation activity.

Traditionally, carbonaceous deposits are thought to simply deactivate catalysts by blocking of active sites. Carbon was however suggested to also influence the selectivity of Pd catalysts in olefin conversions with hydrogen [38, 60, 61]. In line with this suggestion, small amounts of carbon mainly occupying low-coordinated sites, like edges and corners of the Pd particles, were found to dramatically affect the activity and selectivity in the conversion of *cis*-2-butene with D<sub>2</sub> at low temperatures (see chapter 5 and 6). Over the C-free Pd particles, only sustained isomerization activity was observed at low temperatures, while the C-covered Pd catalyst also exhibited persisting hydrogenation activity. High initial hydrogenation rates over the D-presaturated surfaces at the beginning of the experiment showed that hydrogenation is also feasible over the C-free Pd catalyst, when there are no limitations in D availability. These results were interpreted such that D diffusion into the subsurface is inhibited over the C-free surface under reaction conditions at low temperatures, while C deposits facilitate effective D diffusion under reaction conditions allowing for persisting hydrogenation activity even at low temperatures. But carbon was not only found to influence the *selectivity* of the Pd particles at low temperatures, also the *activity* was significantly changed. Contrary to the traditional picture, the C-covered Pd particles exhibited at low temperatures a considerably *higher* overall activity than the C-free Pd model catalyst.

In contrast to these results, it has been recently reported that the presence of large amounts of C suppresses the full hydrogenation of acetylene over Pd(111) which has been attributed to *inhibited* hydrogen diffusion into the subsurface of Pd [38, 58]. This interpretation is in line with previous reports that the formation of the  $\beta$ -PdC<sub>≥0.13</sub> phase prevents the formation of a hydride phase on Pd [58, 62–65]. Thus, different carbonaceous deposits seem to influence the selectivity in olefin conversions in a distinct way. From these opposing results, several questions arise: What is the nature of C that facilitates sustained hydrogenation activity? Is the amount of C decisive or does C located on low-coordinated sites, like steps and edges, have a different effect than C located on (111)-facets? And what is the underlying microscopic mechanism for C-induced promotion of sustained hydrogenation activity at low temperatures?

To investigate the role of low-coordinated sites and their modification by C in the conversion of *cis*-2-butene with D<sub>2</sub>, isothermal pulsed MB experiments were conducted over a Pd/Fe<sub>3</sub>O<sub>4</sub>/Pt(111) model catalyst and compared to equivalent measurements over a Pd(111) single crystal surface. First, the experiments were conducted over the C-free surfaces to obtain a better insight on the role of low-coordinated sites in the activity and selectivity in 2-butene conversion. Secondly, C was deposited on the surfaces. For the supported Pd/Fe<sub>3</sub>O<sub>4</sub>, C predominantly occupies low-coordinated sites like edges and corners of the Pd particles, while the majority of the surface consisting of (111)-facets ( $\approx 80\%$  of the surface area) remains carbon free (see also chapter 5). Reactivity differences compared to the C-precovered Pd(111) surface, where the amount of low-coordinated sites is negligible, provides direct experimental insight into the role of carbon located on low-coordinated sites.

In the first part of this chapter (7.2), the effect of low-coordinated sites and their modification with C on the isomerization pathway will be discussed, while in the second part (7.3), the influence on the hydrogenation activity will be explored. The role of C on low-coordinated sites is discussed in detail in the third section of this chapter (7.4).

## 7.2 Isomerization activity

To investigate the isomerization activity of the C-free and C-covered Pd/Fe<sub>3</sub>O<sub>4</sub> model catalyst as well as of the C-free and C-covered Pd(111) single crystal surface, isothermal pulsed MB experiments were conducted using the same pulse sequence as described in 5.2 and 6.2. Initially, the surfaces were exposed to 280 L of D<sub>2</sub> to saturate the catalysts with both surface adsorbed and subsurface absorbed D. Subsequently, a small flux of *cis*-2-butene ( $\text{flux}_{\text{cis-2-butene}} = 5.6 \cdot 10^{12} \text{ molecules} \cdot \text{cm}^{-2} \cdot \text{s}^{-1}$ ,  $p_{\text{cis-2-butene}} = 2.7 \cdot 10^{-8} \text{ mbar}$ ) was pulsed onto the surface, while D<sub>2</sub> was continuously supplied in a large excess ( $\text{flux}_{\text{D}_2} = 3.2 \cdot 10^{15} \text{ molecules} \cdot \text{cm}^{-2} \cdot \text{s}^{-1}$ ,  $p_{\text{D}_2} = 4.0 \cdot 10^{-6} \text{ mbar}$ ) corresponding to a  $N_{\text{D}_2}:N_{\text{cis-2-butene}}$  ratio of 570. The pulse sequence for *cis*-2-butene consisted of 50 short pulses (4 s on, 4 s off) in the beginning of the experiment to follow the initial reactivity of the catalyst and of 30 longer pulses (20 s on, 10 s off) to study the quasi steady state

regime.

In fig. 7.1, the averaged steady state isomerization rates over the C-free Pd/Fe<sub>3</sub>O<sub>4</sub> model catalyst (upper panels) and the C-free Pd(111) single crystal surface (lower panels) obtained from the last 30 long pulses of the MB experiment are displayed for different reaction temperatures ranging from 220 to 340 K. For a direct comparison, the reaction rates are normalized to the number of surface Pd atoms (for the Pd particles:  $0.6 \cdot 10^{15}$  Pd atoms  $\cdot$  cm<sup>-2</sup>; for Pd(111):  $1.5 \cdot 10^{15}$  Pd atoms  $\cdot$  cm<sup>-2</sup>).

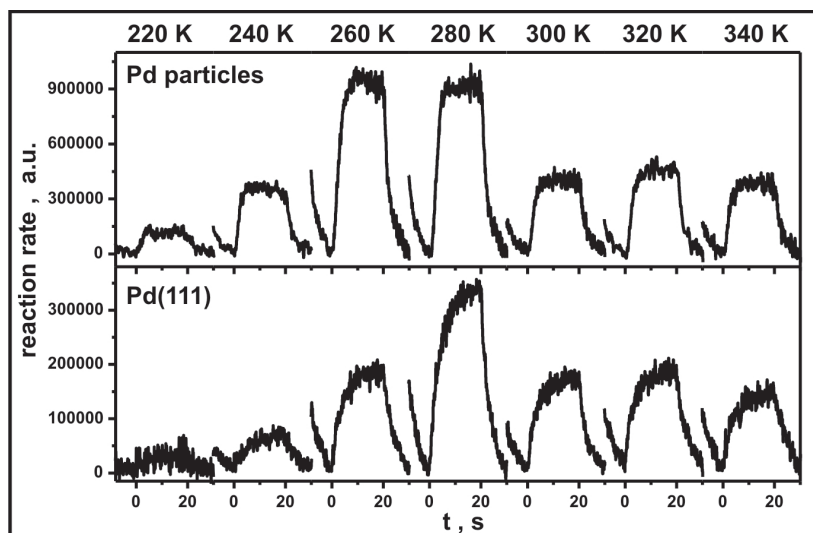


Figure 7.1: Steady state isomerization rates (*trans*-2-butene-*d*<sub>1</sub>) over the C-free Pd(111) single crystal (lower panels) and the C-free Pd/Fe<sub>3</sub>O<sub>4</sub> model catalyst (upper panels) obtained in isothermal pulsed MB experiments for reaction temperatures ranging from 220 to 340 K. For a direct comparison the rates are normalized to the number of Pd surface atoms. The isomerization activity of the Pd(111) surface qualitatively resembles that of the C-free Pd particles. With increasing temperatures, the rates increase reaching a maximum around 280 K and decrease for even higher temperatures. The rates per Pd surface atom are however smaller for the Pd(111) single crystal indicating that the low-coordinated sites on the Pd particles significantly contribute to the observed isomerization activity of the Pd/Fe<sub>3</sub>O<sub>4</sub> model catalyst.

It can be seen in fig. 7.1 that isomerization activity can be sustained in the entire investigated temperature range both over the C-free Pd(111) single crystal surface as well as over the C-free Pd particles. Persisting isomerization activity indicates that both surface D and *cis*-2-butene are available and that the butyl species are effectively formed on the C-free Pd model catalysts. It should be noted that also for the Pd(111) single crystal surface, isomerization (and hydrogenation) activity only begins after an induction

period which was also observed for the *cis*-2-butene conversion over Pd particles. In the induction period, 2-butene is irreversibly adsorbed forming a layer of strongly-adsorbed hydrocarbons, molecular 2-butene and/or other partially dehydrogenated hydrocarbon species, on the surface. Only when a threshold coverage of these hydrocarbon species is reached, formation of gas phase products begins.

With increasing surface temperature, the steady state isomerization rates over the C-free Pd(111) surface display a non-monotonic behavior exhibiting a maximum in reaction rate at 280 K. This behavior is qualitatively very similar to that observed for the C-free Pd particles exhibiting a maximum in isomerization rate around 260-280 K. Two counteracting trends lead to the appearance of a rate maximum: the reaction rate constants increase with increasing temperature resulting in increased isomerization rates, with increasing temperature, however, also the rate constants for desorption of the reactants increase which leads to a decrease of the reaction rates.

A more quantitative comparison shows that the isomerization rates per Pd surface atom are clearly lower on the Pd(111) surface than on the Pd particles indicating that low-coordinated sites, like edges and corners as well as (100)-facets constituting only  $\approx 20\%$  of the particle surface, cause a significant part of the observed isomerization activity of the Pd particles. This observation is in line with olefin conversions under more realistic conditions that report a structure sensitivity for the H/D exchange reaction in alkenes (see [37] and references therein). It should be emphasized however, that the isomerization rates for Pd(111) and the Pd/Fe<sub>3</sub>O<sub>4</sub> are, despite some differences, still in the same order of magnitude.

To study the effect of C deposition on (111)-facets compared to C located on low-coordinated sites of the Pd particles, pulsed isothermal MB experiments as described in the beginning of the section were conducted over the C-precovered Pd(111) single crystal surface and the C-precovered Pd/Fe<sub>3</sub>O<sub>4</sub> model catalyst for reaction temperatures ranging from 220-340 K. Carbon was deposited on both Pd model catalysts by exposure to 280 L of  $D_2$  and 0.8 L of *cis*-2-butene at  $\approx 115$  K and subsequent heating in vacuum to  $\approx 500$  K (see chapter 5 for details). Since C diffusion to subsurface sites of Pd can occur for temperatures higher than 400 K [68, 69], it is expected that some C is situated in subsurface sites after heating to 500 K (see also 2.2.3). On the Pd particles, carbonaceous deposits are mainly located on low-coordinated sites like edges, corners and to a lesser extend (100)-facets, while the majority of the surface consisting of (111)-facets remains C-free (see 5.3 for details). In contrast, on the Pd(111) single crystal surface, the amount of low-coordinated sites in contrast is very small.

Deposition of small amounts of C does not affect the *isomerization* activity over both the Pd(111) surface and the Pd particles significantly (factor of  $\leq 2$ ) compared to the dramatic changes (by several orders of magnitude) found in the *hydrogenation* activity at low temperatures upon C-modification of the Pd particles. The isomerization rates are overall very similar to those obtained over the C-free surfaces, only small differences



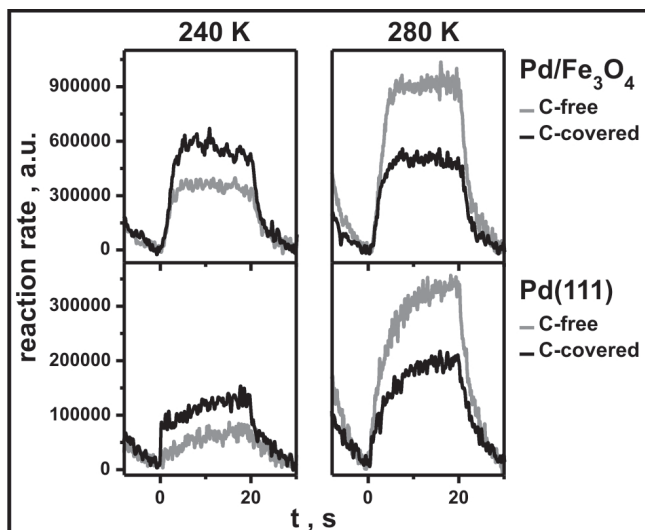


Figure 7.2: Steady state isomerization rates (*trans*-2-butene- $d_1$ ) over the C-free (gray lines) and C-covered (black lines) Pd(111) single crystal (lower panels) and Pd/Fe<sub>3</sub>O<sub>4</sub> model catalyst (upper panels) obtained in isothermal pulsed MB experiments for two reaction temperatures, 240 and 280 K. For a direct comparison the rates are normalized to the number of Pd surface atoms. At 240 K, the isomerization rates are slightly *higher* in the presence of C, while at 280 K, the isomerization rates are *lower* over the C-covered surfaces. The isomerization rates are, however, overall quite similar (factor of  $\leq 2$ ) for the C-free and the C-covered Pd model catalysts compared to the dramatic changes (by several orders of magnitude) in hydrogenation rates observed for the C-covered Pd particles at low temperatures.

are detected as shown in fig. 7.2 for two reaction temperatures, 240 and 280 K, where the effect of C-modification on the isomerization rates is most pronounced. It can be seen that the isomerization rates are slightly higher (factor of  $\leq 2$ ) in the presence of C for both the Pd(111) surface and the Pd particles at the lower reaction temperature of 240 K. In contrast, at a higher surface temperature of 280 K, the C-free Pd surfaces are more active (factor of  $\leq 2$ ) in isomerization compared to the C-modified surfaces.

The exact microscopic mechanism causing this effect is not clear. It can be speculated, however, that the adsorption strength of hydrocarbons/olefins in the vicinity of C is weakened [181, 195] which is expected to result in faster olefin desorption with respect to the C-free surfaces. At low temperatures, faster olefin desorption can potentially result in more open adsorption sites for dissociative D<sub>2</sub> adsorption and thereby in *higher* isomerization rates in the presence of C. In turn, for a potentially higher adsorption strength on the C-free surfaces, it is expected that the reduction of the reaction rates due to fast desorption of the reactants becomes dominant only at higher temperatures

with respect to the C-covered surface, so that for higher temperatures, the isomerization rates over the C-free surfaces are expected to be higher. We note that this is only one possible scenario, which can explain the observed dependencies.

Overall, deposition of small amounts of C does not significantly alter the isomerization activity of both the Pd(111) single crystal surface as well as of the  $Fe_3O_4$  supported Pd nanoparticles. Taking into account that the majority of the regular surface sites remains free of C, this observation supports our earlier interpretation that mainly *surface* adsorbed D which is overall not significantly influenced by a small amount of C is involved in the isomerization reaction, while *subsurface* related H(D) species which were shown to dramatically affect the hydrogenation activity, in contrast, seem not to have a strong influence on the isomerization reaction.

In summary, the isomerization activity over the Pd(111) single crystal surface is qualitatively very similar to that observed for Pd particles. As for the Pd particles, persisting isomerization activity is observed also over the Pd(111) surface in the entire investigated temperature range from 220 to 340 K. With increasing temperature, a maximum in the isomerization rates is observed around 280 K for the C-free Pd(111) surface and around 260-280 K for the C-free Pd particles. Deposition of C does not significantly alter the isomerization activity over the two catalyst. Small changes in the isomerization rates can potentially indicate that deposition of C slightly weakens the adsorption strength of co-adsorbed hydrocarbons in the vicinity of C.

### 7.3 Hydrogenation activity

Next the influence of low-coordinated sites and their modification with carbonaceous deposits on the hydrogenation activity is investigated. Pulsed isothermal MB experiments following the same pulse sequence as described in the preceding section were conducted over the C-free and C-covered Pd(111) single crystal surface as well as over the C-free and C-covered Pd/ $Fe_3O_4$ /Pt(111) model catalyst for surface temperatures ranging from 220 to 340 K. The measurements were conducted applying continuously a large excess of  $D_2$  ( $\text{flux}_{D_2} = 3.2 \cdot 10^{15} \text{ molecules} \cdot \text{cm}^{-2} \cdot \text{s}^{-1}$ ,  $p_{D_2} = 4.0 \cdot 10^{-6} \text{ mbar}$ ) and pulsing a small flux of *cis*-2-butene ( $\text{flux}_{cis-2-butene} = 5.6 \cdot 10^{12} \text{ molecules} \cdot \text{cm}^{-2} \cdot \text{s}^{-1}$ ,  $p_{cis-2-butene} = 2.7 \cdot 10^{-8} \text{ mbar}$ ) corresponding to a  $N_{D_2}:N_{cis-2-butene}$  ratio of 570.

In fig. 7.3, the isomerization and hydrogenation activity over the C-free Pd(111) single crystal surface and the C-free Pd particles is displayed for a reaction temperature of 260 K. Over both Pd model catalysts, isomerization and hydrogenation activity only begin after an induction period in which 2-butene is irreversibly adsorbed on the catalyst forming a layer of strongly-bound hydrocarbon species. After a threshold coverage of these species, molecular 2-butene and/or other partially dehydrogenated hydrocarbons, such as butylidyne, is reached, formation of gas phase products starts.

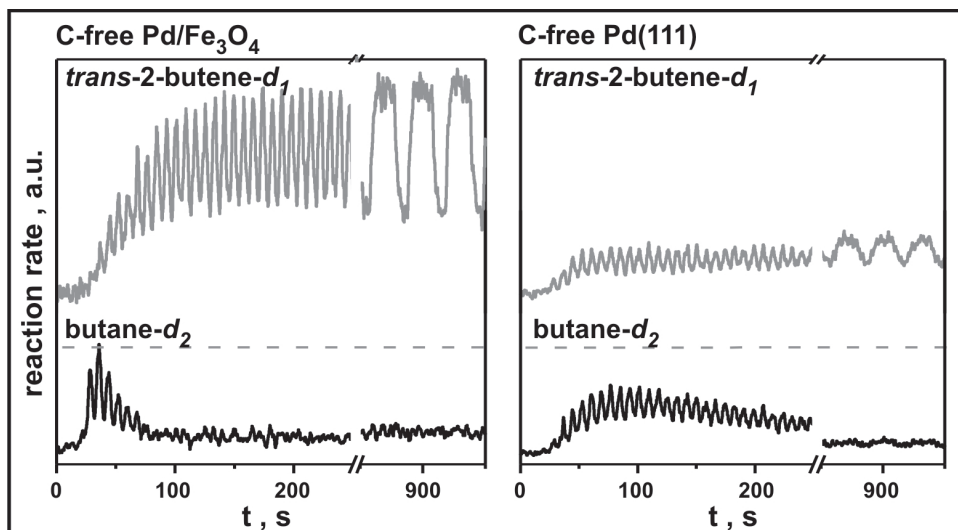


Figure 7.3: Reaction rates for isomerization (upper traces, *trans*-2-butene-*d*<sub>1</sub>) and hydrogenation (lower traces, butane-*d*<sub>2</sub>) obtained in isothermal pulsed MB experiments at 260 K over the C-free Pd(111) single crystal (right panel) and the C-free Pd/Fe<sub>3</sub>O<sub>4</sub> model catalyst (left panel). For a direct comparison, the reaction rates are normalized to the number of Pd surface atoms. Both C-free Pd model catalysts exhibit a qualitatively similar behavior. While isomerization is sustained over long time periods, the hydrogenation rates return to zero after a period of high activity.

While isomerization is sustained, the hydrogenation rates return to zero after a short period of high activity. As discussed in chapter 5, the sustained isomerization rates attest to the availability of surface adsorbed D and *cis*-2-butene as well as to the effective formation of the 2-butyl-*d*<sub>1</sub> intermediate. Since hydrogenation is feasible on the D-presaturated C-free Pd surfaces, thus, when there are no limitations in availability of both surface and subsurface D, zero hydrogenation rates for prolonged olefin exposures indicate that the replenishment of a second D species involved in the second half-hydrogenation is inhibited under reaction conditions. The results presented in chapter 5 suggest that the second D species is associated with subsurface adsorbed D. Over the C-free Pd surfaces, D diffusion into the subsurface is, thus, seemingly inhibited under reaction conditions, in the presence of co-adsorbed hydrocarbons.

A more quantitative comparison of the reaction rates shows that the initial hydrogenation rates per Pd surface atom are comparable and in the same order of magnitude for Pd(111) and the Pd particles. The Pd particles exhibit only a slightly higher initial hydrogenation activity. Thus, the (111)-facets constituting 80 % of the surface of the Pd particles contribute significantly to their hydrogenation activity. The difference in isomerization rates for the Pd(111) surface and the Pd particles is more pronounced

compared to the differences observed for the hydrogenation reaction. This observation is in line with olefin conversions under more realistic conditions that report a more pronounced structure sensitivity for the H/D exchange in alkenes than for the hydrogenation reaction (see [37] and references therein). It should be emphasized however, that the initial reaction rates obtained on the D-saturated surfaces for both isomerization and hydrogenation for the C-free Pd(111) and the C-free Pd/Fe<sub>3</sub>O<sub>4</sub> are, despite some differences, still in the same order of magnitude.

Fig. 7.4 displays the averaged steady state hydrogenation rates over the C-free Pd(111) surface (lower panels) and the C-free Pd particles (upper panels) for surface temperatures ranging from 220 to 340 K. For a direct comparison the rates are normalized to the number of surface Pd atoms.

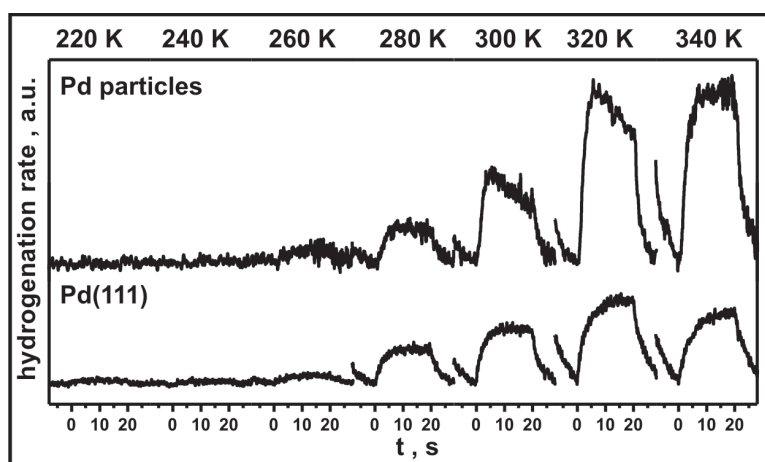


Figure 7.4: Averaged steady state hydrogenation rates as a function of time obtained from the last 30 pulses of isothermal pulsed MB experiments on the conversion of *cis*-2-butene with  $D_2$  over C-free Pd particles (upper panels) and C-free Pd(111) (lower panels) for surface temperatures ranging from 220 – 340 K. The hydrogenation rates are normalized for the number of surface Pd atoms for a quantitative comparison. On the C-free Pd catalysts, hydrogenation is not sustained for temperatures  $\leq 260$  K, while persisting hydrogenation activity is found for temperatures  $\geq 280$  K.

The steady state hydrogenation activity over the C-free Pd(111) surface is qualitatively very similar to that of the C-free Pd/Fe<sub>3</sub>O<sub>4</sub> model catalyst. For C-free Pd(111), no sustained hydrogenation activity is found at low temperatures (up to 260 K) in the steady state which is in agreement with the reactivity observed over C-free Pd particles. It should be emphasized that high hydrogenation rates are however observed at the beginning of the experiment when the surface is saturated with D - both on C-free Pd particles as well as on C-free Pd(111). At higher temperatures ( $\geq 280$  K), persisting hy-

drogenation rates are observed even after prolonged olefin exposures both on the C-free Pd(111) surface and on the C-free Pd particles. For Pd(111), the hydrogenation rates increase with increasing temperature exhibiting a maximum at 320 K. At the highest investigated temperature of 340 K, a slight decrease in the hydrogenation rates over the Pd(111) surface is observed. The shift in rate maximum to higher temperatures for the hydrogenation with respect to isomerization pathway (maximum around 260-280 K) indicates that different rate limiting steps are involved in hydrogenation and *cis-trans* isomerization. While for the isomerization the formation of the 2-butyl- $d_1$  intermediate is most likely rate limiting, for the hydrogenation the second half-hydrogenation step from butyl to butane is determining the rate (see 6.4.1 for a detailed discussion). For the C-free Pd/Fe<sub>3</sub>O<sub>4</sub> model catalyst, a clear maximum in hydrogenation rate was not observed in the investigated temperature range. This shift of the rate maximum to higher temperatures with respect to Pd(111) can be most likely attributed to a higher adsorption strength for the reactants on the Pd particles exhibiting a substantial amount of strongly binding low-coordinated sites.

Overall, the C-free Pd(111) surface exhibits a very similar hydrogenation activity as the C-free Pd particles indicating that the (111)-facets significantly contribute to the hydrogenation activity of the Pd particles. Small differences in the hydrogenation rates may indicate an overall weaker olefin binding on Pd(111) compared to the Pd particles which exhibit next to (111)-facets also a significant amount of more strongly binding, low-coordinated sites. It should be emphasized, however, that the overall reactivity, for both isomerization and hydrogenation, of the C-free Pd(111) surface and the C-free Pd particles is very similar which is an important prerequisite for a meaningful comparison of the reactivities over the C-covered Pd surfaces.

Next the effect of C-deposition on the hydrogenation activity was investigated by pulsed isothermal MB experiments for the Pd(111) single crystal surface and compared to the results obtained for the Pd/Fe<sub>3</sub>O<sub>4</sub> model catalyst. For the formation of carbonaceous deposits, the surface was exposed at low temperature ( $\approx 115$  K) to 280 L D<sub>2</sub> and 0.8 L *cis*-2-butene and subsequently heated in vacuum to 500 K (see 5.3 for details). Since C diffusion to subsurface sites of Pd can occur for temperatures higher than 400 K [68, 69], it is expected that some C is situated in subsurface sites after heating to 500 K (see also 2.2.3 for details).

It should be noted again that on the Pd particles, carbonaceous deposits are mainly located on low-coordinated sites like edges, corners and to a lesser extend on (100)-facets, while the majority of the surface consisting of (111)-facets remains free of carbon (see 5.3 for details). For the Pd(111) single crystal surface, the amount of low-coordinated sites is, in contrast, negligible. Since the reactivity for the C-free Pd(111) and the C-free Pd particles is very similar, comparison of the reactivity changes upon modification by C of the two systems provides direct experimental insight into the role of carbonaceous deposits on low-coordinated sites.

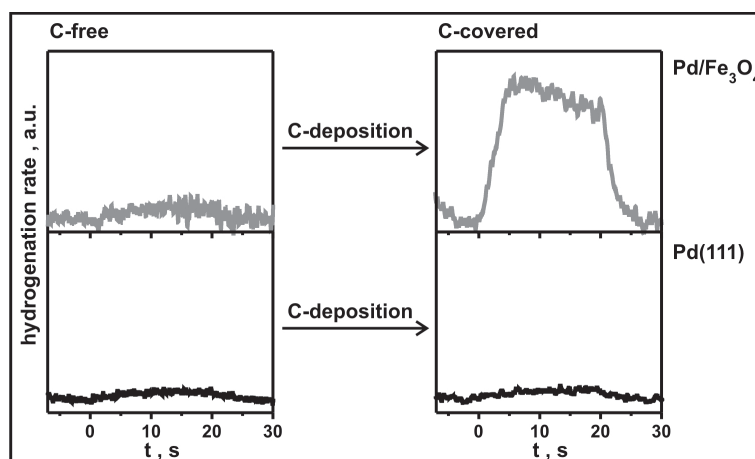


Figure 7.5: Averaged hydrogenation rates as a function of time obtained from the last 30 pulses of isothermal pulsed MB experiments on the conversion of *cis*-2-butene with  $D_2$  at 260 K over C-free (left panels) and C-covered (right panels) Pd(111) (lower traces, black) and Pd particles (upper traces, gray). The hydrogenation rates are normalized for the number of surface Pd atoms for a direct quantitative comparison.

In fig. 7.5, the averaged hydrogenation (butane- $d_2$ ) rates at 260 K obtained from the last 30 long pulses are displayed for Pd particles (upper panels) and Pd(111) (lower panels), both for the C-free (left panels) and the C-covered (right panels) surfaces. For Pd particles, deposition of C was found to promote persisting hydrogenation (butane- $d_2$ ) activity at low temperatures ( $\leq 260$  K) (see also fig. 7.5 (upper panels), hydrogenation rates are normalized to the number of Pd surface atoms). In contrast, C deposition on the Pd(111) surface does not induce sustained hydrogenation activity at 260 K, as depicted in fig. 7.5 (lower panels). While for Pd particles dramatic changes in the activity and selectivity were observed upon C-modification, the reactivity of the C-precovered Pd(111) single crystal surface is at 260 K very similar to the activity and selectivity observed for the C-free Pd(111) surface. In other words, carbonaceous deposits on (111)-facets do not significantly affect the reactivity or selectivity at 260 K as it was observed for carbon deposition on Pd particles where the carbonaceous deposits are located mainly on low-coordinated sites.

To test if C-modification of (111)-facets affects the hydrogenation reaction hypothetically at higher temperatures, the hydrogenation activity of the C-precovered Pd(111) surface was also investigated for different reaction temperatures ranging from 220-340 K.

Fig. 7.6 displays the averaged hydrogenation rates as a function of time obtained from the last 30 long pulses of the isothermal pulsed MB experiment for different reaction temperatures. Next to the hydrogenation rates for the C-precovered Pd(111) surface (lower,

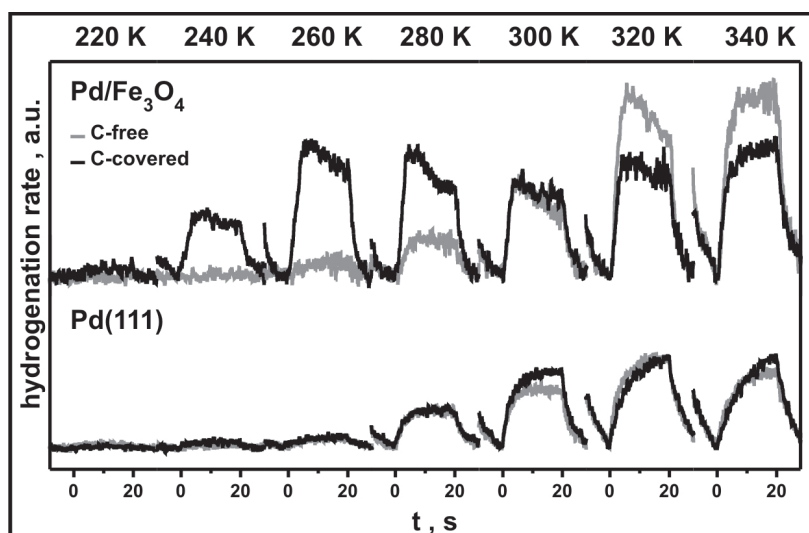


Figure 7.6: Averaged hydrogenation rates (butane- $d_2$ ) as a function of time obtained from the last 30 pulses of isothermal pulsed MB experiments on the conversion of *cis*-2-butene with  $D_2$  at different reaction temperatures in the range from 220 - 340 K. The lower panels display the results obtained over the C-covered (black) and the C-free (gray) Pd(111) single crystal surface. For a more convenient comparison, rates obtained for the C-covered (black) and the C-free (gray) Pd/Fe<sub>3</sub>O<sub>4</sub> model catalyst are shown in the upper panel. All hydrogenation rates are normalized to the number of surface Pd atoms for a quantitative comparison.

black traces), the hydrogenation rates for the C-free Pd(111) single crystal (lower, gray traces) as well as the rates for the C-free (upper, gray traces) and the C-covered (upper, black traces) Pd/Fe<sub>3</sub>O<sub>4</sub> model catalyst are shown for a more convenient examination. All hydrogenation rates are normalized to the number of surface Pd atoms allowing for a direct quantitative comparison.

At low temperatures (up to 260 K), hydrogenation activity is not sustained over the C-covered Pd(111) single crystal. It should be noted however, that even for 220 K an initial hydrogenation activity is found at the beginning of the experiment that returns to zero after prolonged olefin exposure. At higher temperatures ( $\geq 280$  K), persisting hydrogenation is observed displaying a broad maximum in steady state rates between 300 and 340 K. This behavior is very similar to the reactivity of the C-free Pd(111) surface. Even the absolute hydrogenation rates are almost identical for the C-free and the C-covered Pd(111) surface. Only very slight differences are observed for the two surfaces. In contrast, for the Pd particles, significant reactivity changes upon C deposition were found. Deposition of C on Pd particles promotes sustained hydrogenation already at low temperatures, while the C-free Pd particles exhibit a qualitatively similar

hydrogenation activity as the Pd(111) single crystal surfaces.

The almost perfect agreement in the hydrogenation activity for the C-free and the C-covered Pd(111) surfaces in the entire investigated temperature range clearly shows that carbonaceous deposits on (111)-facets do *not* have a significant influence on the hydrogenation activity. This observation can be interpreted that they do not change the availability of subsurface D noticeably. Hence, the sustained hydrogenation activity on C-covered Pd particles arises from the modified properties of the low-coordinated sites and not from C-induced modification of the regular (111)-terraces.

## 7.4 The role of carbon

The results presented in the preceding section clearly showed that modification of *low-coordinated* surface sites with carbon induces sustained hydrogenation activity already at low reaction temperatures ( $\leq 260$  K), while no such effect is observed for C-deposition on (111)-facets. Persisting isomerization activity found for all investigated catalysts with rates in the same order of magnitude indicates that surface adsorbed D is available and that also the common reaction intermediate 2-butyl- $d_1$  is effectively formed. Thus, the high hydrogenation rates over the C-covered Pd particles at low temperatures, which are by several orders of magnitude higher than on the other investigated surfaces, cannot be attributed to strong variations in the concentrations of butyl and/or surface adsorbed D. This clearly shows that the sustained hydrogenation at low temperatures arises from the modified properties of the low-coordinated surface sites and not from C-induced modification of regular (111)-facets.

There are in principle two conceivable ways to understand the role of C-modified low-coordinated surface sites in the promotion of persisting hydrogenation activity at low temperatures. On one hand, these modified sites may exhibit a higher intrinsic hydrogenation activity than regular (111)-facets. On the other hand, C-modified low-coordinated sites may simply allow for the effective replenishment of reactive species required for the hydrogenation as previously suggested in chapter 5.

The first seemingly simple explanation that C-modified low-coordinated sites exhibit an intrinsically higher hydrogenation activity is not supported by the experimental results. Fig. 7.7 displays the initial hydrogenation rates on the D-presaturated surfaces normalized to the number of surface Pd atoms at 260 K obtained on the C-precovered Pd particles (left panel) in comparison to the initial hydrogenation rates obtained for the C-free Pd(111) surface (right panel) and the C-free Pd particles (middle panel). It can be seen in fig. 7.7 that the initial hydrogenation rates on the surface saturated with both surface and subsurface D are in the same range for the different catalysts. The hydrogenation rate over the Pd(111) surface is slightly lower compared to the initial rates over the Pd particles, but of a comparable size indicating that (111)-facets



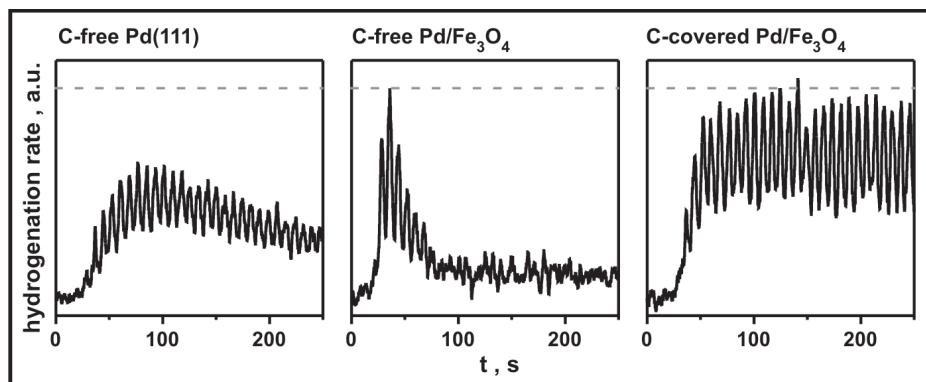


Figure 7.7: The initial hydrogenation rates of *cis*-2-butene obtained in isothermal pulsed MB experiments on D-presaturated surfaces at 260 K for C-free Pd(111) (left panel), C-free (middle panel) and C-covered (right panel) Pd particles. The samples were continuously exposed to a large flux of D<sub>2</sub>, while small amounts of *cis*-2-butene were pulsed onto the surfaces. The rates are normalized to the number of Pd surface atoms.

contribute significantly to the hydrogenation activity of the Pd particles which exhibit about 80 % of (111)-facets. A quantitative comparison of the initial hydrogenation rates of the C-free and the C-covered Pd particles clearly shows that both catalysts display very similar rates when the surface is saturated with D showing that C-modification of low-coordinated sites does *not* result in a higher intrinsic reactivity. As the observed differences in initial hydrogenation rates are relatively small for the different systems, when there are no limitations in surface and subsurface D availability, it is clear that the changes in hydrogenation activity under steady state conditions amounting to several orders of magnitude cannot be merely due to different intrinsic hydrogenation activities for different sites. On the contrary, this observation clearly demonstrates that Pd particles, Pd(111) and C-modified Pd particles exhibit very similar reactivities when there are no limitations in D availability.

As a second explanation for the promotion of sustained hydrogenation activity, a more effective replenishment of reactants under steady state conditions was suggested. Persisting *cis-trans* isomerization activity of comparable size observed for all investigated catalysts indicates that *surface* D species and *cis*-2-butene are available and that also the 2-butyl intermediate is effectively formed. The only remaining species which abundance can be significantly affected under reaction conditions is *subsurface* absorbed D. At a microscopic level, this implies that C-modification of low-coordinated sites alters the catalyst to be highly permeable for D and thereby enables the system to maintain the subsurface D concentration at sufficiently high levels, close to the initially present concentrations. This would result in persisting hydrogenation rates at or close to the initial level which is the experimentally observed result (see fig. 7.7). Thus, we conclude that C-modification of low-coordinated sites merely allows to maintain the concentration

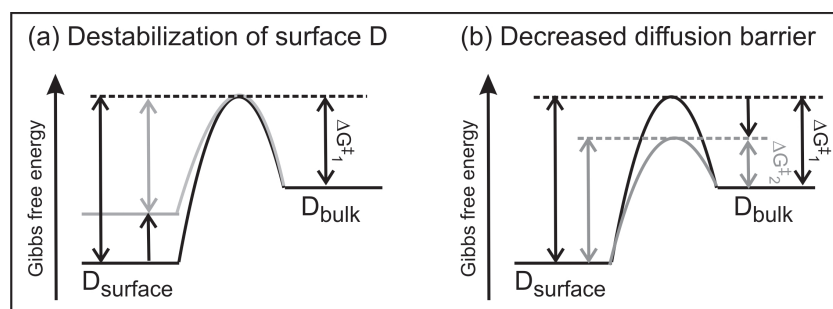


Figure 7.8: Schematic display for the reduction of the effective activation energy for D diffusion into the Pd subsurface by (a) destabilization of surface adsorbed D and by (b) a decreased diffusion barrier. The black lines depict schematically the  $H(D)$  sorption energetics of the C-free surface, while the gray lines indicate presumable changes upon C-modification.

of reactants, in particular the abundance of *subsurface* absorbed D, at a sufficiently high level under reaction conditions.

The microscopic mechanism how C-deposition on low-coordinated sites enables an effective replenishment of subsurface D is most likely based on determining how fast  $H(D)$  can penetrate into the subsurface region of Pd. Under reaction conditions, in the presence of co-adsorbed hydrocarbons, in principle two effects may contribute to a faster D diffusion to subsurface sites. It can be speculated on one hand, that blocking of sites for effective D diffusion by co-adsorbed hydrocarbons may be decreased due to a reduced binding of olefins in the vicinity of C or on the other hand, that C-modification of low-coordinated sites may directly enhance the rate constant for D diffusion.

Assuming that the effect of C modification of low-coordinated sites is exclusively preventing the blocking of diffusion sites for  $H(D)$  is not supported by our experimental results. The length of the induction period at the beginning of the experiment where strongly-bound hydrocarbon species accumulate is basically identical for the C-free and the C-covered Pd particles. This indicates that the amount of accumulated hydrocarbon species on the C-modified Pd particles is not significantly reduced with respect to the C-free particles.

An increase of the D diffusion rate from surface to subsurface sites is also expected when the effective activation barrier for D diffusion becomes reduced. As schematically depicted in fig. 7.8, this can be achieved either by a destabilization of the more strongly bound surface D or by a reduction of the activation barrier itself.

Recent theoretical calculations for hydrogen adsorption on and in Pd nanoparticles show that modification of edge sites by C has a significant influence on the hydrogen sorption energetics [196]. Next to binding energies for surface adsorbed and subsur-

face adsorbed H also the activation energies for H diffusion to subsurface sites were calculated. The density functional (DF) calculations were performed for cuboctahedral Pd<sub>79</sub> clusters which were previously shown to be representative for a realistic description of surface interactions present on larger Pd particles as in the experimentally studied supported Pd model catalyst [201, 202]. In particular, the properties of sites near particle edges are well described. Additionally, calculations on a Pd(111) slab model were performed for comparison (see [196] for details). The results of the calculations on hydrogen sorption and diffusion on Pd nanoparticles are schematically displayed in fig. 7.9.

At a low hydrogen coverage, surface adsorbed H located in an *fcc*-site on the pristine Pd cluster is by  $\approx 30 \text{ kJ} \cdot \text{mol}^{-1}$  more stable than H absorbed in a octahedral subsurface (*oss*) site. A relatively high activation barrier for hydrogen diffusion into the subsurface of  $29 \text{ kJ} \cdot \text{mol}^{-1}$  was obtained. For higher hydrogen coverages, that are experimentally more relevant, hydrogen surface adsorption and subsurface absorption were calculated to be almost isoenergetic. However, a still relatively high activation barrier of  $17 \text{ kJ} \cdot \text{mol}^{-1}$  was obtained for H diffusion to subsurface sites. For the Pd(111) slab model, similar trends were observed when proceeding from low H coverage to high H coverage conditions.

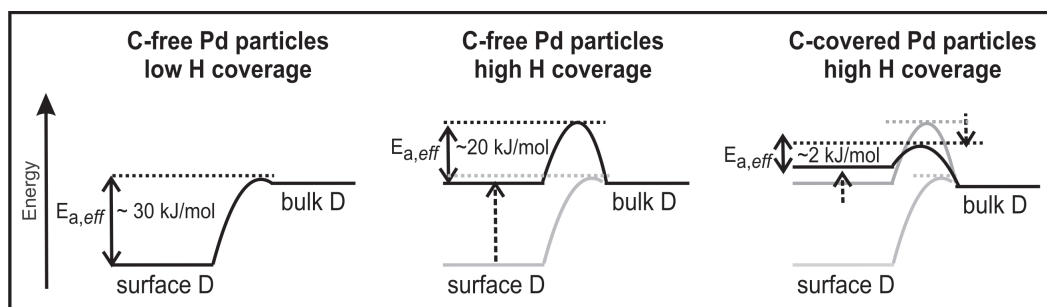


Figure 7.9: Schematic display of the energetics of H sorption and diffusion on small Pd particles as calculated using DFT by Neyman *et al.* (see text and [196] for more details). The left panel depicts schematically the H sorption energetics for a low H coverage on a C-free Pd cluster, while in the middle panel, the energetics for a high H coverage over a C-free Pd cluster (black lines) are displayed (in gray the energetics for a low H coverage are depicted for comparison). The right panel schematically represents the H sorption energetics for C-modified Pd clusters (black lines). For a more convenient comparison, also the energetics for the a low (light gray) and high (gray) H coverage on the C-free Pd clusters are displayed.

When carbon was added to the Pd clusters occupying subsurface sites, which is also expected to some extent for the experimentally applied conditions, subsurface adsorbed H became energetically favored compared to the surface H species by  $\approx 20 \text{ kJ} \cdot \text{mol}^{-1}$ . This shift in binding energies results in a thermodynamic driving force for H diffusion

to subsurface sites. Moreover, for the C-containing Pd cluster the activation barrier for H diffusion into the subsurface is with  $\approx 2 \text{ kJ} \cdot \text{mol}^{-1}$  basically eliminated.

This trend was attributed to Pd cluster distortions assisting H diffusion into the subsurface. It was found that the Pd-Pd bond distance is significantly extended in the presence of carbon. A similar lattice expansion has been previously reported in XRD studies for high C contents (see *e.g.* [60, 130, 131] and 2.2.3 for details). In the DFT calculations, a correlation between this Pd-Pd bond expansion and the decrease of the diffusion barrier was found which showed that for H diffusion a transition state with relatively large Pd bonds is energetically favorable. In the presence of C, the Pd bonds are already significantly elongated so that only a negligibly small activation barrier for H diffusion is found for this situation.

Thus, two effects contribute to a reduction of the effective diffusion barrier for C-modified low-coordinates sites of Pd clusters: C leads, on one hand, to a destabilization of surface adsorbed H. On the other hand, C on atomically flexible edge sites induces local distortions of the Pd lattice which results in a basically vanishing activation barrier for H diffusion to subsurface sites.

For the rigid Pd(111) single crystal surface, a C-induced Pd lattice expansion is not predicted by the DFT calculations. Thus, in the case of the Pd(111) surface, only destabilization of surface adsorbed H in the presence of C is expected to lead to a partial reduction of the diffusion barrier. Therefore, the effect of C-modification of the rigid Pd(111) surface on the reactivity is expected to be only minor compared to the effect of C-modification of atomically flexible, low-coordinated sites of Pd particles which is in good agreement with the experimental results.

In summary, C-modification of low-coordinated sites promotes persisting hydrogenation activity at low temperatures. This promotion is clearly not due to a higher intrinsic reactivity of the modified sites, the C-modification rather allows for an effective replenishment of subsurface hydrogen under reaction conditions. The microscopic mechanism for the facilitated replenishment under reaction conditions at low temperatures can be attributed to two effects. As suggested by theoretical calculations, C destabilizes on one hand surface adsorbed H so that diffusion to subsurface sites becomes energetically favorable and more importantly, C-modification of atomically flexible, low-coordinated sites results in elongated Pd-Pd bonds leading to a reduction of the diffusion barrier enhancing thus, the D diffusion rate. For the rigid Pd(111) surface, in contrast, an expansion of the Pd lattice is not predicted, so that the reduction of the H diffusion barrier in the presence of C and thus, the effect C-modification on the reactivity is expected to be much smaller for Pd(111) which is in line with our experimental results.

## 7.5 Conclusion

To study the role of low-coordinated sites and their modification by carbon deposition in the conversion of *cis*-2-butene with D<sub>2</sub>, pulsed isothermal experiments were conducted on small Pd particles supported on Fe<sub>3</sub>O<sub>4</sub>/Pt(111) and on a Pd(111) single crystal surface. Results were recorded for both the C-free as well as on the C-covered Pd catalysts for different temperatures between 220 and 340 K.

The isomerization activity over the Pd(111) surface exhibits a qualitatively very similar behavior as over the supported Pd particles. With increasing temperature, initially the isomerization rates increase exhibiting a maximum around 280 K, before decreasing for even higher reaction temperatures. A quantitative comparison of the rates indicates that low-coordinated sites are more reactive than the (111)-facets which is in line with previous studies (*e.g.* [37]). The isomerization rates per Pd surface atom are however for the Pd(111) surface and the Pd particles in the same order of magnitude.

Deposition of C does not significantly influence the isomerization activity over the two Pd model catalysts. Small differences in the absolute rates can presumably be attributed to differences in the olefin binding energies on the different surfaces.

Over the C-free Pd(111) surface, the hydrogenation activity is similar to that observed for the C-free Pd particles. Over both C-free Pd surfaces, after an induction period, initially high hydrogenation rates are found that return to zero for longer olefin exposures at low temperatures ( $\leq 260$  K). The observed initial hydrogenation rates per Pd surface atom are similar for the C-free Pd(111) surface and the C-free Pd particles. At higher temperatures ( $\geq 280$  K), similarly to the C-free Pd particles, persisting hydrogenation activity is observed also over the Pd(111) single crystal surface. A quantitative comparison of both the initial and steady state hydrogenation rates per Pd surface atom over the Pd(111) surface and the Pd particles indicates that the (111)-facets contribute significantly to the hydrogenation activity of the Pd particles which is in line with previous studies reporting no pronounced structure sensitivity for alkene hydrogenation over Pd catalysts (*e.g.* [37]).

While carbonaceous deposits on Pd particles, mainly located on low-coordinated sites, induce persisting hydrogenation activity at low temperatures, deposition of C on the Pd(111) single crystal surface does not result in significant changes in the hydrogenation activity in the entire investigated temperature range (220-340 K).

The persisting isomerization activity over all investigated Pd model catalysts indicated that surface D and *cis*-2-butene are available on the surface and that also the 2-butyl intermediate is effectively formed. This suggests that the difference in hydrogenation rates cannot be attributed to large concentration differences of surface D and/or *cis*-2-butene for the different catalysts. This clearly showed that the the promotion of sustained hydrogenation activity observed for C-covered Pd particles arises from the

modified properties of the low-coordinated surface site and not from C-induced modification of regular (111)-facets.

A comparison of the initial rates on the D-presaturated surfaces clearly showed that the intrinsic reactivity is similar for all investigated Pd surfaces, the C-free and C-covered Pd(111) single crystal as well as the C-free and C-covered Pd particles, when there are no limitations in D availability. From this, it was concluded that carbonaceous deposits on low-coordinated sites merely allow for an effective replenishment of reactive species under reaction conditions, *i.e.* of *subsurface* absorbed D.

Recent theoretical calculations indicated that surface adsorbed H is destabilized in the vicinity of C so that H diffusion to subsurface sites becomes energetically favorable. Moreover, C located at atomically flexible edge sites of Pd clusters leads to a local expansion of the Pd lattice which results in a significant reduction of the activation barrier for H diffusion to subsurface sites and thus, an increase of the H diffusion rate. For the rigid Pd(111) surface, in contrast, a C-induced expansion of the Pd lattice is not predicted. Thus, the effect of C-deposition is expected to be minor for the Pd(111) surface compared to C-modification of Pd particles which is in good agreement with the experimental results.

# 8 H/D exchange over Pd model catalysts: Probing the hydrogen distribution

## 8.1 Introduction

Hydrogen sorption on transition metals plays a crucial role in many catalytic reactions, *e.g.* in the hydrogenation of olefins, and is therefore an important subject in catalysis research. Despite numerous classical catalytic and more modern surface science studies, still fundamental questions remain unsolved.

A classical method to probe the hydrogen state on metal surfaces is to study the H/D exchange over these surfaces. The mechanisms of this seemingly simple reaction, where a hydrogen atom recombines with deuterium atom to yield HD, have been under debate since the early 1900's. For a number of transition metal surfaces, a Langmuir-Hinshelwood mechanism was found to describe the H/D exchange well [109]:



On palladium, hydrogen cannot only bind to the surface, but it can also be accommodated in the subsurface and bulk region of palladium [54, 55]. These subsurface absorbed H species were speculated to influence the H/D exchange reaction over Pd surfaces. On one hand, subsurface/bulk absorbed hydrogen was suggested to change the adsorption state of surface bound hydrogen and thereby, influence the H/D exchange. On the other hand, subsurface hydrogen was speculated to be directly involved in the formation of HD providing an additional reaction pathway for the H/D exchange.

Hydrogen adsorbs for low coverages on surface sites in a basically non-activated dissociative adsorption process [27, 104, 105, 109]. For higher coverages, also diffusion to subsurface sites occurs. Hydrogen diffusion into the subsurface/bulk region is known to be a strongly structure sensitive process which is significantly slower for close-packed (111)-facets than for more open surfaces [70–75].

Temperature programmed desorption (TPD) measurements on hydrogen adsorption over Pd surfaces typically display two desorption peaks associated with two hydrogen states on Pd, which were attributed to surface adsorbed and subsurface/bulk absorbed H. While the high temperature desorption peak for hydrogen over Pd single crystal sur-

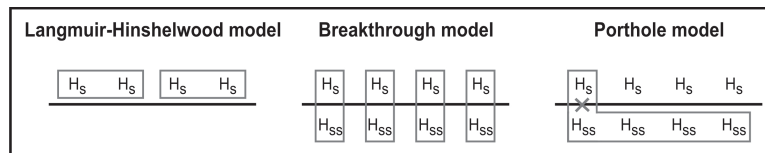


Figure 8.1: Schematical display of models for H<sub>2</sub> formation over Pd (after [203]). Following the Langmuir-Hinshelwood model, H<sub>2</sub> is formed by recombination of two surface adsorbed H species (left). In the *breakthrough* model (middle), recombination of a surface adsorbed H and a subsurface adsorbed H provides an additional H<sub>2</sub> formation channel. Similarly, in the *porthole* model (right), surface H also reacts with subsurface H, but only on special sites, like defects (denoted by x).

faces typically displays a second order behavior, a peak shape indicative of first order desorption was reported for the low temperature desorption feature [27, 70, 71, 104]. For a classical Langmuir-Hinshelwood (LH) mechanism where associative H<sub>2</sub> desorption is rate limiting, a second order desorption behavior is expected as observed for the high temperature H<sub>2</sub> desorption. A first order desorption cannot be explained however by a LH mechanism. Konvalinka *et al.* therefore suggested a *breakthrough* and/or a *porthole* model, schematically displayed in fig. 8.1 [203]. In the *breakthrough* model, subsurface adsorbed hydrogen was suggested to directly react with surface hydrogen to H<sub>2</sub>. The *porthole* model proposed also a direct reaction of subsurface with surface hydrogen, but however only on special sites, like defects.

Engel and Kuipers studied the H/D exchange over a Pd(111) single crystal surface in broad temperature range (250-550 K) using molecular beam techniques [27]. They found, in contrast with the considerations by Konvalinka *et al.*, that HD formation over a Pd(111) surface can be described fairly well by a Langmuir-Hinshelwood mechanism without assuming an activation energy for equilibration of the system stating, in particular, that the equilibrium between surface and subsurface H(D) is reached quickly for surface temperatures > 300 K. It should be noted, however, that some deviations from the Langmuir-Hinshelwood model, *e.g.* higher experimental HD formation rates at temperatures < 300 K than predicted by the model, were observed which were attributed to a surface heterogeneity due to *e.g.* adsorption sites of different binding energies and/or different sticking coefficients for H<sub>2</sub>(D<sub>2</sub>).

Fig. 8.2 displays a D<sub>2</sub> TPD obtained from a supported Pd model catalyst [150]. For a saturation coverage, two desorption maxima at 295 and 325 K are visible with the peaks strongly overlapping [150] which is in line with previous reports in the literature [43]. In combination with nuclear reaction analysis (NRA) measurements for hydrogen depth profiling on Pd particles, it could be demonstrated that the low temperature H<sub>2</sub>(D<sub>2</sub>) desorption is associated with the depletion of subsurface/volume adsorbed H(D) species, while the concentration of surface adsorbed H(D) species remains in this



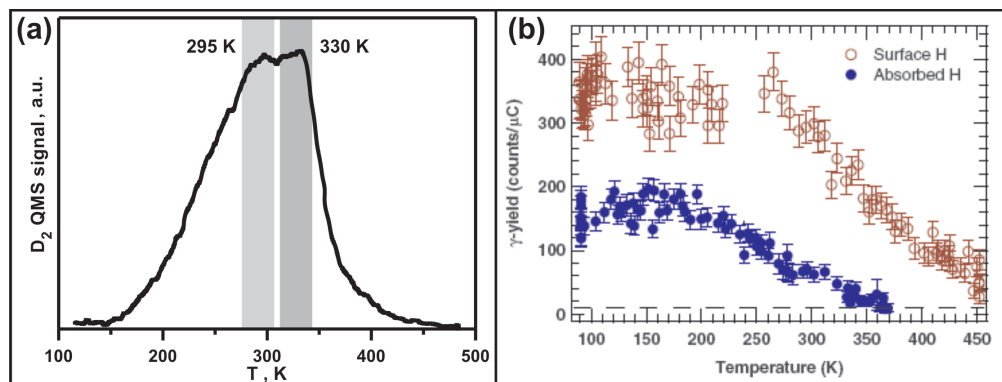


Figure 8.2: (a) D<sub>2</sub> TPD spectrum obtained for Pd particles of  $\approx 7$  nm in diameter supported on Fe<sub>3</sub>O<sub>4</sub> after an exposure of 3.1 L of D<sub>2</sub> at 115 K. The spectrum displays two maxima at 295 and 330 K. (b) Temperature dependent nuclear reaction analysis (NRA) measurements for hydrogen depth profiling obtained for supported Pd particles for a H<sub>2</sub> pressure of  $1 \cdot 10^{-5}$  mbar (from [188]). Depletion of volume-absorbed H occurs at lower temperatures coinciding with the H<sub>2</sub>(D<sub>2</sub>) desorption feature displaying a maximum around 295 K, while depletion of surface adsorbed H is observed only for higher temperatures coinciding with the H<sub>2</sub>(D<sub>2</sub>) desorption peak around 330 K.

temperature region basically unchanged and becomes only depleted for temperatures coinciding with the high temperature H<sub>2</sub>(D<sub>2</sub>) desorption peak [188]. Thus, H<sub>2</sub>(D<sub>2</sub>/HD) formation at rather *low* temperatures (260 K) is expected to be strongly influenced by *subsurface* absorbed H(D) species, while H<sub>2</sub>(D<sub>2</sub>/HD) formation at *higher* temperatures (320 K) is expected to be dominated by recombination of *surface* adsorbed H(D) species.

The weakly-bound subsurface hydrogen was suggested to be more reactive than the more strongly bound surface H and is, thus, expected to play an important role in hydrogenation reactions over Pd surfaces [57–59]. Ceyer *et al.* investigated the role of surface and subsurface H in the hydrogenation of hydrocarbons over Ni surfaces [56, 204–207]. Based on HREELS and TPR measurements using MB techniques for the preparation of subsurface H at low temperatures and for the collision induced desorption of surface H, the authors concluded that weakly-bound subsurface absorbed H is more reactive in hydrogenation than surface adsorbed H which was attributed to the higher energy of subsurface H compared to surface adsorbed H [56, 204–207]. Moreover, they suggested based on their results that subsurface H *directly* reacts with the hydrocarbons upon resurfacing [56, 204–207].

In the preceding chapters, experimental evidence was presented indicating that also the activity and selectivity of Pd model catalysts in *cis*-2-butene conversion with hydrogen crucially depends on the availability of surface adsorbed and subsurface absorbed H. For hydrogenation of *cis*-2-butene over Pd particles, the presence of subsurface hydro-

gen is required, while the *cis-trans* isomerization proceeds effectively when just surface hydrogen is present. It should be emphasized that we do not imply that subsurface absorbed H(D) is directly involved in the formation of the hydrogenation product. Instead, it can merely modify the adsorption properties of surface adsorbed H(D) such that surface adsorbed H(D) becomes more prone to attack the Pd-butyl bond leading to the formation of the hydrogenation product (see chapter 5 for details). Based on our measurements on the 2-butene reactivity, a distinction between these two possible mechanisms is not feasible.

The measurements on the 2-butene reactivity indicated moreover that the hydrogen distribution on and in the Pd particles may vary strongly with different reaction conditions. Small amounts of carbonaceous deposits mainly located on atomically flexible edge sites were found to facilitate the replenishment of subsurface H(D) under reaction conditions inducing thereby sustained hydrogenation already at low temperatures. Recent DFT calculations indicate that this effect can be attributed to an increased diffusion rate due to C-induced distortions of the Pd lattice leading to a reduction of the diffusion barrier [196]. In contrast, co-adsorbed hydrocarbon species, usually present under reaction conditions, were found to inhibit both the dissociative adsorption of H<sub>2</sub>(D<sub>2</sub>) as well as H(D) diffusion into the subsurface.

Several related questions arise from these considerations: Can H/D exchange over Pd be described by a simple Langmuir-Hinshelwood mechanism or is a more complex model required? Does subsurface hydrogen influence the H/D exchange over Pd? Is it possible to probe changes in the H distribution in the presence of carbonaceous deposits on low-coordinated sites as suggested by the measurements on the butene reactivity? And how do co-adsorbed hydrocarbons affect the H/D exchange?

To address these questions with an independent method, isothermal pulsed MB experiments on the H/D exchange over Pd model catalysts were conducted under well-defined UHV conditions. Using this approach, both the *transient* and the *steady state* kinetics can be investigated and it can be studied how they are influenced by different reaction conditions. In the first part of this chapter (8.2), the influence of C-modification of low-coordinated sites on the steady state HD formation rates will be presented. Measurements on the involvement of subsurface H(D) species in the HD formation will be discussed on the second part (8.3), while the effect of co-adsorbed hydrocarbons on the H/D exchange will be addressed in the third part of this chapter (8.4).

## 8.2 The influence of C-modification of low-coordinated sites

To probe the effect of C-modification of low-coordinated sites, isothermal H/D exchange experiments were conducted over the C-free and the C-precovered Pd/Fe<sub>3</sub>O<sub>4</sub>/Pt(111) model catalyst. The measurements were conducted for two reaction temperatures, 260 and 320 K. While for a reaction temperature of 320 K, HD formation is expected to be

dominated by recombination of surface adsorbed H(D) species, as indicated by TPD and NRA measurements [188], subsurface adsorbed H(D) species are expected to strongly influence the H/D exchange at a lower reaction temperature of 260 K. This can mean either that *subsurface* adsorbed H(D) species are *directly* involved in the formation of HD or that they *indirectly* influence the HD formation by modification of *surface* adsorbed H(D) *via e.g.* lowering the binding energy.

In the pulsed isothermal MB experiments on the H/D exchange over C-free and C-covered Pd particles, the model catalysts were continuously exposed to a large excess of D<sub>2</sub>, while a much smaller flux of H<sub>2</sub> was pulsed (60 s on, 60 s off) onto the surfaces using a second independent effusive beam source. The overall pressure was varied ranging from  $1.3 \cdot 10^{-6} - 5.3 \cdot 10^{-6}$  mbar (overall flux:  $1.1 \cdot 10^{15} - 4.3 \cdot 10^{15}$  molecules  $\cdot$  cm<sup>-2</sup>  $\cdot$  s<sup>-1</sup>), while the ratio of the H<sub>2</sub>:D<sub>2</sub> flux was kept constant at 1.4 % in all measurements. Applying a large excess of D<sub>2</sub> ensures that the concentrations of surface adsorbed and subsurface adsorbed D are not notably affected when H<sub>2</sub> is introduced into the system which significantly simplifies the interpretation of the data. The HD formation rate (HD<sup>+</sup> at 3 amu) as well as the evolution of the reactants, D<sub>2</sub> (D<sub>2</sub><sup>+</sup> at 4.8 amu, thus, off the peak maximum to avoid saturation of the detector) and H<sub>2</sub> (H<sub>2</sub><sup>+</sup> at 2 amu), in the gas phase was followed by QMS as a function of time. Toward the end of the H<sub>2</sub> pulse, the HD formation rates approached a constant value indicating steady state conditions. Thus, the rate value at the end of the H<sub>2</sub> exposure was taken as the steady state rate for a given reaction condition.

To obtain a better signal to noise ratio, the HD signal was averaged over several H<sub>2</sub> pulses. As gradual CO adsorption from the background gas was found to significantly poison the H/D exchange, only the first three pulses of an isothermal experiment were used in the averaging procedure. Reference measurements showed that a time-dependent HD signal is found even for the empty chamber presumably due to recombination reactions on the chamber walls and in the ion source of the QMS caused by relatively high pressures. The experimental HD signals were, thus, corrected for this chamber associated time-dependent signal. To obtain a very smooth chamber reference signal, the average of a large number of pulses (typically 70 – 200) was acquired for the empty chamber under equivalent pressure conditions as the corresponding sample measurements.

Fig. 8.3 displays the averaged steady state HD formation rates obtained from several measurements for each reaction condition as a function of the overall pressure. The steady state rates are given for the C-free (black) and the C-covered (gray) Pd/Fe<sub>3</sub>O<sub>4</sub> model catalyst at 260 K (filled circles) and 320 K (open squares). The error bars represent the standard error of the mean of the averaged steady state HD rates and the measured H<sub>2</sub>-QMS signals obtained for several measurements (typically 2-7) for each reaction condition.

For all investigated conditions, the steady state HD formation rates increase with increasing pressure. The H/D exchange rates for a reaction temperature of 260 K are

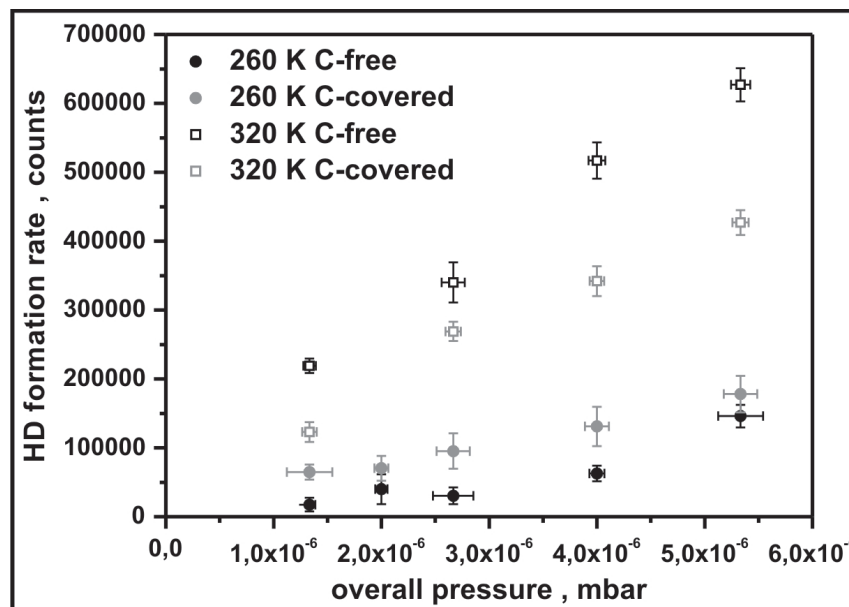


Figure 8.3: Steady state HD formation rates over the C-free (black) and the C-covered (gray) Pd/Fe<sub>3</sub>O<sub>4</sub> model catalyst for 260 K and 320 K as a function of the overall pressure. The ratio of the H<sub>2</sub>:D<sub>2</sub> flux was kept constant and the overall pressure was varied from  $1.3 \cdot 10^{-6} - 5.3 \cdot 10^{-6}$  mbar. The values for the steady state rates were obtained from several measurements for each reaction condition with the error bars indicating the standard error of the mean of the steady state HD rate and the measured H<sub>2</sub> signal. For the C-covered Pd particles significantly different HD formation rates are found with respect to the C-free surfaces.

clearly smaller than those observed for 320 K which can be attributed to increasing reaction rate constants for associative desorption of HD with increasing temperature. Over the C-precovered Pd particles, the steady state H/D exchange rates at 260 K are consistently higher than those observed for the C-free Pd particles. For a reaction temperature of 320 K, in contrast, the HD formation is lower over the C-covered Pd model catalyst. These results clearly demonstrate that the steady state H/D exchange rates are affected by C deposition.

For a reaction temperature of 320 K, where HD formation is expected to be governed by recombination of surface adsorbed H(D) as indicated by TPD and NRA measurements [188], the steady state H/D exchange rates over the C-modified Pd particles are lowered compared to the HD formation rates over the C-free Pd model catalyst. The reduction of the steady state HD formation rate over the C-covered Pd particles can likely be attributed to physical blocking of surface adsorption sites for H(D) by carbonaceous deposits. This poisoning of adsorption sites is expected to lead to decreased coverages

## 8.2 The influence of C-modification of low-coordinated sites

of surface adsorbed H(D) and thus, to reduced steady state HD formation rates which is the experimentally observed result.

At a reaction temperature of 260 K, where H/D exchange is expected to be strongly influenced by subsurface related H(D) species, the C-modification of Pd particles results in *higher* steady state HD reaction rates with respect to the C-free Pd/Fe<sub>3</sub>O<sub>4</sub> model catalyst. Increased HD formation rates on the C-covered Pd model catalyst despite a partial blocking of surface adsorption sites which most probably results in lower surface H(D) concentrations, is an intuitively unexpected result.

The rate of a reaction changes either when the reaction *rate constant* is altered or when the the reactant *concentrations* vary. DFT calculations investigating the influence of C-modification of low-coordinated sites on Pd particles on the hydrogen sorption and diffusion to subsurface sites indicated that C located in subsurface sites near atomically flexible particle edges lowers the activation energy for H(D) diffusion to subsurface sites [196] (see also 7.4 for details). This C-induced decrease in activation energy is expected to result in an increased rate constant for H(D) diffusion into the subsurface and thus, to higher steady state subsurface H(D) concentrations. At a reaction temperature of 260 K, where HD formation is expected to be strongly influenced by subsurface H(D) species, an increase in the steady state H/D exchange rates for C-modified Pd particles would be expected which is the experimentally observed result.

The seemingly intuitive assumption that the C-modified low-coordinated sites exhibit simply a significantly higher rate constant for associative desorption of *surface* H(D) with respect to the unmodified low-coordinated sites due to destabilization of surface adsorbed H(D) [196], is not supported by the experimental results. A similar destabilization of surface adsorbed H(D) is expected for C deposition on a Pd(111) single crystal surface [196]. However, the steady state H/D exchange rates over the C-precovered Pd(111) single crystal surface are not increased with respect to the C-free Pd(111) single crystal.

In summary, the pressure dependent measurements on the steady state H/D exchange rates over the C-free and the C-modified Pd particles at two reaction temperatures, 260 and 320 K, clearly showed that C deposition influences the steady state HD formation rates. For the higher surface temperature of 320 K, where the formation of HD is expected to be dominated by recombination of surface adsorbed H(D), the H/D exchange rates are decreased in the presence of C which can be likely attributed to blocking of surface adsorption sites for H(D) by C. For the lower reaction temperature 260 K, where HD formation is expected to depend largely on the concentration of subsurface H(D) species, an increase of the steady state H/D exchange rates is observed. An increase of the HD formation rate despite the blocking of adsorption sites for H(D) by C is unexpected. The increase in steady state H/D exchange rates in the presence of C at the low reaction temperature (260 K) where a significant influence of subsurface related H(D) species is expected can likely be attributed to an C-induced increase of the rate constant for H diffusion to subsurface sites. This interpretation is in good agreement

with recent DFT calculations predicting a lowering of the activation barrier for H(D) diffusion upon C-modification of atomically flexible edge sites [196].

### 8.3 The influence of subsurface H

It is well known that hydrogen can occupy next to *surface* sites also *subsurface* sites on Pd (see *e.g.* [54, 55, 188]). The influence of the *subsurface* absorbed H(D) species on the H/D exchange has been however still under debate. If just *surface* adsorbed H(D) was involved in the formation of HD over Pd surfaces, a Langmuir-Hinshelwood mechanism is expected to be sufficient to describe the kinetics of the H/D exchange, while, in contrast, more complex mechanisms are expected when also *subsurface* H(D) is involved in the HD formation.

In order to investigate the role of subsurface absorbed H(D) in the HD formation over Pd model catalysts, isothermal pulsed MB H/D exchange experiments were conducted varying the reaction conditions in a broad parameter range. First, the steady state HD formation rates were measured as a function of the reaction temperature in the range from 220 K to 340 K over the C-free and the C-precovered Pd(111) single crystal surface as well as over the C-free and the C-precovered Pd/Fe<sub>3</sub>O<sub>4</sub>/Pt(111) model catalyst. The resulting steady state rates as a function of reaction temperature were compared to values predicted by a simple Langmuir-Hinshelwood (LH) kinetic model assuming HD formation only by recombination of surface adsorbed H(D). Secondly, the steady state H/D exchange rates over the C-free and the C-precovered Pd particles were studied as a function of the H<sub>2</sub>, D<sub>2</sub> and overall pressure for two different reaction temperatures, 260 and 320 K. As indicated by TPD and NRA measurements, for a surface temperature of 320 K, HD formation is expected to be governed by recombination of *surface* adsorbed H(D) species, while *subsurface* H(D) is expected to have a strong influence at a lower reaction temperature of 260 K. The experimentally observed reaction orders are then compared to values predicted by a LH kinetic model assuming just recombination of surface H(D). As a third aspect, the transient kinetic response of the HD signal upon modulation of the H<sub>2</sub> beam is qualitatively analyzed for different Pd model catalysts, *i.e.* the Pd(111) single crystal, C-free and C-modified Pd particles.

#### 8.3.1 Temperature dependence

To investigate the influence of subsurface absorbed H(D) on the steady state H/D exchange rates further, the steady state HD formation rates were measured for different surface temperatures. Isothermal pulsed MB experiments were conducted for the C-free and C-covered Pd(111) single crystal surface as well as for the C-free and C-covered supported Pd/Fe<sub>3</sub>O<sub>4</sub> model catalyst following the same pulse sequence as described in the previous section 8.2. In these experiments, the H<sub>2</sub> ( $4.0 \cdot 10^{-8}$  mbar) and D<sub>2</sub> ( $4.0 \cdot 10^{-6}$  mbar) pressures were kept constant and the reaction temperature was varied in the range from 220 to 340 K. For a direct comparison, all HD formation rates are

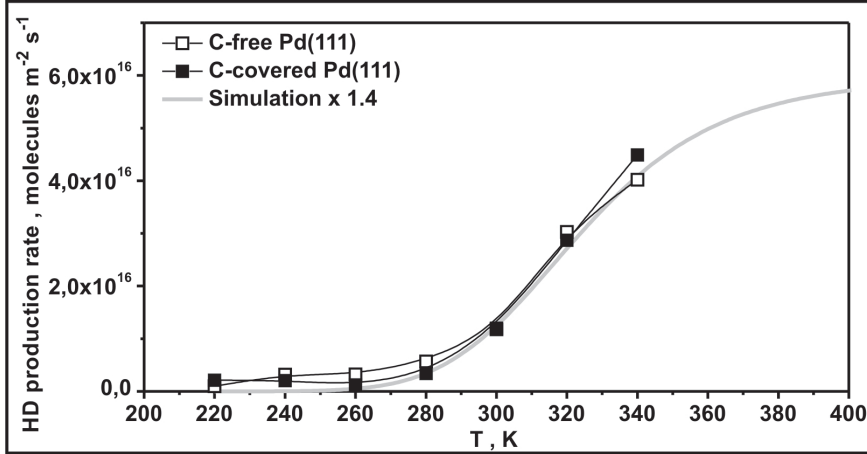


Figure 8.4: Steady state HD formation rates over the C-free (open squares) and the C-covered (filled squares) Pd(111) single crystal surface for different reaction temperatures. The  $H_2$  ( $4.0 \cdot 10^{-8}$  mbar) and  $D_2$  ( $4.0 \cdot 10^{-6}$  mbar) pressures were kept constant for all experiments, while the temperature was varied between 220 and 340 K. For comparison, a kinetic simulation based on a Langmuir-Hinshelwood model assuming HD formation only by recombination of surface adsorbed H(D) is displayed (gray line).

normalized to the number of surface Pd atoms.

In fig. 8.4, the averaged steady state reaction rates obtained for H/D exchange over the C-free (open squares) and the C-covered (filled squares) Pd(111) single crystal surface are displayed. It can be seen that the HD formation rates over the C-free and the C-covered Pd(111) surface are very similar in the entire investigated temperature range. At low temperatures, the HD formation rates are very small and a significant increase of the rates is only observed for temperatures higher than 280 K.

To estimate the possible effect of subsurface hydrogen on the H/D exchange, a kinetic simulation based on a Langmuir-Hinshelwood (LH) mechanism assuming HD formation just by recombination of *surface* H(D) and, thus, neglecting any presumable effect of *subsurface* H(D) was conducted for comparison. As generally believed, the rate limiting step for H(D) removal from the surface was assumed to be the recombination of H(D) followed by fast desorption of the  $H_2$ ,  $D_2$  or HD molecule [55, 208]. The rates of dissociative adsorption and associative desorption were calculated by:

$$R_{ads} = \frac{S_0 \cdot p}{\sqrt{2\pi mk_B T}} \cdot e^{-E_{ads}/RT} \quad (8.4)$$

$$R_{des} = \theta_A \cdot \theta_B \cdot A \cdot e^{-E_{des}/RT_s} \quad (8.5)$$

with  $S_0$  denoting the intrinsic sticking probability,  $p$  the applied pressure of the ad-

Table 8.1: Parameters used for the kinetic simulation for HD formation over Pd (see also [209] for more details).

reaction	$S_0$	$E_{ads}$ , kJ/mol
H <sub>2</sub> + Pd(111)	0.1 [27, 55, 105, 210]	0 [55, 104, 109]
D <sub>2</sub> + Pd(111)	0.1 [27, 55, 105, 210]	0 [55, 104, 109]
reaction	$A$ , s <sup>-1</sup>	$E_{des}$ , kJ/mol
H + D	10 <sup>13</sup> [211–213]	80.0 [27, 55, 208, 212, 213]
H + H	10 <sup>13</sup> [211–213]	85.8 [27, 55, 208, 212, 213]
D + D	10 <sup>13</sup> [211–213]	80.4 [27, 55, 208, 212, 213]

sorbing species,  $m$  the molecular mass of the adsorbing molecule,  $k_B$  the Boltzmann constant,  $T$  the temperature of the incoming gas, and  $E_{ads}$  is the activation energy for dissociative adsorption.  $\theta_A$  and  $\theta_B$  denote the normalized surface coverages of the recombining species,  $T_s$  the surface temperature,  $A$  the pre-exponential factor and  $E_{des}$  the activation energy of the recombination reaction. The values for the activation energies of associative desorption were taken for Pd(111) and assumed to be isotope dependent. These values should also be a good approximation for reaction over the Pd particles which exhibit  $\approx 80\%$  of (111)-facets. The parameters used for the kinetic simulation are summarized in table 8.1.

From fig. 8.4, it can be seen that the H/D exchange over both the C-free and the C-precovered Pd(111) single crystal surface is overall well described by the kinetic model (gray line) which assumes HD formation only by recombination of surface adsorbed H(D). For low reaction temperatures ( $\leq 280$  K), the experimentally observed HD formation rates are slightly higher than the predicted values suggesting for these temperatures a possible influence of subsurface H(D). Overall, the effect is however small for the Pd(111) single crystal surface.

These results, both the overall good agreement of the experimental H/D exchange rates as well as some deviations at relatively low surface temperatures are in line with previous measurements on the H/D exchange over a Pd(111) single crystal surface for temperatures ranging from 250 to 550 K [27]. In this earlier study, the deviations from the LH model were attributed to a surface heterogeneity *e.g.* due to adsorption sites with different binding energies and/or different sticking coefficients for H<sub>2</sub>(D<sub>2</sub>).

Fig. 8.5 displays the steady state HD formation rates over the C-free and the C-covered supported Pd/Fe<sub>3</sub>O<sub>4</sub> model catalyst for different reaction temperatures. For a direct comparison, the rates obtained for the Pd/Fe<sub>3</sub>O<sub>4</sub> model catalyst ( $0.6 \cdot 10^{15}$  Pd surface atoms·cm<sup>-2</sup>) were normalized (scaling factor 2.5) to the number of surface Pd atoms for a Pd(111) surface ( $1.5 \cdot 10^{15}$  Pd surface atoms·cm<sup>-2</sup>). The C-free and the C-modified Pd particles exhibit clear differences in the temperature dependence of the



H/D exchange. In the investigated temperature range, the activity of the C-modified Pd particles increases almost linearly with increasing temperature, while for the C-free Pd particles, the evolution in HD formation activity with temperature qualitatively resembles more that of the Pd(111) surface - for higher temperatures ( $> 280$  K), a significant increase in reaction rate is observed, while at lower temperatures rather small rates are measured. At low temperatures ( $< 280$  K), the HD formation rates are consistently higher over the C-precovered Pd particles, while at higher temperatures ( $\geq 300$  K) the C-free Pd/Fe<sub>3</sub>O<sub>4</sub> model catalyst is more reactive in HD formation.

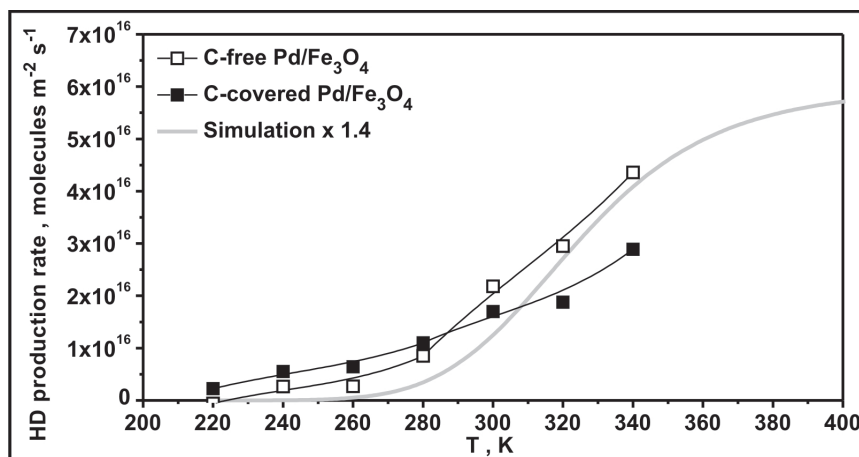


Figure 8.5: Steady state HD formation rates over the C-free (open squares) and the C-covered (filled squares) Pd/Fe<sub>3</sub>O<sub>4</sub> model catalyst for different reaction temperatures (rates are normalized (scaling factor of 2.5) to a number of  $1.5 \cdot 10^{15}$  Pd surface atoms·cm<sup>-2</sup>). The H<sub>2</sub> ( $4.0 \cdot 10^{-8}$  mbar) and D<sub>2</sub> ( $4.0 \cdot 10^{-6}$  mbar) pressures were kept constant for all experiments, while the temperature was varied between 220 and 340 K. For comparison, a kinetic simulation based on a Langmuir-Hinshelwood model assuming HD formation only by recombination of surface adsorbed H(D) is displayed (gray line).

Comparison with the kinetic simulation clearly shows significant differences with the experimental data, both for the C-free and the C-covered Pd particles. For the C-free Pd/Fe<sub>3</sub>O<sub>4</sub> model catalyst, the experimental rates are at low temperatures ( $\leq 300$  K) clearly higher than the values predicted by the kinetic model. At higher temperatures ( $\geq 320$  K), however, a reasonable agreement between experiment and model is found. For the C-covered Pd particles, the simulation does not reflect the experimental data in the entire investigated temperature range. At low temperatures ( $\leq 300$  K), similar to the C-free Pd particles and the Pd(111) single crystal surface, the experimental HD formation rates are higher than the simulation. For high temperatures ( $\geq 320$  K), the H/D exchange rates over the C-covered Pd particles are considerably lower than the model. The latter effect, as previously discussed (see 8.2), can likely be attributed to a

blocking of surface adsorption sites for H(D) by C.

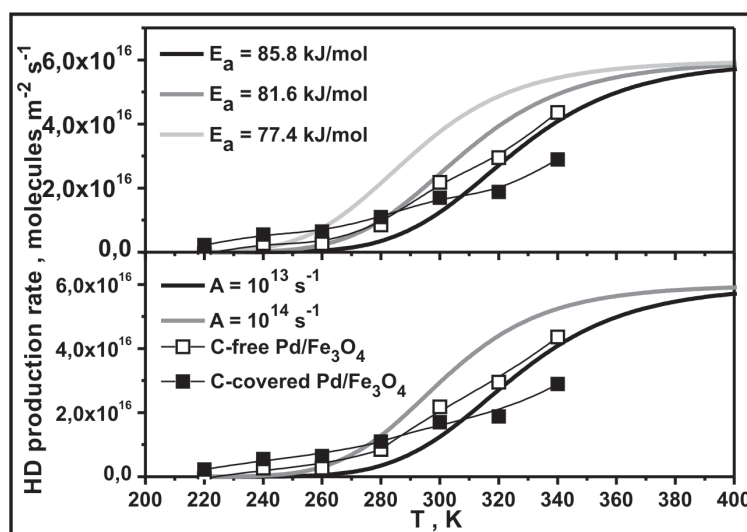


Figure 8.6: Effect of the activation energy,  $E_a$ , (upper panel) and the pre-exponential factor,  $A$ , (lower panel) on the kinetic simulation. For comparison also the steady state HD formation rates over the C-free (open squares) and the C-covered (filled squares) Pd/Fe<sub>3</sub>O<sub>4</sub> model catalyst are displayed.

The strong deviations observed for H/D exchange over the Pd particles which are especially pronounced for low temperatures, clearly show that the kinetic model which reflects fairly well the HD formation over Pd(111) cannot reproduce the H/D exchange rates over Pd particles. It could be speculated that deviations for the Pd particles are due to a different global activation energy and/or a different pre-exponential factor for associative desorption of HD over the Pd particles compared to the Pd(111) surface. As depicted in fig. 8.6, assuming a lower activation energy or a higher pre-exponential factor merely leads to a shift of the curve to lower temperatures, while the shape remains nearly unchanged. The overall agreement between model and experimental data clearly does not improve.

This result strongly suggests that the mechanism is more complex and cannot be adequately described by a Langmuir-Hinshelwood type model. At low temperatures not only recombination of *surface* H(D) is important for H/D exchange over the Pd particles, but that also *subsurface* related H(D) species influence the HD formation. This interpretation is in line with TPD and NRA measurements [188] that indicate that HD formation is expected to depend on the abundance of subsurface H(D) species at low temperatures, while at higher temperatures recombination of surface adsorbed H(D) is predicted to dominate.

The deviations from the kinetic model assuming HD formation only by recombination of surface H(D) are least pronounced for the Pd(111) surface, increase clearly for the C-free Pd particles and are most apparent for the C-modified Pd particles. Following the hypothesis that subsurface absorbed H(D) species cause these deviations, this trend indicates that the influence of subsurface related H(D) species increases from Pd(111), to C-free and C-modified Pd particles. In line with these experimental results, a similar trend is expected for the H(D) diffusion to subsurface sites, a structure sensitive process [70–75, 113], and thus, also for the steady state concentrations of subsurface absorbed H(D) species.

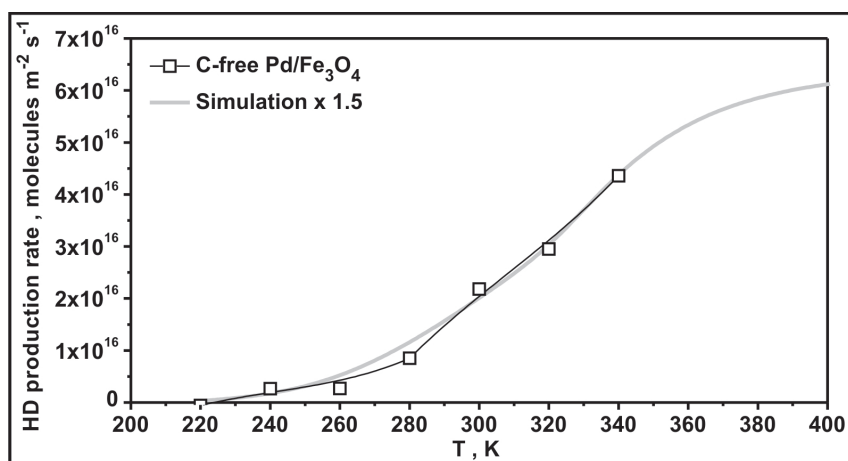


Figure 8.7: Kinetic simulation for a linearly with temperature increasing activation energy to include a possible weakening of the adsorption strength of surface H(D) due to the presence of subsurface H(D) which becomes depleted with increasing temperature. For comparison also the steady state HD formation rates over the C-free Pd/Fe<sub>3</sub>O<sub>4</sub> model catalyst are displayed.

It can be speculated that subsurface absorbed H(D) affects the HD formation merely by lowering the adsorption strength of surface adsorbed H(D) and accordingly the effective activation energy for associative desorption. In such a case, the reduction in adsorption strength can be expected to depend on the abundance of subsurface H(D) which decreases with increasing temperature [188]. Thus, for increasing temperatures due to decreasing concentrations of subsurface H(D) an increase of the adsorption strength and accordingly the activation energy for association can be expected.

To test this hypothesis, we implemented in the kinetic simulation an activation energy that increases with increasing temperature - thus, with decreasing subsurface H(D) concentration - up to 320 K where subsurface H(D) becomes largely depleted [188]. For simplification, a linear increase of the activation energy  $E_a$  was assumed for temperatures  $\leq 320$  K:  $E_a(T) = E_0 + \alpha \cdot T$  with  $E_0$  and  $\alpha$  denoting empirical parameters. It can

be seen in fig. 8.7 exemplarily for the C-free Pd particles that the agreement between the kinetic simulation and the experimental data can be significantly improved (the empirical parameters  $E_0$  and  $\alpha$  were chosen to fit the experimental data). It should be noted however that subsurface H(D) might also be *directly* involved in the H/D exchange. For this case, a considerably more complex reaction mechanism is expected which is beyond the scope of this work.

In summary, the effect of subsurface H(D) species on the steady state H/D exchange rates was investigated by pulsed isothermal MB experiments conducted for different reaction temperatures. Comparison with a kinetic simulation based on a Langmuir-Hinshelwood mechanism assuming HD formation only by recombination of surface H(D) species indicated that H/D exchange over Pd(111) can be described fairly well by this model. Only small deviations from the simulation are observed for low reaction temperatures. For the Pd particles, however, clear deviations were found most pronounced for low temperatures suggesting that subsurface H(D) significantly influences the HD formation over these model catalysts. Over the C-covered Pd particles the most pronounced deviations from the kinetic simulation were measured, while the differences were smaller for the C-free Pd particles and least apparent for the Pd(111) single crystal surface. This trend is in good agreement with previous results and recent DFT calculations indicating that the replenishment of subsurface species is most effective over the C-covered Pd particles and slowest for the Pd(111) surface.

### 8.3.2 Pressure dependence

To investigate the role of subsurface H(D) on the H/D exchange over C-free and C-modified Pd particles further, the steady state HD formation rates were measured by pulsed isothermal MB experiments as a function of the  $D_2$ , the  $H_2$ , and the overall pressure at 260 and 320 K. For these two temperatures, significant differences are expected for the H(D) sorption and consequently, also for the steady state H/D exchange rates. As previously discussed, based on TPD and NRA measurements, a strong influence of *subsurface* related H(D) species on the HD formation is expected for 260 K, while for 320 K, recombination of *surface* H(D) species is expected to dominate the formation of HD [188]. Assuming that two different microscopic reaction mechanisms govern the H/D exchange at these two temperatures, a different pressure dependence is expected for the two reaction temperatures. To better understand a possible involvement of subsurface absorbed H(D) in the H/D exchange over the Pd particles, the experimentally observed pressure dependence is compared to predictions of a simple kinetic model assuming HD formation only by recombination of surface adsorbed H(D) following a Langmuir-Hinshelwood mechanism.

First, the steady state HD reaction rates were investigated as a function of the overall pressure. Fig. 8.3 displays the results obtained for reaction at 260 K (filled circles) and 320 K (open squares) over the C-free and the C-covered Pd/Fe<sub>3</sub>O<sub>4</sub> model catalyst. In these measurements, the  $H_2:D_2$  flux ratio was kept constant (1.4 %) and the overall

Table 8.2: Experimentally obtained formal reaction orders for H/D exchange over a Pd/Fe<sub>3</sub>O<sub>4</sub> model catalyst.

reaction	conditions	overall pressure	D <sub>2</sub> pressure	H <sub>2</sub> pressure
260 K	C-free	+1.29 ± 0.5	+0.03 ± 0.20	+0.58 ± 0.20
	C-covered	+1.08 ± 0.16	+0.18 ± 0.14	+0.62 ± 0.23
320 K	C-free	+0.91 ± 0.05	-0.01 ± 0.03	+0.82 ± 0.05
	C-covered	+0.84 ± 0.09	-0.00 ± 0.05	+0.86 ± 0.08

pressure was varied from  $1.3 \cdot 10^{-6}$  to  $5.3 \cdot 10^{-6}$  mbar. With increasing overall pressure, the HD formation rates increase for all applied conditions. Following a general power law, the HD formation rate  $R_{HD}$  can be expressed as  $R_{HD} = k \cdot p_{D_2}^m \cdot p_{H_2}^n$  with  $k$  denoting the reaction rate constant and  $p_{D_2}$ ,  $p_{H_2}$  the partial pressures of D<sub>2</sub> and H<sub>2</sub>, respectively. At a constant H<sub>2</sub>:D<sub>2</sub> ratio, the slope in the plot of the reaction rates as a function of the overall pressure in a double logarithmic form gives the formal reaction order with respect to the overall pressure. The obtained reaction orders in overall pressure for the different reaction orders are displayed in table 8.2. For all investigated reaction conditions, formal reaction orders with respect to the overall pressure were found to be positive exhibiting values around unity.

Secondly, the dependence on the D<sub>2</sub> pressure on the steady state HD formation rates was investigated. The results for H/D exchange over the C-free (black) and the C-covered (gray) Pd particles at 260 (filled circles) and 320 K (open squares) are displayed in fig. 8.8. In these experiments, the H<sub>2</sub> pressure was kept constant at  $4.0 \cdot 10^{-8}$  mbar and the D<sub>2</sub> pressure was varied from  $1.3 \cdot 10^{-6}$  to  $5.3 \cdot 10^{-6}$  mbar. The corresponding H<sub>2</sub>:D<sub>2</sub> ratios range from 7.0 – 1.1% indicating that even for the lowest D<sub>2</sub> pressure, the reaction is carried out in a large excess of D<sub>2</sub>. For all investigated reaction conditions, a variation of the D<sub>2</sub> pressure does not significantly influence the HD formation rate. The obtained formal reaction orders with respect to the D<sub>2</sub> pressure are consequently around zero for these reaction conditions (see table 8.2).

Next, the influence of the H<sub>2</sub> pressure on the HD formation was investigated. The steady state HD formation rates over the C-free (black) and the C-covered (gray) Pd/Fe<sub>3</sub>O<sub>4</sub> model catalyst at 260 and 320 K are depicted in fig. 8.9 as a function of the H<sub>2</sub> pressure. In these isothermal pulsed MB experiments, the D<sub>2</sub> pressure was kept constant at  $4.0 \cdot 10^{-6}$  mbar and the H<sub>2</sub> pressure was varied between  $1.3 \cdot 10^{-8}$  and  $8.0 \cdot 10^{-8}$  mbar. The corresponding H<sub>2</sub>:D<sub>2</sub> flux ratios vary from 0.5 – 2.8% demonstrating that also in this series a large excess of D<sub>2</sub> was applied in all measurements. As noted before, the error bars in fig. 8.9 indicate the standard error of the mean of the steady state HD formation rate and the measured H<sub>2</sub> signal obtained for several measurements. It can be seen that the steady state H/D exchange rates increase with increasing H<sub>2</sub> pressure for all investigated reaction conditions. The formal reaction orders with respect to the H<sub>2</sub> pressure are consequently positive and exhibit values between 0.5 and unity.

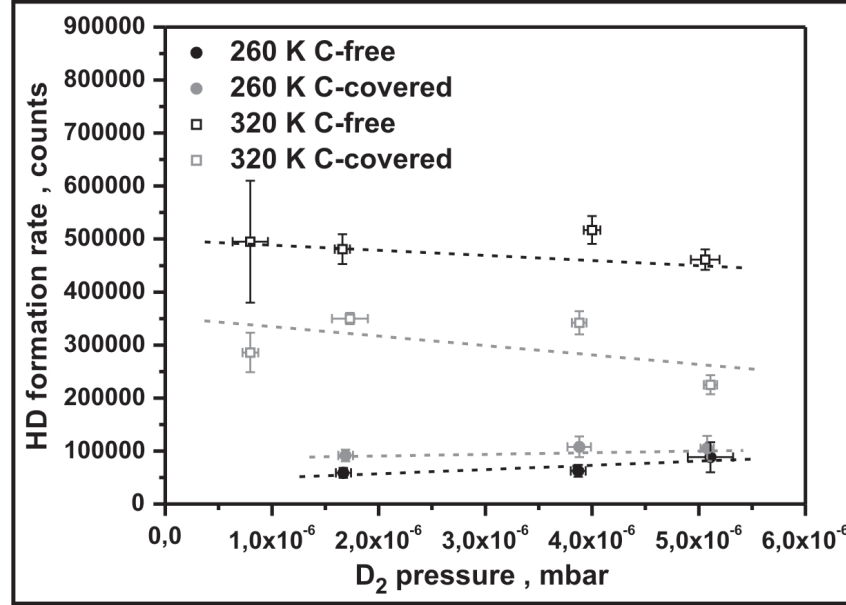


Figure 8.8: Steady state HD formation rates over the C-free (black) and the C-covered (gray) Pd/Fe<sub>3</sub>O<sub>4</sub> model catalyst for 260 K and 320 K as a function of the D<sub>2</sub> pressure. The H<sub>2</sub> pressure was kept constant at  $4.0 \cdot 10^{-8}$  mbar and the D<sub>2</sub> pressure was varied from  $0.8 \cdot 10^{-6} - 5.3 \cdot 10^{-6}$  mbar with the H<sub>2</sub>:D<sub>2</sub> ratios in the range from 7.0 – 1.1%. Thus, even for the lowest D<sub>2</sub> pressure, the experiment is still conducted in a large excess of D<sub>2</sub>. The values for the steady state rates were obtained from several measurements (typically 2 to 7) for each reaction condition with the error bars indicating the standard error of the mean of the steady state HD rate and the measured H<sub>2</sub> signal. The HD formation rates do not change significantly for different D<sub>2</sub> pressures. The dotted lines merely serves as a guide for the eye.

It can be attempted to rationalize the experimentally obtained formal reaction orders by comparison with values predicted by a simple kinetic model assuming a Langmuir-Hinshelwood mechanism. For simplification, a low surface coverage and HD formation only by the reaction of *surface* adsorbed H and D is assumed. Moreover, it is taken into account that the reactions are all carried out in a large excess of D<sub>2</sub> compared to H<sub>2</sub> to simplify the model further.

The rate equation for surface adsorbed D under steady state conditions can be expressed in this case as:

$$\frac{d[D]}{dt} = 2 \cdot flux_{D_2} \cdot S_{D_2} - k_{des,D_2} \cdot [D]^2 - k'_{des,HD} \cdot [H][D] = 0 \quad (8.6)$$

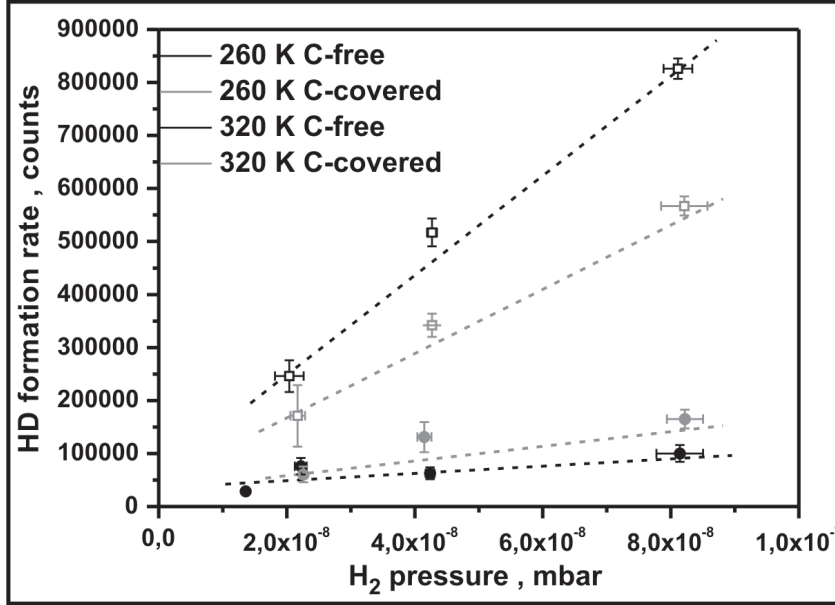


Figure 8.9: Steady state HD formation rates over the C-free (black) and the C-covered (gray) Pd/Fe<sub>3</sub>O<sub>4</sub> model catalyst for 260 K and 320 K as a function of the D<sub>2</sub> pressure. The D<sub>2</sub> pressure was kept constant at  $4.0 \cdot 10^{-6}$  mbar and the H<sub>2</sub> pressure was varied from  $1.3 \cdot 10^{-8}$  –  $8.0 \cdot 10^{-8}$  mbar. The values for the steady state rates were obtained from several measurements for each reaction condition with the error bars indicating the standard error of the mean of the steady state HD rate and the measured H<sub>2</sub> signal. The HD formation rates increase with increasing H<sub>2</sub> pressure. The dotted lines are merely a guide for the eye.

$$\approx 2 \cdot flux_{D_2} \cdot S_{D_2} - k_{des,D_2} \cdot [D]^2 \quad (8.7)$$

with  $flux_{D_2}$  and  $S_{D_2}$  denoting the flux and sticking coefficient of D<sub>2</sub>,  $k_{des,D_2}$  and  $k'_{des,HD}$  the rate constants for associative D<sub>2</sub> and HD desorption, respectively.  $[H]$  and  $[D]$  are the concentrations of surface adsorbed H and D, respectively.

For a large excess of D<sub>2</sub>, recombination of surface D with a small number of surface H species is not expected to affect the concentration of surface D notably and can be thus, neglected (see eq. 8.7). The steady state concentration of surface adsorbed D is then given by:

$$[D]_{st.st.} = \sqrt{\frac{2 \cdot flux_{D_2} \cdot S_{D_2}}{k_{des,D_2}}} \quad (8.8)$$

Similarly, the rate equation for surface H under steady state conditions can be expressed:

$$\frac{d[H]}{dt} = 2 \cdot flux_{H_2} \cdot S_{H_2} - k_{des,H_2} \cdot [H]^2 - k'_{des,HD} \cdot [H][D] = 0 \quad (8.9)$$

$$\approx 2 \cdot flux_{H_2} \cdot S_{H_2} - k'_{des,HD} \cdot [H] [D] \quad (8.10)$$

with  $flux_{H_2}$  and  $S_{H_2}$  denoting the flux and sticking coefficient of  $D_2$ ,  $k_{des,H_2}$  and  $k'_{des}$  the rate constants for associative  $H_2$  and HD desorption, respectively.  $[H]$  and  $[D]$  are the concentrations of surface adsorbed H and D, respectively.

Due to the large excess of  $D_2$ , recombination of two surface adsorbed H species is expected to be negligible (see eq. 8.10), so that the steady state surface H concentration can be approximated by:

$$[H]_{st.st.} = \frac{2 \cdot flux_{H_2} \cdot S_{H_2}}{k'_{des,HD} \cdot [D]} \quad (8.11)$$

$$= \frac{2 \cdot flux_{H_2} \cdot S_{H_2}}{k'_{des,HD} \cdot \sqrt{\frac{2 \cdot flux_{D_2} \cdot S_{D_2}}{k_{des,D_2}}}} \quad (8.12)$$

Using eq. 8.8 and eq. 8.12, the rate of HD formation,  $R_{HD}$ , is then given by:

$$R_{HD} = k'_{des,HD} \cdot [H] [D] \quad (8.13)$$

$$= k'_{des,HD} \cdot \frac{2 \cdot flux_{H_2} \cdot S_{H_2}}{k'_{des,HD} \cdot \sqrt{\frac{2 \cdot flux_{D_2} \cdot S_{D_2}}{k_{des,D_2}}}} \cdot \sqrt{\frac{2 \cdot flux_{D_2} \cdot S_{D_2}}{k_{des,D_2}}} \quad (8.14)$$

$$= 2 \cdot flux_{H_2} \cdot S_{H_2} \quad (8.15)$$

The kinetic model based on a Langmuir-Hinshelwood mechanism assuming a *low* surface coverage and HD formation only by recombination of surface H and surface D species predicts, thus, an upper limit of unity for the formal reaction order with respect to the  $H_2$  pressure and a formal reaction order in  $D_2$  pressure of zero for a large excess of  $D_2$ . Consequently, the predicted formal reaction order with respect to the overall pressure (at a constant  $H_2:D_2$  ratio) is unity.

For a *high* surface coverage close to saturation, in contrast, the number of free adsorption sites is limited, so that the surface H(D) coverage cannot infinitely increase with increasing pressure. Thus, for an increasing overall pressure at a constant  $H_2:D_2$  flux, a formal reaction order in overall pressure of *less* than unity is expected for a basically saturated surface as the H(D) surface coverages and thus, the HD formation rate cannot not significantly increase due to the limited number of free adsorption sites.

For a high surface coverage, the overall H(D) coverage on the surface is expected, thus, to remain roughly constant for increasing pressures. Assuming that the probability for dissociative adsorption of  $H_2$  and  $D_2$  is basically equal, the relative surface coverages of H and D are given by the gas phase ratio of the  $H_2$  and  $D_2$  flux. Thus, when the gas phase ratio of the  $H_2:D_2$  flux is changed, the *relative* coverages of H and D are expected to change accordingly, while the sum of surface H and D is expected to remain constant.



Consequently, when the  $D_2$  pressure is increased, while keeping the  $H_2$  flux constant, the concentration of surface H is expected to *decrease* due to the increase of the surface D concentration. This decrease in the steady state H surface concentration, in turn, is expected to result in decreasing HD formation rates. Consequently, a *negative* formal reaction order with respect to the  $D_2$  pressure is expected for a basically saturated surface. In turn, when the  $H_2$  pressure is varied, the H surface coverage will increase and the D surface coverage will decrease. As  $D_2$  is supplied in a large excess, however, the change in the overall D surface coverage and thus, the effect on the HD formation rate is expected to be rather small. Due to the increasing H surface coverage at a roughly constant D coverage, the HD formation rates are thus, expected to increase with increasing  $H_2$  pressure. Consequently, the reaction order with respect to the  $H_2$  pressure is expected to be positive and basically unity also for a surface close to saturation.

For a reaction temperature of 320 K, the surface concentration of H(D) is expected to be rather small due to fast desorption. This assumption of a low H(D) surface coverage at 320 K is supported also by NRA measurements [188]. Thus, for such a situation, the kinetic model predicts reaction orders of unity with respect to the  $H_2$  and overall pressure and a formal reaction order of zero in the  $D_2$  pressure which is in good agreement with the experimentally observed values.

At 260 K, in contrast, the surface coverage of H(D) is presumably high due to slow desorption - an assumption that is further supported by NRA measurements [188]. As previously discussed, for a high surface coverage, the formal reaction order in  $D_2$  pressure is expected to be *negative* and the reaction order with respect to the overall pressure is predicted to be *lower* than unity. The experimentally observed values clearly do not agree with these predictions for high surface coverages. On the contrary, the experimental values obtained for a reaction temperature of 260 K rather coincide with the values expected for a low coverage situation.

The seemingly obvious consequence that the *surface* coverage at 260 K is low is not supported by experimental results. On one hand, NRA measurements conducted under very similar experimental conditions indicate for 260 K a basically H(D) saturated surface, while at 320 K, the surface concentration was found to be significantly reduced [188]. On the other hand, the low HD formation rates at 260 K clearly show that the rate for associative  $H_2(D_2)$  desorption is compared to 320 K small, so that the steady state H(D) surface coverage at 260 K is expected to be significantly higher than at 320 K.

It should be noted that the experimentally obtained reaction orders with respect to the  $H_2$  pressure are for all investigated reaction conditions below unity. The values obtained for 320 K are with  $+0.82 \pm 0.05$  and  $+0.86 \pm 0.08$ , however, close to the expected value of unity. The values obtained for 260 K are with  $+0.58 \pm 0.20$  and  $+0.62 \pm 0.23$  lower than unity, but exhibit, however, relatively large errors which hampers a further interpretation of these values.

Obviously, the kinetic model assuming HD formation only by recombination of surface H(D) cannot explain the experimentally observed reaction orders for a reaction temperature of 260 K, while the agreement with the experimental data obtained at 320 K is reasonable. This result is in line with TPD and NRA measurements which suggest that at 320 K, HD formation is governed by recombination of surface adsorbed H(D) - for which a good agreement with the LH model is expected -, while for 260 K, a strong influence of subsurface adsorbed H(D) and thus, deviations from the LH model are expected.

The experimental data does not allow to distinguish if subsurface H(D) is *directly* involved in the HD formation or if it merely modifies the adsorption of surface H(D) and thereby, *indirectly* influences the H/D exchange. A more detailed kinetic model may aid in unraveling the exact role of subsurface hydrogen which is however beyond the scope of this work.

In summary, the pressure dependence of the steady state H/D exchange rates was investigated over the C-free and the C-covered Pd/Fe<sub>3</sub>O<sub>4</sub> model catalyst for two reaction temperatures, 260 and 320 K. The formal reaction orders with respect to the H<sub>2</sub>, D<sub>2</sub> and the overall pressure were determined. For the reaction order in H<sub>2</sub> pressure, values between 0.5 and unity were found. The formal reaction orders in D<sub>2</sub> pressure were for all investigated reaction conditions close to zero and with respect to the overall pressure, reaction orders close to unity were measured. A kinetic model assuming HD formation only by recombination of surface H(D) could not predict all experimentally observed reaction orders. For a reaction temperature of 260 K, where a high surface concentration of H(D) as well as a significant population of subsurface sites is expected, clear deviations from the values predicted by the kinetic model are found suggesting that subsurface H(D) has a significant influence on the HD formation.

### 8.3.3 Transient kinetics

The measurements on the *steady steady* HD formation rates as a function of the reaction conditions displayed clear deviations from the kinetic model assuming a Langmuir-Hinshelwood mechanism and HD formation only by recombination of surface adsorbed H(D). This result suggests that next to surface adsorbed H(D) also subsurface adsorbed H(D) affects the H/D exchange over Pd model catalysts. An involvement of subsurface adsorbed H(D) in the HD formation is expected to not only influence the steady state H/D exchange rates, but also the transient kinetic response of the HD signal upon modulation of the H<sub>2</sub> flux.

As earlier discussed, TPD and NRA measurements suggest that the HD formation rate at low temperatures depends strongly on the concentration of subsurface adsorbed H(D) species, while for high temperatures, recombination of surface adsorbed H(D) is expected to dominate the HD formation. Following this model, it can be assumed that

the HD formation rate is given by the following rate equation:

$$R_{HD} = k \cdot [H_s.] [D_s.] + k' \cdot [D_{s.s.}] [H_s.] + k' \cdot [D_s.] [H_{s.s.}] (t) \quad (8.16)$$

with  $[H_s.]$  and  $[D_s.]$  denoting the concentration of surface adsorbed H and D, respectively.  $[D_{s.s.}]$  and  $[H_{s.s.}]$  indicate the concentrations of subsurface related D and H. It should be emphasized that  $H_{s.s.}(D_{s.s.})$  are not necessarily subsurface absorbed H(D) species, but can also be surface adsorbed H(D) which is modified by the presence of subsurface absorbed hydrogen. For simplicity, we refer to these species in the following as *subsurface* H(D).  $k$  denotes the reaction rate constant for recombinative desorption of surface adsorbed H(D) species, while  $k'$  signifies the rate constant for HD formation by reaction of subsurface absorbed D with a surface adsorbed H species and *vice versa*. It should be noted that a possible isotope effect for the latter reactions is neglected.

TPD and NRA measurements indicate that for a low reaction temperature, HD formation by recombination of surface adsorbed H(D) species is presumably slow, so that the first term of the rate equation ( $k \cdot [D_s.] [H_s.]$ ) can be omitted for low reaction temperatures. Thus, HD formation is assumed to occur by reaction of a subsurface absorbed H(D) with a surface adsorbed D(H).

In the pulsed isothermal MB experiments, as described earlier, the surfaces were continuously exposed to a large excess of  $D_2$  ( $\text{flux}_{D_2} = 3.2 \cdot 10^{15} \text{ molecules} \cdot \text{cm}^{-2} \cdot \text{s}^{-1}$ ,  $p_{D_2} = 4.0 \cdot 10^{-6} \text{ mbar}$ ) and a small amount of  $H_2$  ( $\text{flux}_{H_2} = 4.5 \cdot 10^{13} \text{ molecules} \cdot \text{cm}^{-2} \cdot \text{s}^{-1}$ ,  $p_{H_2} = 4.0 \cdot 10^{-8} \text{ mbar}$ ), corresponding to only 1 – 2% of the  $D_2$  flux, was pulsed (60 s on, 60 s off) onto the samples using a second independent effusive beam source.

Applying continuously a large excess of  $D_2$  compared to the  $H_2$  flux ensures that the D concentrations on the sample surface remain basically unchanged in equilibrium when a small flux of  $H_2$  is introduced. The transient kinetic behavior of the HD signal reflects, thus, simply the approach of the H concentrations to steady state conditions.

Upon  $H_2$  exposure, surface adsorbed H is expected build up very fast because the dissociative adsorption of  $H_2$  on Pd surfaces is a basically non-activated process. This instantaneous build up of *surface* adsorbed H,  $H_s.$ , is expected to result in a fast increase of the HD signal upon  $H_2$  exposure due to reaction with already available *subsurface* absorbed D,  $D_{s.s.}$  (second term in eq. 8.16:  $k' \cdot [D_{s.s.}] [H_s.]$ ).

The replenishment of *subsurface* absorbed H by diffusion into the subsurface, in contrast, is an activated process with the activation barrier for H diffusion depending on the surface structure [70–75, 113, 196]. Thus, for a high diffusion barrier, HD formation resulting from the reaction of *subsurface* absorbed H,  $H_{s.s.}$  with *surface* adsorbed D,  $D_s.$  (third term in eq. 8.16:  $k' \cdot [D_s.] [H_{s.s.}] (t)$ ) may reach equilibrium rather slowly, while for a low activation energy for H diffusion a faster approach to equilibrium is predicted.

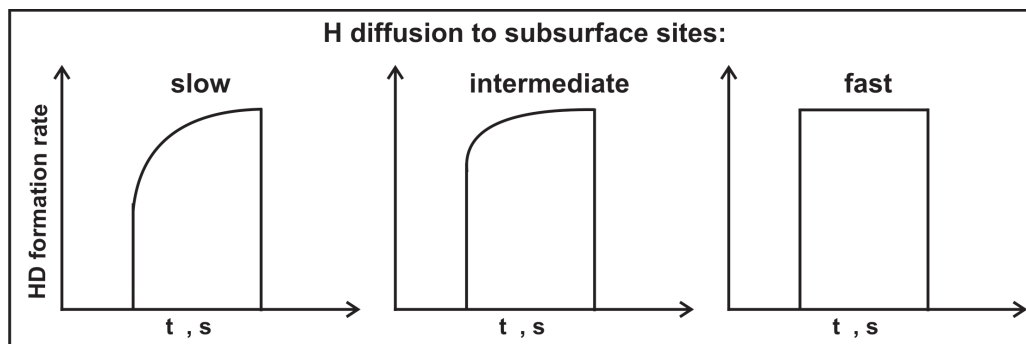


Figure 8.10: Schematical display of the transient kinetic response of the HD signal upon  $\text{H}_2$  exposure based on eq. 8.16 for a low reaction temperature assuming that HD formation by recombination of surface H(D) is negligible. Fast replenishment of surface adsorbed H is expected to result in an instantaneous increase of the HD signal. Replenishment of subsurface adsorbed H by activated diffusion is predicted to depend strongly on the activation barrier for diffusion which in turn depends strongly on the surface structure [70–75, 113, 196]. For a high activation barrier, the steep initial increase of the HD signal due to association of  $H_s$  with already available  $D_{s,s}$  is expected to be followed by a relatively slow growth of the HD formation rate due to recombination of  $D_s$  with  $H_{s,s}$  which population is limited by slow subsurface diffusion. For decreasing diffusion barriers, fast formation of  $H_{s,s}$  should result in a faster achievement of the final steady state rate value.

The predicted transient kinetic behavior of the HD formation upon  $\text{H}_2$  exposure assuming as rate equation for HD formation eq. 8.16 is schematically depicted in fig. 8.10 for three cases, slow, intermediate and high H diffusion to subsurface sites. Initially a fast, instantaneous increase of the HD signal is expected due reaction of *surface* H,  $H_s$  with already available *subsurface* D,  $D_{s,s}$ , (second term in eq. 8.16), which is followed by a further increase due to reaction of *surface* D with *subsurface* H (third term in eq. 8.16) which population is limited by slow diffusion to subsurface sites. For decreasing diffusion barriers (from left to right in fig. 8.10), increasing diffusion rates should result in a faster approach to the final steady state HD formation rate value.

The activation barrier for H diffusion to subsurface sites is expected to be relatively high for a close-packed Pd(111) surface, while for the C-free Pd particles exposing next to (111)-facets also a significant amount of low-coordinated sites, a considerably lower activation energy is predicted [70–75, 113]. For the C-modified Pd particles, recent DFT calculations suggest an even more reduced diffusion barrier [196].

Isothermal pulsed MB experiments were conducted over these three Pd surfaces, *i.e.* a Pd(111) single crystal surface, C-free Pd particles supported on  $\text{Fe}_3\text{O}_4/\text{Pt}(111)$  and

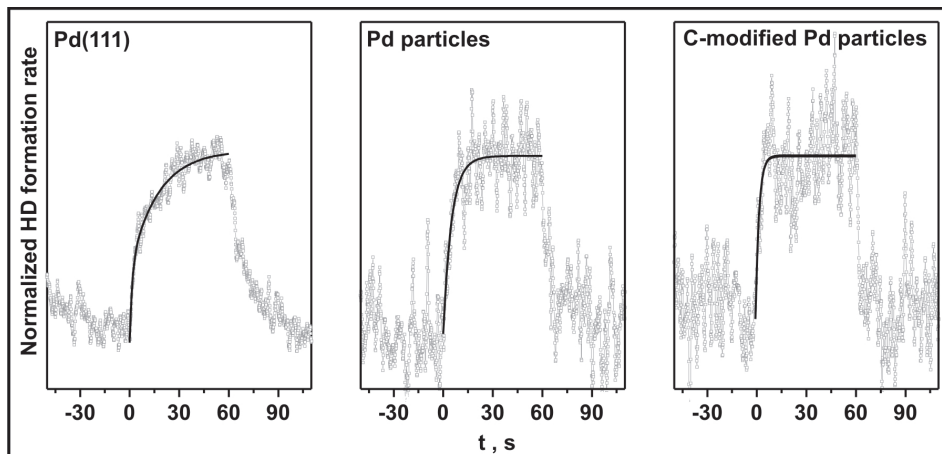


Figure 8.11: Averaged HD reaction rates obtained from isothermal pulsed MB experiments over a Pd(111) single crystal surface (left panel), C-free Pd particles (middle panel) and C-modified Pd particles (right panel) for a reaction temperature of 280 K. The pulse heights are normalized for a more convenient examination of the pulse shape. The black lines are merely a guide for the eye. For all Pd model catalysts, a bi-modal transient response of the HD signal is observed at this temperature. The slow component is pronounced for Pd(111) and becomes faster for C-free and C-covered Pd particles, which is in good agreement with the predictions based on eq. 8.16.

C-modified Pd particles. The results are displayed in fig. 8.11 for a reaction temperature of 280 K with the pulse heights of the HD signals normalized for a more convenient examination of the transient response. It can be seen that the transient kinetic response of the HD formation rate of the three Pd model catalysts agrees well with the predicted structure dependent bi-modal behavior based on eq. 8.16. For all three model catalysts, initially upon  $H_2$  exposure a fast increase of the HD signal is observed which can be tentatively attributed to the reaction of surface H with subsurface D (second term in eq. 8.16:  $k' \cdot [D_{s.s.}] [H_s.]$ ). Over the Pd(111) single crystal, this fast increase is followed by a much slower rise in HD formation which is attributed following eq. 8.16 to reaction of slowly replenishing subsurface H with surface adsorbed D (third term in eq. 8.16:  $k' \cdot [D_s.] [H_{s.s.}] (t)$ ). For the C-free Pd particles, the subsequent increase in HD formation is faster compared to the Pd(111) surface, but slower than for the C-modified Pd particles which is in good agreement with the expected structure dependence of the transient response [70–75, 113, 188]. The clear differences in the transient kinetic response observed for the different Pd model catalysts at this temperature demonstrate that the experimental approach allows to probe kinetically important processes in the H/D exchange over the Pd model catalysts. It should be noted that for an involvement of just *surface* adsorbed H(D) in HD formation not a *bi*-modal behavior is expected.

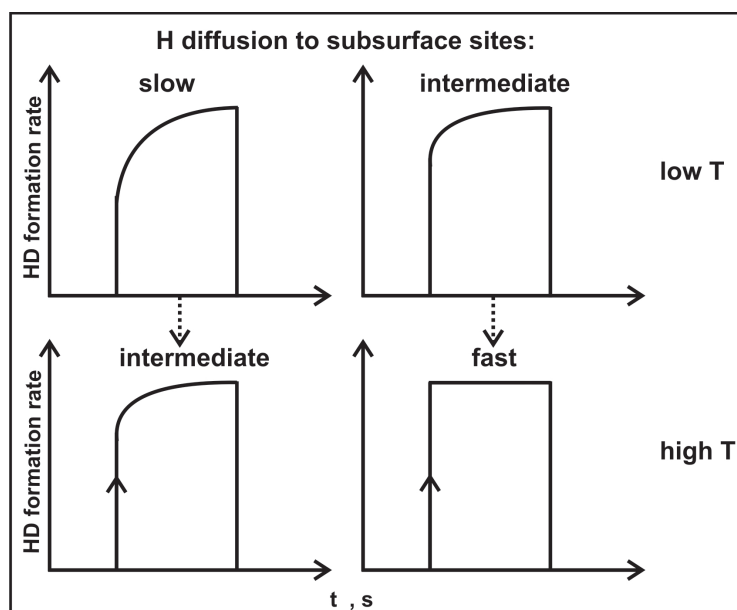


Figure 8.12: Schematical display of the transient kinetic response of the HD signal upon  $H_2$  exposure based on eq. 8.16 for a low and a high reaction temperature. For the high surface temperature, HD formation by recombination of surface H(D) is assumed to contribute to the initial steep increase of the HD signal indicated by the arrows. With respect to the lower temperatures, the rate of H diffusion to subsurface sites is expected to become faster due to the increased temperature. The overall concentration of subsurface H(D) decreases however for higher temperatures [188], so that a smaller contribution of HD formed by reaction of subsurface H(D) with surface D(H) and *vice versa* to the overall HD pulse height is expected.

The bi-modal *transient* response of the experimental HD signal upon  $H_2$  exposure (see fig. 8.11) is in good agreement with the predictions based on the assumed rate equation 8.16. This indicates in line with the temperature and pressure dependent measurements of the *steady state* HD formation rates that *not only* surface adsorbed H(D) is involved in the H/D exchange. The good agreement of the experimental results with the qualitative predictions on the structure dependence of the transient kinetic response based on eq. 8.16 strongly suggests that indeed *subsurface* adsorbed H(D) is also involved in the formation of HD as for these H species a pronounced structure dependence for the replenishment by activated diffusion is expected.

For a higher reaction temperature, TPD and NRA measurements indicate that HD formation by recombination of *surface* adsorbed H and D is expected to gain importance. HD formed by this reaction (first term in eq. 8.16:  $k \cdot [D_s] [H_s]$ ) is expected to result also in an additional fast increase of the HD signal upon  $H_2$  exposure. At higher

temperatures, moreover, H diffusion to subsurface sites and consequently, the related HD increase (third term in eq. 8.16:  $k' \cdot [D_s] [H_{s.s.}] (t)$ ) is predicted to become faster due to the increase in temperature. Overall, the contribution of the HD formation by reaction of *subsurface* adsorbed D(H) and surface adsorbed H(D) and *vice versa* (second and third term in eq. 8.16) is however expected to decrease due to a reduction in the steady state concentrations of subsurface adsorbed H(D) at higher temperatures as indicated by NRA measurements [188]. The expected evolution of the transient response of the HD signals for a transition from a low (upper panels) to a higher (lower panels) reaction temperature is schematically depicted in fig. 8.12. Next to an additional fast component indicated by the arrows due to HD formation by recombination of surface H(D), the slow growth of the HD signal due to reaction of subsurface H with surface D (third term in eq. 8.16) is expected to become faster and decrease in relative intensity for a higher reaction temperature (see fig. 8.12 lower panels).

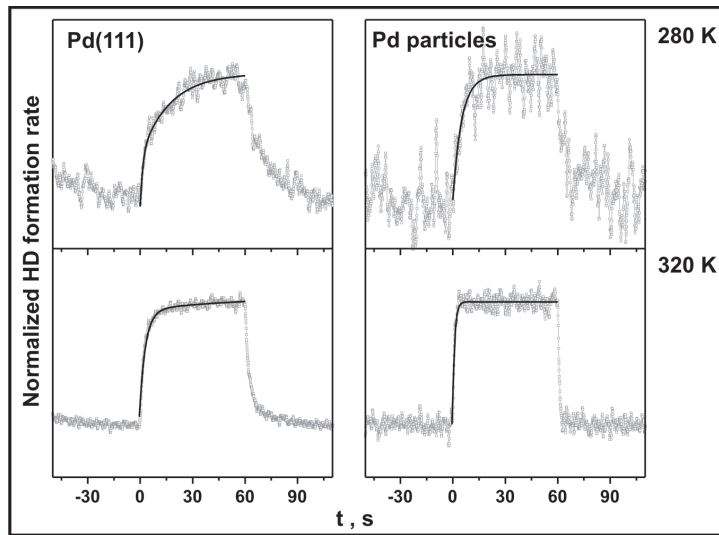


Figure 8.13: Normalized HD reaction rates obtained from isothermal pulsed MB experiments over a Pd(111) single crystal (left panels) and C-free Pd particles (right panels) for 280 K (upper panels) and 320 K (lower panels). For the higher temperature, the slow component becomes faster and contributes less to the signal height with respect to 280 K which is in line with the predictions based on eq. 8.16.

The experimental transient response curves of the HD signal obtained over the Pd(111) single crystal surface and the Pd particles are displayed in fig. 8.13 for a reaction temperature of 280 K and of 320 K. For a more convenient examination of the transient kinetics, the pulse heights are normalized. While at 280 K, the initial steep increase of the HD signal is followed by a relatively slow further growth for both Pd surfaces, this slow component becomes significantly faster for a reaction temperature of 320 K, both over

Pd(111) and the C-free Pd particles. Moreover, the relative contribution of the slower component to the signal height decreases at 320 K with respect to a reaction temperature of 280 K for both Pd model catalysts. These observations are in good agreement with the predictions based on eq. 8.16 supporting the earlier hypothesis that next to surface adsorbed H(D) also subsurface adsorbed H(D) is involved in the formation of HD.

In summary, the transient kinetics of the H/D exchange were studied by pulsed isothermal MB experiments over different Pd model catalysts. For a surface temperature of 280 K, a clearly bi-modal transient kinetic response is observed which supports the assumption that not only surface adsorbed H(D) is involved in the formation of HD, but most likely also subsurface adsorbed H(D). For the replenishment of subsurface adsorbed H by activated diffusion to subsurface sites, a strong structure dependence is expected with the rates increasing from Pd(111), to C-free Pd particles and even further for C-modified Pd particles. This structure dependent behavior of the transient response is qualitatively observed in the experiments supporting the earlier hypothesis that *subsurface* related H is involved in the HD formation. For higher temperatures, an increasing contribution of recombination of surface adsorbed H(D) is expected next to a faster H diffusion to subsurface sites as well as an overall reduction of the contribution of subsurface H(D) species to the HD formation. This is in good agreement with the experimentally observed trend for the transient response curves for H/D exchange over Pd(111) and C-free Pd particles at 320 K compared to the lower reaction temperature of 280 K. These results are in line with the temperature and pressure dependent measurements of the steady state HD formation rates which also suggested an involvement of *subsurface* adsorbed H(D) in the H/D exchange next to recombination of *surface* adsorbed H(D) species.

## 8.4 Effect of hydrocarbons

The reactivity of the Pd model catalysts in the conversion of *cis*-2-butene with D<sub>2</sub> suggested that the availability of different D species differs significantly for the different model catalysts under steady state conditions or in other words, in the presence of hydrocarbon species. Moreover, comparison of the reaction rates in 2-butene conversion over the D-saturated surface and the surface under steady state reaction conditions provided experimental evidence that co-adsorbed hydrocarbon species inhibit the dissociative adsorption of D<sub>2</sub> as well as the D diffusion to subsurface sites. To test if these changes in the D distribution can be probed more directly, the H/D exchange experiments were conducted in the presence of hydrocarbon species. In all experiments, the surfaces were continuously exposed to a large excess of D<sub>2</sub> ( $4.0 \cdot 10^{-6}$  mbar) and a small flux of H<sub>2</sub> ( $4.0 \cdot 10^{-8}$  mbar) was pulsed onto the model catalysts. Measurements were conducted over the C-free and the C-covered Pd/Fe<sub>3</sub>O<sub>4</sub> model catalysts as well as over the C-free and the C-covered Pd(111) single crystal surface for reaction temperatures ranging from 220 to 340 K.



To mimic the reaction conditions of the *cis*-2-butene reactivity measurements during olefin exposure, the surfaces were continuously exposed to *cis*-2-butene in one series of H/D exchange measurements. The same 2-butene pressure ( $2.7 \cdot 10^{-8}$  mbar) was applied as in the majority of the butene reactivity measurements. The pulsed isothermal MB experiments on the *cis*-2-butene conversion indicated however also that for a broad range of reaction conditions, the availability of the different D species increases significantly *between* the olefin pulses, thus, in the absence of olefin supply from the gas phase, but in the presence of co-adsorbed hydrocarbon species. To mimic these conditions, a 2-butene reactivity measurement as described in the preceding chapters (see *e.g.* 5) was conducted prior to the H/D exchange experiment. The HD formation was then studied without an additional supply of 2-butene from the gas phase.

In fig. 8.14, the results on the HD formation in the presence of co-adsorbed hydrocarbon species are displayed for the C-covered Pd/Fe<sub>3</sub>O<sub>4</sub> model catalyst (black traces). The experiments were conducted for different surface temperatures ranging from 220 to 340 K. During the H/D exchange measurement, no additional 2-butene was supplied from the gas phase. For comparison, also the corresponding H/D exchanges rates in the absence of hydrocarbon species (gray traces) are shown which were obtained for the same surface temperatures and applying the same D<sub>2</sub> and H<sub>2</sub> pressures. It can be seen that the HD formation rates remain negligible in the entire investigated temperature range, when hydrocarbon species are present on the catalyst. Even for the highest applied temperature, where the H/D exchange in the absence of hydrocarbons displays high values, no significant HD formation rates are found for the hydrocarbon-covered surface. Also for the other Pd model catalysts, both C-free and C-covered Pd particles as well as the single crystal, no significant H/D exchange rates are measured in the presence of hydrocarbon species (data not shown). It should be noted that no *cis*-2-butene was supplied from the gas phase during the experiments displayed in fig. 8.14. Thus, it can be excluded that H(D) is consumed in reactions with olefins. Moreover, the HD formation rates remained negligible even for prolonged H<sub>2</sub>(D<sub>2</sub>) exposure (> 1 h) at high temperatures (340 K) indicating that H(D) does not effectively hydrogenate the co-adsorbed hydrocarbon species under these reaction conditions which could presumably be a depletion channel for H(D).

The absence of noticeable HD formation can either indicate that H<sub>2</sub>(D<sub>2</sub>) is not effectively adsorbed on the surfaces or that the recombination of H(D) is inhibited. Both dissociative adsorption and associative desorption require an ensemble of free, neighboring adsorption sites [104, 110, 111]. Co-adsorbed hydrocarbon species presumably may break up these ensembles and thereby, inhibit both the dissociation of hydrogen as well as the recombinative desorption. In particular, the recombination to HD requiring that both H and D reach simultaneously a free space, which constitutes basically a three particle process, is expected to be significantly slower compared to the hydrocarbon-free surface.

This interpretation is in good agreement with the results obtained for the 2-butene conversion. On one hand, these experiments indicated that hydrocarbons may inhibit

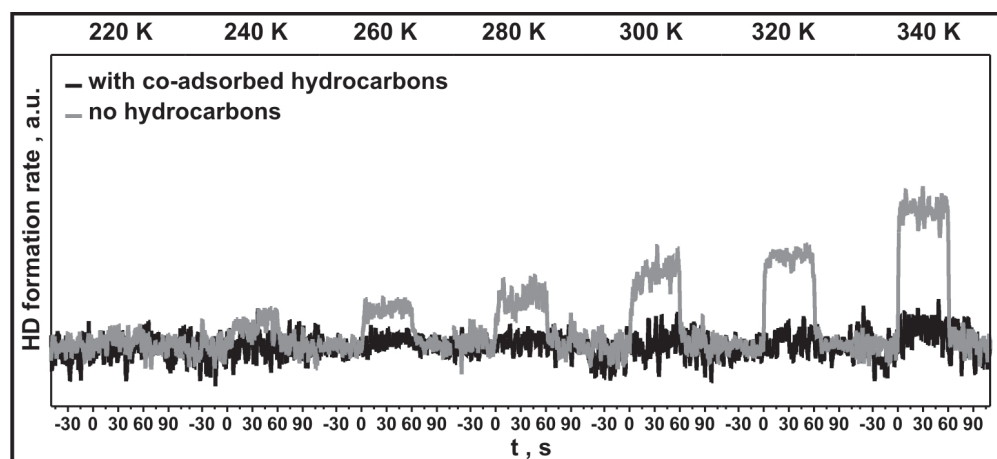


Figure 8.14: HD formation rates as a function of time over the C-covered Pd/Fe<sub>3</sub>O<sub>4</sub> model catalyst obtained in the presence (black trace) and absence (gray trace) of co-adsorbed hydrocarbons. For the hydrocarbon covered surface basically no HD formation is detected over the entire investigated temperature range.

hydrogen sorption for certain reaction conditions. On the other hand, the formal reaction orders obtained in pressure dependent measurements also suggested that H<sub>2</sub>(D<sub>2</sub>) desorption may be inhibited under reaction conditions (see chapter 6 for details). Both of these effects are expected to result in reduced HD formation rates, so that the corresponding HD signals become too low for the detection sensitivity of the experiment.

In summary, co-adsorbed hydrocarbons effectively inhibit the formation of HD even at high temperatures and when no additional 2-butene is supplied from the gas phase. A possible explanation for this inhibition is that co-adsorbed hydrocarbons break up ensembles of neighboring free adsorption sites which are required for both the dissociative adsorption as well as for the associative desorption of hydrogen. In particular, the probability for the recombination process is significantly reduced as both H and D are required to reach a free ensemble simultaneously. Both a reduction of the H(D) concentration on the surface as well as an inhibition of the recombination are expected to result in significantly reduced HD formation rates that are too low for the sensitivity of the experiment.

## 8.5 Conclusion

To probe the H(D) distribution with an independent method under reaction conditions, pulsed isothermal MB experiments on the H/D exchange were conducted over the C-free and C-covered Pd/Fe<sub>3</sub>O<sub>4</sub> model catalyst as well as over the C-free and C-covered Pd(111) single crystal surface.

Measurements on the steady state HD formation for C-free and C-modified Pd particles conducted for two reaction temperatures, 260 and 320 K, showed that C located on low-coordinate sites of the Pd particles influences the H/D exchange. On one hand, deposition of C blocks surface adsorption sites for H(D) which results in decreased HD formation rates in the presence of C at 320 K where HD production is expected to be governed by recombination of surface adsorbed H(D) species. On the other hand, at 260 K, where HD formation is expected to be strongly influenced by subsurface related H(D) species, increased rates are observed for the C-modified Pd particles. In line with recent DFT calculations, this experimental result is interpreted that C-modified low-coordinated sites allow for a faster H(D) diffusion to subsurface sites resulting in an increased steady state concentration of subsurface H(D) species and therefore in higher HD formation rates with respect to the C-free Pd particles.

To investigate the possible influence of *subsurface* adsorbed H(D) on the H/D exchange over Pd model catalysts further, the temperature and pressure dependence of the steady state HD formation rate was studied for different Pd model catalysts. The experimental results were compared to a simple kinetic model based on a Langmuir-Hinshelwood (LH) mechanism assuming, in contrast, HD formation only by recombination of *surface* H(D). Also the transient response of the HD signal was qualitatively analyzed to unravel the role of subsurface H(D) in the H/D exchange further.

The temperature dependent measurements showed for the Pd particles strong deviations from the LH model, while the H/D exchange over a Pd(111) single crystal is described fairly well by this model. The deviations are most pronounced for the C-modified Pd particles. It was demonstrated that the agreement between model and experimental data does not improve assuming simply a different activation energy or pre-exponential factor for the HD formation. This suggests that not only recombination of surface H(D) influences the H/D exchange over Pd. The structure dependence of the deviations from the LH model indicate that also *subsurface* adsorbed H(D) may influence the HD formation over Pd model catalysts.

Pressure dependent measurements on the steady state H/D exchange rates over C-free and C-covered Pd particles were conducted for two reaction temperatures, 260 and 320 K. Comparison with values predicted by a LH model assuming HD formation only by recombination of surface adsorbed H(D), clearly showed that the experimentally obtained formal reaction orders cannot be explained when just reaction of surface species is considered suggesting that subsurface H(D) is also involved in the formation of HD.

For a low reaction temperature (280 K), the transient kinetic response of the HD signal over different Pd model catalysts, *i.e.* a Pd(111) single crystal surface as well as C-free and C-covered Pd particles, exhibits a bi-modal behavior suggesting, in line with previous results, that HD formation occurs not only by recombination of *surface* adsorbed H(D). A qualitative analysis showed a structure dependence of the transient

response for the three investigated Pd model catalysts. The observed structure dependence is in good agreement with the structure dependence expected for H diffusion to subsurface sites supporting further the earlier hypothesis that *subsurface* absorbed H(D) is also involved in the HD formation over Pd model catalysts.

Co-adsorbed hydrocarbons were found to strongly inhibit the HD formation over all investigated Pd model catalysts even for the highest applied temperatures. A plausible microscopic mechanism for the inhibition of the H/D exchange due to co-adsorbed hydrocarbons is that the hydrocarbon species break up ensembles of free neighboring adsorption sites which are required for both the dissociative adsorption of H<sub>2</sub>(D<sub>2</sub>) and the associative desorption of hydrogen (HD), and thereby inhibit these processes. In particular, the recombination to HD requiring that both H and D reach simultaneously a free space, which constitutes basically a three particle process, is expected to be significantly slower compared to the hydrocarbon-free surface. An inhibition of both the dissociative adsorption of H<sub>2</sub> and D<sub>2</sub> as well as of the recombinative desorption of HD is expected to result in overall strongly reduced HD formation rates. In line with this interpretation are results on the 2-butene reactivity indicating an inhibition of both the H<sub>2</sub>(D<sub>2</sub>) sorption and the associative desorption of H<sub>2</sub>(D<sub>2</sub>) in the presence of co-adsorbed hydrocarbon species.

# 9 Isophorone adsorption and reaction with $D_2$ on Pd(111)

## 9.1 Introduction

Tuning the selectivity of catalytic reactions is one of the most important and challenging subjects in catalysis research. For a rational design of new, improved catalysts, it is essential to understand the microscopic factors governing the selectivity. In the preceding chapters, it was shown that the availability of different hydrogen species under reaction conditions strongly controls the selectivity toward *cis-trans* isomerization and hydrogenation in the conversion of *cis*-2-butene with hydrogen over Pd model catalysts.

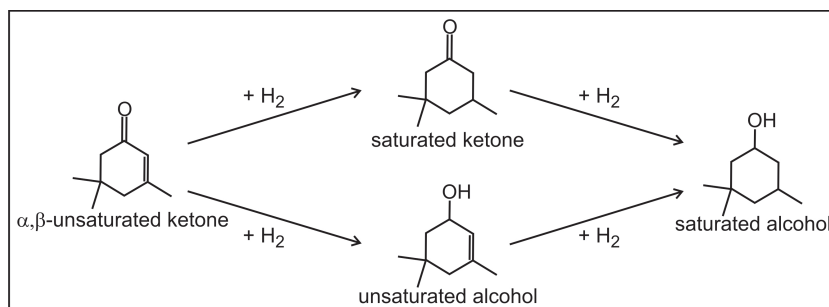


Figure 9.1: Schematical display of isophorone hydrogenation yielding different products. Selective hydrogenation of the C=C double bond results in the formation of a saturated ketone, while hydrogenation of the C=O double bond produces an unsaturated alcohol. Further reaction of the partial hydrogenation products yields a saturated alcohol.

For molecules containing several double bonds, like *e.g.* the  $\alpha,\beta$ -unsaturated ketone isophorone, hydrogenation can yield different products. In the case of isophorone, the C=C, the C=O double bond or both can be hydrogenated yielding a saturated ketone, an unsaturated alcohol or a saturated alcohol, respectively (see also fig. 9.1). Since separation of these similar products is often difficult and cost intense, a high chemoselectivity is desirable. Over Pd catalysts, the hydrogenation of isophorone yields under realistic conditions with a high selectivity the saturated ketone ( $\approx 100\%$ ) [214–216]. Thus, over Pd catalysts, the hydrogenation of the C=C double bond is favored over the hydrogenation of the C=O bond. The origin of this chemoselectivity is, however, not fully understood.

Using modifiers, heterogeneous catalysts may be applied also for enantioselective hydrogenations traditionally catalyzed by homogeneous catalysts (see *e.g.* [217–220] and references therein). The use of heterogeneous catalysts is often economically and environmentally advantageous, so that heterogeneously catalyzed enantioselective hydrogenation was quickly recognized to be a promising field of research. Consequently, numerous catalytic systems, *i.e.* combinations of molecules, modifiers and heterogeneous catalysts, exhibiting pronounced enantioselectivities (with *e.e.* > 90% for selected cases) were identified. A number of different modifiers have been also tested for the enantioselective hydrogenation of isophorone (see *e.g.* [217, 221–228]) including cinchonine (CN) and cinchonidine (CD) (see fig. 9.2) which are versatile modifiers yielding opposing enantiomers for isophorone and a variety of other reactant molecules. Modifiers, like CN and CD, are thought to induce enantioselectivity by providing a chiral adsorption site on the surface for the reactant molecules (see also fig. 9.2), but also other mechanism have been proposed, *e.g.* the formation of a chiral surface by ensemble effects as well as complex formation in the liquid phase rather than on the surface (see *e.g.* [220]).

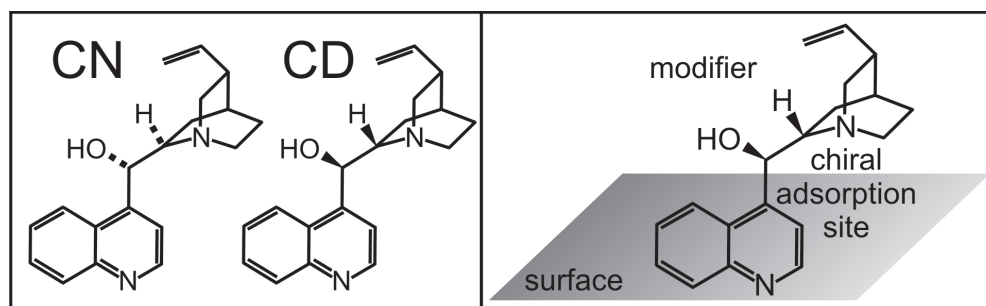


Figure 9.2: The molecular structure of the modifiers cinchonine (CN) and cinchonidine (CD) (left panel); schematical display of the suggested working principle of cinchona modifiers: formation of a chiral adsorption site for the reactant molecule on the surface (right panel).

To unravel the effect of cinchona modifiers in the hydrogenation of isophorone, it is necessary to first understand the chemistry of the *unmodified* system. Due to the relatively high complexity of the isophorone molecule, the adsorption and reaction of isophorone was initially studied over a simple Pd(111) single crystal under well-defined UHV conditions by IRAS and TPR measurements. To study the effect of hydrogen(deuterium), experiments were conducted both on the clean and the D-precovered Pd(111) single crystal. Next to isophorone also the adsorption and reaction of its partial hydrogenation product TMCH (3,3,5-trimethyl-cyclohexanone) was investigated. In the first part of this chapter, results of IRAS measurements on the adsorption of isophorone and the saturated ketone TMCH will be presented, while the second part focuses on the reactivity over Pd(111) studied by TPR.

## 9.2 Adsorption on Pd(111)

The adsorption of isophorone and its partial hydrogenation product TMCH (3,3,5-trimethyl-cyclohexanone) on a Pd(111) single crystal surface was investigated by IRAS measurements to obtain information on the interactions with the surface determining the activity and selectivity in conversion reactions. To investigate also the effect of co-adsorbed hydrogen, the measurements were conducted both on the clean and the D-precovered Pd(111) surface. First, the adsorption of the reactant isophorone over the clean and the D-precovered Pd(111) single crystal surface is presented. Secondly, the interaction of the partial hydrogenation product TMCH with the clean and the D-precovered Pd(111) surface is discussed.

### 9.2.1 Isophorone on Pd(111)

In fig. 9.3, IRAS measurements on the adsorption of isophorone over clean Pd(111) are depicted in the wavenumber range from 3200 to 1000  $\text{cm}^{-1}$ . In these measurements, the Pd(111) surface was exposed at  $\approx 100$  K to different amounts of isophorone ranging from 0.05 to 1.0 ML (1 ML is defined as  $0.6 \cdot 10^{15}$  molecules corresponding to the number of surface Pd atoms of the Pd/Fe<sub>3</sub>O<sub>4</sub> model catalyst). The IR spectra of isophorone adsorbed on clean Pd(111) exhibit numerous signals consisting often of several contributions. The precise assignment of the peaks to certain molecular vibrations is not trivial. For the adsorbed molecules, interactions with the surface and with other co-adsorbed molecules may lead to shifts in the peak positions as well as to changes in the relative peak intensities (see also chapter 2 for further details). Currently, theoretical calculations are conducted to aid in the assignment of the experimentally observed IR spectra. But even without a precise assignment, three main spectral regions can be distinguished in the isophorone IR spectra: The region between 2800 and 3200  $\text{cm}^{-1}$  is characteristic for signals due to C-H stretching vibrations, while signals attributed to the C-H deformation vibrations are expected for wavenumbers below 1500  $\text{cm}^{-1}$ . Between 1550 and 1850  $\text{cm}^{-1}$ , signals due to C=C and C=O stretching vibrations may be observed.

For low coverages ( $\leq 0.15$  ML), only signals in the C-H stretching and C-H deformation regions are observed, while no IR absorption is detected in the region characteristic for C=C and C=O stretching vibrations (see fig. 9.3). With increasing coverage, the intensities of the signals attributed to C-H vibrations increase and for coverages  $\geq 0.2$  ML, a broad signal centered around  $\approx 1610$   $\text{cm}^{-1}$  appears in the C=C and C=O stretching region. This initially weak signal increases quickly with further increasing isophorone coverage and the peak maximum shifts to  $\approx 1660$   $\text{cm}^{-1}$ . At high coverages, it can be clearly seen that this signal is composed of several contributions.

For the highest coverages, where the formation of isophorone multilayers is expected, the IR spectrum resembles the gas phase isophorone spectrum well, while for lower coverages, the absence of signals in the C=C and C=O stretching region attests to pronounced interactions of the isophorone molecules with the underlying surface. For molecules ad-

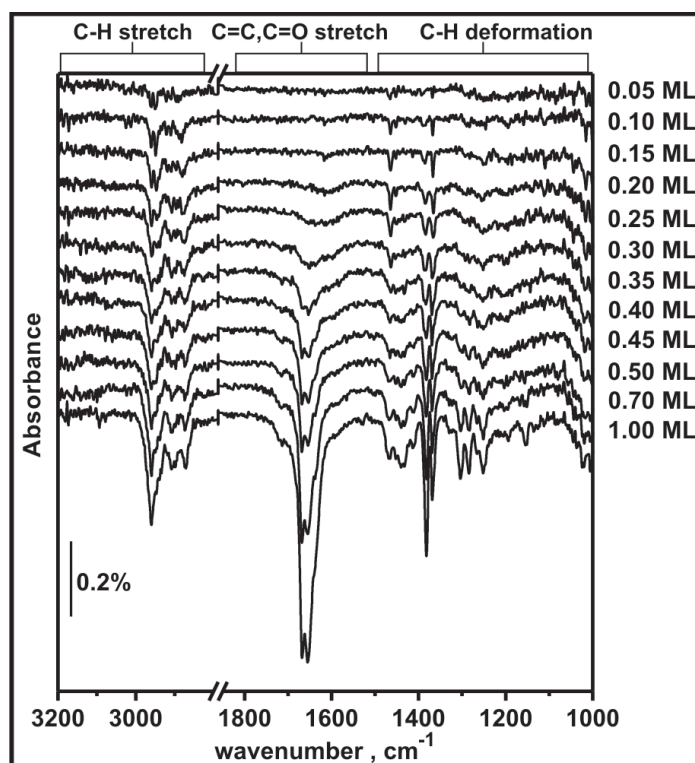


Figure 9.3: IR spectra of isophorone adsorbed on clean Pd(111). The IRAS measurements were conducted for isophorone coverages ranging from 0.05 to 1.0 ML at a surface temperature of  $\approx 100$  K. Three main spectral regions can be distinguished characteristic for C-H stretching ( $2800 - 3200 \text{ cm}^{-1}$ ), C=C and C=O stretching ( $1550 - 1850 \text{ cm}^{-1}$ ) and to C-H deformation vibrations ( $< 1500 \text{ cm}^{-1}$ ).

sorbed on a metal surface, the absence of IR signals may indicate that the corresponding bonds are oriented parallel to the surface and/or that these bonds are strongly perturbed due to interactions with the surface (see 2.3.2 for further details). Both cases suggest an adsorption geometry with the C=C and the C=O bonds in the isophorone ring lying flat on the surface. For a flat adsorption geometry of the isophorone ring, not only for the C=C and the C=O bonds relatively strong interactions with the underlying Pd(111) single crystal surface are expected, but also for C-H bonds close to the surface. Recent theoretical calculations support this hypothesis suggesting that a flat adsorption geometry for isophorone is only obtained when Van-der-Waals interactions of the isophorone ring with the surface are taken into account [229].

For isophorone coverages  $\geq 0.2$  ML, the appearance of IR absorption signals in the C=C and C=O stretching region indicates changes in the adsorption geometry with respect to lower coverages. At higher coverages, the isophorone C=C and/or the C=O



bond are no longer oriented completely parallel to the surface which can be indicative of a reduced interaction strength with the Pd surface. These changes in the adsorption strength and geometry affecting the C=C and/or the C=O double bonds are expected to have a pronounced influence on the hydrogenation activity and selectivity of the adsorbed isophorone.

To investigate the influence of co-adsorbed H(D), IRAS measurements for different isophorone coverages were conducted over the D-presaturated Pd(111) single crystal surface. In these experiments, the sample was first exposed at 100 K to 190 L of D<sub>2</sub> to saturate the surface with D and subsequently, isophorone was dosed onto the Pd(111) single crystal. Fig. 9.4 displays the resulting IR spectra obtained for isophorone coverages ranging from 0.05 to 0.40 ML for the D-precovered Pd(111) surface (black traces) and for comparison, also the corresponding spectra for the clean Pd(111) single crystal (gray traces).

The IR spectra obtained for the D-precovered surface exhibit several differences with respect to the measurements over the clean Pd(111) single crystal demonstrating that co-adsorbed H(D) affects the adsorption of isophorone. Changes are apparent for the C-H vibrations as well as for the C=C and C=O stretching region. In the C-H stretching region, the most pronounced difference upon D-precovering is the vanishing of the IR signal at 2880 cm<sup>-1</sup> present in the spectra of the clean Pd(111) surface. Similarly, in the region characteristic for C-H deformation vibrations, the signal at 1465 cm<sup>-1</sup> is absent in the presence of co-adsorbed H(D). In this spectral region, an additional peak appears at 1435 cm<sup>-1</sup>. These changes in the C-H vibrations clearly show that the interactions of one or several C-H bonds with the surface are altered by the presence of co-adsorbed H(D). It can either indicate changes in the adsorption geometry and/or H/D exchange within the isophorone molecule. It should be noted that no signals clearly characteristic for C-D stretching vibrations (around 2100 cm<sup>-1</sup>) could be detected suggesting that H/D exchange is not the predominate cause for the changes in the IR spectra.

For the D-precovered surface, a broad signal around 1635 cm<sup>-1</sup> is observed even for the lowest applied coverage (0.05 – 0.10 ML), while for the clean Pd(111) surface, IR absorption in this region is only observed for coverages  $\geq 0.2$  ML. Moreover, the signal observed for low coverages over the clean surface is centered around 1605 cm<sup>-1</sup>, thus, shifted to lower wavenumbers compared to the D-precovered Pd(111) single crystal. These differences demonstrate that co-adsorbed H(D) not only influences the interactions of the C-H bonds in isophorone with the surface, but that also the interactions of the C=C and/or the C=O bond with the Pd(111) surface are altered in the presence of H(D). The appearance of a signal already at very low coverages demonstrates that the C=C and/or the C=O stretching vibration exhibits a dipole moment with a component perpendicular to the surface indicating a non-parallel orientation of these bonds with respect to the Pd surface. Changes in the adsorption geometry, especially regarding the C=C and/or C=O double bonds, are expected to have a distinct influence on the hydrogenation activity and selectivity of isophorone.

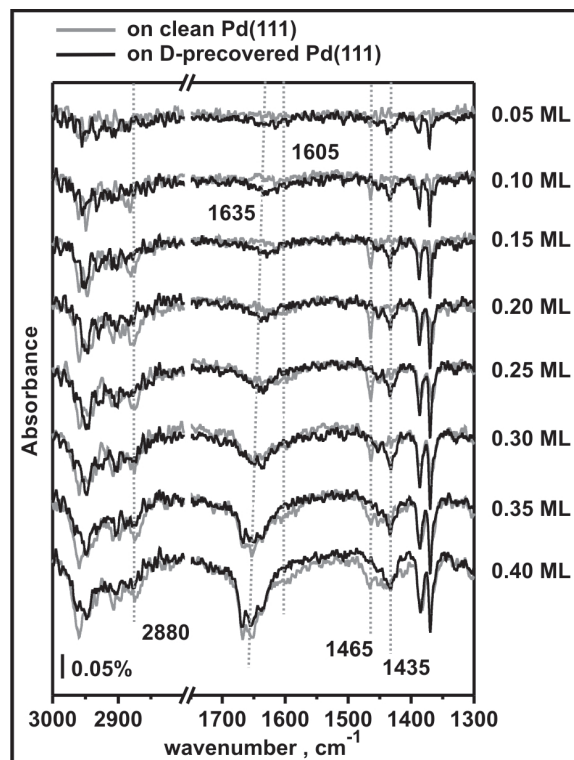


Figure 9.4: IR spectra of isophorone adsorbed on D-precovered Pd(111). In these experiments, the Pd(111) surface was exposed at 100 K to 190 L of  $D_2$  and subsequently isophorone was dosed onto the sample. IRAS measurements for isophorone coverages ranging from 0.05 to 0.40 ML are displayed for the D-precovered (black traces) and the clean (gray traces) Pd(111) single crystal surface for comparison. Several changes upon D-precovering indicate that co-adsorbed H(D) affects the adsorption of isophorone on Pd(111).

### 9.2.2 3,3,5-trimethyl-cyclohexanone on Pd(111)

Under realistic conditions, the hydrogenation of isophorone over Pd catalysts yields with a very high selectivity the saturated ketone, 3,3,5-trimethyl-cyclohexanone, denoted TMCH for simplicity in the following [214–216]. The adsorption of this predominant hydrogenation product on the Pd(111) single crystal surface was studied by IRAS.

Fig. 9.5 displays results for 3,3,5-trimethyl-cyclohexanone (TMCH) adsorption over the D-presaturated Pd(111) surface for coverages ranging from 0.1 to 1.0 ML. The experiments were conducted as described in the previous part. The Pd(111) surface was exposed at  $\approx 100$  K to 190 L of  $D_2$  and subsequently, TMCH was dosed onto the sample. For a more convenient comparison, the corresponding spectra for isophorone adsorption on D-precovered Pd(111) (gray traces) are displayed next to the data obtained for the partial hydrogenation product, TMCH (black traces).

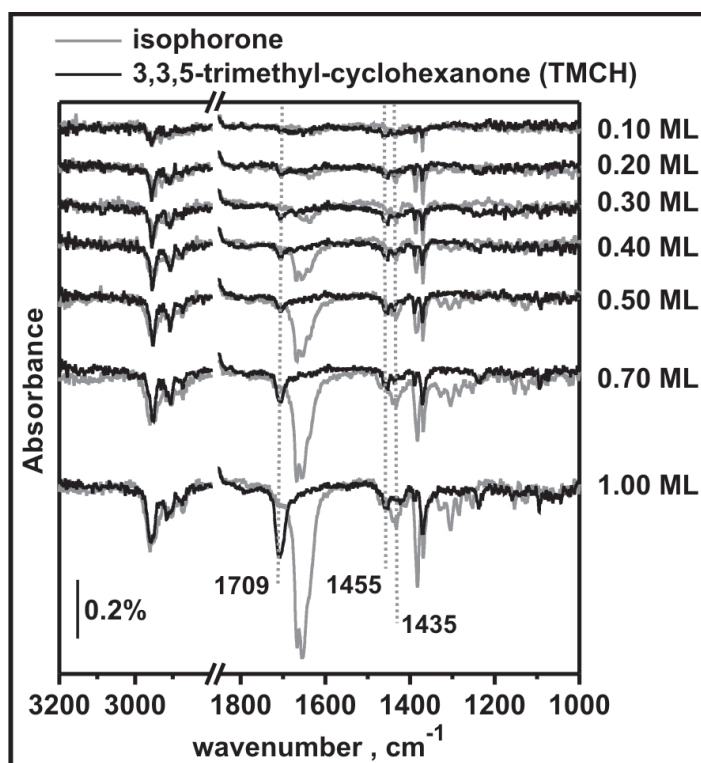


Figure 9.5: IR spectra of the partial hydrogenation product 3,3,5-trimethyl-cyclohexanone TMCH adsorbed on D-precovered Pd(111). In these experiments, the Pd(111) surface was exposed at 100 K to 190 L of D<sub>2</sub> and subsequently TMCH was dosed onto the sample. IRAS measurements were conducted for coverages ranging from 0.05 to 1.0 ML. Next to the data obtained for TMCH (black traces), the corresponding measurements of isophorone adsorption are displayed (gray traces).

To use IRAS as a detection method in reactivity measurements, it is important that isophorone and its hydrogenation products can be spectroscopically distinguished from each other. The spectra of isophorone and TMCH display very similar IR absorption signals in the C-H stretching region, while some differences are notable for the C-H deformation vibrations. The peak at 1435 cm<sup>-1</sup> observed for adsorbed isophorone is basically absent in the spectra of the hydrogenation product, while the spectra of adsorbed TMCH display a signal at 1455 cm<sup>-1</sup> that is not present for adsorption of the reactant isophorone. The signals in the C=O(C=C) stretching region clearly differ for the two molecules. For the hydrogenation product exhibiting only a C=O double bond, a relatively narrow peak at 1709 cm<sup>-1</sup> is observed, while isophorone containing both a C=C and a C=O double bond displays a relatively broad signal around 1635-1660 cm<sup>-1</sup>, thus, clearly at lower wavenumbers. These distinct differences in the static spectra of

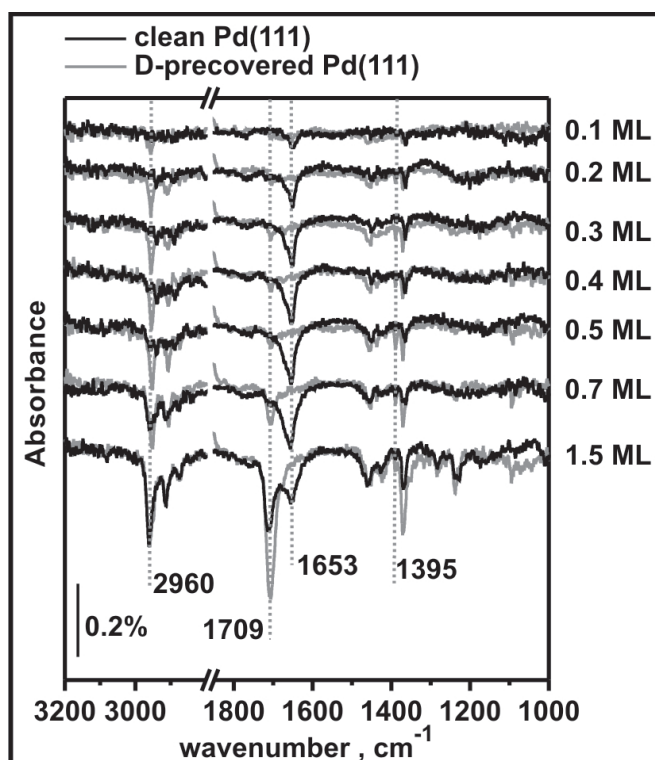


Figure 9.6: IR spectra of the partial hydrogenation product (3,3,5-trimethylcyclohexanone) TMCH adsorbed on clean Pd(111). In these experiments, the Pd(111) surface was exposed at 100 K to TMCH with exposures ranging from 0.05 to 1.0 ML. Next to the data obtained for TMCH adsorbed on clean Pd(111) (black traces), the corresponding measurements of adsorption on the D-precovered Pd(111) single crystal are displayed (gray traces). Several differences are visible for the IR spectra obtained for the clean and the D-precovered Pd(111) surface.

isophorone and its predominant hydrogenation product allow to use IRAS as a detection method in future dynamic reactivity measurements, like *e.g.* in pulsed isothermal MB experiments.

The adsorption of TMCH was also studied for the clean Pd(111) single crystal surface. The experiments were conducted as previously described and the results are displayed in fig. 9.6 (black traces). The clean Pd(111) surface was exposed to TMCH at surface temperature of 100 K. The exposures ranged from 0.10 to 1.50 ML. For a more convenient comparison, also the corresponding IR spectra obtained for the D-precovered Pd(111) surface are shown (gray traces).

The IR spectra for TMCH adsorption on the clean and the D-precovered Pd(111)

single crystal surface exhibit several differences most pronounced at low coverages where a strong influence of the underlying surface is expected. With respect to C-H vibrations, the most prominent difference is found in the C-H stretching region. For adsorption on the D-precovered Pd(111) surface, a strong signal at  $2960\text{ cm}^{-1}$  is detected even for low TMCH coverages, while no notable IR absorption is found at these wavenumbers for low TMCH coverages on the clean Pd(111) surface. In the C-H deformation region only small differences are observed. The signal at  $1395\text{ cm}^{-1}$  exhibits for TMCH adsorbed on the clean Pd(111) surface a lower intensity with respect to adsorption on the D-precovered Pd surface. It should be noted that also for TMCH, no notable signals characteristic for C-D stretching vibrations were detected indicating that H/D exchange is not the predominant cause for the observed changes. With respect to the relatively small changes in the C-H vibrations, co-adsorbed H(D) dramatically affects IR signals in the C=O stretching region. Over the clean Pd(111) surface, a strong signal at  $1653\text{ cm}^{-1}$  is detected, with respect to the peak observed for the D-precovered surface shifted to lower wavenumbers and exhibiting a high intensity already at low coverages. A signal at  $1709\text{ cm}^{-1}$  as detected for the D-precovered sample is also observed for the clean Pd(111) surface, but only at higher coverages ( $> 0.5\text{ ML}$ ) where multilayer formation is expected.

The pronounced difference in the C=O stretching region clearly demonstrates that co-adsorbed H(D) significantly affects the adsorption of TMCH on Pd(111). The shift of the low coverage signal for the clean surface with respect to the multilayer peak at  $1709\text{ cm}^{-1}$  indicates strong distortions of the molecule upon adsorption on the clean Pd(111) surface. While the comparably small intensity of the  $1709\text{ cm}^{-1}$  signal observed for low coverages on the D-precovered surface suggests a relatively parallel orientation of the C=O bond to the Pd surface, the high intensity of the low coverage signal of the clean Pd(111) surface at  $1653\text{ cm}^{-1}$  indicates a clearly non-parallel orientation of the C=O bond and thus, a significantly different adsorption geometry in the absence of co-adsorbed H(D).

In summary, the adsorption of isophorone and its saturated ketone, 3,3,5-trimethylcyclohexanone (TMCH), was investigated by IRAS measurements over the clean and the D-precovered Pd(111) single crystals surface. For low isophorone coverages, signals due to C=C and C=O stretching vibrations are not observed in the IR spectra. This can indicate either that the C=C and C=O bonds are oriented parallel to the surface or that these bonds are strongly perturbed in the adsorbed molecule, *e.g.* by formation of a di- $\sigma$  complex or by bond breaking. For higher coverages, the adsorption geometry most probably changes with the C=C and/or the C=O stretching vibration exhibiting a transition dipole moment perpendicular to the surface. Co-adsorbed H(D) induces changes in the IR spectrum demonstrating that the adsorption of isophorone is altered in the presence of H(D). For the partial hydrogenation product TMCH distinct differences in the static IR spectra are observed compared to isophorone which allows for the use of IRAS as detection method in dynamic reactivity measurements. Pronounced changes in the IR spectra of TMCH show that also the adsorption of the partial hydrogenation product is significantly influenced by the presence of co-adsorbed H(D). The observation

of characteristic IRAS signals even at low coverages reflecting also changes in the adsorption geometry constitute the foundation for further investigations of this catalytic system.

### 9.3 Reactivity on Pd(111)

TPR measurements were conducted to investigate the reactivity of isophorone over Pd(111) in the conversion with H<sub>2</sub>(D<sub>2</sub>) under well-defined UHV conditions. In these measurements, the Pd(111) single crystal surface was exposed at 100 K to 190 L of D<sub>2</sub> and to isophorone with the exposures ranging from 0.1 to 0.3 ML. Subsequently, the sample was heated in vacuum to  $\approx$  700 K. During the heating, the evolution of products in the gas phase was followed by QMS. For large molecules, like isophorone and its hydrogenation products, fragmentation in the ion source is an important process resulting in characteristic fragmentation patterns with the maximum signal intensity typically on a fragment and not on the parent ion peak, the signal of the unfragmented ionized molecule. Due to the similar molecular structure of isophorone and its hydrogenation products, often identical fragments are formed so that several characteristic peaks including the corresponding parent ion and their relative intensity are required for an unambiguous assignment to a certain hydrocarbon species. Table 9.1 summarizes the masses detected for isophorone and its hydrogenation products stating the approximately expected intensity (based on [230]) and if other molecules may contribute to the signal intensity of the mass. Next to signature peaks for isophorone and its hydrogenation products, also decomposition products, like H<sub>2</sub> (at 2 amu), CO (at 28 amu) and CH<sub>4</sub> (at 15 amu), were detected during the heating.

In fig. 9.7, TPR spectra of characteristic species for isophorone desorption and reaction from D-precovered Pd(111) are displayed for different isophorone coverages. For the lowest applied coverage of isophorone (0.1 ML), no molecular desorption is observed as indicated by the absence of signals on the mass where the maximum signal intensity of isophorone is expected (82 amu, C<sub>5</sub>OH<sub>6</sub><sup>+</sup>-fragment) and as on the mass of the parent ion peak of isophorone (138 amu). Also the masses characteristic for the hydrogenation products of isophorone do not display any significant signals for the lowest applied isophorone coverage. At this coverage, merely decomposition products, like H<sub>2</sub>, CO and CH<sub>4</sub>, are detected in the gas phase (data not shown). Only for higher isophorone exposures ( $\geq$  0.2 ML), molecular desorption is observed next to decomposition. Thus, for low isophorone coverages, the interactions with the underlying Pd(111) surface are seemingly so strong that basically all adsorbed molecules decompose, while for higher coverages, the interactions with the surface become for a part of the adsorbed isophorone molecules sufficiently small to allow for desorption of the intact molecule.

In the case of molecular desorption (masses 82 and 138 amu in fig. 9.7), two features at 207 and 270 K can be clearly distinguished likely attributed to multilayer and monolayer desorption, respectively. Next to molecular desorption, for isophorone exposures

Table 9.1: Masses monitored for isophorone and its hydrogenation products in TPR measurements. The expected intensity is given relative to the maximum signal based on [230]. It can be seen that for most masses presumably several molecules may contribute to the signal intensity. Therefore, several masses and their relative intensity have to be considered for an unambiguous assignment to a certain molecule.

Molecule	$m/z$ , amu	intensity, %	unique	presumable fragment
isophorone- $d_0$	82	100	no	$(C_5OH_6^+)$ or $(C_6H_{10}^+)$
	83	7	no	
	138	23	yes	parent ion
TMCH- $d_0$	83	100	no	$(C_5OH_7^+)$ or $(C_6H_{11}^+)$
	84	10	no	
	125	7	no	$(C_8OH_{13}^+)$
	140	14	no	parent ion
TMCH- $d_2$	85	$\leq 100$	no	$(C_5OH_5D_2^+)$
	86	$\leq 10$	no	
	127	$\leq 7$	no	$(C_8OH_{11}D_2^+)$
	142	14	no	
isophorol- $d_0$	82	8	no	$(C_5OH_8^+)$ $(C_8H_{11}^+)$ $(C_8OH_{13}^+)$ parent ion
	83	30	no	
	84	59	no	
	107	64	yes	
	125	100	yes	
	140	20	no	
isophorol- $d_2$	85	$\leq 30$	no	$(C_5OH_6D_2^+)$ $(C_8H_{11-10}D_{0-1}^+)$ $(C_8OH_{11}D_2^+)$ parent ion
	86	$\leq 59$	no	
	107/108	$\leq 64$	yes	
	127	$\leq 100$	no	
	142	20	no	
dihydro- isophorol- $d_0$	82	11	no	$(C_6H_{11}^+)$ $(C_8H_{13}^+)$ $(C_9H_{16}^+)$ parent ion
	83	48	no	
	84	4	no	
	109	100	yes	
	124	11	yes	
	142	0.5	yes	
dihydro- isophorol- $d_2$	109/110	$\leq 100$	no	$(C_8H_{13-12}D_{0-1}^+)$ $(C_9H_{16}^+)$ parent ion
	124	$\leq 11$	yes	
	144	0.5	yes	
dihydro- isophorol- $d_4$	111/112	$\leq 100$	yes	$(C_8H_{11-10}D_{2-3}^+)$ $(C_9H_{16-15}D_{2-3}^+)$ parent ion
	126/127	$\leq 11$	no	
	146	0.5	yes	

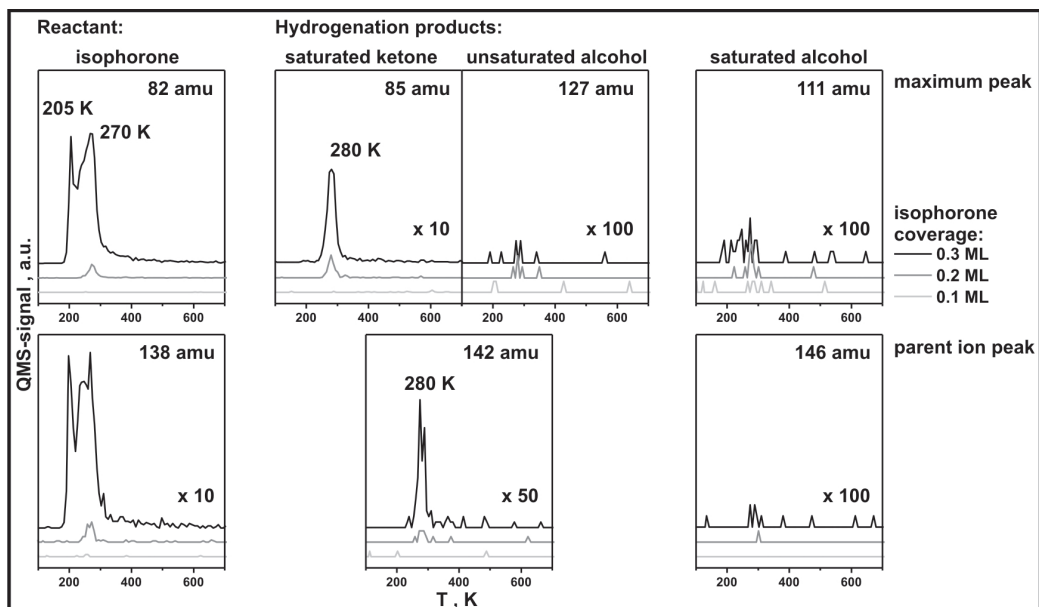


Figure 9.7: TPR spectra for isophorone adsorbed on a D-precovered Pd(111) single crystal surface. The isophorone exposure was varied from 0.1 to 0.3 ML. Displayed are masses characteristic for isophorone (82 amu maximum signal intensity and 138 amu parent ion peak of isophorone) and the hydrogenation products: the saturated ketone, 3,3,5-trimethyl-cyclohexanone(TMCH)- $d_2$  (maximum signal intensity on mass 85, parent ion peak on 142 amu), the unsaturated alcohol, isophorol- $d_2$  (maximum signal intensity on 127 amu and parent ion peak at 142 amu) as well as the saturated alcohol, dihydroisophorol- $d_4$  (maximum signal on 111 amu and parent ion peak on 146 amu).

$\geq 0.2$  ML, signals around 280 K are detected on masses characteristic for hydrogenation products. Desorption is observed on the mass where the maximum signal intensity of the saturated ketone, TMCH- $d_2$ , is expected (85 amu, likely  $C_5OD_2H_5^+$ -fragment). At the same temperature also a signal is found on the mass significant for the parent ion peak of TMCH- $d_2$  (142 amu) which coincides however with the parent ion peak of the unsaturated alcohol, isophorol- $d_2$ . For isophorol- $d_2$ , in contrast to TMCH- $d_2$ , no significant desorption features are observed for the expected maximum signal (127 amu,  $C_8OD_2H_{11}^+$ -fragment) demonstrating that the formation of the unsaturated alcohol involving the hydrogenation of the C=O bond is negligible. The absence of significant signals on the masses characteristic for the saturated alcohol dihydroisophorol- $d_4$  (111 amu, maximum signal intensity, likely  $C_8D_2H_{11}^+$ -fragment, and 146 amu, parent ion peak) indicates that under the applied conditions the full hydrogenation to the saturated alcohol is also insignificant. Thus, in good agreement with studies under more realistic conditions [214–216], the hydrogenation of isophorone over Pd(111) yields under the applied



conditions with a high selectivity the saturated ketone, while the formation of alcohols involving the hydrogenation of the C=O double bond is negligible.

TPR measurements were also conducted for the partial hydrogenation product TMCH. In these experiments, the Pd(111) surface was first exposed to 190 L of D<sub>2</sub> and then to different amounts (0.05 – 0.20 ML) of TMCH. Subsequently, the sample was also heated in vacuum to  $\approx 700$  K and the evolution of gas phase products was followed by QMS. As can be seen in fig. 9.8, even for the lowest applied exposure (0.05 ML), molecular desorption of TMCH-*d*<sub>0</sub> (see masses 83 amu, maximum signal intensity, and 140 amu, parent ion peak of TMCH-*d*<sub>0</sub>) is observed next to decomposition evidenced by H<sub>2</sub>, CO and CH<sub>4</sub> desorption (data not displayed). For low coverages of isophorone ( $\leq 0.2$  ML), in contrast, only decomposition and no molecular desorption was detected suggesting a stronger interaction of isophorone with the D-precovered Pd(111) surface compared to the saturated ketone.

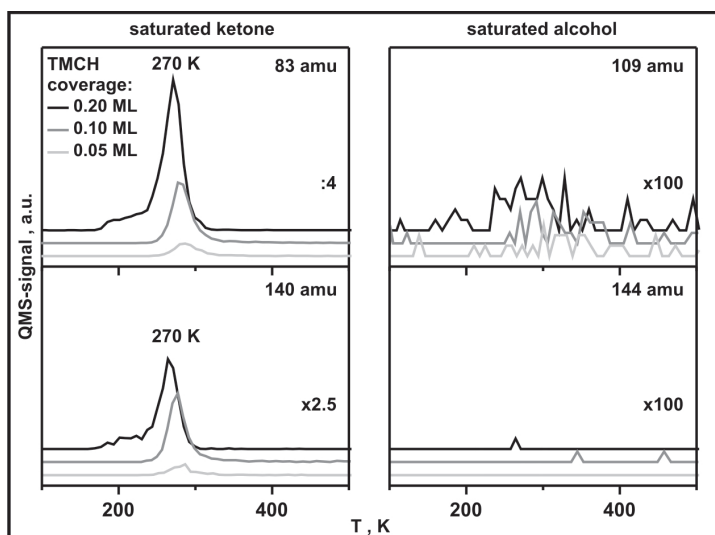


Figure 9.8: TPR spectra for TMCH adsorbed on a D-precovered Pd(111) single crystal surface. The isophorone exposure was varied from 0.05 to 0.20 ML. Displayed are masses characteristic for TMCH-*d*<sub>0</sub> (83 amu maximum signal intensity and 140 amu parent ion peak of TMCH) and the hydrogenation product, dihydroisophorol-*d*<sub>2</sub>, the saturated alcohol (maximum signal on 109 amu and parent ion peak on 144 amu).

Further hydrogenation of the TMCH molecule to the saturated alcohol is not observed in these experiments. For the parent ion peak of dihydroisophorol-*d*<sub>2</sub> (144 amu), clearly no notable desorption is detected and even on the expected maximum signal (109 amu) for the saturated alcohol, the intensity is negligible compared to the formation of the saturated ketone from isophorone. Thus, under the applied reaction conditions, TMCH

does not react further to form the saturated alcohol dihydroisophorol over the Pd(111) single crystal surface. This finding is in good agreement with realistic catalytic studies where formation of the saturated alcohol remains typically negligible over Pd catalysts [214–216].

In summary, the TPR measurements on the reactivity of isophorone over the D-precovered Pd(111) single crystal surface showed that isophorone merely decomposes at low coverages. For higher coverages, also molecular desorption and formation of hydrogenation products occurs. In the hydrogenation, no significant amounts of alcohols are formed indicating that mainly the C=C double bond is hydrogenated yielding the saturated ketone. TPR measurements on the reactivity of TMCH, the saturated ketone of isophorone, also do not show further hydrogenation to the saturated alcohol. Thus, a high selectivity toward the hydrogenation of the C=C double bond over Pd(111) is found in the TPR measurements which is in good agreement with catalytic studies conducted under more realistic conditions. The observation of a similar reactivity of the model system under UHV condition as for realistic conditions is the basis for further reactivity studies under well-defined conditions to unravel the microscopic mechanisms governing the activity and selectivity of this catalytic reaction.

## 9.4 Conclusion and outlook

In this chapter, the first measurements on the adsorption and reaction of isophorone with  $H_2(D_2)$  over Pd model catalysts under well-defined UHV conditions were presented. The adsorption of isophorone on a clean and D-precovered Pd(111) single crystal surface was investigated by IRAS measurements at 100 K. To study the reactivity in the conversion with  $H_2(D_2)$ , TPR measurements were conducted for isophorone and its partial hydrogenation product, 3,3,5-trimethyl-cyclohexanone (TMCH), over the D-precovered Pd(111) surface.

The IRAS measurements indicated for low isophorone coverages, an adsorption geometry with the C=C and the C=O bond parallel to the surface. Co-adsorbed H(D) was found to induce changes in the IR spectra indicating an altered interaction of isophorone with the Pd(111) surface in the presence of H(D). The absence of significant signals attributable to C-D vibrations suggested that the changes in the presence of co-adsorbed H(D) are likely due to an altered adsorption geometry. Next to C-H vibrations, also the IR absorption in the C=C/C=O stretching region was affected. The altered adsorption geometry of isophorone can potentially be expected to influence the activity and selectivity in the partial hydrogenation of isophorone.

The static IR spectra of the saturated ketone TMCH exhibited clear differences with respect to the isophorone spectra demonstrating that these two molecules can be spectroscopically distinguished and thus, allowing the use of IRAS as a detection method in future dynamic reactivity measurements, like *e.g.* pulsed isothermal MB experiments.

The presence of H(D) was found to also significantly affect the adsorption of the saturated ketone on the Pd(111) surface. The changes in the IR spectra suggested on one hand strong distortions of the molecule adsorbed on the clean Pd(111) surface and on the other hand, a relatively flat lying adsorption geometry for TMCH adsorption over the D-precovered Pd surface.

TPR experiments on the conversion of isophorone with H(D) over Pd(111) showed that at low coverages only decomposition occurs, while for higher coverages, also molecular desorption and hydrogenation is found. In line with more realistic catalytic studies, the partial hydrogenation product could be identified as the saturated ketone, while the unsaturated alcohol isophorol involving hydrogenation of the C=O bond is not formed in notable amounts. Also the saturated alcohol is not formed under the applied conditions regardless, if isophorone or the saturated ketone is used as reactant.

The presented experiments conducted for a simple Pd(111) single crystal surface clearly show that it is possible to investigate the adsorption and reaction of a relatively large and complex molecule like isophorone under well-defined UHV conditions using modern surface science techniques which is the base for further studies over more complex supported Pd model catalysts. In the determination of the the exact adsorption geometry, NEXAFS (near edge X-ray absorption fine structure) measurements may aid, while isothermal pulsed MB experiments using time-resolved IRAS and MS as detection methods may help to understand the factors governing the activity, selectivity as well as the underlying reaction kinetics in the conversion of isophorone with H<sub>2</sub>(D<sub>2</sub>) over Pd catalysts. Thus, the results presented in this chapter build a base for further investigations on the microscopic origins of selectivity in complex catalytic reactions.



## 10 Summary

Understanding microscopic factors that govern the activity and selectivity in catalytic reactions is one of the main goals in catalytic research. The conversion of olefins with hydrogen constitutes a major application for heterogeneous catalysts, in particular Pd catalysts are often used in these reactions. The aim of this work was to unravel important microscopic factors governing the activity and selectivity in hydrocarbon conversions with hydrogen over Pd catalysts using a surface science approach.

The conversion of *cis*-2-butene with hydrogen was studied over well-defined Pd model catalysts under UHV conditions by pulsed isothermal molecular beam (MB) experiments. As model catalysts, on one hand a Pd(111) single crystal surface was employed and on the other hand a supported Pd/Fe<sub>3</sub>O<sub>4</sub>/Pt(111) model catalyst was used exhibiting important features of applied catalysts, while still providing a well-defined and well-characterized surface morphology.

In the conversion with hydrogen over transition metal surfaces, *cis*-2-butene can either undergo *cis-trans* isomerization or hydrogenation following the generally accepted Horiuti-Polanyi mechanism which consists of a series of sequential hydrogenation and dehydrogenation steps. When D<sub>2</sub> is used instead of H<sub>2</sub>, each *cis-trans* isomerization step is accompanied by an H/D exchange allowing for a distinction of the reactant *cis*-2-butene and the product *trans*-2-butene-*d*<sub>1</sub> in the gas phase by mass spectrometry. As a third reaction pathway, *cis*-2-butene can decompose yielding other hydrocarbon species, like butylidyne, and strongly dehydrogenated carbonaceous deposits after heating to high temperatures. Despite the practical importance of these carbonaceous deposits which are usually present under realistic reaction conditions, most surface science studies are conducted over clean, C-free surfaces.

We found that formation of gas phase products, only occurs once the surface is covered with hydrocarbon species that build up during an initial induction period. At low temperatures ( $\leq 210$  K), these hydrocarbon species inhibit the dissociative adsorption of H<sub>2</sub>(D<sub>2</sub>) under reaction conditions resulting in vanishing conversion activity for prolonged olefin exposures. For higher temperatures ( $> 210$  K), persisting isomerization activity attests to effective formation of butyl species, the common reaction intermediate for isomerization and hydrogenation, indicating that also surface H(D) is effectively replenished under reaction conditions. The hydrogenation activity over the C-free Pd model catalyst, in contrast, returns to zero after a period of high activity indicating the involvement of a second hydrogen species which is present on the D-saturated particles, but is depleted under these conditions for longer olefin exposures. In the presence

of strongly dehydrogenated carbonaceous deposits which are mainly located on low-coordinated sites of the Pd particles, like edges and corners, the activity and selectivity changes dramatically. Next to isomerization also hydrogenation activity persists for surface temperatures  $> 210$  K indicating that also the second hydrogen species is effectively replenished under reaction conditions when the surface is C-precovered.

Using a combination of nuclear reaction analysis (NRA) for hydrogen depth profiling and transient MB experiments, it was possible to show that the second hydrogen species which is required for the hydrogenation reaction is associated with the presence of subsurface hydrogen. Either subsurface hydrogen is directly inserted into the metal-carbon bond of the butyl intermediate or surface hydrogen is modified in the presence of subsurface hydrogen to be more prone to attack the Pd-butyl bond. Thus, while the replenishment of subsurface hydrogen is inhibited over the C-free Pd surface, carbonaceous deposits seem to facilitate the H(D) diffusion into the subsurface under reaction conditions allowing for persisting hydrogenation activity.

To elucidate the role of hydrogen-related processes, such as dissociative adsorption on the surface and diffusion to subsurface sites, and how these processes influence the activity and selectivity, the reactivity over the D-saturated surface and over the surface under steady state conditions was investigated by pulsed MB experiments for different reaction conditions. Next to the temperature dependence, the influence of the reactant pressures and their relative ratio was studied. With increasing  $D_2$  pressure and increasing temperature, a shift in selectivity toward hydrogenation is observed, while increasing *cis*-2-butene pressures favor the *cis-trans* isomerization pathway. For temperatures  $\geq 280$  K, hydrogenation is also sustained over the C-free Pd/Fe<sub>3</sub>O<sub>4</sub> model catalyst. The formal reaction orders with respect to the  $D_2$  pressure were around unity, while the formal reaction orders in *cis*-2-butene pressure were around zero under steady state conditions for a reaction temperature of 260 K. These general trends are all in good agreement with more applied catalytic studies.

The formal reaction orders in  $D_2$  pressure were found to be in fair agreement with values predicted by a simple Langmuir-Hinshelwood mechanism. This model exhibited however not enough detail to reproduce the experimentally observed results exactly. The formal reaction orders in 2-butene pressure with values around zero indicated a strong inhibition of hydrogen sorption by co-adsorbed hydrocarbon species. This interpretation was further corroborated by the qualitative analysis of the pulse shapes. The formation of subsurface H(D) is more strongly inhibited by co-adsorbed hydrocarbon species than the formation of surface H(D).

With increasing reaction temperature, a maximum in reaction rates was observed for both hydrogenation and isomerization. Compared to the isomerization, the maximum of the hydrogenation rates is shifted to higher temperatures clearly demonstrating that different elementary steps determine the rates of the hydrogenation and the isomerization reactions. While isomerization is limited in a broad range of reaction conditions by

the formation of the butyl intermediate, the rate of the second half-hydrogenation step from butyl to butane determines the formation of hydrogenation products for a large range of reaction conditions.

To investigate the influence of low-coordinated sites of the Pd particles and their modification with carbonaceous deposits further, pulsed isothermal MB experiments were conducted over a C-free and a C-precovered Pd(111) single crystal surface and compared to the corresponding measurements over the supported Pd/Fe<sub>3</sub>O<sub>4</sub> model catalyst. The C-free Pd model catalysts, both Pd(111) and the Pd particles, exhibit a qualitatively very similar reactivity in the conversion of *cis*-2-butene with H<sub>2</sub>(D<sub>2</sub>). At low temperatures, only isomerization activity is sustained, while hydrogenation activity ceases after an initial period of high activity. For higher temperatures ( $\geq 280$  K), both *cis-trans* isomerization and hydrogenation activity persist. The high hydrogenation activity over the Pd(111) surface indicates that the (111)-facets constituting  $\approx 80\%$  of the surface of the Pd particles significantly contribute to the hydrogenation rates over the supported Pd/Fe<sub>3</sub>O<sub>4</sub> model catalysts, while the clearly lower isomerization rates over the Pd(111) single crystal surface suggest that low-coordinated sites of the Pd particles exhibit a higher activity for *cis-trans* isomerization than the (111)-facets. This finding is in good agreement with realistic catalytic studies reporting a more pronounced structure sensitivity for the isomerization pathway.

Deposition of C onto the Pd(111) single crystal surface does not result in pronounced reactivity changes with respect to the C-free surface which is in strong contrast to the dramatic effect of C-precovering on the Pd particles which induces persisting hydrogenation activity already at low temperatures (220 – 260 K). Sustained isomerization over all Pd model catalysts - displaying similar rates for the C-free and the C-modified surfaces - attests to the availability of the reactants 2-butene and surface H(D) as well as to the effective formation of the common reaction intermediate butyl. Thus, the reactivity changes are clearly connected to the modification of low-coordinated sites by C and not to C-induced changes of regular (111)-facets. Similarly high initial hydrogenation rates observed for all Pd model catalysts clearly demonstrate, moreover, that the intrinsic reactivity of the C-modified low-coordinated sites is not significantly higher, when there are no limitations in H(D) availability. Thus, the effect of C-deposition on low-coordinated sites was attributed to the replenishment of the second hydrogen species associated with the presence of subsurface hydrogen under reaction conditions. Theoretical calculations suggest that C-modification of atomically-flexible, low-coordinated sites facilitates H(D) diffusion to subsurface sites by two effects. On one hand, surface adsorbed H is destabilized in the vicinity of C and on the other hand, C-induced local distortions of the Pd lattice lead to a basically vanishing of the diffusion barrier. For the rigid Pd(111) surface, in contrast, an expansion of the Pd lattice is not predicted so that the effect of C-deposition is expected to be minor for the Pd(111) surface which is the experimentally observed result.

To probe the hydrogen distribution more directly, isothermal pulsed MB experiments

on the H/D exchange over Pd model catalysts were conducted. Measurements on the steady state H/D exchange rates as a function of the overall pressure over the C-free and the C-covered Pd particles conducted for 260 and 320 K showed that C-modification affects the HD formation. TPD and NRA measurements indicate that H/D exchange at 320 K is governed by recombination of surface H(D). For this temperature, a reduction of the steady state rates in the presence of C is observed which can likely be attributed to physical blocking of H(D) surface adsorption sites by C that is expected to result in lower steady state H(D) surface coverages. For a reaction temperature of 260 K, TPD and NRA measurements suggest, in contrast, that HD formation is strongly influenced by subsurface related H(D) species. At this temperature, an increase in the steady state H/D exchange rates is observed for the C-modified Pd particles with respect to the C-free model catalyst. The interpretation that C-modification of atomically flexible, low-coordinated sites results in increased H(D) diffusion rates to subsurface sites and thereby, in higher steady state HD formation rates at 260 K is consistent with our experimental results and in line with DFT calculations.

Temperature dependent H/D exchange measurements were conducted for the C-free and the C-covered Pd(111) surface and the C-free and the C-covered Pd particles. The experimental results were compared to a kinetic simulation based on a Langmuir-Hinshelwood type kinetic model assuming HD formation solely by recombination of surface H(D) species. The comparison of the experimental data to the predictions of this model was used to reveal a possible involvement of subsurface adsorbed H(D). While the kinetic simulation was found to describe fairly well the steady state H/D exchange rates over the Pd(111) surfaces, clear deviations from the model, especially for low temperatures, were found for the Pd particles, which were most pronounced for the C-modified Pd particles. Assuming simply different activation energies and/or pre-exponential factors for HD formation over Pd particles cannot account for the observed deviations which supports the earlier hypothesis that not only surface H(D), but also subsurface H(D) is involved in the H/D exchange reaction.

Pressure dependent measurements on the steady state H/D exchange over the C-free and the C-covered Pd particles were conducted at 260 and 320 K. The obtained formal reaction orders were compared to values predicted by a simple Langmuir-Hinshelwood model assuming HD formation only by association of surface adsorbed H(D). The experimentally observed reaction orders agree fairly well with the model for a reaction temperature of 320 K where H/D exchange is expected to be governed by reaction of surface H(D) species. For 260 K, the simple kinetic model taking only surface H(D) species into account cannot adequately describe the experimentally observed reaction orders supporting the assumption that next to surface H(D), subsurface H(D) species influence the HD formation at this temperature.

The transient response of the HD formation rates reflecting the approach of the H concentrations to equilibrium indicated that two processes with different characteristic times are involved in the HD formation. These can be attributed to a fast replenishment



of surface hydrogen by basically non-activated dissociative adsorption of H<sub>2</sub> and to a slower replenishment of subsurface hydrogen species by activated diffusion into the Pd bulk. Activated H diffusion to subsurface sites is known to be a structure sensitive process. The diffusion rate and thus, the achievement of the final steady state HD formation rates are expected to increase from Pd(111), to the C-free and the C-covered Pd particles as well as for one particular surface when the reaction temperature is increased. This prediction is in good agreement with the experimental results. At 280 K, the transient response curves of the HD signal obtained for the Pd(111) surface, the C-free and the C-modified Pd particles exhibit the expected structure dependence. Comparison of the experimental transient response curves obtained at 320 K with those at 280 K show, moreover, also the predicted temperature dependence. These results are, as the results of the temperature and pressure dependent measurements, consistent with the interpretation that subsurface absorbed H(D) influences the HD formation over Pd surfaces.

Co-adsorbed hydrocarbon species were found to strongly inhibit the H/D exchange. Even for the highest applied temperatures, no significant HD formation rates were observed. This effect is understood such that hydrocarbon species break up ensembles of free neighboring adsorption sites which are required for both the dissociative adsorption of H<sub>2</sub>(D<sub>2</sub>) as well as for the associative desorption. In particular, the latter process where both a H and a D species need to simultaneously reach a free space is expected to be significantly slower.

For molecules containing several double bonds, like *e.g.* the  $\alpha,\beta$ -unsaturated ketone isophorone exhibiting both a C=C and a C=O double bond, hydrogenation can yield different products. Over Pd catalysts, typically a pronounced chemoselectivity toward the hydrogenation of the C=C double bond is observed. In the presence of certain modifiers, it is possible to hydrogenate isophorone even enantioselectively over heterogeneous Pd catalysts. To first understand the chemoselectivity of isophorone over Pd catalysts, the adsorption and reaction of isophorone with hydrogen was investigated by IRAS and TPR measurements over a simple Pd(111) surface. IRAS experiments showed that isophorone adsorbs at 100 K for low coverages in a relatively flat lying adsorption geometry, either with the C=C and the C=O bond parallel to the surface or with these bonds strongly perturbed by *e.g.* di- $\sigma$ -complex formation or bond breaking. For higher coverages, a presumably more tilted adsorption geometry is observed. Co-adsorbed H(D) induces changes in the adsorption geometry affecting also the C=C and/or the C=O bonds which can potentially influence the reactivity.

Corresponding IRAS measurements on 3,3,5-trimethyl-cyclohexanone (TMCH), the predominant hydrogenation product of isophorone over Pd catalysts, showed that the spectra for adsorption on Pd(111) differ even at low coverages from the isophorone spectra which is an important prerequisite to use IRAS as detection method in future reactivity measurements. Co-adsorbed H(D) also influences the adsorption of the partial hydrogenation product with the IR spectra exhibiting the most pronounced changes for the C=O stretching vibration.

In the TPR measurements, full decomposition of isophorone was found for low coverages suggesting strong interactions with the underlying Pd surface. For higher coverages, also molecular desorption and formation of hydrogenation products occurs. The hydrogenation product could be identified as the saturated ketone TMCH formed *via* the hydrogenation of the C=C double bond. Hydrogenation of the C=O double bond resulting in the formation of alcohols is not observed over the Pd(111) surface under the applied reaction conditions, regardless if isophorone or TMCH is used as reactant. This selectivity is in good agreement with catalytic studies conducted under more realistic reaction conditions.

These first measurements demonstrate that it is possible to investigate the adsorption and reaction of complex molecules like isophorone over well-defined model catalysts under chemically clean UHV conditions using modern surface science techniques. This promising result constitutes the foundation for future experiments over more complex supported Pd model catalysts and in the presence of surface modifiers. Based on the first successful measurements, also the use of techniques like NEXAFS to study the adsorption in more detail and pulsed isothermal MB experiments for reactivity measurements under more realistic reaction conditions is projected to further advance the understanding of the microscopic origins for selectivity in catalytic reactions.

# Bibliography

- [1] E. K. Rideal. *Concepts in Catalysis*. Academic Press, 1968.
- [2] G. Ertl, H. Knözinger, and J. Weitkamp. *Environmental Catalysis*. Wiley VCH, 1999.
- [3] J. M. Thomas and W. J. Thomas. *Principle and Practice of Heterogeneous Catalysis*. Wiley VCH, 1997.
- [4] G. Ertl, H. Knözinger, F. Schüth, and J. Weitkamp. *Handbook of Heterogeneous Catalysis*. Wiley VCH, 2008.
- [5] M. Boudart. Catalysis by supported metals. *Adv. Catal.*, 20:153, 1969.
- [6] M. Che and C. O. Bennett. The influence of particle size on the catalytic properties of supported metals. *Adv. Catal.*, 36:55, 1989.
- [7] G. C. Bond. The origins of particle size effects in heterogeneous catalysis. *Surf. Sci.*, 156(2):966, 1985.
- [8] J. A. Dumesic, D. F. Rudd, L. M. Aparicio, J. E. Rekoske, and A. A. Trevino. *The Microkinetics of Heterogeneous Catalysis*. American Chemical Society, 1993.
- [9] G. Ertl. Reactions at surfaces: From atoms to complexity (Nobel lecture). *Angew. Chem. Int. Ed.*, 47(19):3524, 2007.
- [10] R. J. Farrauto and R. M. Heck. Environmental catalysis into the 21st century. *Catal. Today*, 55(1-2):179, 2000.
- [11] C. R. Henry. Surface studies of supported model catalysts. *Surf. Sci. Rep.*, 31(7-8):157, 1998.
- [12] J. Libuda and H.-J. Freund. Molecular beam experiments on model catalysts. *Surf. Sci. Rep.*, 57(7-8):157, 2005.
- [13] M. P. D'Evelyn and R. J. Madix. Reactive scattering from solid surfaces. *Surf. Sci. Rep.*, 3:413, 1984.
- [14] G. Scoles. *Atomic and Molecular Beam Methods*. Oxford University Press, 1988.
- [15] C. T. Rettner, D. J. Auerbach, J. C. Tully, and A. W. Kleyn. Chemical dynamics at the gas-surface interface. *J. Chem. Phys.*, 100(31):13021, 1996.

## Bibliography

- [16] A. W. Kleyn. Molecular beams and chemical dynamics at surfaces. *Chem. Soc. Rev.*, 32(2):87, 2003.
- [17] A. W. Kleyn. *The chemical physics of solid surfaces and heterogeneous catalysis, Volume 11 (Surface Dynamics)*. D. A. King and D. P. Woodruff (Editors), Elsevier, Amsterdam, 2003.
- [18] V. P. Zhdanov and B. Kasemo. Simulations of the reaction kinetics on nanometer supported catalyst particles. *Surf. Sci. Rep.*, 39(2-4):29, 2000.
- [19] M. Bäumer and H.-J. Freund. Metal deposits on well-ordered oxide films. *Prog. Surf. Sci.*, 61(7-8):127, 1999.
- [20] T. P. St. Clair and D. W. Goodman. Metal nanoclusters supported on metal oxide thin films: bridging the materials gap. *Top. Catal.*, 13(1-2):5, 2000.
- [21] C. T. Campbell, A. W. Grant, D. E. Starr, S. C. Parker, and V. A. Bondzie. Model oxide-supported metal catalysts: energetics, particle thickness, chemisorption and catalytic properties. *Top. Catal.*, 14(1-4):43, 2001.
- [22] H.-J. Freund, M. Bäumer, J. Libuda, T. Risse, G. Rupprechter, and Sh. Shaikhutdinov. Preparation and characterization of model catalysts: from ultra-high vacuum to in situ conditions at the atomic dimension. *J. Catal.*, 216(1-2):223, 2003.
- [23] H.-J. Freund. Adsorption on gases on complex solid surfaces. *Angew. Chem. Int. Ed.*, 36(5):452, 1997.
- [24] H.-J. Freund. Clusters and islands on oxides: from catalysis via electronics and magnetism to optics. *Surf. Sci.*, 500(1-3):271, 2002.
- [25] H.-J. Freund and G. Pacchioni. Oxide ultra-thin films on metals: new materials for the design of supported metal catalysts. *Chem. Soc. Rev.*, 37(10):2224, 2008.
- [26] R. J. Madix and J. A. Schwarz. Chemical relaxation molecular beam studies of reactive gas-solid scattering: I. Reaction of silicon and germanium with molecular chlorine. *Surf. Sci.*, 24(1):264, 1971.
- [27] T. Engel and H. Kuipers. A molecular-beam investigation of the scattering, adsorption and absorption of H<sub>2</sub> and D<sub>2</sub> from/on/in Pd(111). *Surf. Sci.*, 90:162, 1979.
- [28] D. F. Padowitz and S. J. Sibener. Kinetics of hydrogen oxidation to water on the Rh(111) surface using multiple source modulated molecular-beam techniques. *Surf. Sci.*, 254(1-3):125, 1991.
- [29] M. Bonn, A. W. Kleyn, and G. J. Kroes. Real time chemical dynamics at surfaces. *Surf. Sci.*, 500(1-3):475, 2002.

- [30] J. Libuda, I. Meusel, J. Hartmann, and H.-J. Freund. A molecular beam/surface spectroscopy apparatus for the study of reactions on complex model catalysts. *Rev. Sci. Instr.*, 71(12):4395, 2000.
- [31] J. Horiuti and K. Miyahara. *Hydrogenation of Ethylene on Metallic Catalysts*. Report NSRDS-NBC No. 13, National Bureau of Standards, 1986.
- [32] G. C. Bond and J. M. Winterbottom. Hydrogenation of olefins: 6. Reaction of *n*-butenes with hydrogen and with deuterium over alumina supported palladium. *Trans. Farad. Soc.*, 65:2779, 1969.
- [33] J. P. Boitiaux, J. Cosyns, and S. Vasudevan. Hydrogenation of highly unsaturated-hydrocarbons over highly dispersed palladium catalysts. 1. Behavior of small metal particles. *Appl. Catal.*, 6(1):41, 1983.
- [34] S. Hub, L. Hilaire, and R. Touroude. Hydrogenation of but-1-yne and but-1-ene on palladium catalysts - particle size effect. *Appl. Catal.*, 36(1-2):307, 1988.
- [35] K. S. Sim, L. Hilaire, F. Le Normand, R. Touroude, V. Paul-Boncour, and A. Percheron-Guegan. Catalysis by palladium-rare-earth-metal intermetallic compounds: Hydrogenation of but-1-ene, buta-1,3-diene and but-1-yne. *J. Chem. Soc. Farad. Trans.*, 87(9):1453, 1991.
- [36] S. P. Bressa, O. M. Martinez, and G. F. Barreto. Kinetic study of the hydrogenation and hydroisomerization of the *n*-butenes on a commercial palladium/alumina catalyst. *Ind. Eng. Chem. Res.*, 42(10):2081, 2003.
- [37] G. C. Bond. *Metal-Catalysed Reactions of Hydrocarbons*. Springer Science, 2005.
- [38] D. Teschner, E. Vass, M. Hävecker, S. Zafeirotos, P. Schnörch, H. Sauer, A. Knop-Gericke, R. Schlögl, M. Chamam, A. Woosch, A. S. Canning, J. J. Gamman, S. D. Jackson, J. McGregor, and L. F. Gladden. Alkyne hydrogenation over Pd catalysts: A new paradigm. *J. Catal.*, 242:26, 2006.
- [39] X.-C. Guo and R. J. Madix. Selective hydrogenation and H-D exchange of unsaturated hydrocarbons on Pd(100)-p(1 × 1)-H(D). *J. Catal.*, 155:336, 1995.
- [40] J. C. Bertolini, A. Cassuto, Y. Jugnet, J. Massardier, B. Tardy, and G. Tourillon. A comparative study of 1,3-butadiene and 1-butene chemisorbed on Pt(111) and Pd(111). *Surf. Sci.*, 349:88, 1996.
- [41] G. Tourillon, A. Cassuto, Y. Jugnet, J. Massardier, and J. C. Bertolini. Buta-1,3-diene and but-1-ene chemisorption on Pt(111), Pd(111), Pd(110) and Pd<sub>50</sub>Cu<sub>50</sub>(111) as studied by UPS, NEXAFS, and HREELS in relation to catalysis. *J. Chem. Soc. Farad. Trans.*, 92(23):4835, 1996.
- [42] S. Katano, H. S. Kato, M. Kawai, and K. Domen. Selective partial hydrogenation of 1,3-butadiene to butene on Pd(110): specification of reactant adsorption states and product stability. *J. Phys. Chem. B*, 107(16):3671, 2003.

## Bibliography

- [43] A. M. Doyle, Sh. K. Shaikhutdinov, S. D. Jackson, and H.-J. Freund. Alkene chemistry on the palladium surface: nanoparticles vs single crystals. *J. Catal.*, 223(2):444, 2004.
- [44] J. Silvestre-Albero, G. Rupprechter, and H.-J. Freund. Atmospheric pressure studies of selective 1,3-butadiene hydrogenation on Pd single crystals: effect of CO addition. *J. Catal.*, 235:52, 2005.
- [45] C. Breinlich, J. Haubrich, C. Becker, A. Valcarcel, F. Delbecq, and K. Wandelt. Hydrogenation of 1,3-butadiene on Pd(111) and Pd/Sn/Pd(111) surface alloys under UHV conditions. *J. Catal.*, 251:123, 2007.
- [46] J. Silvestre-Albero, M. Borasio, G. Rupprechter, and H.-J. Freund. Combined UHV and ambient pressure studies of 1,3-butadiene adsorption and reaction on Pd(110) by GC, IRAS and XPS. *Catal. Comm.*, 8:292, 2007.
- [47] P. Beccat, J. C. Bertolini, Y. Gauthier, J. Massardier, and P. Ruiz. Crotonaldehyde and methylcrotonaldehyde hydrogenation over Pt(111) and Pt<sub>80</sub>Fe<sub>20</sub>(111) single crystals. *J. Catal.*, 126(2):451, 1990.
- [48] M. Bron, D. Teschner, A. Knop-Gericke, B. Steinhauer, A. Scheybal, M. Hävecker, D. Wang, R. Födisch, D. Hönicke, A. Woosch, R. Schlögl, and P. Claus. Bridging the pressure and materials gap: in-depth characterisation and reaction studies of silver catalysed acrolein hydrogenation. *J. Catal.*, 234:37, 2005.
- [49] M. E. Chiu, D. J. Watson, G. Kyriakou, M. S. Tikhov, and R. M. Lambert. Tilt the molecule and change the chemistry: mechanism of S-promoted chemoselective catalytic hydrogenation of crotonaldehyde on Cu(111). *Angew. Chem. Int. Ed.*, 45:7530, 2006.
- [50] C. J. Kliever, M. Bieri, and G. A. Somorjai. Hydrogenation of the  $\alpha$ ,  $\beta$ -unsaturated aldehydes acrolein, crotonaldehyde and prenal over Pt single crystals: A kinetic and sum-frequency generation vibrational spectroscopy study. *J. Am. Chem. Soc.*, 131:9958, 2009.
- [51] K. Brandt, M. E. Chiu, D. J. Watson, M. S. Tikhov, and R. M. Lambert. Chemosselective hydrogenation of acrolein on Ag(111): Effect of molecular orientation on reaction selectivity. *J. Am. Chem. Soc.*, 131:17286, 2009.
- [52] L. E. Murillo, C. A. Menning, and J. G. Chen. Trend in the C=C and C=O bond hydrogenation of acrolein on Pt-M(M = Ni, Co, Cu) bimetallic surfaces. *J. Catal.*, 268:335, 2009.
- [53] A. M. Doyle, Sh. K. Shaikhutdinov, S. D. Jackson, and H.-J. Freund. Hydrogenation on metal surfaces: Why are nanoparticles more active than single crystals? *Angew. Chem. Int. Ed.*, 42(42):5240, 2003.

- [54] E. Wicke and H. Brodowsky. *Hydrogen in Metals, Volume 2*, page 73. G. Alefeld and J. Völkl (Editors), Springer, Berlin, 1978.
- [55] H. Conrad, G. Ertl, and E. E. Latta. Adsorption of hydrogen on palladium single crystal surfaces. *Surf. Sci.*, 41(2):435, 1974.
- [56] S. P. Daley, A. L. Utz, T. R. Trautman, and S. T. Ceyer. Ethylene hydrogenation on Ni(111) by bulk hydrogen. *J. Am. Chem. Soc.*, 116(13):6001, 1994.
- [57] A. Michaelidis, P. Hu, and A. Alavi. Physical origin of the high reactivity of subsurface hydrogen in catalytic hydrogenation. *J. Chem. Phys.*, 111(4):1343, 1999.
- [58] D. Teschner, J. Borsodi, A. Wootsch, Z. Revay, M. Hävecker, A. Knop-Gericke, S. D. Jackson, and R. Schlögl. The roles of subsurface carbon and hydrogen in palladium-catalyzed alkyne hydrogenation. *Science*, 320:86, 2008.
- [59] F. Studt, F. Abild-Pedersen, T. Bligaard, R. Z. Sørensen, C. H. Christensen, and J. K. Nørskov. On the role of surface modifications of palladium catalysts in the selective hydrogenation of acetylene. *Angew. Chem. Int. Ed.*, 47:9299, 2008.
- [60] A. Sarkany. Hydrocarbonaceous deposit assisted *n*-butane formation in hydrogenation of 1,3-butadiene over Pd catalysts. *Appl. Catal. A*, 175:245, 1998.
- [61] A. Sarkany. Features of deposit formation from 1,3-butadiene over Pd catalysts. *React. Kinet. Catal. Lett.*, 68(1):153, 1999.
- [62] S. B. Ziemecki, G. A. Jones, D. G. Swartzfager, and R. L. Herlow. Formation of interstitial Pd-C phase by interaction of ethylene, acetylene, and carbon monoxide with palladium. *J. Am. Chem. Soc.*, 107:4547, 1985.
- [63] J. Stachurski. Hydrogen sorption by a supersaturated solution of carbon in palladium. *J. chem. Soc. Farad. Trans.*, 81:2813, 1985.
- [64] J. A. McCaulley. In-situ X-ray absorption spectroscopy studies of hydride and carbide formation in supported palladium catalysts. *J. Phys. Chem.*, 97:10372, 1993.
- [65] P. Albers, J. Pietsch, and S. F. Parker. Poisoning and deactivation of palladium catalysts. *J. Mol. Catal. A*, 173:275, 2001.
- [66] F. C. Tompkins. *Chemisorption of gases on metals*. Academic Press, 1978.
- [67] K. W. Kolasinski. *Surface science: foundations of catalysis and nanoscience*. Wiley, 2002.
- [68] H. Yokoyama, H. Numakura, and M. Koiwa. The solubility and diffusion of carbon in palladium. *Acta Mater.*, 46(8):2823, 1998.

## Bibliography

- [69] M. Morkel, V. V. Kaichev, G. Rupprechter, and H.-J. Freund. Methanol dehydrogenation and formation of carbonaceous overlayers on Pd(111) studied by high-pressure SFG and XPS spectroscopy. *J. Phys. Chem. B*, 108:12955, 2004.
- [70] G. E. Gdowski, T. E. Felter, and R. H. Stulen. Effect of surface temperature on the sorption of hydrogen by Pd(111). *Surf. Sci. Lett.*, 1881(3):L147, 1987.
- [71] R. J. Behm, V. Penka, M. G. Cattania, K. R. Christmann, and G. Ertl. Evidence for subsurface hydrogen on Pd(110) - an intermediate between chemisorbed and dissolved species. *J. Chem. Phys.*, 78(12):7486, 1983.
- [72] M.-G. Cattania, V. Penka, R. J. Behm, K. Christmann, and G. Ertl. Interaction of hydrogen with a palladium(110) surface. *Surf. Sci.*, 126(1-3):382, 1983.
- [73] K. H. Rieder, M. Baumberger, and W. Stocker. Selective transition of chemisorbed hydrogen to subsurface sites on Pd(110). *Phys. Rev. Lett.*, 51(19):1799, 1983.
- [74] A. W. Aldag and L. D. Schmidt. Interaction of hydrogen with palladium. *J. Catal.*, 22(2):260, 1971.
- [75] A. Couper and C. S. John. Sorption of hydrogen by palladium and palladium silver alloys. *J. Chem. Soc. Farad. Trans.*, 74(2):326, 1978.
- [76] B. D. Kay, C. H. F. Peden, and D. W. Goodman. Kinetics of hydrogen absorption by Pd(110). *Phys. Rev. B*, 34(2):817, 1986.
- [77] E. Wicke and H. Brodowsky. *Hydrogen in Metals, Volume 28*, page 321. G. Alefeld and J. Völkl (Editors), Springer, Berlin, 1978.
- [78] C. N. Hinshelwood. *The kinetics of chemical change*. Clarendon Press, 1940.
- [79] D. D. Eley and E. K. Rideal. Parahydrogen conversion on tungsten. *Nature*, 146(3699):401, 1940.
- [80] J. Harris and B. Kasemo. On precursor mechanisms for surface reactions. *Surf. Sci.*, 105(2-3):L281, 1981.
- [81] G. Pacchioni and N. Rösch. Modeling of supported metal-clusters: A density-functional study of CO adsorption on Ni clusters deposited on alumina. *Surf. Sci.*, 306(1-2):169, 1994.
- [82] Sh. K. Shaikhutdinov, R. Meyer, D. Lahav, M. Bäumer, T. Klüner, and H.-J. Freund. Determination of atomic structure of the metal-oxide interface: Pd nanodeposits on an FeO(111) film. *Phys. Rev. Lett.*, 91(7):076102, 2003.
- [83] R. Meyer, M. Bäumer, Sh. K. Shaikhutdinov, and H.-J. Freund. Two-dimensional growth of Pd on a thin FeO(111) film: A physical manifestation of strong metal-support interaction. *Surf. Sci. Lett.*, 546(2-3):L813, 2003.



- [84] T. Schalow. *Bildung und katalytische Aktivität partiell oxidiertes Pd-Nanopartikel*. PhD thesis, Fakultät II (Mathematik und Naturwissenschaften), Technische Universität, Berlin, 2006.
- [85] T. Schalow, B. Brandt, D. E. Starr, M. Laurin, S. Schauerer, Sh. K. Shaikhutdinov, J. Libuda, and H.-J. Freund. Oxygen-induced restructuring of a Pd/Fe<sub>3</sub>O<sub>4</sub> model catalyst. *Catal. Lett.*, 107(3-4):189, 2006.
- [86] G. Blyholder. Molecular orbital view of chemisorbed carbon monoxide. *J. Phys. Chem.*, 68(10):2772, 1964.
- [87] M. Tüshaus, W. Berndt, H. Conrad, A. M. Bradshaw, B. Persson, and A. Nilson. Understanding the structure of high coverage CO adlayers. *Appl. Phys. A*, 51(2):91, 1990.
- [88] H. Othani, M. A. van Hove, and G. Somorjai. LEED intensity analysis of the surface-structures of Pd(111) and of CO adsorbed on Pd(111) in a  $(\sqrt{3} \times \sqrt{3}) R30^\circ$  arrangement. *Surf. Sci.*, 187(2-3):372, 1988.
- [89] M. K. Rose, T. Mitsui, J.C. Dunphy, A. Borg, D. F. Ogletree, M. Salmeron, and P. Sautet. Ordered structures of CO on Pd(111) studied by STM. *Surf. Sci.*, 512(1-2):48, 2002.
- [90] A. M. Bradshaw and F. M. Hoffmann. The chemisorption of carbon monoxide on palladium single crystal surfaces: IR spectroscopic evidence for localised site adsorption. *Surf. Sci.*, 72:513, 1978.
- [91] D. Loffreda, D. Simon, and P. Sautet. Dependence of stretching frequency on surface coverage and adsorbate-adsorbate interactions: A density-functional theory approach of CO on Pd(111). *Surf. Sci.*, 425(1):68, 1999.
- [92] T. Gießel, O. Schaff, C. J. Hirschmugl, V. Fernandez, K.-M. Schindler, A. Theobald, S. Bao, R. Lindsay, W. Berndt, A. M. Bradshaw, C. Baddeley, A. F. Lee, R. M. Lambert, and D. P. Woodruff. A photoelectron diffraction study of ordered structures in the chemisorption system Pd(111)-CO. *Surf. Sci.*, 406(1-3):90, 1998.
- [93] S. Surnev, M. Sock, G. M. Ramsey, F. P. Netzer, M. Wiklund, M. Borg, and J. N. Andersen. CO adsorption on Pd(111): A high-resolution core level photoemission and electron energy loss spectroscopy study. *Surf. Sci.*, 470(1-2):171, 2000.
- [94] W. K. Kuhn, J. Szanyi, and D. W. Goodman. CO adsorption on Pd(111) - the effects of temperature and pressure. *Surf. Sci. Lett.*, 274(3):L611, 1992.
- [95] H. Unterhalt, G. Rupprechter, and H.-J. Freund. Vibrational sum frequency spectroscopy on Pd(111) and supported Pd nanoparticles: CO adsorption from ultra-high vacuum to atmospheric pressure. *J. Phys. Chem. B*, 106(2):356, 2002.

## Bibliography

- [96] A. Ortega, F. M. Hoffman, and A. M. Bradshaw. The adsorption of CO on Pd(100) studied by IR reflection absorption-spectroscopy. *Surf. Sci.*, 119(1):79, 1982.
- [97] S. A. Francis and A. H. Ellison. Infrared spectra of monolayers on metal mirrors. *J. Opt. Soc. Am.*, 49(2):131, 1959.
- [98] X. P. Xu and D. W. Goodman. An infrared and kinetic-study of CO oxidation on model silica-supported palladium catalysts from  $10^{-9}$  to 15 torr. *J. Phys. Chem.*, 97(29):7711, 1993.
- [99] C. Goyhenex, M. Croci, C. Claeys, and C. R. Henry. FTIR studies of the adsorption of CO on supported metallic clusters Pd/MgO(100). *Surf. Sci.*, 352:475, 1996.
- [100] K. Wolter, O. Seiferth, H. Kuhlenbeck, M. Bäumer, and H.-J. Freund. Infrared spectroscopic investigation of CO adsorbed on Pd aggregates deposited on an alumina model support. *Surf. Sci.*, 399(2-3):190, 1998.
- [101] S. Bertarione, D. Scarano, A. Zecchina, V. Johnnek, J. Hoffmann, S. Schauer mann, M. M. Frank, J. Libuda, G. Rupprechter, and H.-J. Freund. Surface reactivity of Pd nanoparticles supported on polycrystalline substrates as compared to thin film model catalysts: Infrared study of CO adsorption. *Surf. Sci.*, 108(11):3603, 2004.
- [102] M. Morkel, H. Unterhalt, M. Salmeron, G. Rupprechter, and H.-J. Freund. SFG spectroscopy from  $10^{-8}$  to 1000 mbar: less ordered CO structures and coadsorption on Pd(111). *Surf. Sci.*, 532:103, 2003.
- [103] P. Hollins. The influence of surface-defects on the infrared-spectra of adsorbed species. *Surf. Sci. Rep.*, 16(2):51, 1992.
- [104] R. J. Behm, K. Christmann, and G. Ertl. Adsorption of hydrogen on Pd(100). *Surf. Sci.*, 99:320, 1980.
- [105] K. Christmann. Interaction of hydrogen with solid surfaces. *Surf. Sci. Rep.*, 9:1, 1988.
- [106] F. Besenbacher, I. Stensgaard, and K. Mortensen. Adsorption position of deuterium on the Pd(100) surface determined with transmission channeling. *Surf. Sci.*, 191(1-2):288, 1987.
- [107] G. Alefeld and J. Völkl. *Hydrogen in Metals*. Springer, 1978.
- [108] V. Ledentu, W. Dong, and P. Sautet. Heterogeneous catalysis through subsurface sites. *J. Am. Chem. Soc.*, 122:1796, 2000.
- [109] K. Nobuhara, H. Kasai, W. A. Dino, and H. Nakanishi. H<sub>2</sub> dissociative adsorption on Mg, Ti, Ni, Pd and La surfaces. *Surf. Sci.*, 566:703, 2004.
- [110] T. Mitsui, M. K. Rose, E. Fomin, D. F. Ogletree, and M. Salmeron. Hydrogen adsorption and diffusion on Pd(111). *Surf. Sci.*, 540:5, 2003.

- [111] T. Mitsui, M. K. Rose, E. Fomin, D. F. Ogletree, and M. Salmeron. Dissociative hydrogen adsorption on palladium requires aggregates of three or more vacancies. *Nature*, 422(6933):705, 2003.
- [112] T. E. Felter, E.C. Sowa, and M. A. van Hove. Location of hydrogen adsorbed on palladium(111) studied by low-energy electron-diffraction. *Phys. Rev. B*, 40(2):891, 1989.
- [113] K. Christmann, G. Ertl, and O. Schober. LEED intensities for clean and hydrogen covered Ni(100) and Pd(111) surfaces. *Surf. Sci.*, 40(1):61, 1973.
- [114] T. E. Felter, S. M. Foiles, M. S. Daw, and R. H. Stulen. Order-disorder transitions and subsurface occupation for hydrogen on Pd(111). *Surf. Sci. Lett.*, 171(1):L379, 1986.
- [115] W. Eberhardt, S. G. Louie, and E. W. Plummer. Interaction of hydrogen with a Pd(111) surface. *Phys. Rev. B*, 28(2):465, 1983.
- [116] R. Lamber, S. Wetjen, and N. I. Jaeger. Size dependence of the lattice parameter of small palladium particles. *Phys. Rev. B*, 51(16):10968, 1995.
- [117] M. Suleiman, N. M. Jisrawi, O. Dankert, M. T. Reetz, C. Bätz, R. Kirchheim, and A. Pundt. Phase transition and lattice expansion during hydrogen loading of nanometer sized palladium clusters. *J. Alloys Comp.*, 356:644, 2003.
- [118] H. Kobayashi, M. Yamauchi, H. Kitagawa, Y. Kubota, K. Kato, and M. Takata. On the nature of strong hydrogen atom trapping inside Pd nanoparticles. *J. Am. Chem. Soc.*, 130(6):1828, 2008.
- [119] P.G. Menon. Coke on catalysts - harmful, harmless, invisible and beneficial types. *J. Mol. Catal.*, 59:207, 1990.
- [120] P. G. Menon. Diagnosis of industrial catalyst deactivation by surface characterization techniques. *Chem. Rev.*, 94:1021, 1994.
- [121] R. Lamber, N. Jaeger, and G. Schulz-Ekloff. Electron microscopy study of the interaction of Ni, Pd and Pt with carbon. *Surf. Sci.*, 227:15, 1990.
- [122] S. M. Kozlov, I. V. Yudanov, H. A. Aleksandrov, and N. Rösch. Theoretical study of carbon species on Pd(111): Competition between migration of C atoms to the subsurface interlayer and formation of  $C_n$  clusters on the surface. *Phys. Chem. Chem. Phys.*, 11:10955, 2009.
- [123] N. Seriani, F. Mittendorfer, and G. Kresse. Carbon in palladium catalysts: A metastable carbide. *J. Chem. Phys.*, 132:024711, 2010.
- [124] I. V. Yudanov, K. M. Neyman, and N. Rösch. Density functional study of Pd nanoparticles with subsurface impurities of light elements. *Phys. Chem. Chem. Phys.*, 6:116, 2003.

## Bibliography

- [125] D. Teschner, Z. Revay, J. Borsodi, M. Hävecker, A. Knop-Gericke, R. Schlögl, D. Milroy, S. D. Jackson, D. Torres, and P. Sautet. Understanding palladium hydrogenation catalysts: When the nature of the reactive molecule controls the nature of the catalyst active phase. *Angew. Chem. Int. Ed.*, 47(48):9274, 2008.
- [126] H. Gabasch, K. Hayek, A. Knop-Gericke, and R. Schlögl. Carbon incorporation in Pd(111) by adsorption and dehydrogenation of ethene. *J. Phys. Chem. B*, 110:4947, 2006.
- [127] F. Viñes, C. Loschen, F. Illas, and K. M. Neyman. Edge sites as a gate for subsurface carbon in palladium. *J. Catal.*, 266:59, 2009.
- [128] L. Nykänen, J. Andersin, and K. Honkala. First-principles calculations of the initial incorporation of carbon into flat and stepped Pd surfaces. *Phys. Rev. B*, 81:075417, 2010.
- [129] L. Garcia, M. Calatayud, J. Andres, and M. Salmeron. Migration of the subsurface C impurity in Pd(111). *Phys. Rev. B*, 71:033407, 2005.
- [130] Z. Kaszukur, J. Stachurski, and J. Pielaszek. X-ray diffraction study of the palladium-carbon system. *J. Phys. Chem. Solids*, 47(8):795, 1986.
- [131] M. Maciejewski and A. Baiker. Incorporation of carbon into palladium during low-temperature disproportionation of CO over Pd/Zr<sub>2</sub> prepared from glassy Pd-Zr alloys. *J. Phys. Chem.*, 98:285, 1994.
- [132] M. K. Rose, A. Borg, T. Mitsui, D. F. Ogletree, and M. Salmeron. Subsurface impurities in Pd(111) studied by scanning tunneling microscopy. *J. Chem. Phys.*, 115(23):10927, 2001.
- [133] D. A. King and M. G. Wells. Molecular-beam investigation of adsorption kinetics on bulk metal targets - nitrogen on tungsten. *Surf. Sci.*, 29(2):454, 1972.
- [134] D. A. King and M. G. Wells. Reaction-mechanism in chemisorption kinetics - nitrogen on the (100) plane of tungsten. *Prog. Roy. Soc. London, Ser. A*, 339:245, 1974.
- [135] P. H. Dawson. *Quadrupole mass spectrometry and its applications*. Elsevier, 1976.
- [136] J. H. Gross. *Mass spectrometry*. Springer, 2004.
- [137] H. Budzikiewicz and M. Schäfer. *Massenspektrometrie*. VHC, 2005.
- [138] F. M. Hoffmann. Infrared reflection-absorption spectroscopy of adsorbed molecules. *Surf. Sci. Rep.*, 3(2-3):107, 1983.
- [139] B. E. Hayden. *Vibrational Spectroscopy of Molecules on Surfaces, Volume 1 of Methods of Surface Characterization*, page 267. J. T. Yates Jr. and T. E. Madey (Editors), Plenum Press, New York, 2002.

- [140] H. Günzler and H. M. Heise. *IR-Spektroskopie: eine Einführung*. VHC, 1996.
- [141] N. B. Colthup, L. H. Daly, and S. E. Wiberley. *Introduction to Infrared and Raman Spectroscopy*. Academic Press, 1990.
- [142] R. J. Bell. *Introductory Fourier Transform Spectroscopy*. Academic Press, 1972.
- [143] A. E. Martin. *Infrared Interferometric Spectrometers, Volume 8 of Vibrational Spectra and Structure: A Series of Advances*. J. R. Durig (Editor), Elsevier, Amsterdam, 1980.
- [144] P. R. Griffiths. *Chemical Infrared Fourier Transformed Spectroscopy*. John Wiley and Sons, 1975.
- [145] P. W. Atkins. *Molecular Quantum Mechanics*. Oxford University Press, 1983.
- [146] J. J. Sakurai. *Modern Quantum Mechanics*. Addison-Wesley, 1994.
- [147] M. Moskovits and J. E. Hulse. Frequency-shifts in spectra of molecules adsorbed on metals, with emphasis on infrared spectrum of adsorbed CO. *Surf. Sci.*, 78(2): 397, 1978.
- [148] R. M. Hammaker, S. A. Francis, and R. P. Eischens. Infrared study of intermolecular interactions for carbon monoxide chemisorbed on platinum. *Spectrochim. Acta*, 21(7):1295, 1965.
- [149] I. Meusel. *Aufbau einer Molekularstrahlapparatur für oberflächenkinetische Untersuchungen*. PhD thesis, Fakultät II (Mathematik und Naturwissenschaften), Technische Universität, Berlin, 2002.
- [150] B. Brandt. *Selectivity in hydrocarbon conversions and methanol decomposition on a Pd/Fe<sub>3</sub>O<sub>4</sub> model catalyst*. PhD thesis, Mathematisch-Naturwissenschaftliche Fakultät I, Humboldt Universität, Berlin, 2008.
- [151] G. H. Vurens, V. Maurice, M. Salmeron, and G. A. Somorjai. Growth, structure and chemical properties of FeO overlayers on Pt(100) and Pt(111). *Surf. Sci.*, 268 (1-3):170, 1992.
- [152] W. Weiss, A. Barbieri, M. A. van Hove, and G. A. Somorjai. Surface-structure determination of an oxide film grown on a foreign substrate - Fe<sub>3</sub>O<sub>4</sub> multilayer on Pt(111) identified by low-energy-electron-diffraction. *Phys. Rev. Lett.*, 71(12): 1848, 1993.
- [153] A. Barbieri, W. Weiss, M. A. van Hove, and G. A. Somorjai. Magnetite Fe<sub>3</sub>O<sub>4</sub>(111) - surface-structure by LEED crystallography and energetics. *Surf. Sci.*, 302(3):259, 1994.
- [154] W. Weiss. Structure and composition of thin epitaxial iron oxide films grown onto Pt(111). *Surf. Sci.*, 377(1-3):943, 1997.

## Bibliography

- [155] Y. J. Kim, C. Westphal, R. X. Ynzunza, Z. Wang, H. C. Galloway, M. Salmeron, M. A. van Hove, and C. S. Fadley. The growth of iron oxide films on Pt(111): A combined XPD, STM and LEED study. *Surf. Sci.*, 416(1-2):68, 1998.
- [156] M. Ritter and W. Weiss. Fe<sub>3</sub>O<sub>4</sub>(111) surface structure determined by LEED crystallography. *Surf. Sci.*, 432(1-2):81, 1999.
- [157] W. Weiss and M. Ritter. Metal oxide heteroepitaxy: Stranski-Krastanov growth for iron oxides on Pt(111). *Phys. Rev. B*, 59(7):5201, 1999.
- [158] Sh. K. Shaikhutdinov, M. Ritter, X.-G. Wang, H. Over, and W. Weiss. Defect structures on epitaxial Fe<sub>3</sub>O<sub>4</sub>(111) films. *Phys. Rev. B*, 60(15):11062, 1999.
- [159] Y. Joseph, G. Ketteler, C. Kuhrs, W. Ranke, W. Weiss, and R. Schlögl. On the preparation and composition of potassium promoted iron oxide model catalyst films. *Phys. Chem. Chem. Phys.*, 3(18):4141, 2001.
- [160] W. Weiss and W. Ranke. Surface chemistry and catalysis on well-defined epitaxial iron-oxide layers. *Prog. Surf. Sci.*, 70(1-3):1, 2002.
- [161] C. Lemire, R. Meyer, V. E. Henrich, Sh. K. Shaikhutdinov, and H.-J. Freund. The surface structure of Fe<sub>3</sub>O<sub>4</sub>(111) films as studied by CO adsorption. *Surf. Sci.*, 572(1):103, 2004.
- [162] C. Lemire, S. Bertarione, A. Zecchina, D. Scarano, A. Chaka, Sh. K. Shaikhutdinov, and H.-J. Freund. Ferryl (Fe=O) termination of the hematite  $\alpha$ -Fe<sub>2</sub>O<sub>3</sub>(0001) surface. *Phys. Rev. Lett.*, 94(16):166101, 2005.
- [163] L. Zhu, K. L. Yao, and Z. L. Liu. First-principles study of the polar (111) surface of Fe<sub>3</sub>O<sub>4</sub>. *Phys. Rev. B*, 74(3):035409, 2006.
- [164] Y. J. Kim, Y. Gao, and S. A. Chambers. Selective growth and characterization of pure, epitaxial  $\alpha$ -Fe<sub>2</sub>O<sub>3</sub>(0001) and Fe<sub>3</sub>O<sub>4</sub>(001) films by plasma-assisted molecular beam epitaxy. *Surf. Sci.*, 371(2-3):358, 1997.
- [165] Y. Joseph, W. Ranke, and W. Weiss. Water on FeO(111) and Fe<sub>3</sub>O<sub>4</sub>(111): Adsorption behavior on different surface terminations. *J. Phys. Chem. B*, 104(14):3224, 2000.
- [166] A. F. Wells. *Structural inorganic chemistry*. Clarendon Press, 1984.
- [167] K. H. Hansen, T. Worren, S. Stempel, E. Lægsgaard, M. Bäumer, H.-J. Freund, F. Besenbacher, and I. Stensgaard. Pd nanoparticles on Al<sub>2</sub>O<sub>3</sub>: Structure and adhesion energy. *Phys. Rev. Lett.*, 83(20):4120, 1999.
- [168] R. Meyer, Sh. K. Shaikhutdinov, and H.-J. Freund. CO oxidation on a Pd/Fe<sub>3</sub>O<sub>4</sub>(111) model catalyst. *Z. Phys. Chem.*, 218(8):905, 2004.

- [169] T. I. Taylor. *Catalysis, Volume 5*, page 257. P. H. Emmet (Editor), Reinhold, New York, 1957.
- [170] C. Kemball. *Advances in Catalysis and Related Subjects, Volume 11*, page 223. D. D. Eley, P. W. Selwood and P. B. Weisz (Editors), Academic Press, New York, 1959.
- [171] G. A. Somorjai. *Introduction to Surface Science Chemistry and Catalysis*. John Wiley and Sons, 1994.
- [172] V. Ponec and G. C. Bond. *Catalysis by Metals and Alloys*. Elsevier, 1995.
- [173] F. Zaera. Probing catalytic reactions at surfaces. *Prog. Surf. Sci.*, 69(1-3):1, 2001.
- [174] J. Horiuti and M. Polanyi. Exchange reactions of hydrogen on metallic catalysts. *Trans. Farad. Soc.*, 30:1164, 1934.
- [175] Z. Ma and F. Zaera. Organic chemistry on solid surfaces. *Surf. Sci. Rep.*, 61(5):229, 2006.
- [176] R. J. Koestner, J. C. Frost, P. C. Stair, M. A. Van Hove, and G. A. Somorjai. Evidence for the formation of stable alkylidyne structures from C-3 and C-4 unsaturated-hydrocarbons adsorbed on the Pt(111) single-crystal surface. *Surf. Sci.*, 116(1):85, 1982.
- [177] F. Zaera. On the mechanism for the hydrogenation of olefins on transition-metal surfaces: The chemistry of ethylene on Pt(111). *Langmuir*, 12(1):88, 1996.
- [178] D. Zscherpel, W. Ranke, W. Weiss, and R. Schlögl. Energetics and kinetics of ethylbenzene adsorption on epitaxial FeO(111) and Fe<sub>3</sub>O<sub>4</sub>(111) films studied by thermal desorption and photoelectron spectroscopy. *J. Chem. Phys.*, 108(22):9506, 1998.
- [179] Y. Joseph, M. Wühn, A. Niklewski, W. Ranke, W. Weiss, C. Wöll, and R. Schlögl. Interaction of ethylbenzene and styrene with iron oxide model catalyst films at low coverages: A NEXAFS study. *Phys. Chem. Chem. Phys.*, 2(22):5314, 2000.
- [180] C. Kuhrs, Y. Arita, W. Weiss, W. Ranke, and R. Schlögl. Understanding heterogeneous catalysis on an atomic scale: a combined surface science and reactivity investigation for the dehydrogenation of ethylbenzene over iron oxide catalysts. *Topics Catal.*, 14(1-4):111, 2001.
- [181] B. Brandt, J.-H. Fischer, W. Ludwig, J. Libuda, F. Zaera, S. Schauerermann, and H.-J. Freund. Isomerization and hydrogenation of *cis*-2-butene on Pd model catalyst. *J. Phys. Chem. C*, 112(30):11408, 2008.
- [182] F. Zaera and G. A. Somorjai. *Hydrogen Effects in Catalysis: fundamentals and Practical Applications*, page 425. Z. Paal, G. P. Menon (Editors), Marcel Dekker, New York, 1988.

## Bibliography

- [183] C. Yoon, M. X. Yang, and G. A. Somorjai. reactions of 1-butene and *cis*-2-butene on platinum surfaces: Structure sensitivity of *cis*-2-butene isomerization. *J. Catal.*, 176(1):35, 1998.
- [184] S. Schauer mann, J. Hoffmann, V. Johane k, J. Hartmann, J. Libuda, and H.-J. Freund. Catalytic activity and poisoning of specific sites on supported metal nanoparticles. *Angew. Chem. Int. Ed.*, 41(14):2532, 2002.
- [185] S. Schauer mann, J. Hoffmann, V. Johane k, J. Hartmann, J. Libuda, and H.-J. Freund. The molecular origins of selectivity in methanol decomposition on Pd nanoparticles. *Catal. Lett.*, 84(3-4):209, 2002.
- [186] M. Frank and M. Bäumer. From atoms to crystallites: adsorption on oxide-supported metal particles. *Phys. Chem. Chem. Phys.*, 2(18):3723, 2000.
- [187] M. Wilde, K. Fukutani, W. Ludwig, B. Brandt, J.-H. Fischer, S. Schauer mann, and H.-J. Freund. Influence of carbon deposition on the hydrogen distribution in Pd nanoparticles and their reactivity in olefin hydrogenation. *Angew. Chem. Int. Ed.*, 47(48):9289, 2008.
- [188] M. Wilde, K. Fukutani, M. Naschitzki, and H.-J. Freund. Hydrogen absorption in oxide-supported palladium nanocrystals. *Phys. Rev. B*, 77(11):113412, 2008.
- [189] M. Wilde and K. Fukutani. Penetration mechanisms of surface-adsorbed hydrogen atoms into bulk metals: Experiment and model. *Phys. Rev. B*, 78(11):115411, 2008.
- [190] H. Öfner and F. Zaera. Isothermal kinetic measurements for the hydrogenation of ethylene on Pt(111) under vacuum: Significance of weakly-bound species in the reaction mechanism. *J. Phys. Chem. B*, 101(3):396, 1997.
- [191] G. C. Bond. *Catalysis by Metals*. Academic Press, 1962.
- [192] H.-P. Koh and R. Hughes. Kinetics of ethylene hydrogenation over a supported nickel-catalyst. *J. Catal.*, 33(1):7, 1974.
- [193] F. Zaera. Surface chemistry of hydrocarbon fragments on transition metals: towards understanding catalytic processes. *Catal. Lett.*, 91(1-2):1, 2003.
- [194] I. Lee, F. Delbecq, R. Morales, M. A. Albiter, and F. Zaera. Tuning selectivity in catalysis by controlling particle shape. *Nature Materials*, 8(2):132, 2009.
- [195] Sh. K. Shaikhutdinov, M. Frank, M. Bäumer, S. D. Jackson, R. J. Oldman, J. C. Hemminger, and H.-J. Freund. Effect of carbon deposits on reactivity of supported Pd model catalysts. *Catal. Lett.*, 80(3-4):115, 2002.
- [196] K. M. Neyman and S. Schauer mann. Hydrogen diffusion into Pd nanoparticles: Pivotal promotion by carbon. *Angew. Chem. Int. Ed.*, 49(28):4743, 2010.



- [197] B. Brandt, W. Ludwig, J.-H. Fischer, J. Libuda, F. Zaera, S. Schauermaun, and H.-J. Freund. Conversion of *cis*- and *trans*-2-butene with deuterium over a Pd/Fe<sub>3</sub>O<sub>4</sub> model catalyst. *J. Catal.*, 265(2):191, 2009.
- [198] F. Zaera. Study of the surface-chemistry of ethyl groups on Pt(111) using partially deuterated ethyl iodide. *J. Phys. Chem.*, 94(21):8350, 1990.
- [199] F. Zaera. Mechanisms for ethylene hydrogenation and H-D exchange over Pt(111). *J. Phys. Chem.*, 94(12):5090, 1990.
- [200] C.-B. Hwang, Y.-S. Fu, Y.-L. Lu, S.-W. Jang, P.-T. Chou, C. R. C. Wang, and S. J. Yu. Synthesis, characterization and highly efficient catalytic reactivity of suspended palladium nanoparticles. *J. Catal.*, 195(2):336, 2000.
- [201] I. V. Yudanov, R. Sahnoun, K. M. Neyman, and N. Rösch. Metal nanoparticles as models of single crystal surfaces and supported catalysts: Density functional study of size effects for CO/Pd(111). *J. Chem. Phys.*, 117(21):9887, 2002.
- [202] F. Viñes, A. Desikusumastuti, T. Staudt, A. Görling, J. Libuda, and K. M. Neyman. A combined density-functional and IRAS study on the interaction of NO with Pd nanoparticles: Identifying new adsorption sites with novel properties. *J. Phys. Chem. C*, 112(42):16539, 2008.
- [203] J. A. Konvalinka and J. J. F. Scholten. Sorption and temperature-programmed desorption of hydrogen from palladium and from palladium on activated carbon. *J. Catal.*, 48(1-3):374, 1977.
- [204] A. D. Johnson, S. P. Daley, A. L. Utz, and S. T. Ceyer. The chemistry of bulk hydrogen embedded in nickel with adsorbed CH<sub>3</sub>. *Science*, 257(5067):223, 1992.
- [205] K. L. Haug, T. Bürgi, T. R. Trautman, and S. T. Ceyer. Distinctive reactivities of surface bound H and bulk H for the catalytic hydrogenation of acetylene. *J. Am. Chem. Soc.*, 120(34):8885, 1998.
- [206] S. T. Ceyer. The unique chemistry of hydrogen beneath the surface: Catalytic hydrogenation of hydrocarbons. *Accounts Chem. Research*, 34(9):737, 2001.
- [207] K. L. Haug, T. Bürgi, M. Gostein, T. R. Trautman, and S. T. Ceyer. Catalytic hydrogenation of acetylene on Ni(111) by surface-bound H and bulk H. *J. Phys. Chem. B*, 105(46):11480, 2001.
- [208] F. Leardini, J. F. Fernandez, J. Bodega, and C. Sanchez. Isotope effects in the kinetics of simultaneous H and D thermal desorption from Pd. *J. Chem. Phys. Solids*, 69(1):116, 2008.
- [209] A. Savara, W. Ludwig, R. J. Madix, S. Schauermaun, and H.-J. Freund. HD exchange over Pd nanoparticles and Pd(111): Influence of subsurface hydrogen. in preparation.

## Bibliography

- [210] C. A. Ramirez and H. F. Busnengo. Comparative dynamical study of the HD and H<sub>2</sub> isotopomers interacting with Pd(111) and Cu(110) surfaces. *Surf. Sci.*, 603(21):3171, 2009.
- [211] R. J. Madix, G. Ertl, and K. Christmann. Pre-exponential factors for hydrogen desorption from single-crystal metal-surfaces. *Chem. Phys. Lett.*, 62(1):38, 1979.
- [212] E. G. Seebauer, A. C. F. Kong, and L.D. Schmidt. The coverage dependence of the pre-exponential factor for desorption. *Surf. Sci.*, 193(3):417, 1988.
- [213] V. P. Zhdanov. Arrhenius parameters for rate-processes on solid-surfaces. *Surf. Sci. Rep.*, 12(5):183, 1991.
- [214] M. G. Hitzler, F. R. Smail, S. K. Ross, and M. Poliakoff. Selective catalytic hydrogenation of organic compounds in supercritical fluids as a continuous process. *Organic Process Research & Development*, 2(3):137, 1998.
- [215] T. Sato, C. V. Rode, O. Sato, and M. Shirai. Hydrogenation of isophorone with noble metal catalysts in supercritical carbon dioxide. *Appl. Catal. B*, 49(3):181, 2004.
- [216] D. I. Enache, G. J. Hutchings, S. H. Taylor, and E. H. Stitt. The hydrogenation of isophorone to trimethyl cyclohexanone using the downflow single capillary reactor. *Catal. Today*, 105(3-4):569, 2005.
- [217] A. Tungler and G. Fogassy. Catalysis with supported palladium metal, selectivity in the hydrogenation of C=C, C=O and C=N bonds, from chemo- to enantioselectivity. *J. Mol. Catal. A*, 173(1-2):231, 2001.
- [218] Studer. M., H.-U. Blaser, and C. Exner. Enantioselective hydrogenation using heterogeneous modified catalysts: An update. *Adv. Synth. Catal.*, 345(1-2):45, 2003.
- [219] H.-U. Blaser, B. Pugin, and F. Spindler. Progress in enantioselective catalysis assessed from an industrial point of view. *J. Mol. Catal. A*, 231(1-2):1, 2005.
- [220] T. Mallat, E. Orglmeister, and A. Baiker. Asymmetric catalysis at chiral metal surfaces. *Chem. Rev.*, 107(11):4863, 2007.
- [221] T. Tarnai, A. Tungler, T. Mathe, J. Petro, R. A. Sheldon, and G. Toth. A new chiral auxiliary in enantioselective hydrogenations: (-)-dihydrovinpocetine. Part I. Hydrogenation of isophorone. *J. Mol. Catal. A*, 102(1):41, 1995.
- [222] A. Tungler, K. Fodor, T. Mathe, and R. A. Sheldon. Enantioselective hydrogenation of ethyl pyruvate and isophorone over modified Pt and Pd catalysts. *Heterog. Catal. Fine Chem. IV*, 108:157, 1997.

- [223] G. Farkas, K. Fodor, A. Tungler, T. Mathe, G. Toth, and R. A. Sheldon. New chiral auxiliaries in enantioselective heterogeneous catalytic hydrogenations: (-) and (+)-dihydro-apovincaminic acid. comparison with (-)-dihydro-apovincaminic acid ethyl ester. iii. *J. Mol. Catal. A*, 138(2-3):123, 1999.
- [224] A. Tungler, Y. Nitta, K. Fodor, G. Farkas, and T. Mathe. Comparison of chiral modifiers in the Pd catalysed hydrogenation of phenylcinnamic acid and isophorone. *J. Mol. Catal. A.*, 149(1-2):135, 1999.
- [225] E. Sipos, A. Tungler, and I. Bitter. Solvent and support effects in enantioselective hydrogenation of isophorone with (s)- $\alpha$ , $\alpha$ -diphenyl-2-pyrrolidinemethanol modified palladium. *React. Kinet. Catal. Lett.*, 79(1):101, 2003.
- [226] E. Sipos, A. Tungler, and G. Fogassy. New substrates and modifiers in the enantioselective heterogeneous catalytic hydrogenation of the C=C double bond. *J. Mol. Catal. A*, 216(2):171, 2004.
- [227] M. Fodor, A. Tungler, and L. Vida. Heterogeneous catalytic asymmetric hydrogenations with modifiers of axial chirality. *React. Kinet. Catal. Lett.*, 90(2):413, 2007.
- [228] S. Li, E. Zhan, Y. Li, Y. Xu, and W. Shen. Enantioselective hydrogenation of isophorone and kinetic resolution of 3,3,5-trimethyl-cyclohexanone over Pd catalysts in the presence of (S)-proline. *Catal. Today*, 131(1-4):347, 2008.
- [229] W. Liu, X. Ren, A. Tkatchenko, and M. Scheffler. Private communication. Not published, 2010.
- [230] NIST WebBook. <http://webbook.nist.gov/chemistry/>.



# Abbreviations

AES	Auger electron spectroscopy
CEM	channeltron electron multiplier
DF	density functional
DFT	density functional theory
EB	effusive beam
EI	electron impact (ionization)
ER	Eley-Rideal
FT	Fourier transform
HOMO	highest occupied molecular orbital
IR	Infrared
HREELS	high-resolution electron energy loss
IRAS	infrared reflection absorption spectroscopy
L	Langmuir - measure for exposure ( $1 \text{ L} = 1.0 \cdot 10^{-6} \text{ Torr} \cdot \text{s}$ )
LEED	low energy electron diffraction
LH	Langmuir-Hinshelwood
LUMO	lowest unoccupied molecular orbital
MB	molecular beam
MCP	multi channel plate
MCT	mercury cadmium telluride (IR detector material)
ML	monolayer
MS	mass spectrometry
MSSR	metal surface selection rule
NEXAFS	near edge X-ray absorption fine structure
NRA	nuclear reaction analysis
PES	photoelectron spectroscopy
PVD	physical vapor deposition
QMS	quadrupole mass spectrometry
SSB	supersonic beam
STM	scanning tunneling microscopy
TMCH	3,3,5-trimethyl-cyclohexanone
TMP	turbomolecular pump
TDS	thermal desorption spectroscopy
TPD	temperature programmed desorption
TPR	temperature programmed reaction
TR	time-resolved
TTL	transistor-transistor-logic
UHV	ultra-high vacuum
XPD	X-ray photoelectron diffraction
XRD	X-ray diffraction



# Danksagung

An erster Stelle möchte ich *Prof. Freund* für seine Unterstützung und sein Interesse an dieser Arbeit danken sowie für die Möglichkeit, an dieser interessanten Themenstellung unter hervorragenden experimentellen Bedingungen in einem inspirierenden wissenschaftlichen Umfeld zu arbeiten.

Als nächstes möchte ich mich bei *Prof. Rademann* von der Humboldt-Universität bedanken, der sich bereit erklärt hat, die Arbeit zu begutachten und zu unterstützen.

Besonders herzlich danke ich meiner Arbeitsgruppenleiterin *Dr. Svetlana Schauer-mann* für die unkomplizierte, effiziente und nette Betreuung. Die Diskussionen, Anregungen und allgemeine Unterstützung haben nicht nur maßgeblich zum Gelingen der Arbeit beigetragen, sondern auch das Arbeiten selbst sehr erfreulich gemacht.

Für die gute Zusammenarbeit in der Arbeitsgruppe und experimentelle Unterstützung möchte ich meinen Kollegen *Dr. Börn Brandt* und *Dr. Aditya Savara* danken sowie *Jan-Henrik Fischer Wolfarth*, *Jose-Manuel Flores-Camacho* und *Matthias Peter* für anregende Diskussionen, schnelle Hilfe bei experimentellen Fragen und eine sehr angenehme Arbeitsatmosphäre in der Arbeitsgruppe. *Jens Hartmann* danke ich einerseits für die kompetente und besonnene Hilfe bei technischen Problemen und andererseits für viele wohlthuende Kurzpausen.

Des Weiteren möchte ich *Prof. Madix*, der die Messungen zum H/D-Austausch angeregt hat, für sein Interesse sowie ausführliche Diskussionen und Denkanstöße danken.

Selbstverständlich möchte ich mich auch bei den anderen Kollegen aus der Abteilung Chemische Physik bzw. dem Fritz-Haber-Institut für das nette und unkomplizierte Arbeitsklima sowie für schnelle Hilfe bei unterschiedlichsten Fragen, Problemen oder Problemchen bedanken. Meinen Büromitbewohnern *Jan-Henrik Fischer-Wolfarth*, *Alexander Uhl* und *Elena Primorac* sowie der gesamten Mittagessensgruppe möchte ich für sowohl wissenschaftliche Diskussionen als auch nicht-wissenschaftliche Unterhaltungen danken.

Schließlich danke ich meinen Eltern und meiner gesamten Familie, insbesondere *Jens Riedel*, für die ausdauernde Unterstützung in allen Lebenslagen.

Vielen, vielen Dank!





# Selbständigkeitserklärung

Ich erkläre, dass ich die vorliegende Arbeit selbständig und nur unter Verwendung der angegebenen Literatur und Hilfsmittel angefertigt habe.

Berlin, den 18.10.2010

Wiebke Ludwig